Technical University of Denmark

Gas Phase Sulfur, Chlorine and Potassium Chemistry in Biomass Combustion

Løj, Lusi Hindiyarti; Glarborg, Peter; Jappe Frandsen, Flemming; Livbjerg, Hans

Publication date:
2007

Link back to DTU Orbit

DTU Library
Technical Information Center of Denmark

Gas Phase Sulfur, Chlorine and Potassium Chemistry in Biomass Combustion

Lusi Hindiyarti

PhD Thesis
CHEC Research Centre
Department of Chemical Engineering
Technical University of Denmark
2007

Preface

This thesis is a partial fulfillment of the requirements of the PhD degree. The work was carried out at the CHEC Research Centre, at the Department of Chemical Engineering, Technical University of Denmark with Associate Professors Peter Glarborg, Flemming Frandsen, and Professor Hans Livbjerg as my supervisors. The PhD project is funded by PSO-Elkraft (Grant FU-2207).

First of all, I would like to express my deepest gratitude to my supervisor Peter Glarborg who has introduced me to this very subject and has been very kind, supportive and helpful during the whole period of my PhD.

I also would like to thank my supervisors Flemming Frandsen and Hans Livbjerg for all the discussions, feedback and support. I thank Paul Marshall for the discussion and collaboration. I would also like to thank Kim Dam-Johansen and Anker Degn Jensen who have been my first contact persons and introduced me to Peter Glarborg prior to my PhD study here at DTU.

I thank the technicians who have been very helpful during my experimental works, Thomas Wolfe, Carsten Nørby, Jørn Hansen, and Lilian Holgersen. I would also like to thank PhD students Jacob Zeuthen, for all the help and discussions and Christian Lund Rasmussen for the help and introduction to the potassium experiments and also for the thesis summary in Danish.

Thanks a lot to Michelangelo Dall'ora and Kim Pedersen for additional reviews of the general part of the thesis. I am also thankful to my friends and officemates, Miche, Kim, Martin, Suzan, Pavle, Simone, Ayten, Sandra, Ana, Diego, Kaare, Claus, Jakob, Yuanjing, Michael, Francesco and lots of others which I can not mention all here, who have provided me with a 'family' at CHEC during this period. Not to forget, I would also like to thank Lisbeth and Lone for all the kindness and help, especially with the administrative things.

Last but not least, I would like to thank my family back home, Ibu, Bapak, Mbak Susi, and Lis who have let me take this opportunity, my husband Ole Løj, for all the love and support, my 'sviger' family here in DK, who has been always like my real family back home, thanks a lot for all of the support.

February, 2007

Lusi Hindiyarti

Summary

Concern about aerosols formation, deposits, corrosion, and gaseous emissions during biomass combustion, especially straw, continues to be a driving force for investigation on S, Cl, K-containing species under combustions conditions. These trace species contained in the biomass structure will be released to the gas phase during combustion and contribute to the problems generated during the process. The investigation during this PhD project is done to step by step improve our understanding in the chemistry and reduce the uncertainties. This study is divided into 3 parts which are K/O/H/Cl chemistry, sulfur chemistry, and their interaction (K/O/H/Cl/S chemistry).

The study on K/O/H/Cl chemistry was done by conducting CO oxidation experiments under reducing conditions with KCl addition. The experiments were performed using a laboratory flow reactor at atmospheric pressure and temperatures in the range 773-1373 K. The addition of KCl results in a strong inhibition of the CO oxidation. The inhibition increases with the KCl level, but the effect levels off at high concentrations. The experimental data were interpreted in terms of a detailed chemical kinetic model. In general a satisfactory agreement between experimental data and kinetic modeling was achieved. The work on K/O/H/Cl chemistry is presented in detail in chapter 3 and paper I in appendices. Analysis of the modeling results indicates that the reaction $K+OH+M \rightleftharpoons KOH+M$ is rate controlling for the radical recombination.

The ratio of SO_2/SO_3 in the gas phase system has been suggested to be the rate limiting step in the homogeneous sulfation process prior to aerosol formation. As presented in detail in papers II-IV in appendices and summarized in chapter 4, the work on sulfur chemistry has significantly improved our understanding of the mechanisms important for the SO_2/SO_3 ratio under combustion conditions. The modeling results using an updated chemistry give a good agreement when compared to experimental data for the SO_2/SO_3. The calculations indicate that oxidation of SO_2 to SO_3 with and without presence of combustibles involve primarily recombination of SO_2 with O and OH radicals. The reaction SO_3+H may limit the SO_3 concentration, while SO_3 reactions with O or OH are unimportant for the SO_2/SO_3 ratio under most conditions of interest. In conclusion, the ratio of SO_2/SO_3 in the gas phase system is mainly determined by reactions $SO_2 +O/OH$, reactions involving intermediate $HOSO_2$, and reaction SO_3+H.

The updated K/O/H/Cl and sulfur chemistry is then used to investigate the interaction of those species important for sulfation prior to aerosols formation, deposits, and corrosion as presented in chapter 5 and in paper V in appendices. It is still an open question whether alkali sulfate aerosols in bio-

mass combustion are formed in the gas phase by a homogeneous mechanism or if it does only involve heterogeneous contact between solid or condensed alkali salt and gas phase S-containing species.

This study investigates sulfate aerosol formation using homogeneous gas phase modeling. The model was validated with data from laboratory experiments available in the literature. The sulfate aerosol formation was modeled using four different approaches. The model consists of a detailed chemical kinetic mechanism containing subsets for O_2/H_2, chlorine chemistry, sulfur chemistry, potassium chemistry, and the interactions of those species. It has been suggested that the rate limiting step in the gas phase sulfate aerosol formation is the oxidation of SO_2 to SO_3. This study suggests that apart from the oxidation of SO_2 to SO_3, there may be other limiting steps which include reactions of SO_2 and O_2 with K-containing species or catalytic reaction by solid surfaces. In general, the sulfate aerosols formation is influenced by the SO_2, O_2, KCl inlet concentrations, residence time and temperature history.

Resume (Danish)

Stigende bekymringer for aerosoldannelse, belgningsdannelse, korrosion, og emissioner af skadelige gasarter i forbindelse med afbrænding af biomasse; især strå, er fortsat den drivende kraft bag undersøgelser af K-, Cl-, og S-holdige stoffers omsætning under forbrændingsbetingelser. Disse stoffer findes i sporstofmængder i biomasse, men frigives til gasfasen under forbrændingsprocessen, hvorfra de spille en afgørende roller i ovennævnte problemstillinger, som har stor industriel og miljømæssig betydning. Dette PhD projekt har til formål at forbedre den nyværende forståelsen af den styrende kemi for disse stoffer i gasfasen under typiske forbrændingsbetingelser. Arbejdet består af tre dele: De første to dele omhandler separarte undersøgelser af K/O/H/Cl- og S-kemi, efterfulgt af et studie af interaktionerne mellem K/O/H/Cl/S.

Det kemiske system K/O/H/Cl er blevet undersøgt både eksperimentel og teoretisk. I det eksperimentelle arbejde blev KCl introduceret i et velkendt kemisk system, hvor CO oxideres under reducerende betingelser. Forsøgene blev udført under veldefinerede forhold i en flowreaktor i laboratorieskala under atmosfæriske betingelse og temperaturer fra 773 til 1373 K med varierende koncentrationer af både CO og KCl. Tilsætningen af KCl har en stærkt inhiberende effekt på CO oxidationen, som forstærkes ved højere KCl koncentrationer indtil et vist koncentrationsniveau er nået, hvorefter effekten stabiliserer sig. De eksperimentelle resultater viser god overensstemmelse med en detaljeret kemisk kinetisk model, som efterfølgende har dannet grundlag for en analysering af de grundliggende reaktionsmekanismer. Denne analyse har vist, at radikal rekombinationsreaktionen $K+OH+M \rightleftharpoons KOH+M$ er et vigtigt hastighedskontrollerende trin i processen. Arbejdet med K/O/H/Cl kemien er gennemgået i detaljer i Kapitel 3, samt i Artikel I i appendiks.

Relevant svovlkemi er også blevet undersøgt udfra et samspil mellem veldefinerede eksperimenter og detaljeret kemisk kinetisk modellering. Arbejdet fokuserer primært på reaktioner, der knytter sig til SO_2/SO_3 forholdet under typiske forbrændingsbetingelser, eftersom det tidligere er blevet foreslået, at dette forhold repræsenterer det hastighedsbegrænsende trin i den homogene sulfaneringsproces forud for aerosoldannelse. Arbejdet med svovlkemi er præsenteret i Kapitel 4 samt i Artikel II-IV i appendiks. De vigtigste resultater er som følger: Termisk dekomponering af SO_3 er for første gang blevet undersøgt eksperimentelt ved 1000-1400 K. Eksperimenterne blev udført i en laminar flowreaktor ved atmosfærisk tryk med nitrogen som bæregas. På baggrund af disse data har det været muligt at udlede hastighedskonstanten for $SO_3+N_2 \rightarrow SO_2+O+N_2$ indenfor temperaturintervallet 1273-1348

v

K. Temperatur- og trykafhængigheden for $SO_2+O(+N_2)$ er ydermere blevet estimeret på basis af ekstrapolation fra eksperimentelle data ved lave temperaturer samt den estimerede broadening-faktor og højtryksgrænse fra nylige studier af Naidoo, Goumri og Marshall (Proc. Combust. Inst. 2005, 30, 1219-1225). Den teoretisk baserede hastighedskonstant er i god overensstemmelse med de eksperimentelle resultater. Flowreaktormålinger ved 1073-1373 K er desuden gennemført for $SO_3/SO_2/N_2O$ systemet mhp. at undersøge reaktionen $SO_3+O \rightleftharpoons SO_2+O_2$. Disse målinger er blevet sammenlignet med detaljeret kinetisk modellering, hvilket antyder, at hastighedskonstanten har en lavere værdi end forventet. Resultaterne er dog ikke vurderet fyldestgørende til at understøtte en endelig konklusion herom, eftersom det kemiske system viste sig at være meget følsomt overfor tilstedeværelsen af vand; selv i sporstoffermængder, hvilket det ikke har været muligt at kvantificere med tilstrækkelig nøjagtig. Dette giver anledning til en vis usikkerhed omkring målingerne. Endelig er radikalreaktioner mellem SO_3 og H, O, og OH blevet karakteriseret vha. ab initio beregninger. De derved fremkomne hastighedskonstanter er inkluderet som en opdateringen af det kinetisk skema for svovlkemi. Efterfølgende modelleringsresultater passer godt overens med litteraturdata fra batch- og flowreaktorer, samt laminar flammer, der involverer oxidation af SO_2 til SO_3. Modelbetragtninger antyder, at reaktionen mellem SO_3+O er ubetydelig under de fleste betingelser, som kan have interesse i forbrændingssammenhæng; selv i flammer under oxiderende betingelser er forbruget af SO_3 primært styret af SO_3+H.

Den opdaterede K/O/H/Cl- samt S-kemi er efterfølgende blevet udnyttet til at undersøge stoffernes vekselvirkning i forbindelse med homogen sulfanering forud for aerosoldannelse, belægningsdannelse samt korrosion, som beskrevet i Kapitel 5 og Artikel V i appendiks. Det er stadig et åbent spørgsmål, hvorvidt alkalisulfat-aerosoler fra biomasseafbrænding bliver dannet som følge af en homogen gasfasemekanisme, eller involverer heterogen kontakt mellem svovlholdige gasfasekomponenter og faststof eller kondenserede alkalissalte. Det aktuelle arbejde hermed har været baseret på homogen gasfasemodellering, der involverer fire forskellige tilgangesvinkler til problematikken. Den anvendte model er valideret mod eksperimentelle data fra litteraturen. Tidligere er det foreslået, at oxidationen af SO_2 til SO_3 er det hastighedsbegrænsende trin, men de nuværende undersøgelser antyder, at der godt kan være andre begrænsende reaktioner; heriblandt reaktioner mellem K-holdige stoffer og SO_2 og O_2, samt reaktioner katalyseret af sulfataerosol-partikler. Overordnet viser undersøgelserne, at sulfataerosol-dannelsen er afhængig af indgangskoncentrationen af SO_2, O_2, KCl, samt opholdstid og temperaturudvikling i systemet.

Contents

Chapter 1

Introduction

This thesis contains a summary of the PhD project and five papers, which fully detail each part of the specific subject investigated during this PhD study. First, the background and objectives are presented. A literature study, to give an overview of the release of S, Cl, and K-containing species and their transformations under combustion conditions, follows the introduction. Furthermore, operational and health problems caused by these species and their interactions during combustion are presented. The important mechanism which controls the gas phase chemistry and aerosol formation is summarized. The results of the work are presented in chapters 3-5. Chapter 3 contains K/O/H/Cl chemistry, while chapter 4 contains sulfur chemistry. The interactions between those species including aerosol formation are presented in chapter 5. General conclusions are presented in chapter 6. Finally, possible practical applications and future work are presented in chapter 7. In order to get more details on the entire project, it is necessary to read the detailed reports, which are presented as five papers in appendices. These papers are presented in the following order:

- **Paper I**: Influence of Potassium Chloride on Moist CO Oxidation under Reducing Conditions: Experimental and Kinetic Modeling Study. (published in FUEL, 85, 978-988, 2006)

- **Paper II**: Thermal Dissociation of SO_3 at 1100-1400 K. (published in Journal of Physical Chemistry A, 110, 6654-6659, 2006)

- **Paper III**: The Fate of SO_3/SO_2 in the System with N_2O Addition. (additional report)

- **Paper IV**: Reactions of SO_3 with O/H Radical Pool under Combustion Conditions. (accepted for publication in Journal of Physical Chemistry A, 2006)

- **Paper V**: Mechanism of Alkali Sulfate Aerosol Formation during Biomass Combustion. (accepted for publication in FUEL, 2007)

The first paper contains a study of potassium and chlorine chemistry involving both experimental work and detailed kinetic modeling. The second to fourth papers provide a study of gas phase sulfur chemical kinetics, which was intended to improve the understanding of the sulfur chemistry. In particular, it aimed to reduce the uncertainties in the important reactions which determine the ratio of SO_2 to SO_3 under combustion conditions. Finally, in the fifth paper, the chemistry for potassium, chlorine, sulfur, and their interactions is used to model the sulfation process and aerosols formation.

1.1 Background

In biomass combustion, especially in the case of straw combustion, some problems arise during the process. Corrosion, fouling, plugging of boiler heat transfer surfaces, gaseous emissions and aerosol formation are probably the most significant operational problems during straw combustion. The species responsible for these problems are typically alkali metal chlorides, and alkali metal sulfates. Chlorine, sulfur, and alkali metals contained in the biomass structure will be released to the gas phase and possibly react to form chemical species e.g: KCl, K_2SO_4.

Combustion and gasification of renewable fuels (biomass, waste) involves a number of chemical reactions, important for emissions, aerosol formation, deposition, and corrosion. The high-temperature sulfur, chlorine, and potassium chemistry has important implications for those problems generated during the combustions, involving both gas phase and condensed phase reactions. Despite the practical importance of Cl/S/K-interactions, only few attempts have been made in order to understand the detailed kinetics of the system. A better understanding of the gas phase chemistry of these components may facilitate development of more efficient methods to minimize emission and operation problems in biomass or waste combustion systems.

1.2 Objectives

The objective of this project has been to improve the fundamental knowledge of the gas phase chemistry, which is important for the emissions, aerosol or deposit formation at combustion of biomass and waste. The aim is to improve the available detailed chemical kinetic model for conversion of chlorine, sulfur and alkali-containing species and their interaction at high temperatures. Such a chemical description can be implemented in reactor models and used to simulate the effect of fuel and process parameters on emissions and operation.

Chapter 2

Literature Study

2.1 S, Cl, and Alkali Metal in Straw

The most widely used annual biomass fuel for combustion to produce heat and power in Denmark is cereal straw [1]. The occurrence of ash forming elements in the biomass structure is important for the release behavior [2–5]. Nutrients needed for plant growth are the majority of the ash forming elements found in annual biomass. Nevertheless, the inorganic impurities can also occur as a result of contamination of the biomass with soil during harvest transport or handling. The most abundant ash forming elements in annual biomass are K, Cl, S, Ca, Mg, P, and Si.

In annual biomass, K and Cl are normally present in high concentrations. These will remain in ionic form and are not metabolized by the plant [6]. The ionic association of K and Cl is in accordance with the fact that typically more than 90 % can be removed by leaching with H_2O [4]. The K^+ and Cl^- main function in the plants is to maintain the pH and charge neutrality, regulate the osmotic pressure, and stimulate enzyme activity. The K^+ and Cl^- ions are characterized by a high mobility at all levels in the plant.

Sulfur is present in biomass as inorganic sulfate and as organically associated sulfur of aliphatic nature such as in proteins, sulfate esters, and sulfur lipids. Annual crops are characterized by high grow rates compared to wood tree, and thereby high production rates of proteins which require a rich sulfur supply [2].

2.2 Release of S, Cl, and Alkali Metal to the Gas Phase

Several studies on the release of S, Cl, and alkali metal from biomass and its waste are available in the open literature [3, 4, 7–9]. An investigation using molecular beam mass spectrometry (MBMS) by Dayton and coworkers indicates that HCl and SO_2 were released during fuel devolatilization, whereas potassium was mainly volatilized during the char burnout, mainly as KCl. At temperatures from 800 to 1100 °C, the amount of potassium released as gas phase KCl was found to increase from 17 to 23 %. During char burnout at higher temperature, additional SO_2 was detected. It was also found that there is no significant effect of the O_2 concentration on the release of inorganic material. More KOH and HCl were found when 20 % more steam was added to the system. Investigations by Jensen et al. [5] indicate that during pyrolysis, a substantial fraction of the total chlorine and potassium contents in wheat straw can be released. Potassium starts to volatilize from around 700 °C, and at 1050 °C approximately 25 % was volatilized. Around 60 % of the chlorine was released when the pyrolysis temperature increased from 200 to 400 °C, and the rest of the chlorine was released in ranges 700 to 900 °C.

Investigations by Knudsen [8], showed that both the combustion temperature and the ash chemical composition significantly affected the quantity of Cl, K and S release to the gas phase. Despite the uncertainties and the variations between the different quantification methods, Knudsen [8] suggests that in grate combustion of straw, more than 80 % Cl, 50-80 % S and 10-40 % K were volatilized. From full scale measurement, Christensen et al. suggest that the average fractional volatilization of K, Cl, and S during combustion of straw is 18 %, 66 %, and 43 % respectively [10]. Figure 2.1 illustrates the release and fate of the S, Cl, and K-containing species during biomass combustion.

2.2.1 Sulfur Transformations

The sulfur contained in a fuel (biomass, fossil fuels) is released to the gas phase during combustion, in the form of H_2S or some complex organic compounds. These gaseous sulfur is then oxidized to sulfur oxides, mainly SO_2 [11, 12]. During combustion, a small part of SO_2 will be oxidized into SO_3. A recent study [2] suggests that sulfur may be recaptured by reaction with char to form strong bonds to inorganic elements. Part of the sulfur will also react with some alkali metal forming sulfates. This sulfate is known to cause problems such as aerosols formation, deposit and corrosion.
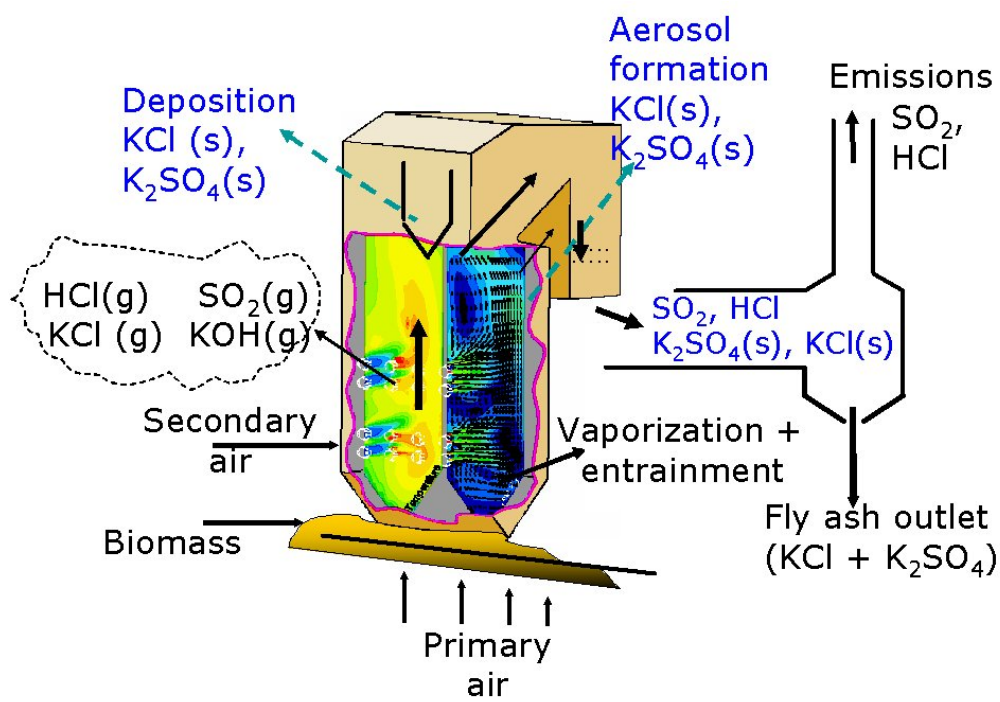
Figure 2.1: Fate and release of sulfur, chlorine, and alkali metal during biomass combustion on a grate. Adapted from [8]

Dayton et al. [4] directly sampled the hot gases released from the devolatilization and combustion of small samples of various types of biomass fuels in a quartz-tube reactor employing a molecular beam mass spectrometer (MBMS) system. They identified gaseous SO_2 during devolatilization of various types of biomass fuels (i.e.: rice straw, wheat straw, switchgrass, and wood) and suggested that this release of SO_2 was due to the oxidation of organic S in the plant matrix. Knudsen et al. [6] found a relatively high release of S (around 25-60 %, depending on the fuel type) at 500 °C in the case of the combustion of annual biomass. In earlier work, Knudsen et al. [2] found that during pyrolysis of wheat straw, the fraction of sulfatic sulfur in the char remains constant up to 500-600 °C, whereas the total S content in the char is decreasing in this temperature range. This result confirms that the S release is due to the decomposition of organic S compounds rather than inorganic sulfates. In this respect, the quantity of S released at 500 °C is highly related to the association of S in the fuel (i.e., to the ratio of organic versus inorganic S), rather than to the composition of the fuel.

According to their experimental work and theoretical considerations [2], the net sulfur transformations during combustion of straw may be summarized as described in figure 2.2 below,
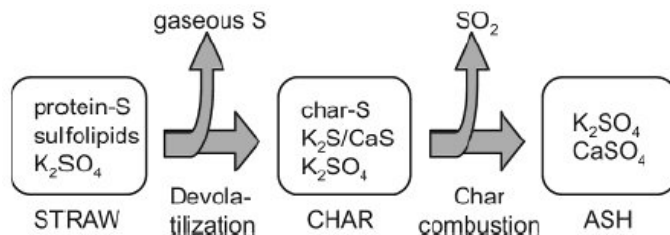
Figure 2.2: Overall sulfur transformations during thermal conversion of straw [2]

From figure 2.2, during the devolatilization sulfur is released from its primary binding sites in organic molecules such as proteins and sulfolipids. The released sulfur may subsequently be captured by reactive sites in the char matrix and become bound to the char. Sulfur present as inorganic sulfate in straw, e.g. K_2SO_4, may partially react with char during devolatilization and become attached to the char matrix or transformed to CaS/K_2S depending on the temperature. During char burnout, inorganic sulfides and sulfur bound to the char matrix are oxidized and released to the gas phase as SO_2 or transformed into solid $CaSO_4$ and K_2SO_4.

2.2.2 Chlorine Transformations

During pyrolysis of Cl-containing fuels, the chlorine is released to the gas phase as chlorinated hydrocarbons (e.g: CH_3Cl), hydrogen chloride (HCl) or alkali chloride (KCl). During combustion, chlorine will be oxidized and released as HCl. Hydrogen chloride is typically the desired chlorine containing product in combustion, since by using a scrubbing system it will be easily removed [12]. Chlorine will also react with alkali metal to form chloride which is involved in the formation of aerosols and deposits.

On the basis of the inorganic composition alone, it is expected that chlorine would mainly be released as KCl for fuels with relatively high concentrations of readily available K, i.e., low Cl/K and high K/Si. Apparently, this is not the case because most Cl is released as HCl from this type of fuel, which implies that the low-temperature HCl release is related to the interaction with the organic structure [6].

Jensen et al. [5] found a two-step release of Cl during pyrolysis of wheat straw; in the first step about 60 % of the Cl was released between 200 and 400 °C. They suggested that during pyrolysis of wheat straw the original straw matrix is destructed and the Cl is released from its solid-phase bonding sites and transferred to a liquid tar phase in the temperature range of 200-400 °C. From there, Cl may be released to the gas phase as HCl(g) or undergo secondary reactions with K to form KCl(s) or with basic functionalities on the char surface. However, it is believed that also in this case, the low-temperature Cl release during pyrolysis may have been due to the reaction of KCl with the char [13].

2.2.3 Alkali Metal Transformations

Alkali metals contained in the fuels will partly be released to the vapor phase during combustion. Wood and annual biomass mainly contain potassium [2, 9]. Chlorine contained in the fuel is believed to facilitate alkali release as alkali chlorides during combustion [3, 9]. These alkali chlorides may be partially converted to alkali hydroxide or alkali sulfates [14]. Alkali chlorides and sulfates are known to be the main composition of aerosols formed in biomass combustion systems, but they are also components which may cause deposit build-up and corrosion.

Knudsen et al. [6] observed a K release of 5-10 % during combustion of annual biomass fuels at 500 °C. The larger fraction of K released during devolatilization (or combustion) at temperatures above 500-700 °C in the case of annual biomass fuels [4–6,13] is suggested to be mainly due to vaporization of potassium salts. This is supported by the fact that water-leaching of

biomass fuels greatly reduces the release of K during devolatilization at high temperature.

The presence of Cl in the fuel has been found to enhance the release of K during pyrolysis and combustion of straw and other annual biomass fuels [6]. In the case of Cl-rich annual biomass, the release of K in the form of KCl occurs mainly between 700 and 800 °C [6], the fraction of K released being dependent on the K/Cl molar ratio of the fuel (20% release in the case of wheat straw, which has a K/Cl ratio of around 4, and 40-50 % release in the cases of rice and barley, which have a K/Cl ratio of around 2).

2.3 Problems in Biomass Combustion

The most severe operational problems in biomass combustion include aerosols, deposit formations, corrosion, and gaseous emissions.

2.3.1 Aerosols Formations and Gaseous Emissions

The flue gas from combustion of biomass (especially straw) contains submicron aerosol particles, SO_2, and HCl in varying but often significant concentrations. During straw combustion, the submicron particle concentration before the particle filter varies considerably but often exceeds 1000 mg/m^3 [10], which leads to high particle emissions through the stack due to the high penetration of submicron particles through electrostatic precipitator [15] or scrubbers [16]. Apart from that there is a potential for enrichment of trace heavy metals in the fine mode aerosol as observed for coal combustion aerosols.

Several studies [17–19] suggest that the sub micron particles are formed during cooling of the flue gas by recondensation of alkali volatilized in the combustion zone in similar way as found in coal combustion. The further evolution of the aerosol is determined by condensation of the volatile on the surface of the particles, coagulation, and deposition. Figure 2.3 illustrates the mechanisms leading to formation of both the small and large particles during combustion of coal.

Sodium or potassium is recovered in the effluent particles mainly as their chloride and sulfate salts. It was suggested that particles are formed from the homogeneous nucleation of salt seeds, which grow by condensation and coagulation [10,18,19]. The process is controlled by chemical reactions in the gas between, e.g., alkali, chlorine, and sulfur species. The rate and equilibrium of these reactions determine the chemical composition of the particles as well as the deposits and the relative amounts of the gas pollutants HCl and SO_2. A study by Christensen et al. [10] investigated aerosol formation
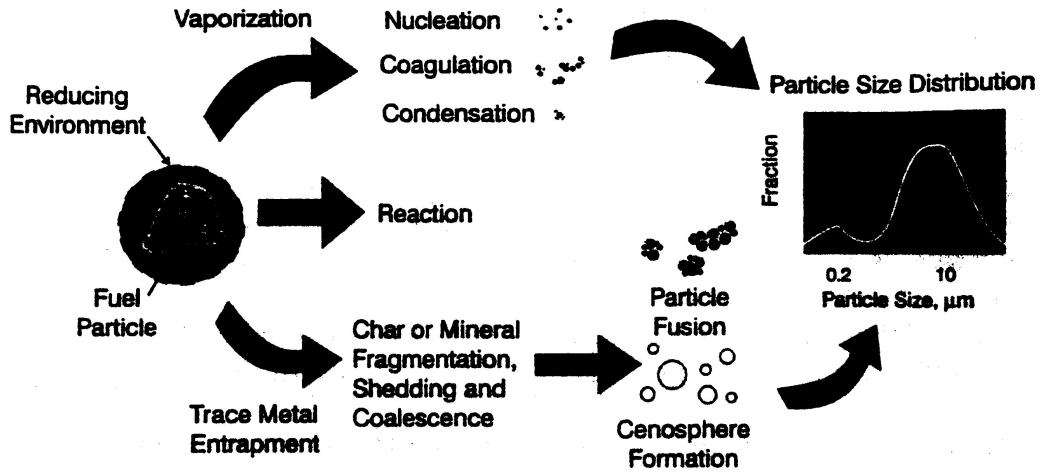
Figure 2.3: Trace metal transformations and partitioning in thermal fuel conversions of coal. [20]

during biomass combustion using a modeling approach and full scale measurements on two straw fired boilers in Denmark (The Haslev and Slagelse CHPs). The aerosols collected consisted of KCl and K_2SO_4. A quenched equilibrium theory by which the KCl, K_2SO_4, HCl and SO_2 is determined by the equilibrium for sulfation at 812 ± 10 ° C, was used to explain the chemical composition of the aerosol particles, HCl and SO_2 outlet concentrations. The authors suggest that aerosol formation is initiated by homogeneous nucleation of K_2SO_4. The particles grow by heterogeneous condensation of K_2SO_4 and KCl. Christensen et al. suggest that oxidation of SO_2 to SO_3 is the rate limiting step.

Livbjerg [15] suggested that several field studies show evident data for the interaction between the gas species SO_2, HCl and the particle composition due to chemical reactions between vapor phase species, prior to particle formation. It was suggested that during the cooling of the flue gas, the reactions shown in figure 2.4 is shifted to the right direction, with the important routes being those leading to chloride and sulfate. It was also suggested that while those reactions tend to be in equilibrium at high temperatures, some of them, especially the oxidation of SO_2 to SO_3 becomes kinetically controlled at low temperature [15].

It was also suggested that the chemical equilibrium seems to determine the composition of the flue gas at temperature of approximately 820 °C.
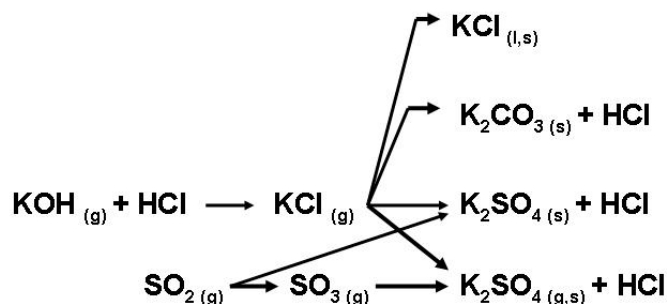
11

Figure 2.4: Possible pathways to particles for vaporized potassium species, adapted from [15]

Below this temperature, only phase transformations occur [15].

2.3.2 Deposits

Deposits are formed due to accumulation of fly ash particles and aerosols as well as condensation of inorganic vapors on exposed surfaces in the furnace. Subsequent chemical reactions within the deposit and sintering will further contribute to the buildup of the deposits layers. Deposits formed in industrial boilers are often divided into slagging and fouling. Slagging occurs in the combustion zone where the radiant heat transfer is dominant. The deposits often consist of an inner powdery layer followed molten or partly molten ash. Fouling forms on the heat transfer surfaces in the convective pass of the boiler. It consists of fly ash particles and condensed volatile species and are loosely bonded [21].

Potassium plays a major role in biomass deposits. Potassium sulfate and chloride have been found to be main components in the deposits formed on the heat transfer surfaces. Jensen et al. [22] studied deposit formation on probes when burning of eight types of cereal straws in two grate boilers in Denmark (the Haslev and Slagelse CHPs). The average composition of the superheater deposits from the investigation was 28-38 wt% K, 14-22 wt% Cl, 5-7 wt% Si, 4.7-5.4 wt% S and 3.1-6.0 wt% Ca.

When there is enough available sulfur in the system, the deposits are mainly found as sulfate with minor chloride. The main component of the hotter deposits is alkali sulfates, while samples from colder sampling points contained both sulfates and chlorides [21]. An example of deposits formed in the superheater during biomass combustion is shown in figure 2.5. However, in the figure shown the deposits formed are not severe enough to cause any

operational problem.

Figure 2.5: An example of deposit formed on the superheater during pulverized biomass combustion

2.3.3   Corrosion

The presence of alkali chloride in deposits enhances corrosion at temperatures above their melting points. Corrosion is generally related to fouling, but fouling does not always mean corrosion problems. A boiler can operate with thick deposits without corrosion problems. Corrosion of heat transfer surfaces is caused either by molten salts on the tubes or by acid components in the flue gases. Generally, hydrogen sulfide (H_2S) and hydrogen chloride (HCl) are the most harmful gaseous species in the flue gases. However, both H_2S and HCl require reducing conditions, high concentrations, or high temperatures to initiate the corrosion process. Whenever molten salts appear on the tubes, corrosion problems hardly ever can be avoided [23].

Corrosion of the superheater tubes in waste incineration and biomass combustion systems are reported to be caused by sulfation of potassium chloride, causing a high partial pressure of chlorine near the metal surface [21, 24], when water is presence following the mechanism below. When there is no water presence, Cl_2 is formed instead of HCl.

$$2KCl(g,c) + SO_2(g) + \frac{1}{2}O_2(g) + H_2O \rightarrow 2K_2SO_4(g,c) + 2HCl(g) \qquad (2.1)$$
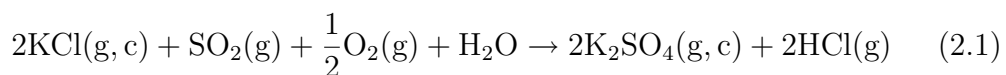
2.4 Sulfation of KCl to K$_2$SO$_4$

The sulfation of alkali chlorides are important for the aerosol formation [10, 19], fouling, corrosion [24, 25], and gaseous emissions [12, 15]. Previous studies on alkali sulfate formation have been motivated mostly by the problems with deposition and corrosion in combustion systems [26]. The mechanism of formation of condensed or solid alkali sulfates in deposits has long been in dispute [14]. Both homogeneous [27–29] and heterogeneous [26,30–34] mechanisms have been discussed in the literature.

During the cooling of the flue gases, alkali chlorides will condense and may deposit on the heat transfer surfaces [19, 23]. The chlorides may react with sulfur dioxide and form sulfate according to mechanism below.

$$2\text{KCl}(g, c) + \text{SO}_2(g) + \frac{1}{2}\text{O}_2(g) + \text{H}_2\text{O} \rightarrow \text{K}_2\text{SO}_4(g, c) + 2\text{HCl}(g) \qquad (2.2)$$

$$2\text{NaCl}(g, c) + \text{SO}_2(g) + \frac{1}{2}\text{O}_2(g) + \text{H}_2\text{O} \rightarrow \text{Na}_2\text{SO}_4(g, c) + 2\text{HCl}(g) \qquad (2.3)$$
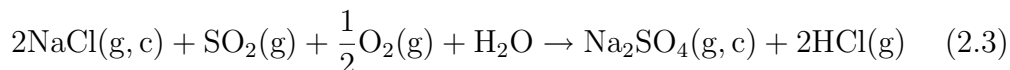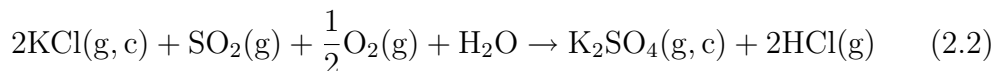
There is still disagreement whether potassium sulfate will be formed in the gas phase and subsequently condense on the heat transfer surfaces or forming aerosol particles, or whether potassium chlorides or hydroxides are deposited, followed by sulfation of these deposits.
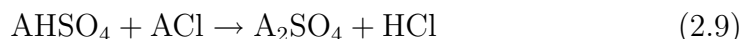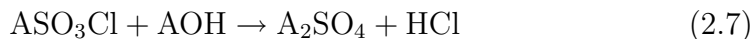
2.4.1 Homogeneous Gas Phase Sulfation

Homogeneous gas phase reaction mechanisms involve formation of alkali sulfates in the gas phase, followed by condensation on the surface or homogeneous nucleation to form aerosols. Some studies suggest that alkali sulfate is mostly formed in the gas phase [10, 14, 18, 19, 23]. Investigation on sulfation of KCl under combustion conditions by Iisa et al. [23] suggests that the sulfation rate is slow in the condensed phase, while the sulfation in the gas phase is quite fast.

Even though gaseous K$_2$SO$_4$ [35–37] and Na$_2$SO$_4$ [38–41] have been shown in vaporization experiments to be stable at moderate to high temperatures, it has been questioned [30–32] whether they are formed in the combustion systems. As reported by Glarborg and Marshall [14] some investigations have detected gaseous Na$_2$SO$_4$ by mass spectrometry in the post flame zone of a CH$_4$/O$_2$ flame doped with SO$_2$ and NaCl [27] and in black liquor combustion experiments [7, 42], but such measurements may be affected by a deposit forming around the sampling orifice [32]. Glarborg and Marshall [14] proposed a homogeneous mechanism of sulfation process which involves the intermediates alkali oxysulfur (ASO$_3$Cl) and alkali hydrogen sulfate (AHSO$_4$).

According to Glarborg and Marshall [14], the oxidation of SO_2 to SO_3 is the first step in the gaseous alkali sulfate formation. The subsequent step [14] is most likely an association reaction involving alkali hydroxide (AOH) and alkali chloride (ACl) (i.e.: KOH or KCl) with SO_3 following reactions:

$$AOH + SO_3(+M) \rightarrow AHSO_4(+M) \tag{2.4}$$

$$ACl + SO_3(+M) \rightarrow ASO_3Cl(+M) \tag{2.5}$$
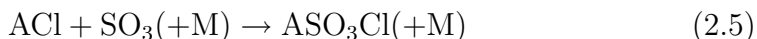
If the alkali hydrogen sulfate and alkali oxysulfur chloride are sufficiently stable at high temperatures, they may participate in a series of shuffle reactions leading to alkali sulfate formation following reactions:

$$ASO_3Cl + H_2O \rightarrow AHSO_4 + HCl \tag{2.6}$$

$$ASO_3Cl + AOH \rightarrow A_2SO_4 + HCl \tag{2.7}$$

$$AHSO_4 + AOH \rightarrow A_2SO_4 + H_2O \tag{2.8}$$

$$AHSO_4 + ACl \rightarrow A_2SO_4 + HCl \tag{2.9}$$
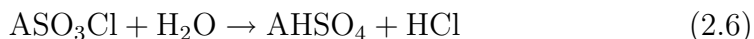
It was also suggested that the proposed mechanism indicates a fast and efficient gas phase sulfation process, with oxidation of SO_2 being the rate limiting step rather than alkali transformations. The plausibility of the proposed gas phase mechanism depends on the thermal stability of the alkaline hydrogen sulfates and the alkaline oxysulfur chlorides in the gas phase [14]. The pathway proposed from their work is shown in figure 2.6.

2.4.2 Heterogeneous Sulfation Mechanism

Several studies on heterogeneous sulfation are published in the literature [29–31, 43–49]. The mechanism may include transportation of gas phase alkali containing precursors to the surface where it is sulfated by reactions in either condensed or solid phase. Heterogeneous formation of alkali sulfate deposits is supported by flame experiments with sodium and potassium salt deposition [31, 45]. Sulfation of solid alkali chloride has been studied both theoretically [43, 44] and experimentally [29, 46–49]. According to some gas phase kinetical considerations [30], only a small fraction of the equilibrium value for gas phase alkali sulfate is expected to form. The earlier work done by Steinberg and Schofield [30, 45, 50] on homogeneous interactions of sodium and sulfur in gas flames implied that the kinetics limitations ruled out a homogeneous Na_2SO_4 formation mechanism in flames. The formation was actually a surface phenomenon, and occurred at a rate that was directly proportional to the flame total sodium content [30]. In this case the alkali metal
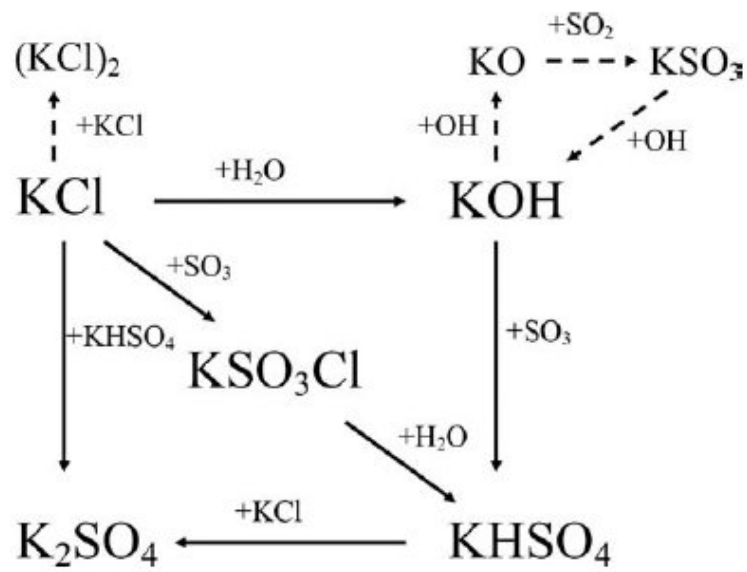
15

Figure 2.6: Pathways of sulfation process proposed by Glarborg and Marshall [14] to simulate experimental data from an entrained flow reactor at 1373 K [23]. Inlet conditions contained 2 % SO_2, 5 % O_2, 10 % H_2O, N_2 to balanced and KCl feed rate : 0,24 g/min

(sodium/potassium) is expected to condense as chlorides. The condensed chloride will then react with available S-containing gas to form sulfates in the condensed (solid) phase. Below 900 K the sulfation is slow with low activation energy [29, 46, 49]. The rate constant sharply increased above this temperature [47, 49]. The presence of molten sodium chloride may shift the mechanism; mixtures of Na_2SO_4 + NaCl form a melt in this range of temperature. Availability of SO_3 promotes the heterogeneous sulfation [29, 44, 48]. Sulfation of molten alkali sulfate is less known, but it is reported [23] to be comparatively slow even in the presence of SO_3.

2.4.3 Aerosol Formation

Aerosol particles are suggested to be formed from homogeneous nucleation of salt seeds, which grow by condensation and coagulation [10, 17–19]. The process is controlled by chemical reactions in the gas between, e.g., alkali, chlorine, and sulfur species. Alkali sulfates play an important role in the formation of submicron particles [10, 18, 19, 51]. The fact that alkali sulfate aerosols were detected in biomass combustion [10, 18, 19] and in experiments using a laboratory flow reactor [17, 23] support the idea of gas phase mechanism. The reaction time for aerosol formation is only about a few seconds, in contradiction to the deposit formation, which may develop over long times. Glarborg and Marshall [14] reported that extrapolation of the results for heterogeneous sulfation [23, 47, 49] indicates that even at high temperatures, the sulfation of solid and molten alkali chloride by SO_2, H_2O, and O_2 is too slow to play an important role on a short times. Christensen et al. [10] concluded from their theoretical analysis of the measured submicron particles concentration in biomass combustion, that the gas to particle conversion occurs by homogeneous nucleation of K_2SO_4 particles, which act as a condensation nuclei for the subsequent condensation of KCl. Observations on aerosol formation during cooling of synthetic flue gas containing $KCl/O_2/H_2O/N_2$ in a laboratory reactor [17] support this interpretation. Christensen and co-workers [10] suggested from their calculation, that SO_2 oxidation plays a key role in the process mentioned above. Several studies suggest that the rate limiting step in the homogeneous gas phase sulfation mechanism is the oxidation of SO_2 to SO_3 [10, 14, 18, 19, 23]. This reaction is discussed further below.

2.5   Oxidation of SO_2 to SO_3

There are several studies addressing the oxidation of SO_2 to SO_3 both homogeneously [11, 52–56] and heterogeneously [57–60]. There has been some controversy regarding the relative importance of two mechanisms of formation of the sulfur trioxide. On the one hand, this compound may be produced by the reaction of atomic oxygen with sulfur dioxide; alternatively, it may be formed by the catalytic oxidation of sulfur dioxide on solid surfaces and at lower temperatures, where the equilibrium is more in favor of sulfur trioxide.
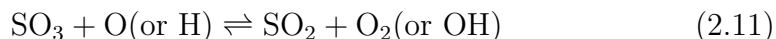
2.5.1   Homogeneous SO_2 Oxidation

The degree of SO_2 oxidation to SO_3 in combustion gases is quite low, in range of 1-2 % [52, 53]. The SO_3 produced in the combustion process will vary with the concentration of SO_2, O_2, and the operational conditions in the system. The oxidation of SO_2 to SO_3 proceeds at an extremely slow rate in the homogeneous gas phase system, even at temperatures above 1073 K. Even though SO_3 can be formed in the gas phase from reaction between SO_2 and O_2 at high temperatures and from the reaction of SO_2 with nitrogen oxides, neither reaction appears to be a major contributor to SO_3 formation in fuel burning systems. The major SO_3 in the system appears to originate from the homogeneous gas phase reaction between sulfur dioxide and oxygen atoms as discussed later. There is no doubt that some of the SO_3 is formed through a heterogeneous catalyzed oxidation of SO_2 on iron oxide surfaces, but substantial experimental data indicate that this reactions is unlikely to be a major source of SO_3 in combustion gases [52,54]. Catalysts on surfaces such as oxidized or V_2O_3 coated superheater elements in boiler furnaces definitely contribute to external corrosion processes, but this case does not directly affect the SO_3 concentration in the gas phase stream flowing through a boiler [52].

The reaction between sulfur dioxide and oxygen atoms has received attention for many years. Investigation by Dooley and Wittingham [55] on SO_2 in flames showed that the amount of flame produced SO_3 increased in the order methane; hydrogen; carbon monoxide. This order also indicates the order of the O atom concentrations observed to increase in these three flames [61]. This suggests that the oxidation of SO_2 in flames occurs by reaction with O-atoms.

A study by Levy and Merryman obtained SO_3-profiles showing the formation of SO_3 just above the visible flame zone. It was concluded that the SO_3 was formed only from the reaction of SO_2 with O atoms, since if the O_2 molecules were oxidizing the SO_2 to SO_3, the SO_3 concentration would

continue to increase in the post flame region. This conclusion was derived from the nearly constant temperature and SO_3 concentrations observed in the post flame probing. Fenimore and Jones [62] proposed the mechanism below to observe steady-state ratios of SO_3 to SO_2 in lean flames.

$$SO_2 + O(+M) \rightleftharpoons SO_3(+M) \tag{2.10}$$

$$SO_3 + O(\text{or } H) \rightleftharpoons SO_2 + O_2(\text{or } OH) \tag{2.11}$$

Levy et al. [52] suggested that the depletion of flame produced SO_3 occurs mostly by O or H attack rather than thermal decomposition.

The homogeneous oxidation of SO_2 by oxygen molecules at temperatures below 1173 K can be neglected according Cullis and Mulcahy [11]. Flint and Lindsay [56] conducted experiments using a quartz tube to measure the SO_3 outlet. Air containing 8% H_2O and 0.14% SO_2 was drawn at a controlled rate through the quartz tube. They concluded that for residence time less than 2 s and below 1073 K, there was negligible oxidation. From a thorough investigation applying spectroscopically dry gases and humidified gases by Dennis and Hayhurst [57] over temperature range studied (973-1198K), concluded that the oxidation of SO_2 was not affected by the presence of H_2O. In addition, an investigation by Glarborg et al. [63] to study the SO_2 conversion during moist CO oxidation suggests that the SO_2 oxidation under the conditions investigated is low, below 5 %.

2.5.2 Heterogeneous SO_2 Oxidation

An investigation on the SO_3 formation in a fluidized bed done by Dennis and Hayhurst [57] indicated that the homogeneous reactions at 973-1198 K result in a very minor conversion of SO_2 to SO_3. Heterogeneous catalytic reactions on the surface of the sand are suggested to be active in the oxidation.

A laboratory study in a silica tube by Marier and Dibbs [59] indicates that the conversion of SO_2 to SO_3 in the presence of fly ash was between 10 - 30 %, and increased linearly with the iron oxide content of the ash. It was suggested that the oxidation of SO_2 was catalyzed by some species contained in the particles (i.e.: iron oxides in fly ash). Experiments of SO_3 formation without adding fly ash in the system indicate that the supporting material, fibrous alumina silica, catalyzes the sulfur conversion into around 1 % conversion. Adding some fly ash containing Fe_2O_3 increase the oxidation of SO_2 to SO_3 significantly. It is generally known that the formation of SO_3 is catalyzed by iron oxide in the fly ash from a coal-fired boiler [58,59].

The alkali-promoted vanadium catalyst for SO_2 oxidation is one of the most important agents in the chemical industry [64]. Hundreds million tons

of sulfuric acid are produced annually, not only as a primary product in the fertilizer industry, but also as a necessary by-product in mineral ore processing. The temperature profile of a common 4-pass SO_2 converter is 420 to 620 °C in the first pass followed by a gradual temperature decline from 440 to 420 °C in the inlet to the last three passes. The SO_2 inlet concentration varies from 7 % in a pyrite-roaster gas to 10.5 % in a sulfur-burning plant, and conversion of SO_2 is almost 100 %. These widely varying process conditions are all accounted for by the use of often a single catalyst type-a 6-wt% V_2O_5 promoted by K_2SO_4 and supported on a diatomaceous earth pellets or extrudates. It was suggested that at the reaction temperature of SO_2 oxidation, a small part of binary K_2SO_4-V_2O_5 is molten [64].

A study on emissions of sulfur trioxide from coal-fired power plants [60] indicates that the SO_3 formations from gas phase modeling prediction is very low, around 0.1-0.65 %. It was suggested that in addition to the SO_3 formation in the furnace, formation of SO_3 also takes place in the temperature range 427-593 °C, found in the economizer region of the boiler. This formation results from oxidation of SO_2 catalyzed by iron oxides, and difficult to characterize the extent, depends on site-specific factors (e.g. : cleanliness of the tube surfaces).

2.6 Detailed Chemistry

2.6.1 Homogeneous Mechanism

The homogeneous gas phase mechanism can be studied using a detailed kinetic modeling approach. Detailed chemical kinetic modeling is a concept for modeling chemical reactions, by studying the individual elementary reactions taking place. The concept is opposed to global chemical kinetic modeling, in which the overall reaction is modeled disregarding any intermediate steps. Detailed kinetics is often found to be necessary in complex processes with a relatively high number of intermediates, which may or may not participate in reactions. This is often the case in combustion processes, which are the subject of this study. When using detailed kinetic modeling of a process, the model will be based on a description of transport processes and the chemistry. The transport processes may be described by fluid dynamics, but often idealized reactor models are used, such as an assumption of plug flow. Kinetic models that are based on elementary reactions offer the best accuracy and reliability. Moreover, the knowledge of a specific elementary reaction can be re-used for completely different operating conditions and in different species mixtures.

Recently Glarborg and Marshall [14] developed a detailed kinetic model for sulfation of KCl through a homogeneous gas phase mechanism. The reaction mechanism developed in their work consists of subsets for H_2/CO oxidation, sulfur chemistry, chlorine chemistry, and potassium/sodium chemistry.

The CO/H_2 subset was drawn from their earlier work [65]. Reactions involving sodium and chlorine species are fairly well known and have been characterized experimentally [66–68], especially reactions of Na, NaO, NaOH and NaO_2 with HCl or Cl_2 to form NaCl. For K/Cl subset, only the K+HCl rate constant has been determined experimentally [69], the authors have estimated the other rate constants in this subset by analogy to sodium reactions [14]. The chlorine subset involving reactions of HCl and Cl_2 was drawn from evaluation of Baulch et al. [70], with few reactions were updated with more accurate data available [14].

The sulfur subset is better known compared to the other subsets. Decades of work have provided fairly good knowledge of the chemistry. Quite a number of the rate constants have been measured experimentally [71–73]. The S/H/O subset was drawn from earlier work [63, 73, 74]. The subset of SO_2/SO_3 includes reactions of SO_2 with O and OH, to form SO_3 either directly or through $HOSO_2$, as well as reactions that recycle SO_3 to SO_2 by reaction with O and SO. All of these reactions both forward and backward are important for the SO_2/SO_3 ratio. This chemistry is believed to play a significant role in the sulfation of KCl. Despite the importance of the reactions in the SO_2/SO_3 subsets, there are still a significant uncertainty in some of the important reactions.

Glarborg and Marshall have also estimated most of the rate constants of the reactions involving alkaline species with sulfur compounds theoretically. Only the recombination reactions of Na and K with SO_2 have been determined experimentally [75, 76].
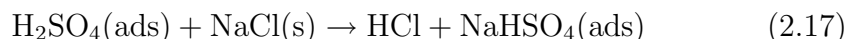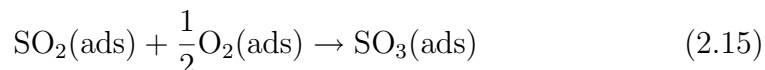
2.6.2 Heterogeneous Mechanism

There are two important mechanism available in the literatures which can be used to describe the heterogeneous/ catalytic reactions for SO_2 oxidation and also for heterogeneous sulfation. Those are Langmuir Hinshelwood and Eley Rideal.

Mechanisms of heterogeneous oxidation of SO_2 over commercial catalysts have been proposed by Ashmore [77]. Dennis and Hayhurst [57] proposed several mechanisms for the case in a fluidized reactor, based on the principle that O_2 chemisorbs dissociatively on the surface of a sand particle in competition with SO_2 and SO_3. The rate of the reaction is assumed to be

governed by either, gas phase SO_2-molecules reacting with adsorbed O-atoms in an Eley-Rideal mechanism or by reaction between adsorbed O-atoms and adsorbed SO_2-molecules in a Langmuir-Hinshelwood mechanism.

A study by Henriksson and Warnqvist [47] investigated the sulfation of NaCl using an alumina tube in an electrically heated furnace. The study was conducted in the temperature range from 500 to 800 °C, which covers both solid and molten phases of NaCl and Na_2SO_4 mixtures. They proposed the following reaction mechanisms for the sulfation of NaCl by SO_2 in the absence of SO_3,

$$SO_2 \rightarrow SO_2(\text{ads}) \tag{2.12}$$

$$O_2 \rightarrow O_2(\text{ads}) \tag{2.13}$$

$$H_2O \rightarrow H_2O(\text{ads}) \tag{2.14}$$

$$SO_2(\text{ads}) + \frac{1}{2}O_2(\text{ads}) \rightarrow SO_3(\text{ads}) \tag{2.15}$$

$$SO_3(\text{ads}) + H_2O(\text{ads}) \rightarrow H_2SO_4(\text{ads}) \tag{2.16}$$

$$H_2SO_4(\text{ads}) + NaCl(\text{s}) \rightarrow HCl + NaHSO_4(\text{ads}) \tag{2.17}$$

$$NaHSO_4(\text{ads}) + NaCl(\text{s}) \rightarrow HCl + Na_2SO_4(\text{ads}) \tag{2.18}$$

The SO_2, O_2, and H_2O are adsorbed on the NaCl surface, and the adsorbed species react to form $SO_3(\text{ads})$. The $SO_3(\text{ads})$ reacts with adsorbed water and NaCl to form HCl and Na_2SO_4. The intermediates was proposed to be $H_2SO_4(\text{ads})$ and $NaHSO_4$ (ads). These sequential reactions they proposed followed the Langmuir-Hinshelwood mechanism.

Two possible approaches which can be used to model the kinetic phenomena of the heterogeneous/catalytic reactions will be discussed further below.

Langmuir Hinshelwood and Eley Rideal

Langmuir-Hinshelwood reaction kinetics describes most catalytic reactions. The basic idea of this kinetic mechanism is that all reactants are adsorbed prior to the actual reaction event. These adsorbed reactants are then ready for reacting with another species. The catalytic reaction consists of a sequence of reaction steps, each step is assumed to be an elementary step, meaning that the reaction is supposed to occur exactly as it is written.

Taking as an example the catalytic reaction of SO_2 to SO_3 over a solid surface, the catalytic mechanism might be described using this method. The gaseous SO_2 and O_2 will be adsorbed into the surface of solid particles, and this adsorbed reactants will react further to form SO_3 as illustrated in figure 2.7 below,
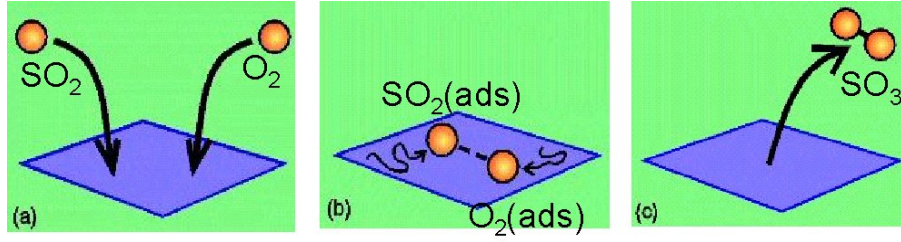
Figure 2.7: The schematic description of Langmuir Hinshelwood mechanisms for SO_3 formation adapted from [78]

A study by Graham and Sarofim [58] investigated the submicometer ash catalyzed SO_2 oxidation. Heterogeneous oxidation of SO_2 with inlet gas contained 5 % O_2 and 1000 ppm SO_2 using submicrometer ash Fe_2O_3 showed a non linear arrhenius plot, especially in higher temperature (around above 950 K). There was an indication of sintering being a caused of non-Arrhenius behaviour. The experiments done after applying heat to the submicrometer samples, the linear Arrhenius plot was achieved with activation energy for 43 kcal/mole. The determination of reaction order from the sintered samples indicated that the reaction is 0.5 order in O_2 and first order in SO_2.

A langmuir-Hinshelwood model for adsorption and reaction where the rate limiting step was assumed to be this surface reaction:

$$SO_2 \cdot L + O \cdot L \Rightarrow SO_3 \cdot L + L \qquad (2.19)$$
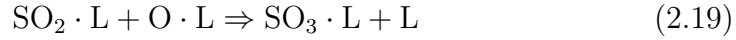
was in a good fit with the kinetic information above. Where L=active adsorption site, and k_f=forward reaction-rate constants. The kinetic expression they used was derived from the Langmuir-Hinshelwood model and the assumption of the above rate limiting step is as follows :

$$\frac{dC_{SO_3}}{dt} = \frac{ak_f K_{O_2}^{1/2} K_{SO_2} [P_{O2}^{1/2} P_{SO2} - (1/K) P_{SO3}]}{[1 + K_{SO2} P_{SO2} + K_{SO3} P_{SO3} + (K_{O2} P_{O2})^{1/2}]^2} \qquad (2.20)$$

where K_{O2}, K_{SO_2}, and K_{SO3}=adsorption equilibrium constants, a=catalyst surface area/reactor volume, K=equilibrium constant for the overall reaction, and P_i=partial pressure of species i. The terms $K_{SO2} P_{SO2}$, $K_{SO3} P_{SO3}$, $(K_{O2} P_{O2})^{1/2}$ are assumed to be much smaller than 1 ($<< 1$, i.e. only a small fraction of the active sites is occupied - a condition not uncommon at high temperatures and low gas partial pressures), then the denominator can be assumed to be 1. This leads to a kinetic expression which has the reactions orders of 1/2 in O_2 and 1 in SO_2

23

Another assumption used by Boonsongsup et al. [46] may also be applied, depending on the system conditions investigated. They investigated the kinetics of sulfation of solid NaCl at combustion conditions. The results implied that the adsorption of SO_2 on the alkali chloride surface limited the overall reaction rate. Thus, the overall rate of reaction can be approximated by the adsorption rate of SO_2. Langmuir isotherms are used to describe the adsorption process assuming that the surface is energetically ideal and that forces of interaction between adsorbed species are negligible. The difference between the Langmuir Hinshelwood and Eley Rideal can be seen in figure 2.7-2.8. In Eley Rideal, the mechanism following these steps; a. an atom adsorbs onto the surface; b. another atom passes by which interacts with the one on the surface; c. a molecule is formed which desorbs. While in Langmuir Hinshelwood, the mechanism following these steps; a. two atoms adsorb onto the surface; b. they diffuse across the surface, and interact when they are close; c. a molecule is formed which desorbs.
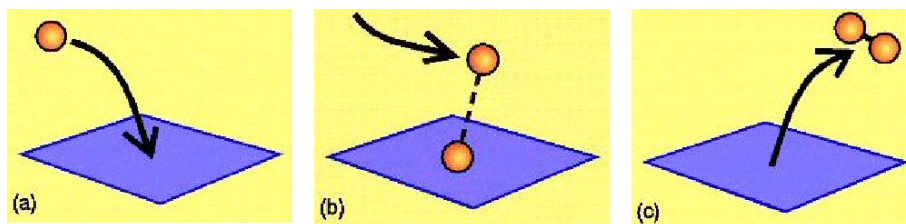

Figure 2.8: The schematic description of Eley Rideal mechanisms adapted from [78]

2.7 Concluding Remarks

Annual biomasses, especially straw, contain trace amounts of alkali metal, sulfur, and chlorine in their structure. These species will be released to the gas phase and react further to cause problems such as aerosols formation, deposits, corrosion, and gaseous emissions. According to some literature, the vapor phase of these species and their interactions in the gas phase having a significant role in the problems caused by those species during combustion and cooling of the flue gas.

In literature, there is only very limited study on the gaseous alkali metal chemistry. Previous attempts to develop detailed reaction mechanisms for the potassium and sodium chemistry are limited. The first detailed mechanisms for alkali metal chemistry in flames were reported by Steinberg and co-workers [30, 32, 79]. They focused on alkali atom removal, catalyzed radical recombination, and sodium/sulfur interactions. Zamansky and co-workers [80–84] investigated sodium chemistry in relation to NO_x reduction in combustion and reburning zone. In a recent kinetic study on gas phase alkali chemistry, Glarborg and Marshall [14] updated the thermochemistry and high-temperature gas-phase reaction mechanisms of sodium and potassium. More work is needed to improve the understanding of alkali metal chemistry, especially for the reaction of K-containing species and the radical pool under combustion conditions.

There are quite a number of reports on gaseous sulfur chemistry, results of decades of work. While the overall mechanisms for SO_3 formation and destruction are fairly well known, kinetic modeling of the process still suffers from a lack of accurate kinetic data, and refinements are required in order to establish a reliable mechanism. The oxidation of SO_2 to SO_3 under combustion conditions has been suggested to be the rate limiting step in the gaseous sulfation process prior to aerosols formation. According to available literature, only few percent of the SO_2 will be oxidized to SO_3 homogeneously above 1073 K; heterogeneously, a catalytic oxidation by for instance iron oxide contained in the fly ash will enhance the sulfur conversion significantly. The homogeneous and/or heterogeneous mechanism may be active in the SO_3 formation depending on the system and operating conditions. More work is needed on the sulfur chemistry especially to improve the understanding of the mechanism important for SO_2/SO_3 ratio under combustion conditions.

There is clearly still an open question regarding the fundamental mechanism of sulfate aerosols formation, whether it involves homogeneous gas phase mechanism or only involves a heterogeneous mechanism. Recently, Glarborg and Marshall [14] proposed a homogeneous gas phase sulfation mechanism. However, the results are not conclusive, yet other studies suggest that the sul-

fation phenomena can only occur through heterogeneous mechanism involving solid alkali chloride. The only available study on K/O/H/Cl/S gaseous chemistry is one by Glarborg and Marshall [14]. Most of the rate constants used in their study is results of theoretical estimation. In order to improve the understanding of that chemistry and minimize the uncertainties, further work is needed. This attempt can be done by i.e., evaluating the available mechanism to a broader range of experimental data and operating conditions.

From literature, both homogeneous and heterogeneous mechanism may contribute to the sulfation process depending on the system and operating conditions. For lower residence time, a heterogeneous mechanism seems too slow to be important in the sulfation process, while it may become important for longer residence times. Kinetic models of either mechanism can be evaluated using different approaches available in the literature, depending on the conditions of the system. If only considering a homogeneous mechanism, a detailed kinetic model seems to be the right tool to investigate the complex gas phase chemistry of those species under combustion conditions and cooling of the flue gases. Further work is necessary to improve the understanding of the sulfur, chlorine and alkali metal chemistry both in terms of minimizing uncertainties in the rate constants of some important reactions and in improving the understanding of the fundamental mechanism of the sulfation process. This work needs to be done step by step to improve our understanding and minimizing uncertainties in the K chemistry and interactions of radical pool, sulfur chemistry important for SO_2/SO_3 ratio, and their interactions (K/O/H/Cl/S chemistry) under combustion conditions. Also the importance of surface reactions for K/Cl/S transformations needs to be addressed.

Chapter 3

K/O/H/Cl Chemistry

3.1 Introduction

This chapter contains most of the work presented in paper I [85]. The intention of the work has been to improve the understanding of gaseous K chemistry and its interactions with radical pool under combustion conditions. The knowledge of alkali metal chemistry and its interactions with radical pool is limited. Most of the rate constants used in the mechanism were results of estimations. Only very limited number of rate constants have been calculated from experimental work. There are clearly significant uncertainties both in the mechanism and the rate constants reported in the literature.

To the author knowledge, previous attempts to develop detailed reaction mechanisms for the potassium and sodium chemistry are limited. The first detailed mechanisms for alkali metal chemistry in flames were reported by Steinberg and co-workers [30, 32, 79]. They focused on alkali atom removal, catalyzed radical recombination, and sodium/sulfur interactions. Zamansky and co-workers [80–84] investigated sodium chemistry in relation to NO_x reduction in combustion and reburning zone. In a recent kinetic study on gas phase alkali chemistry, Glarborg and Marshall [14] updated the thermochemistry and high-temperature gas-phase reaction mechanisms of sodium and potassium.

The objective of this work is to improve the understanding of potassium chemistry and its interactions with the radical pool under combustion conditions by studying the effect of KCl on CO oxidation in a flow reactor under reducing conditions and 873 - 1373 K. The work involves both experiments and a kinetic modeling study.

The CO oxidation system was chosen because the mechanism is quite well known. The K chemistry and its interactions with radical pool can be

investigated by introducing some gaseous KCl to the CO oxidation system under very reducing conditions. The reducing conditions were chosen to slower the oxidation of CO to CO_2. By comparing the measured CO and CO_2 outlet from the $CO/H_2O/N_2$ system with and without addition of potassium chloride, the effect of the KCl addition can be analysed. The experimental data can be used to evaluate the detailed kinetic modeling on K chemistry and its interaction with radical pool.

3.2 Experimental Work

The experiments were done in an alumina tube reactor to simulate plug flow under well controlled reaction conditions. A picture of the setup is shown in figure 3.1, while the schematic of the reactor used can be seen in figure 3.2. The inner diameter of the main tube was 24 mm and it had a wall thickness of 3 mm. The length of the reactor and reaction zones was 750 mm and 300 mm, respectively. The alumina inner tube for KCl feeding was 12 mm in diameter and 150 mm in length, with a wall thickness of 2 mm.

The reactor inlet consisted of main and secondary inlet flows. Potassium was fed by saturating a nitrogen flow from the main inlet with potassium vapor in a packed bed of inert porous alumina pellets impregnated with potassium chloride. The packed bed of pellets was inserted in the inner tube close to the entrance section of the reactor. It was critical to maintain a constant temperature in the potassium feeding section in order to get a certain amount of potassium vapor. In order to avoid contact with the KCl in the pellets, the reactive gas was fed to the secondary flow. The two inlet flows were merged at the end of the inner tube. A reactor set-up equipped with a three-heating-zone oven was used for the experiment. The separate heating zones were useful to maintain a constant temperature in the KCl feeding tube, and a certain setting temperature in the reaction zones.

The alumina pellets were prepared by heating them in an oven at a temperature of about 573 K for one day to remove the volatiles. Then the pellets were impregnated with a saturated KCl solution for about one day, and the slurry was filtered in order to separate the particles. The particles were gently flushed with water before being placed in an oven for 24 hours at 473 K. The KCl solution was prepared by adding a sufficient amount of solid KCl in a beaker glass filled with distilled water, applying continuous agitation to the slurry until no more solid KCl dissolved in the water.

For the present investigation a total gas flow of about 1 NL/min was used. Feed gases contained CO, H_2O, and N_2. Two different CO inlet concentrations were used in the experiments and the amount of KCl vapor was varied
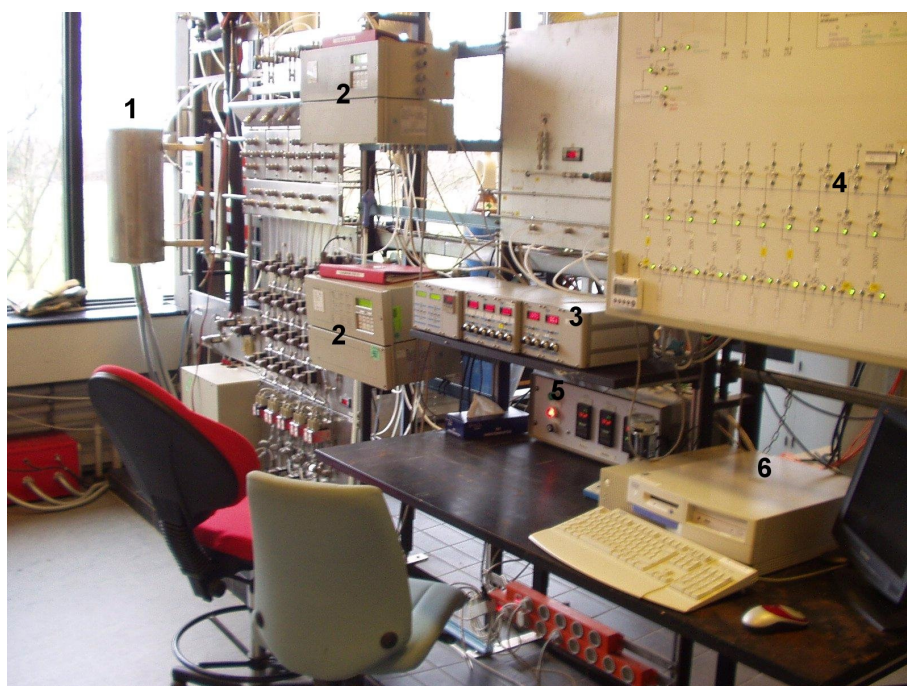
28

Figure 3.1: A picture of the experimental setup used to investigate K/O/H/Cl chemistry, 1: flow reactor, 2: gas analyzer, 3: gas flow controller, 4: gas mixing system, 5: oven controller, 6: a computer for data acquisition.
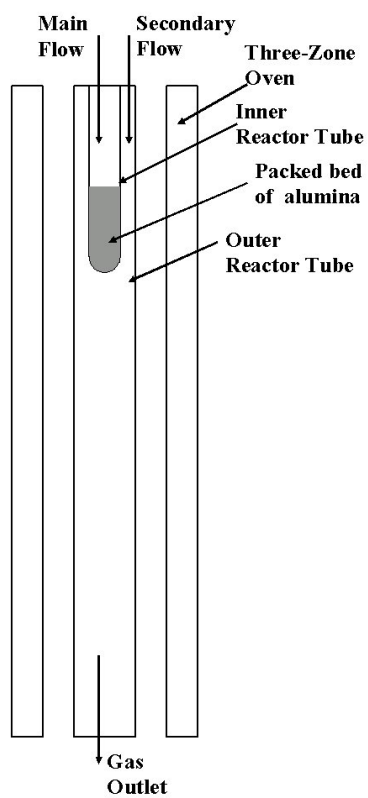
Figure 3.2: A schematic of the alumina reactor used in the experimental setup for K/O/H/Cl chemistry.

by setting the flow to the alumina packed bed. The gas outlet was analyzed for CO and CO_2 after gas conditioning. Pure CO oxidation experiments were done for reference.

The temperature profile along the reactor was measured by a K type thermocouple, which was displaced axially in small steps, allowing sufficient time for stabilization of the temperature between each reading.

To obtain a mass balance for potassium chloride, the amount of potassium condensed on the tube wall and those caught by aerosols filter was measured. The alumina tube was withdrawn and flushed with distilled water. The filter samples were also flushed with distilled water in backward direction using a vacuum. The wall and filter condensate of potassium chloride was analyzed from the electrical conductivity of the flushed water.

The experiments on potassium chemistry were quite challenging. The potassium is very difficult to handle during the experiments, since it is very easy to be deposited on any surfaces available in the system. Mass balance experiments indicate a significant loss of potassium in the system investigated. During present experiments, a certain amount of potassium was found to be deposited on the alumina tube surface, and affect the homogeneous chemistry. Surface reactions need to be attributed to the homogeneous mechanism to account for this effect.

3.3   Detailed Kinetic Model

The Senkin code [86] which runs in conjunction with Chemkin-II [87] was used to model the flow reactor experiments, assuming plug flow. The reaction mechanism and thermodynamic properties used in this study were drawn mainly from the work of Glarborg and Marshall [14]. The thermodynamic data for the key species, and rate coefficients for important reactions in the potassium subset are listed in Table 1-2 in paper I.

The reaction mechanism consists of subsets for CO/H_2 oxidation, chlorine chemistry, and potassium chemistry. The chlorine chemistry, involving reactions of HCl and Cl_2, is an update of the evaluation by Baulch et al. [70]. Few of the rate constants in the K/H/O/CO reaction subset have been determined experimentally. Therefore estimated values for the rate constants are assigned to most of the reactions. While Glarborg and Marshall [14] focused on lean conditions, the present study involves strongly reducing conditions. For this reason we have included a reaction subset for KH (R30–R36), with rate constants as estimated by Klingenberg and Heimerl [88]. The reaction numbering is in accord with the mechanism listed in table 2 (see paper I). The most important reaction in the K/H/O/CO subset for the present in-

vestigation is the recombination of K with OH to form KOH (R2).

Among the potassium/chlorine interaction, only one reaction has been determined experimentally, K + HCl (R24). The other rate constants are estimated to be the same as the corresponding sodium reactions. Data on corresponding K and Na reactions show very similar rate constants [14]. The sodium and chlorine species interaction, primarily the reactions of Na, NaO, NaOH, and NaO_2 with HCl (or Cl_2 to form NaCl), is fairly well established, as all those reactions have been determined experimentally.

3.4 Results and Discussions

Oxidation of CO by water vapor was studied in the range of temperature from 773 to 1373 K. Experiments were performed by increasing the temperature in steps of 25 K. The initial mole fractions of CO were around 1900-2150 ppm or 7800 ppm. The mole fraction of the oxidizing agent, H_2O, was kept constant as 0.052, with N_2 as balance gas. The KCl vapor concentration was varied as 0, 157, 313, 470, or 626 ppm. Oxygen was present as an impurity due largely to diffusion through the teflon tubes in the feeding system; the concentration was estimated to be approximately 75 ppm. The isothermal zone residence times for the experiments were 0.95-1.70 seconds; it varied with temperature since the mass flow was held constant. Mass balance experiments performed at 1073 K showed a significant amount of KCl condensation in the reactor system (in the range of 40-80%), but we expect only a fraction of the KCl to deposit in the high temperature, isothermal part of the reactor.

3.4.1 CO Oxidation without KCl Present

The oxidation of carbon monoxide (CO) under very reducing conditions was studied as shown in Fig. 3.3, for a mixture of CO and H_2O with CO inlet concentrations around 1900 or 7800 ppm. The results from the experiments are shown as symbols, while solid lines denote modeling results. Comparing Figs. 3.3a and 3.3b, it can be seen that by increasing the inlet ratio between H_2O and CO, the oxidation of CO occurs at lower temperatures. The temperature for 50% conversion of CO, i.e. where CO and CO_2 reach the same value, is shifted from around 923 K (for the higher inlet ratio between H_2O and CO (a)) to around 1023 K (for the lower ratio (b)). This is caused by the reaction sequence $H_2O + H \rightleftharpoons OH + H_2$, $CO + OH \rightleftharpoons CO_2 + H$. The promoting effect of water vapor in larger amounts is opposite to what has been observed for CO oxidation under oxidizing condition; here an increase in the H_2O/CO inlet ratio will typically decelerate the CO oxidation [89,90].
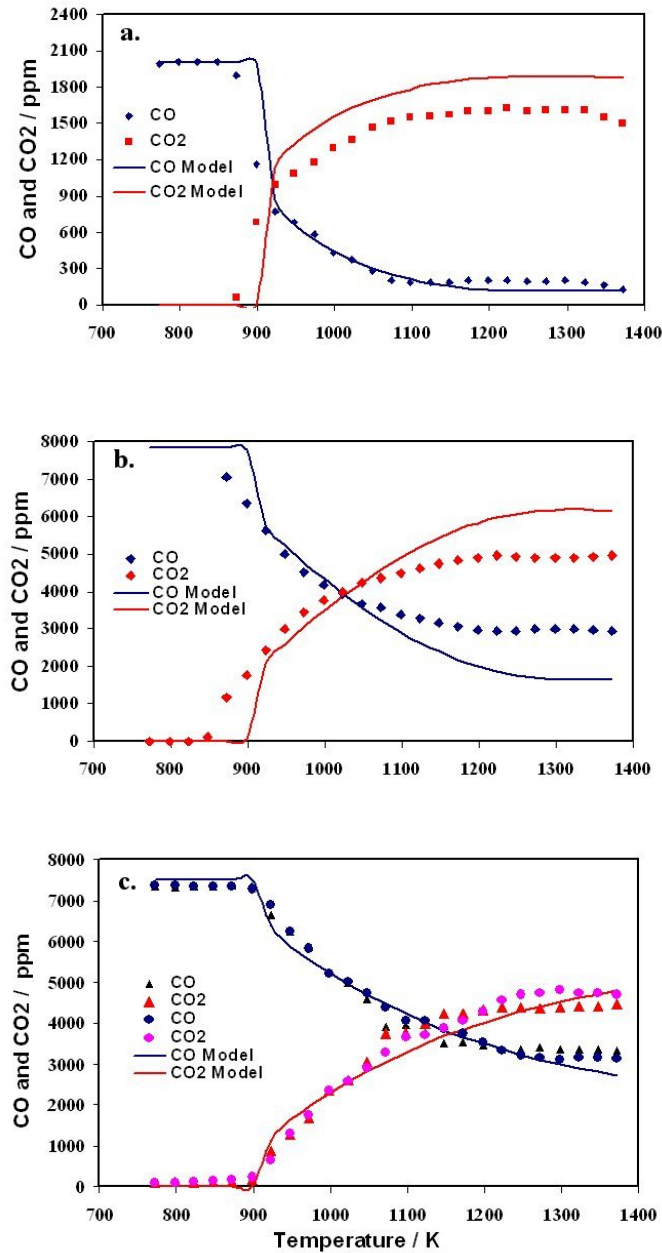
Figure 3.3: The outlet mole fractions of CO and CO_2 in a CO oxidation experiment in a clean reactor for lower CO inlet concentration (a), for higher CO inlet concentration (b) and for higher CO inlet concentration with dirty reactor (c) without KCl addition in the gas phase. Inlet composition CO:1900 ppm or 7800 ppm; H_2O: 0.052; N_2: balance gas and O_2 from kinetic modeling estimation (75 ppm), residence time: 0.95 - 1.70 s (1305/T[K]). The solid lines denote modeling results and the symbols are experimental results. Note that for the conditions of (a) and (b) the CO inlet concentration decreased slightly over the time of the experimental run.

33

From pathway analysis and sensitivity analysis the key reactions in the CO/H_2 subset under the present conditions were identified. The CO conversion is dominated by $CO+OH \rightleftharpoons CO_2+H$, which is also the most sensitive reaction in the system. Since the OH radical is required for the reaction to occur, the availability of water will control the system. Most of the OH radicals are generated through the reaction $H_2O+H \rightleftharpoons OH+H_2$ and only a small amount is formed by the reaction $H_2O+O \rightleftharpoons OH+OH$.

In the interpretation of the flow reactor results, the potential impact of oxygen impurities and of reactions on the alumina reactor surface had to be taken into consideration. The presence of trace amounts of O_2 enhances the oxidation rate through $H + O_2 \rightleftharpoons O + OH$, and $O + H_2O \rightleftharpoons 2OH$. The amount of oxygen was estimated by kinetic modeling and assumed to be the same in all experiments. Modeling predictions of the present experiments tend to overpredict the conversion of CO to CO_2. Since the rate constants for the key reactions in the system are well known, the difference between the experimental and modeling results cannot be explained in terms of uncertainties in the kinetic model. Consequently, the discrepancy was attributed to surface reactions. While data on moist CO oxidation have shown little indication of surface reactions on a quartz wall under lean to slightly reducing conditions [63, 73, 89], experiments on CO/H_2 oxidation under reducing conditions [74] indicate some radical recombination on the quartz reactor wall.

Following Dagaut et al. [74] the surface reaction was represented by a hydrogen atom loss at the reactor walls. As the O/H radical pool starts establishing, the presence of CO causes the production of hydrogen atoms through the reaction $CO+OH \rightleftharpoons CO_2+H$. This reaction enhances the radical pool build-up. Hydrogen atom recombination kinetics at the surface was included by fitting a sticking probability to match the experimental results, assuming an activation energy of 9800 cal/mole as observed for quartz [74]. The resulting hydrogen loss rate constant for the (clean) alumina reactor, $k_{clean} = 5.0 \cdot \exp(-9800/RT)$ s^{-1}, was implemented in the mechanism and used in the plug-flow calculation. The results of the model equipped with the hydrogen atom loss mechanism agree quite well with data for the clean reactor (Fig. 3.3a and b). The presence of potassium chloride could be expected to alter the surface reactivity. Various potassium powders have been shown to enhance radical recombination on their surface [91]. Figure 3.3 (b and c) shows results of CO oxidation experiments with the high CO inlet concentration in a clean and a dirty reactor, respectively. The dirty reactor has been exposed to KCl. The results show a significant inhibition of the CO oxidation in the dirty reactor, compared to the behavior in the clean reactor. In the clean reactor the initiation temperature is around 873 K; this value is

34

shifted to 923 K in a dirty reactor. The temperature for 50% conversion of CO, i.e. where CO and CO_2 reach the same value, is shifted from around 1023 K (clean reactor) to around 1148 K (dirty reactor). These results suggest that the surface reactivity towards radicals has increased considerably due to the presence of potassium on the wall. Similar to the procedure used for the clean reactor, a hydrogen atom loss rate at the reactor wall was derived based on trial and error to achieve the closest agreement between modeling and experimental results. The resulting rate constant, $k_{dirty} = 2.8 \cdot 10^3 \exp(-9800/RT)$ s^{-1} for the dirty reactor is more than two orders of magnitude higher than the value for the clean reactor. We have assumed here for simplicity that the activation energy for the rate constant is similar to that of the clean surface. This revised mechanism subset for the dirty reactor is used in the subsequent modeling with KCl addition.

3.4.2   CO Oxidation with KCl Present

A number of experiments with KCl addition to the $CO/H_2O/N_2$ system were conducted, varying the CO and KCl inlet concentrations. The results are summarized in Figs. 3.4 and 3.5. The presence of KCl clearly has an inhibiting effect on the CO oxidation; as the inlet KCl level increases, the CO conversion into CO_2 decreases, resulting in a higher fraction of $CO/CO_{initial}$ (higher CO outlet). The inhibiting effect of KCl addition can be seen in the experimental data both with lower and higher CO inlet concentration. The addition of KCl in concentrations of 157, 313, 470, or 626 ppm to the CO oxidation system shifts the initiation temperature from around 923 K for conditions without KCl addition to 1023 K for experiments with KCl present. The temperature for 50% conversion of CO is also shifted. Similar to what has been observed in flames [92] the effect of potassium is non-linear, with increasing seeding levels resulting only in minor additional inhibition of the oxidation.

To investigate the importance of surface deposits compared to gas phase potassium reactions additional experiments were conducted. Similar to the other experiments the inlet gases consisted of carbon monoxide, water vapor and nitrogen; the temperature was kept at 1073 K. The concentrations of CO and CO_2 from the gas outlet was measured continuosly during the course of the reaction. By passing a nitrogen flow through the packed alumina bed with KCl, KCl vapor was fed in a certain amount to the reaction zone. After around 2 hours, when the outlet concentrations of CO and CO_2 had achieved steady state values, the nitrogen flow to the KCl feeding system was stopped, terminating the KCl vapor fed to the system. When the CO and CO_2 concentrations again achieved steady state, the nitrogen flow to the
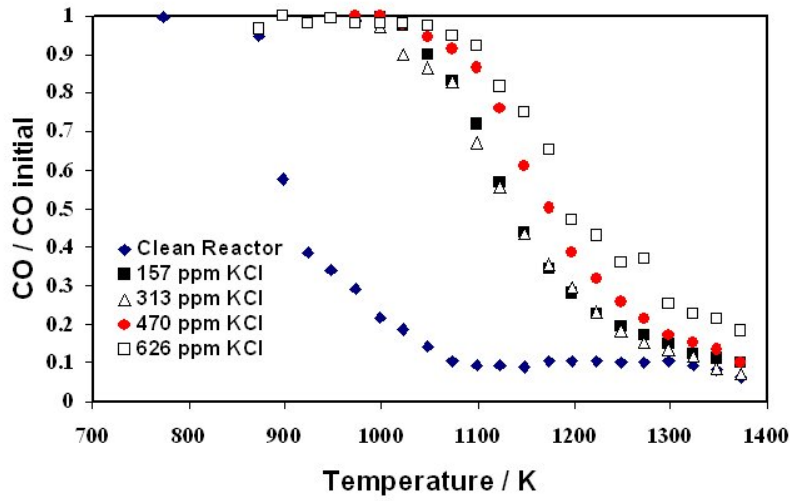
Figure 3.4: The fractions of $CO/CO_{initial}$ from the reactor from a CO oxidation experiment with 0-626 ppm KCl addition, inlet composition CO: 2150 ppm; H_2O: 0.052; N_2: balance gas; and O_2 from kinetic modeling estimation (75 ppm).
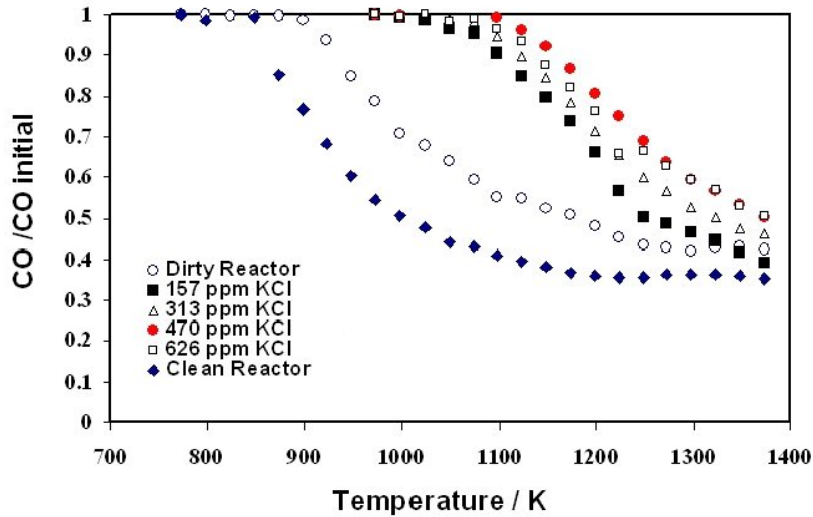

Figure 3.5: The fractions of $CO/CO_{initial}$ from the reactor from CO oxidation experiment with 0-626 ppm KCl addition KCl addition, inlet composition CO: 7800 ppm; H_2O: 0.052; N_2: balance gas; and O_2 from kinetic modeling estimation (75 ppm).

packed alumina bed with KCl was resumed.

The results from this experiment (Fig. 3.6) show that the CO and CO_2 concentrations depend strongly on the KCl feeding. Initially the potassium chloride causes a strong inhibition of CO oxidation. When the KCl feeding is terminated, the inhibition of the CO oxidation is reduced significantly, resulting in a lower CO outlet concentration. After an initial instant decrease, the CO concentration continues to decrease for 45-60 min, approaching the values typical of the dirty reactor experiments (Fig. 3.3c). The inhibition of CO oxidation may indicate that potassium is slowly released from the deposit on the surface to the gas phase. When the KCl feeding to the gas phase is resumed, the CO outlet concentration increases almost instantaneously to the initial level, followed by a slow further increase. The slow increase in CO at this point may be attributed to a slight increase in surface reactivity as the wall deposit builds up.

Overall the results confirm that the potassium deposited on the alumina reactor surface reactivity is active and has some influence on the CO conversion in the reactor. However, the gas phase potassium chemistry dominates the CO oxidation rate and despite the surface reactions the experimental results are useful for characterizing the potassium/radical pool interaction.

Figures 3.7 and 3.8 compare the experimental data with KCl feeding (Figs. 3.4 and 3.5) with kinetic modeling results. The modeling predictions agree well with the experimental data for the lower CO inlet concentration (Fig. 3.7), while the agreement for the data with higher CO inlet concentration is less satisfactory (Fig. 3.8). In general, for the higher CO inlet concentration the proposed kinetic scheme predicts a lower inhibition effect of the KCl addition compared to the experimental results.

Reaction-path analysis and sensitivity analysis were conducted to identify the key reactions under the present conditions. According to our kinetic model, the presence of KCl does not alter the key reactions for CO conversion. As discussed previously, CO oxidation mainly occurs by reaction with OH radicals, $CO + OH \rightleftharpoons CO_2 + H$. The hydroxyl radical is mostly formed by the reaction $H_2O + H \rightleftharpoons OH + H_2$, with a little amount generated through $H_2O + O \rightleftharpoons OH + OH$.

Figure 3.9 is a pathway diagram for the potassium transformations at 1050 K with 313 ppm KCl addition for both high and low CO inlet concentration. The contribution of various elementary reactions in the production and destruction of a species is analyzed. The main form of gaseous potassium under the present conditions is potassium chloride, with small amounts of KOH and the K atom, their relative importance depending on the temperature and residence time. Potassium hydride (KH) does not attain a significant concentration.
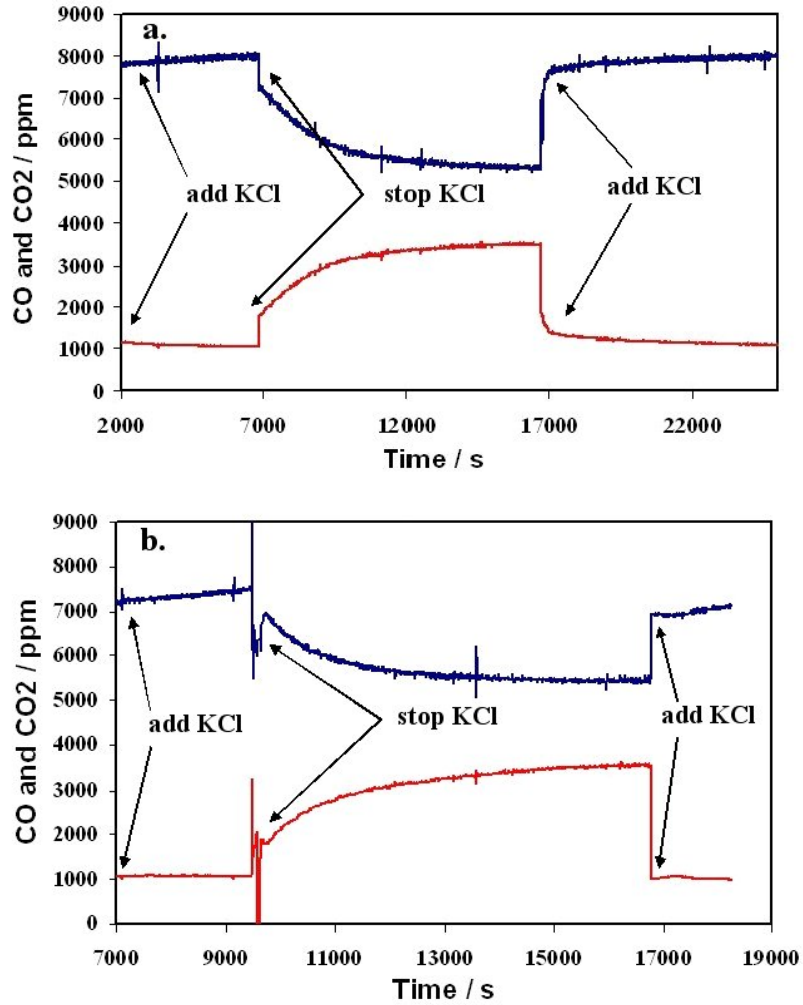
Figure 3.6: The outlet mole fractions of CO and CO_2 in CO oxidation experiments with 157 (a) and 313 (b) ppm KCl addition, inlet composition CO: 7800 ppm; H_2O: 0.052; N_2: balance gas; and O_2 from kinetic modeling estimation (75 ppm). The KCl feeding was terminated after about 7000 s (upper) and 9500 s (lower), respectively, and resumed after nearly 17000 s.
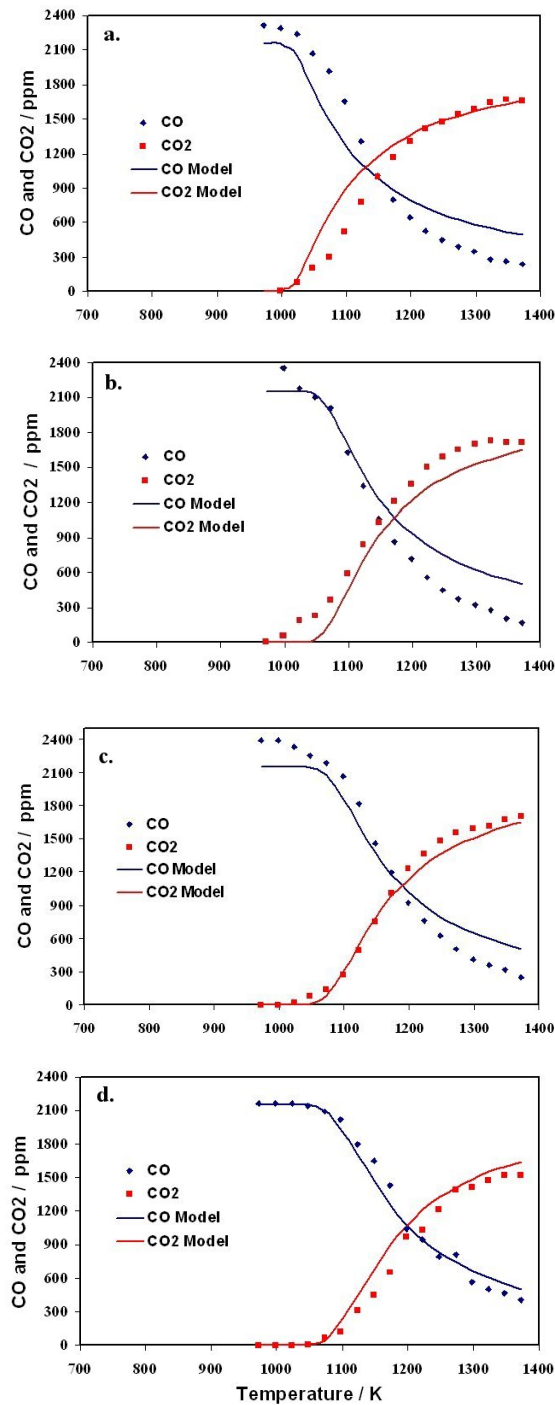
Figure 3.7: The outlet molar fractions of CO and CO_2 in CO oxidation experiments with 157 (a), 313 (b), 470 (c), or 626 (d) ppm KCl addition respectively, inlet composition CO: 2150 ppm; H_2O: 0.052; N_2: balance gas; and O_2 from kinetic modeling estimation (75ppm), residence time: 0.95 - 1.70 s (1305/T[K]). The solid lines denote modeling results and the symbols are experimental results.
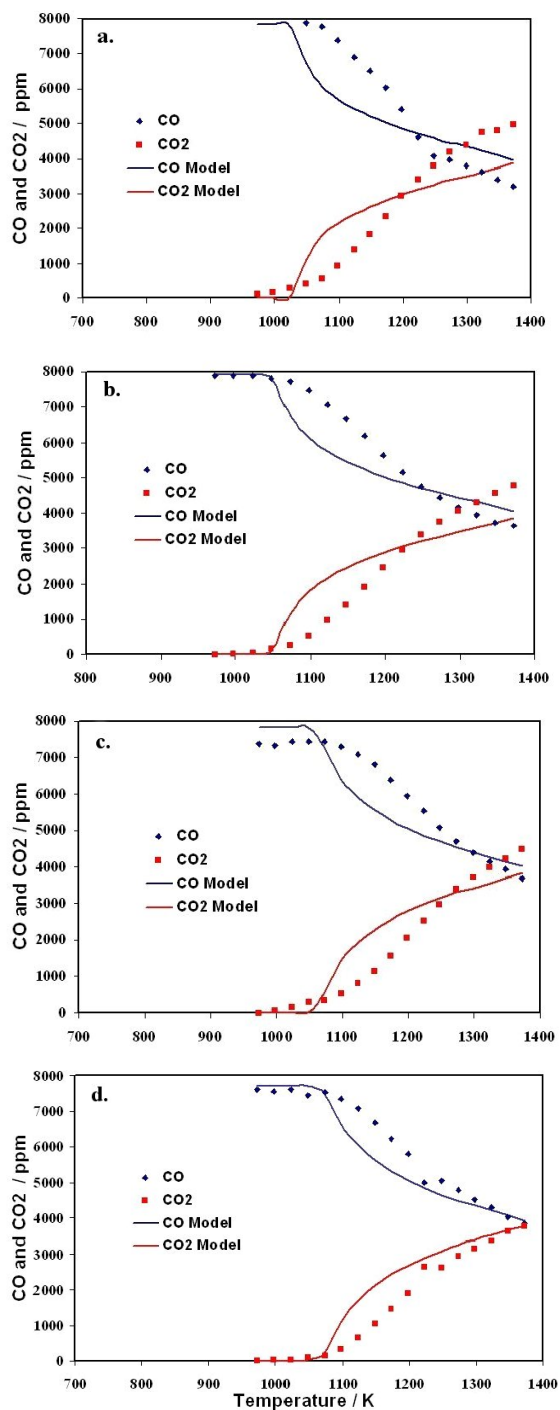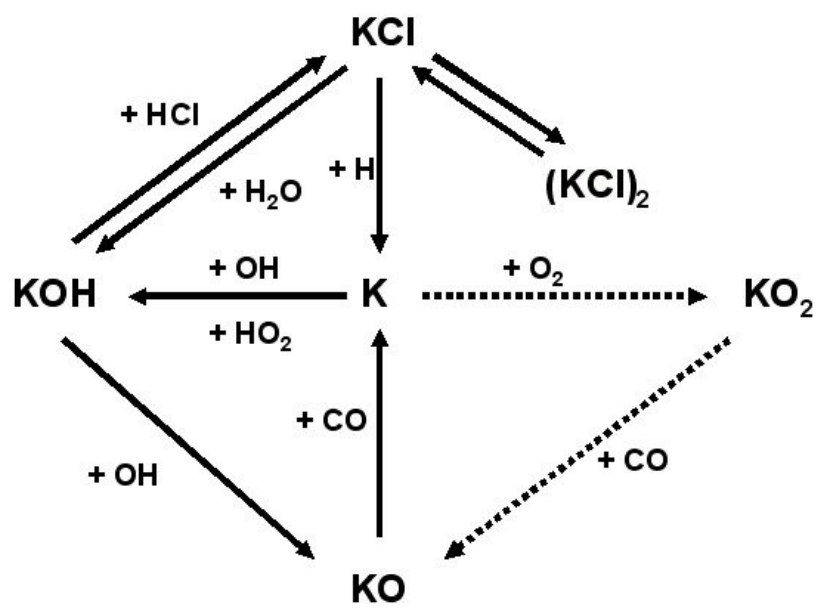
Figure 3.8: The outlet mole fractions of CO and CO_2 in CO oxidation experiments with 157 (a), 313 (b), 470 (c), or 626 (d) ppm KCl addition respectively. Inlet composition CO: 7800 ppm; H_2O: 0.052; N_2: balance gas;and O_2 from kinetic modeling estimation (75 ppm), residence time: 0.95 - 1.70 s (1305/T[K]). The solid lines denote modeling results and the symbols are experimental results.

Figure 3.9: The pathway diagram for potassium transformation under the condition of temperature 1050 K with 313 ppm KCl addition for higher and lower CO inlet concentration.

After vaporization, part of the KCl is converted to KOH by the reaction

$$KCl + H_2O \rightleftharpoons KOH + HCl \qquad \text{(R27b)}$$

The b in (27b) denotes a reverse reaction. In the early stage (within 0.5 ms) this reaction is the major consumption step for KCl, while at longer times (above 0.5 ms) it becomes a net producer of KCl. At 1050 K it reaches equilibrium very fast, in just about 1 ms. Potassium hydroxide is predicted to build up to a few ppm and then slowly decay. As the H atom concentration builds up, KCl is converted mainly to K atoms through reaction

$$KCl + H \rightleftharpoons K + HCl \qquad \text{(R24)}$$

The K atom reacts through several reactions, mainly

$$K + HO_2 \rightleftharpoons KOH + O \qquad \text{(R3)}$$

$$K + OH + M \rightleftharpoons KOH + M \qquad \text{(R2)}$$

with minor contributions through reaction

$$K + O_2(+M) \rightleftharpoons KO_2(+M) \qquad \text{(R4)}$$

Potassium dioxide will form KO by reacting with CO through reaction below,

$$KO_2 + CO \rightleftharpoons KO + CO_2 \qquad \text{(R22)}$$

Potassium hydroxide will react further according to the reactions below,

$$KOH + HCl \rightleftharpoons KCl + H_2O \qquad \text{(R27)}$$

$$KOH + OH \rightleftharpoons KO + H_2O \qquad \text{(R13)}$$

According to the model, KO reacts almost solely through reaction with CO,

$$KO + CO \rightleftharpoons K + CO_2 \qquad \text{(R14)}$$
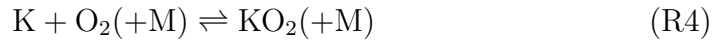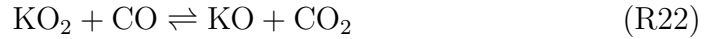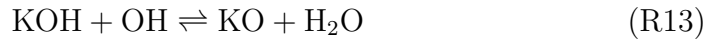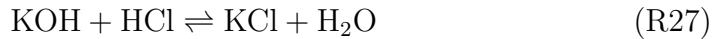
During the course of reaction, potassium chloride remains the dominant form of potassium in the gas phase. Figure 3.10 shows the predicted distribution of the minor potassium species as a function of temperature for conditions with a lower CO inlet concentration and 470 ppm KCl addition. At lower temperatures a major part of the KCl recombines to form the dimeric form of potassium chloride through the reaction $KCl + KCl \rightleftharpoons (KCl)_2$ (R29). As the temperature increases, KCl is thermodynamically favored compared to $(KCl)_2$ and the dimer becomes a less important.
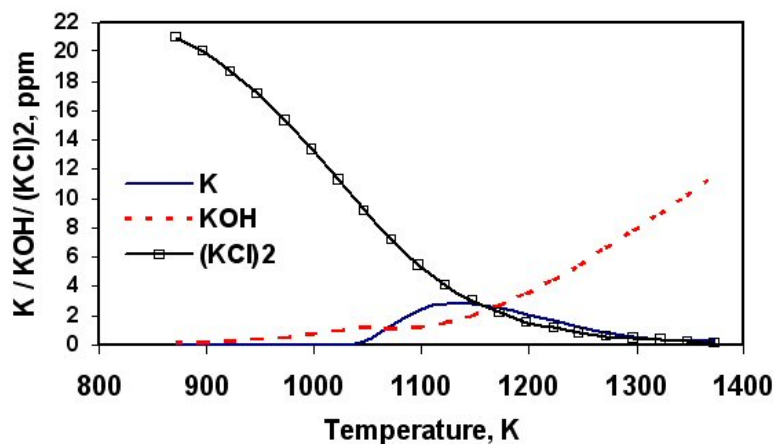
Figure 3.10: Concentration of $(KCl)_2$ (scaled by a factor of 1/10), K and KOH during the course of the gas phase reaction. Inlet composition : KCl: 470 ppm; CO: 2150 ppm; H_2O: 0.052; N_2 : balance gas; and O_2 from kinetic modeling estimation (75 ppm), residence time: 0.95 - 1.70 s (1305/T[K]). The combined symbols and line denotes $(KCl)_2$, dashed line the KOH concentration and the solid line the K concentration.

Apart from the KCl monomer and dimer, KOH is the most important potassium species over most of the temperature range investigated. However, the K atom starts to build up above 1050 K and peaks at 1100 K, where it is present in higher concentrations than KOH. Above this temperature [K] decreases and at 1175 K it is again lower in concentration than KOH. Since key reactions, such as (R27), are close to equilibration, the relative importance of KOH and K will depend on the thermodynamic properties of the involved species, and particularly the heat of formation of KOH needs to be determined with higher accuracy. It should be noted that the trends from the simulations shown in Fig. 3.10 are different from what has been observed in flames [93] where most of the potassium is present as K but with a smaller, although significant, proportion present as KOH.

To identify the rate limiting steps in the inhibition of CO oxidation by KCl, an A-factor sensitivity analysis was performed. Figure 3.11 shows the results of a first order sensitivity analysis of the predicted CO concentration with respect to the reaction rate constants for the conditions above. The analysis indicates that the oxidation rate is mainly sensitive to the reactions that generate or consume free radicals in the system. The oxidation rate is enhanced by reactions that increase the radical pools of OH and H such as

43

$H_2O+H \rightleftharpoons OH+H_2$, $HO_2+H_2O \rightleftharpoons H_2O_2+OH$ and $H_2O+O \rightleftharpoons OH+OH$ and inhibited by chain terminating reactions mainly involving alkali species. The reactions $K+HCl \rightleftharpoons KCl+H$ (R24), $KOH+H \rightleftharpoons K+H_2O$ (R15), $KO+CO \rightleftharpoons K+CO_2$ (R14), $K+H_2O_2 \rightleftharpoons KOH+OH$ (R5), and $K+OH+M \rightleftharpoons KOH+M$ (R2) inhibit the CO oxidation, whereas the reaction $K+HO_2 \rightleftharpoons KOH+O$ (R3) enhances the CO oxidation. The analysis confirms that the inhibiting effect of potassium on the CO oxidation in the present work is caused by decreasing the availability of active radicals.
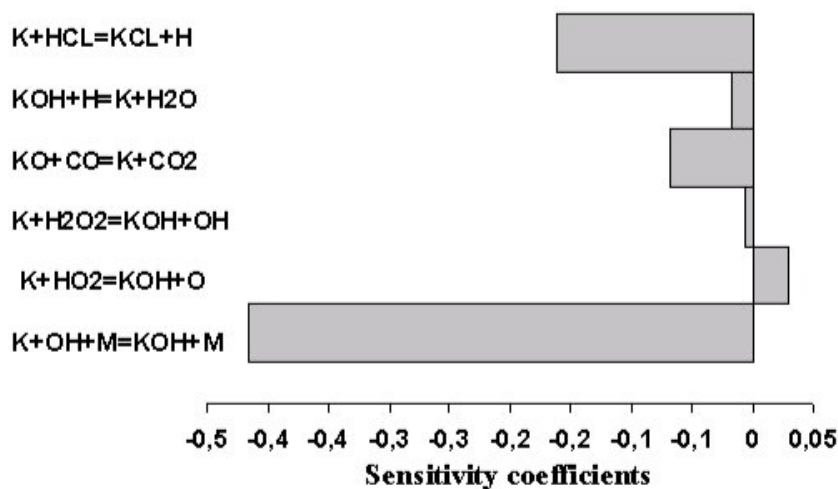

Figure 3.11: A-factor sensitivity coefficients for key elementary reactions with respect to formation of CO_2 with conditions corresponding to the experiments in fig. 3.10.

The sensitivity analysis indicates that the chain terminating reaction $K+OH+M \rightleftharpoons KOH+M$ (R2) is the rate limiting step of the potassium inhibition to the CO oxidation system. For this reason the value of rate constant for this reaction has a considerable impact on the model predictions. Glarborg and Marshall [14] adopted the rate constant proposed by Husain et al. [94], $k_2 = 5.4 \cdot 10^{21} T^{-1.55}$ cm^6 mol^{-1} s^{-1}. Using this value, experimental results and modeling prediction agree qualitatively, but the inhibiting effect of KCl is underpredicted. The expression by Husain et al. was based on a direct measurement at 530 K (with He as bath gas) and an extrapolation to high temperatures by RRKM theory. In the present work, we have chosen a rate constant for (R2) of $k_2 = 3.8 \cdot 10^{19} T^{-0.65}$ cm^3 mol^{-1} s^{-1}. This value is in agreement with the measurement of Husain et al. at 530 K, assuming the collision efficiency of N_2 to be twice that of He, and with the high temperature data of Jensen et al. [93], obtained from analysis of $H_2/O_2/N_2$ flames
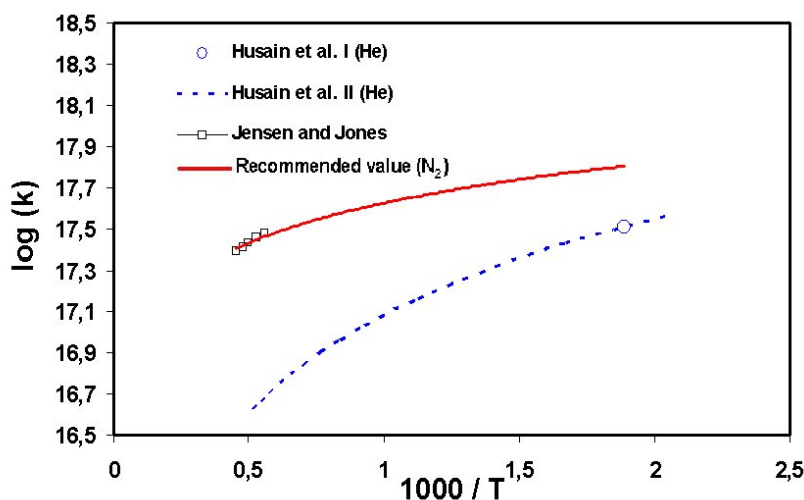
Figure 3.12: Arrhenius plot for the K+OH+M reaction. Units are Kelvin and cm^6 mol^{-2} s^{-1}. The open symbols denote data from a direct measurement by Husain et al. [95] and the indirect determination from the flame measurement by Jensen et al. [93]. The dashed line shows the theoretical values predicted by Husain et al. [96], while the solid line denotes the value recommended from the present work.
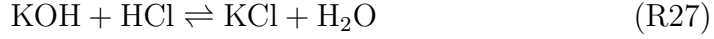
doped with potassium.

Figure 3.12 shows an Arrhenius plot for the K+OH+M reaction (R2). The open symbols denote data from a direct measurement by Husain [95] and the indirect determination from the flame measurement by Jensen et al. [93]. The dashed line shows the theoretical values predicted by Husain [96], while the solid line denotes the value recommended from the present work.
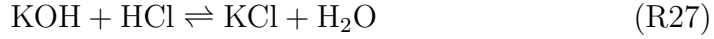
The chosen rate constant for (R2) results in a significantly improved agreement between modeling predictions and experimental results, compared to calculations with the lower rate constant proposed by Husain et al. [94]. However, experimental uncertainties and uncertainties in the chemical kinetic model preclude a determination of k$_2$ from the present work. The experimental uncertainties include the amount of KCl fed to the gas phase, the oxygen concentration, and surface reactions at the reactor wall. The model uncertainties involve the heat of formation of KOH and the rate constants for potential key reactions, for instance the K+H+M reaction (R30) which could become an important chain terminating step if the rate constant was comparable to that of K+O+M (R1) and K+OH+M (R2).

The reaction-path analysis and sensitivity analysis indicate that there are

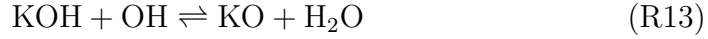several active mechanisms for catalyzed radical recombination by potassium. These include:

$$KCl + H \rightleftharpoons K + HCl \tag{R24}$$

$$K + OH + M \rightleftharpoons KOH + M \tag{R2}$$

$$KOH + HCl \rightleftharpoons KCl + H_2O \tag{R27}$$

The net reaction is $H + OH \rightleftharpoons H_2O$.

$$KCl + H \rightleftharpoons K + HCl \tag{R24}$$

$$K + HO_2 \rightleftharpoons KOH + O \tag{R3}$$

$$KOH + HCl \rightleftharpoons KCl + H_2O \tag{R27}$$

The net reaction is $H + HO_2 \rightleftharpoons H_2O + O$.

$$KOH + OH \rightleftharpoons KO + H_2O \tag{R13}$$

$$KO + CO \rightleftharpoons K + CO_2 \tag{R14}$$

$$K + OH + M \rightleftharpoons KOH + M \tag{R2}$$
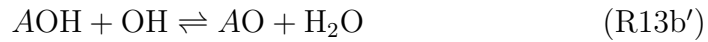
The net reaction is $CO + 2OH \rightleftharpoons CO_2 + H_2O$.

These mechanisms are different from those proposed based on flame studies. Jensen et al. [93] found the key reactions in fuel-rich flames to be,

$$KOH + H \rightleftharpoons K + H_2O \tag{R15}$$

$$K + OH + M \rightleftharpoons KOH + M \tag{R2}$$

Reaction (R2) is also important under our conditions, while (R15) is rapidly equilibrated and found not to be an important reaction in this work.

Research on sodium chemistry [50,81,97] indicate that the impact of alkali metals on oxidation is largely controlled by the reactions

$$A + OH + M \rightleftharpoons AOH + M \tag{R2$'$}$$

$$A + H_2O \rightleftharpoons AOH + H \tag{R15b$'$}$$

$$AOH + OH \rightleftharpoons AO + H_2O \tag{R13b$'$}$$

$$A + O_2 + M \rightleftharpoons AO_2 + M \tag{R4$'$}$$

$$AO_2 + H \rightleftharpoons AO + OH \tag{R18$'$}$$

The reactions numbers correspond to the similar steps in the potassium mechanism. The alkali superoxide AO_2 has also been suggested to be important in K-doped flames [92], but with the present thermochemistry it is doubtful

that these compounds are sufficiently stable at high temperatures to play a role. In the present work at lower temperatures there is only trace amounts of oxygen present and KO_2 reactions are not significant.

It is interesting that alkali metals, similar to nitrogen oxides [89] and sulfur oxides [73], may act as sensitizers or inhibitors, depending on reaction conditions. All of these compounds have the ability to inhibit or catalyze some particular reactions depending on gas composition and reaction conditions. For example in the case of sulfur dioxide, it catalyzes CO oxidation under specific conditions even though it generally acts to inhibit fuel oxidation [73]. The idea that alkali metals can remove radicals if its concentration is sufficient is well documented in literature, e.g. [30, 32, 79], as well as in the present work. However, under other conditions addition of alkali metals may serve to promote reaction [80–84]. Zamansky and co-workers [80, 84] propose that Na can add or remove radicals depending on factors such as concentrations of radicals, of other species, and temperature. They investigated the effect of sodium on the reburning process for NO_x reduction. It was found that Na atoms inhibited the combustion process by reducing H and OH if radical concentrations in the combustion system are high (main combustion zone and the initial part of the reburning zone where injection, mixing, and oxidation of the reburning fuel occurs). If radical concentrations were low (end of the reburning zone), Na atoms increased the concentrations of H and OH [84].

Promotion of reaction by alkali metals may occur through the reaction sequence

$$A\text{OH} + \text{M} \rightleftharpoons A + \text{OH} + \text{M} \qquad\qquad (\text{R2b}')$$

$$A + \text{H}_2\text{O} \rightleftharpoons A\text{OH} + \text{H} \qquad\qquad (\text{R15b}')$$

which corresponds to the net reaction $\text{H}_2\text{O} \rightleftharpoons \text{H} + \text{OH}$. More research in the interaction of the alkali species with the radical pool is desirable, as this chemistry may have important practical implications.

3.5   Conclusions

Experimental work on the influence of gas phase potassium on CO oxidation under reducing conditions has been conducted to evaluate the K/O/H/Cl gas phase chemistry. The experiments were performed using a laboratory flow reactor at atmospheric pressure and temperatures in the range 773-1373 K, varying the CO inlet concentration and the KCl level. The addition of KCl results in a strong inhibition of the CO oxidation. The inhibition increases with the KCl level, but the effect levels off at high concentrations. The

experimental data were interpreted in terms of a detailed chemical kinetic model. In general a satisfactory agreement between experimental data and kinetic modeling was achieved. Analysis of the modeling results indicates that the reaction $K+OH+M \rightleftharpoons KOH+M$ is rate controlling for the radical recombination. The experimental data support a high rate constant for this reaction, but an estimation of the value from the present work is difficult due to uncertainties in the potassium chemistry and in the experimental conditions. From this study, the understanding of the K chemistry and interaction with the radical pool has been improved. A comparison between results of the modeling and experimental data gives a favorable agreement, which indicates that the suggested chemistry in this work in general is fairly good. Having the K/O/H/Cl chemistry validated and updated, the next step is to investigate the sulfur chemistry which is important for the SO_2/SO_3 ratio under combustion conditions as presented in the next chapter.
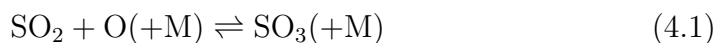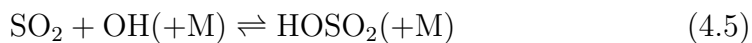
Chapter 4

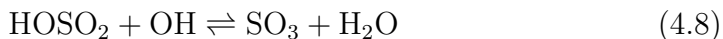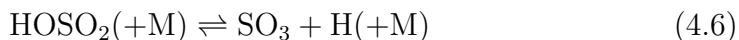# Sulfur Chemistry

4.1   Introduction

This chapter contains a summary of the study on sulfur chemistry as presented in papers II-IV [98–100]. As previously suggested, oxidation of SO_2 to SO_3 is proposed to be the rate limiting step in the homogeneous sulfation of potassium prior to aerosol formation during biomass combustion [10, 14, 17–19, 23]. In this study, investigations to minimize the uncertainties of the sulfur chemistry important for the SO_2/SO_3 ratio under combustion conditions were done. While the overall mechanisms for SO_3 formation and destruction are fairly well known, kinetic modeling of the process still suffers from a lack of accurate kinetic data, and refinements are required in order to establish a reliable mechanism [14, 63]. Detailed studies are presented in papers II-IV.

A better understanding of the mechanisms for SO_2/SO_3 formation and destruction is a necessary step in the effort to investigate the ratio of SO_2 to SO_3 under combustion conditions. A number of reactions below may affect the SO_2/SO_3 concentration, (b) indicate the reaction number in reverse direction than normally used in detailed kinetic modeling in the present study.
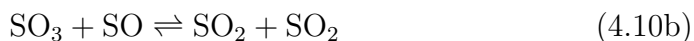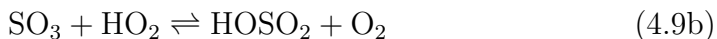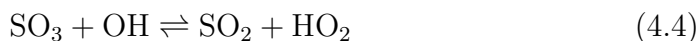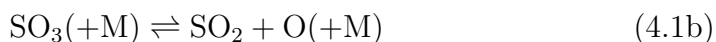
$$SO_2 + O(+M) \rightleftharpoons SO_3(+M) \qquad (4.1)$$

$$SO_2 + OH \rightleftharpoons SO_3 + H \qquad (4.3b)$$

$$SO_2 + O_2 \rightleftharpoons SO_3 + O \qquad (4.2b)$$

$$SO_2 + HO_2 \rightleftharpoons SO_3 + OH \qquad (4.4b)$$

or it may involve $HOSO_2$ as an intermediate,

$$SO_2 + OH(+M) \rightleftharpoons HOSO_2(+M) \qquad (4.5)$$

49

$$HOSO_2(+M) \rightleftharpoons SO_3 + H(+M) \tag{4.6}$$

$$HOSO_2 + O \rightleftharpoons SO_3 + OH \tag{4.7}$$

$$HOSO_2 + OH \rightleftharpoons SO_3 + H_2O \tag{4.8}$$

$$HOSO_2 + O_2 \rightleftharpoons SO_3 + HO_2 \tag{4.9}$$

And the destruction of SO_3 may involve reactions,

$$SO_3(+M) \rightleftharpoons SO_2 + O(+M) \tag{4.1b}$$

$$SO_3 + H \rightleftharpoons SO_2 + OH \tag{4.3}$$

$$SO_3 + O \rightleftharpoons SO_2 + O_2 \tag{4.2}$$

$$SO_3 + OH \rightleftharpoons SO_2 + HO_2 \tag{4.4}$$

$$SO_3 + HO_2 \rightleftharpoons HOSO_2 + O_2 \tag{4.9b}$$

$$SO_3 + SO \rightleftharpoons SO_2 + SO_2 \tag{4.10b}$$

It is believed that the SO_2/SO_3 ratio in the gas phase system is mainly controlled by reactions below [11, 63, 73, 101].

$$SO_2 + O(+M) \rightleftharpoons SO_3(+M) \tag{4.1}$$

$$SO_3 + O \rightleftharpoons SO_2 + O_2 \tag{4.2}$$
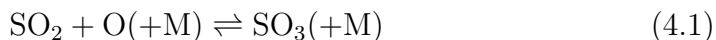
The rate of reaction 4.1 is characterized over a wide range of temperature and pressure [98]. Even though the rate constant for reaction 4.1 is probably known more accurately than most sulfur reactions, it is noteworthy that there are no measurements under the conditions of practical interest in combustion and industrial processes, i.e. temperatures between 1000 and 1500 K. Furthermore, the only direct measurements of the rate constant for nitrogen as collision partner were obtained at room temperature [98, 102]. Reaction 4.1 is important not only for formation of SO_3 in combustion systems, but also in some industrial processes. The reverse reaction,

$$SO_3(+M) \rightleftharpoons SO_2 + O(+M) \tag{4.1b}$$
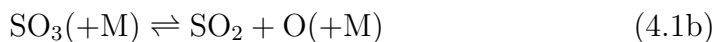
is believed to be the rate limiting for the conversion of spent sulfuric acid to SO_2 [103].

Reported rate constants for reaction 4.2 vary by several orders of magnitude [62, 73, 104–108]. While most of the data support a high rate constant for this reaction; only the investigation by Alzueta et al. [73] suggest a low rate constant.

50

The objective of the present work is to improve the understanding of sulfur chemistry important for SO_2/SO_3 ratio under combustion conditions. Reactions of particular interest are those of SO_2 with O, SO_3 thermal dissociation and reactions of SO_3 with H, O, and OH.

Experimental work was conducted in order to derive rate constants for SO_3 destruction by the thermal dissociation (paper II) and by O atoms (papers II-III) in the 1000-1373 K range from flow reactor experiments with nitrogen as inert gas. A gas containing a mixture of SO_2 and O_2 in N_2 is led to the catalysts, where SO_2 is partly oxidized to SO_3 at 673 K. The resulting gas is then led to a flow reactor, where SO_3 is converted back to SO_2 by thermal dissociation or by reaction with O atoms. Finally, as presented in paper IV, ab initio calculations were conducted by Paul Marshall, to provide reliable estimates for the reactions of SO_3 with H, O, and OH. The mechanism for sulfur chemistry is updated with the new values of those rate constants from ab initio calculations. Modeling predictions with the revised model are compared to a range of experimental results from literature on the oxidation of SO_2 to SO_3.

4.2   Experimental Work

The experimental setup consisted of two quartz reactors in series in separate ovens. In the first reactor, SO_2 was oxidized to SO_3 over the V_2O_5-WO_3-TiO_2 catalyst doped with KCl. The temperature along the catalytic reactor was set to 673 K. The product gas from the first reactor was fed into the second reactor. The second reactor was homogeneous, operated at high temperatures (up to 1373 K). A schematic of the experimental setup used in the sulfur chemistry study is shown in figure 4.1.

Sulfur dioxide, oxygen and nitrogen were mixed and directed either to bypass (the flow meter - G) or to the catalytic reactor (B). The bubble flow meter (G) served to measure the flow of the input gases from the gas cylinders as a check for mass flow meters. The output of the catalytic reactor was directed either to the homogeneous reactor (C) or to the gas conditioning and analyzers (F). By-pass lines were available for both reactors so that input and output gases could be analyzed and the setup could be used in a flexible way. Prior to the analyzers, a condenser (D), two filters (E) and a condense alarm were located to protect the analyzer from any aerosols and/or condensed liquids.

The catalytic reactor was a heterogeneous quartz reactor with a 2 cm inner diameter. The total length of the reactor occupied by the catalyst material was 16 cm. This reactor was operated at 673 K and the reactor
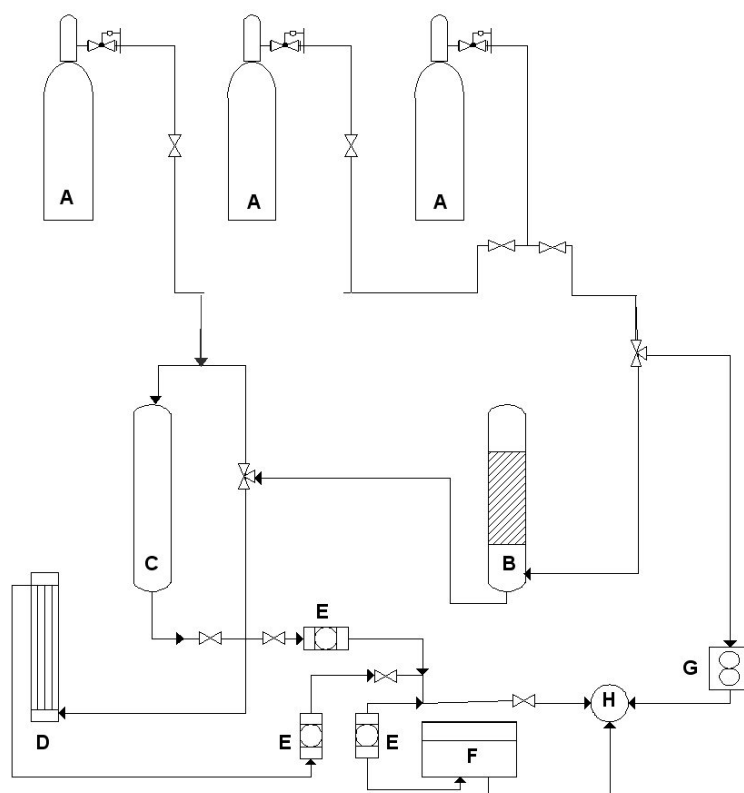
Figure 4.1: A schematic of the experimental setup used to investigate sulfur chemistry. Some modifications are made when necessary in order to run different type of experiments

residence time was about 3 s.

The homogeneous reactor consisted of a quartz tube located in a three-zone electrically heated oven. The homogeneous reactor was operated at high temperatures (up to 1373 K). The tubes used for the second reactor were designed to approximate plug flow in the laminar flow regime. While no gases were added to the mixture between the first and the second reactor in the experiments presented in paper II, in the work presented in paper III, N_2O was introduced to the gases prior to entering the homogeneous reactor. N_2O was introduced as a source of O atoms in the homogeneous system.

Characteristic temperature profiles for the reactor are shown in 4.2. In most of the temperature range investigated, a flat temperature profile was obtained in the isothermal region of the reactor, but at the highest temperatures variations within ±15 K were observed. The concentration of SO_2 and/or N_2O was measured continuously using gas analysers.
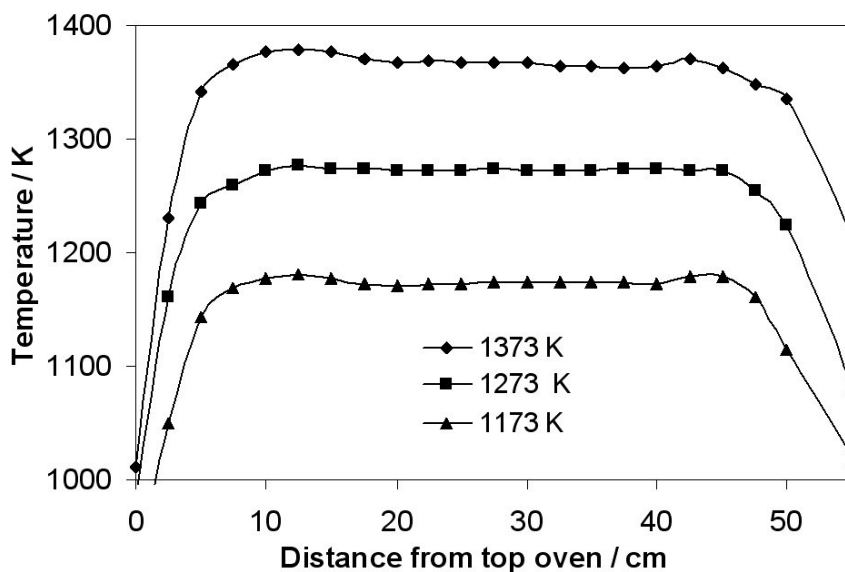

Figure 4.2: Characteristic temperature profiles in the homogeneous reactor

4.3 Detailed Kinetic Model

The experimental results were interpreted in terms of a detailed reaction mechanism. SENKIN [86], which is part of the CHEMKIN library [87] was

Table 4.1: Rate coefficients for reactions in the sulfur chemistry important for the SO_2/SO_3 ratio used or results of present work as presented in papers II-IV. Units are cm, mol, s, K.

No	Reaction	A	n	E/R	Note
4.1	$SO_2+O(+M) \rightleftharpoons SO_3(+M)^a$	3.7E11	0.00	850	[110], papers II-IV
	Low pressure limit	2.4E27	-3.60	2610	
	Troe parameters 0.442 316 7442				
	Low pressure limit (N_2)	2.9E27	-3.58	2620	papers II-IV
	Troe parameters (N_2) 0.43 371 7442				
4.2.	$SO_3 + O \rightleftharpoons SO_2 + O_2$	7.8E11	0.00	3070	[107], paper II
	$SO_3+O \rightleftharpoons SO_2+O_2$	2.0E12	0.00	10000	[73], paper III
	$SO_3+O \rightleftharpoons SO_2+O_2$	2.8E04	2.57	14700	paper IV
4.3	$SO_3+H \rightleftharpoons SO_2+OH$	8.4E09	1.22	1670	paper IV
4.3b	$SO_2 + OH \rightleftharpoons SO_3 + H$	4.9E02	2.69	12000	[63], papers II-III
4.4	$SO_3+OH \rightleftharpoons SO_2+HO_2$	4.8E04	2.46	13700	paper IV
4.4b	$SO_2+HO_2 \rightleftharpoons SO_3+OH$	1.0E12	0.00	8000	[109], paper III

^{a}: Enhanced third body coefficients: $N_2=0$, $SO_2=10$, $H_2O=10$

used for the simulation, assuming plug flow. The results of the SENKIN calculations were compared to experimental data.

The reaction mechanism consisted of a $H_2/O_2/N_2O$ subset and a full description of the H/S/O reaction system. The H_2/O_2 subset was included in the model to account for effects of water vapor. Presence of water vapor, even in small concentrations, may conceivably lead to an O/H radical pool, initiated by the reaction

$$O + H_2O \rightleftharpoons OH + OH$$
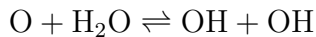
With a few exceptions, the H/S/O subset and the corresponding thermochemistry were adopted from previous work [14,73,109]. Oxidation of SO_2 to SO_3 may occur through reaction of SO_2 with O or with OH, either directly or through $HOSO_2$. In addition to thermal dissociation of SO_3, reactions that consume SO_3 may include SO_3+O, SO_3+H and SO_3+HO_2.

Rate constants of selected reactions used in this study (papers II-IV), are listed in Table 4.1. The value of a rate constant used for a specific reaction may differ from paper II to IV (see note).

4.4   Results and Discussion

4.4.1   SO$_3$ Thermal Dissociation

The experiments were performed at atmospheric pressure with temperatures in the homogeneous reactor in the range 973 to 1373 K. Typical conditions involved SO$_3$ and SO$_2$ concentrations into the homogeneous reactor of about 500 ppm, with around 2.5-5% O$_2$ in N$_2$. Also trace amounts of water vapor were present, estimated to be in the range 30-150 ppm [111].
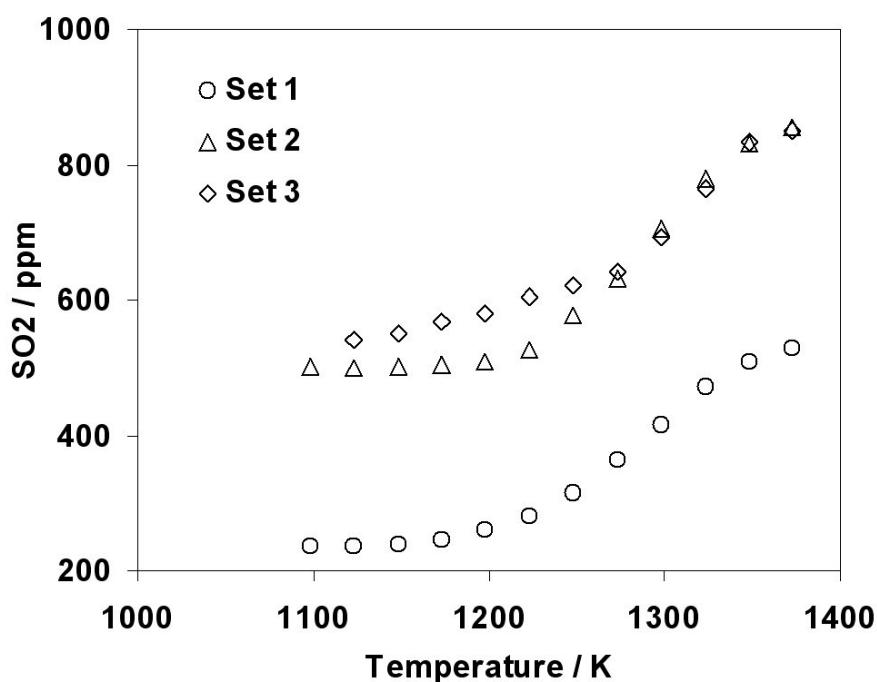

Figure 4.3: Experimental results for thermal decomposition of SO$_3$. Set 1: SO$_3$ = 342 ppm, SO$_2$ = 238 ppm, O$_2$ = 4.7%; residence time 2320/T[K]. Set 2: SO$_3$ = 420 ppm, SO$_2$ = 500 ppm, O$_2$ = 2.6%; residence time 2550/T[K]. Set 3: SO$_3$ = 406 ppm, SO$_2$ = 540 ppm, O$_2$ = 4.7%; residence time 2901/T[K]. All experiments are carried out with N$_2$ as carrier gas, with H$_2$O $\approx$ 100 ppm, and with a pressure of about 1.05 atm. The residence time, varying with reactor temperature as indicated (constant mass flow), applies to the isothermal part of the reactor (about 40 cm of the length).

Some of the experimental results for decomposition of SO$_3$ in the temperature range 1073 to 1373 K are shown in figure 4.3. The oxygen level affects

55

the oxidation of SO_2 to SO_3 in the catalytic reactor, but has little effect on the SO_3 decomposition in the homogeneous reactor.
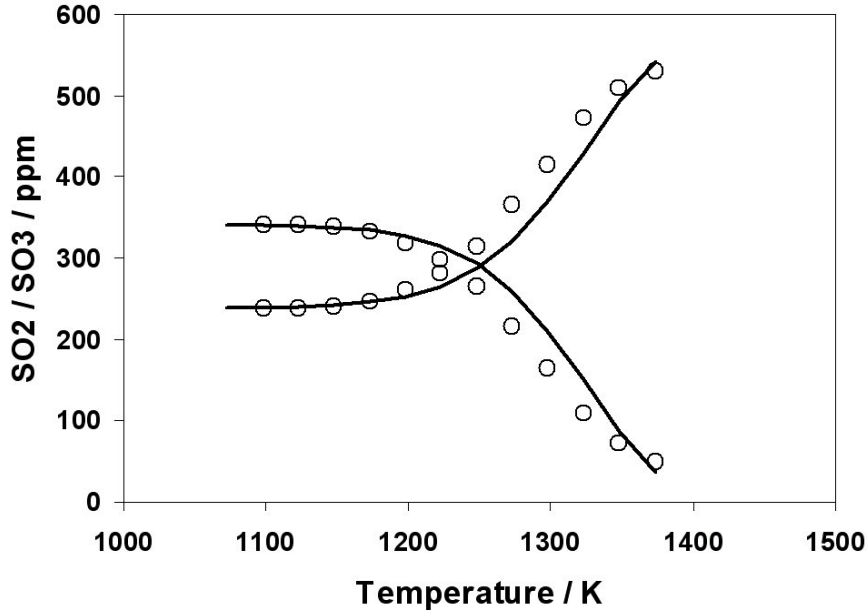

Figure 4.4: Experimental results (symbols) compared to modeling prediction (lines) for thermal decomposition of SO_3. Set 1: $SO_3 = 342$ ppm, $SO_2 = 238$ ppm, $O_2 = 4.7\%$; residence time 2320/T[K]. The experiments are carried out with N_2 as carrier gas, with $H_2O \approx 100$ ppm, and with a pressure of about 1.05 atm.

Figure 4.4 compares selected experimental data (set 1) to modeling prediction with the detailed reaction mechanism (solid lines). Without any adjustments, the kinetic model is seen to describe the experimental results quite well. For all sets the kinetic model is in agreement with the experimental data within the experimental uncertainty.

Sensitivity analysis of the calculations with the detailed chemical kinetic model shows that the SO_3 decomposition rate is only sensitive to two reactions,

$$SO_3(+M) \rightleftharpoons SO_2 + O(+M) \tag{4.1b}$$

$$SO_3 + O \rightleftharpoons SO_2 + O_2 \tag{4.2}$$
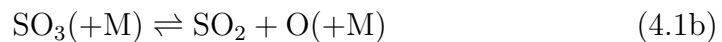
The chemistry is not affected by the trace impurities of water vapor present. The rate constant of reaction 4.1b was determined from optimization of the

value of $k_{4.1b}$ at selected experimental conditions using the detailed chemical kinetic model. Rate constant for reaction

$$SO_3 + O \rightleftharpoons SO_2 + O_2 \tag{4.2}$$

could be obtained from a simple analysis of the (4.1b)-(4.2) reaction sequence, assuming the oxygen atom to be in steady state. The present flow reactor data apparently support a comparatively high value for $k_{4.2}$. This result is not in accord with the latter studies as discussed in the next section (papers III-IV).

Figure 4.5 compares the data for the thermal dissociation rate of SO_3 with the only other measurements of this reaction, the shock tube study of Astholz et al. [112]. While the present study involved nitrogen as collision partner, Astholz et al. conducted their experiments in argon. The two sets of data appear to be consistent, but a direct comparison is difficult due to the differences in temperature regime and bath gas.
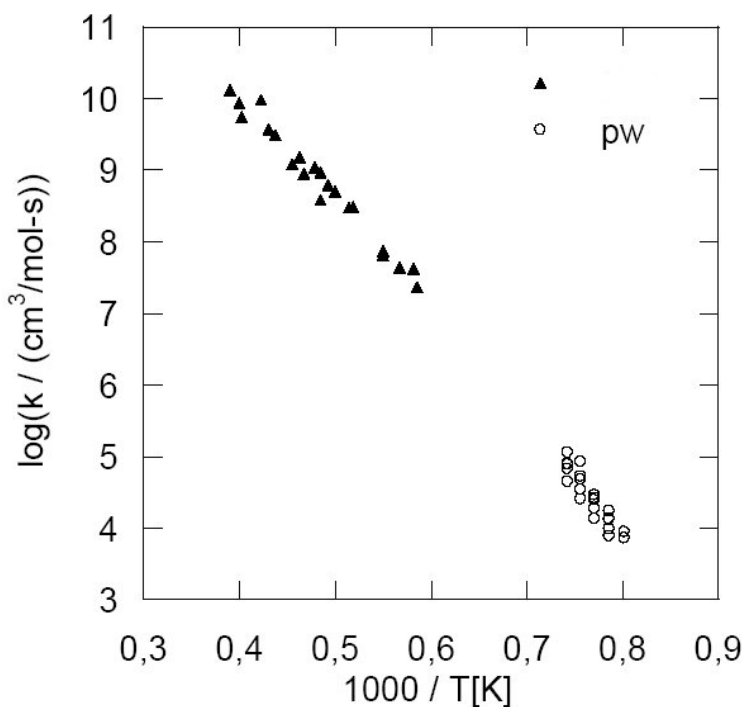

Figure 4.5: Arrhenius plot for the reaction $SO_3 + M \longrightarrow SO_2 + O + M$ (R1b). The closed symbols denote values obtained in the present work, while the open symbols represent the measurements of Astholz et al. [112] with Ar as third body [98].

The rate constant of reaction (R4.1b) was determined from optimization of the value of $k_{4.1b}$ at selected experimental conditions using the detailed chemical kinetic model. There are some scatter in the data, but within the uncertainty values appear to be independent of the SO_x inlet level and the O_2 concentration, as would be expected. The flow reactor data are consistent with a rate constant for $SO_3 + N_2 \rightleftharpoons SO_2 + O + N_2$ of $5.7 \cdot 10^{17} \exp(-40000/T)$ cm^3/(mole s) in the temperature range 1248–1348 K.

It is noteworthy that a very low value for $k_{4.2}$, such as that proposed by Alzueta et al. [73], leads to $k_{4.1}[SO_2][M] >> k_{4.2}[SO_3]$ and thereby the decomposition rate for SO_3, $\dot{R}_{SO_3} = 0$. This is in conflict with the experimental observations; the present flow reactor data support a comparatively high value for $k_{4.2}$.

The error analysis conducted includes an experimental uncertainty and a modeling uncertainty. The experimental uncertainty involves uncertainty in inlet concentrations, outlet concentrations, reactor residence time in the isothermal zone, reactor temperature, and potential loss of SO_3 or O atoms on the reactor surface; the modeling uncertainty involves uncertainty in the value of $k_{4.2}$.

4.4.2   SO$_2$/SO$_3$/N$_2$O System

The reaction $SO_3+O \rightleftharpoons SO_2+O_2$ (4.2) which is believed to be an important consumption step for SO_3 under combustion conditions, previously has not been measured directly and the rate constant is associated with a considerable uncertainty [63, 73]. In paper II [98], the rate constant for reaction $SO_3+O \rightleftharpoons SO_2+O_2$ was evaluated, and this analysis supports a high value of a rate constant.

A set of experiments were conducted to evaluate the reaction 4.2 in range of temperature from 1073 to 1373 K. N$_2$O gas was used during experiments as an O source. The fate of SO_2/SO$_3$ in the system with N$_2$O addition under those conditions is evaluated using a detailed kinetic modeling [98, 109]. In the present study, SO_3 is expected to decompose through reaction involving O. The availability of N$_2$O in the system is expected to be a source of O from the N$_2$O dissociation. The SO_2 measured from the experiments is shown in figure 4.6, while figure 4.7 shows the decomposition of N$_2$O.

The experimental data was used to evaluate the sulfur chemistry, taking into account the updated rate constants and thermodynamic data [98,109]. If a high rate constant for reaction $SO_3+O \rightleftharpoons SO_2+O_2$ (4.2) from paper II [98] was applied, the agreement between experimental data and the predicted model is not achieved. While applying a low rate constant from Alzueta
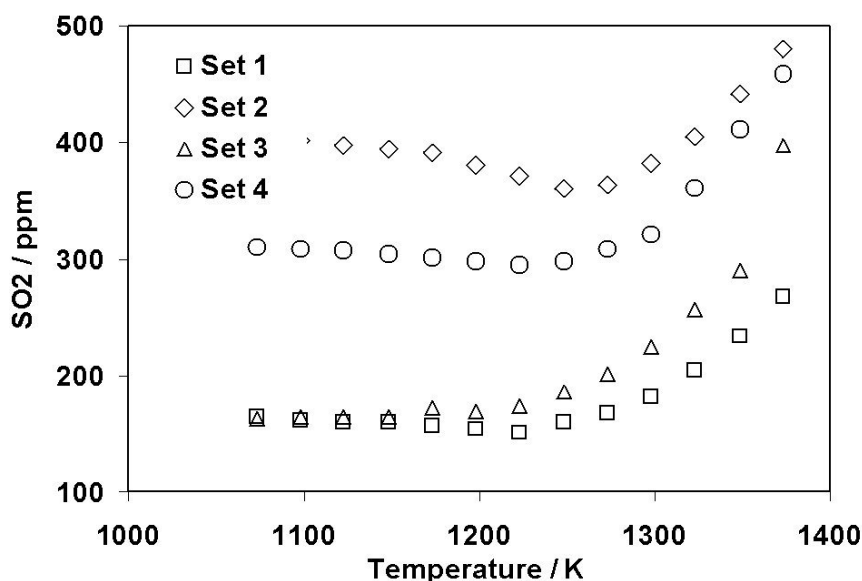
Figure 4.6: Experimental results for decomposition of SO_3 in $SO_3/SO_2/N_2O$ system. Set 1: $SO_3 = 214.7$ ppm, $SO_2 = 156$ ppm, $N_2O = 164$ ppm, $O_2 = 4.07$ %; residence time $1441.28/T[K]$. Set 2: $SO_3 = 201.2$ ppm, $SO_2 = 401$ ppm, $N_2O = 131$ ppm, $O_2 = 1.02$ %; residence time $1356.3/T[K]$. Set 3: $SO_3 = 387.4$ ppm, $SO_2 = 156$ ppm, $N_2O = 176$ ppm, $O_2 = 4.27\%$; residence time $1519.65/T[K]$. Set 4: $SO_3 = 310.8$ ppm, $SO_2 = 300.4$ ppm, $N_2O = 143$ ppm, $O_2 = 1.02\%$; residence time $1377.45/T[K]$. All experiments are carried out with N_2 as carrier gas, with traces $H_2O \approx 0\text{-}100$ ppm, and with a pressure of about 1.05 atm. The residence time, varying with reactor temperature as indicated (constant mass flow), applies to the isothermal part of the reactor (about 40 cm of the length).

et al. [73], a good agreement is achieved. It is noteworthy that the system investigated is sensitive to traces of water. If only around 5-10 ppm water was introduced, the kinetic model is seen to describe the experimental results for SO_2, SO_3 and N_2O quite well for all sets.

The results are shown in figure 4.8. It appears that the results from N_2O doped experiments support the suggestion of reaction $SO_3+O\rightleftharpoons SO_2+O_2$ being very slow, contrary to the suggestion presented in paper II [98]. The reaction $SO_3+O \rightleftharpoons SO_2+O_2$ (4.2), which is previously suggested to be an important consumption step for SO_3 decomposition, appears to be slow and play insignificant role under most condition of interest in the $SO_2/SO_3/N_2O$ system. Rate of production analysis suggests that the decomposition of SO_3
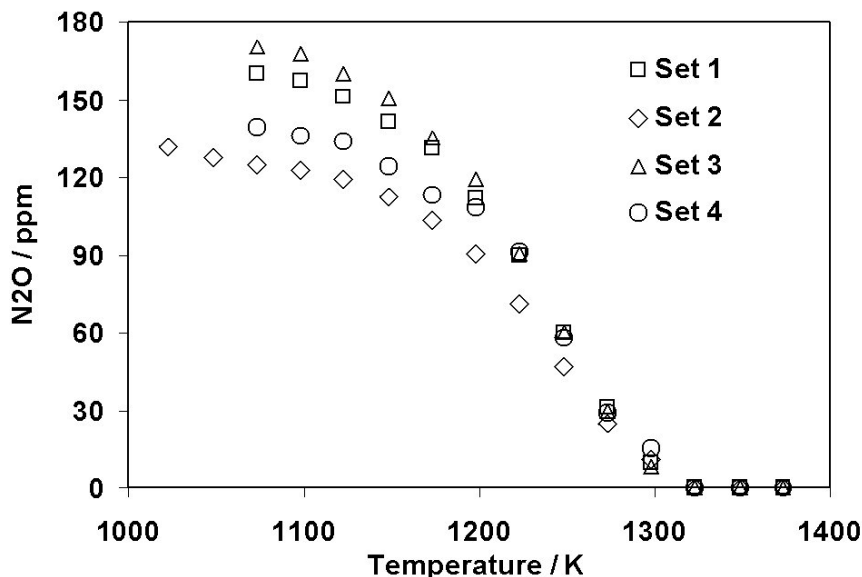
59

Figure 4.7: Experimental results for decomposition of N_2O in $SO_3/SO_2/N_2O$ system. Set 1: $SO_3 = 214.7$ ppm, $SO_2 = 156$ ppm, $N_2O = 164$ ppm, $O_2 = 4.07$ %; residence time $1441.28/T[K]$. Set 2: $SO_3 = 201.2$ ppm, $SO_2 = 401$ ppm, $N_2O = 131$ ppm, $O_2 = 1.02$ %; residence time $1356.3/T[K]$. Set 3: $SO_3 = 387.4$ ppm, $SO_2 = 156$ ppm, $N_2O = 176$ ppm, $O_2 = 4.27\%$; residence time $1519.65/T[K]$. Set 4: $SO_3 = 310.8$ ppm, $SO_2 = 300.4$ ppm, $N_2O = 143$ ppm, $O_2 = 1.02\%$; residence time $1377.45/T[K]$. All experiments are carried out with N_2 as carrier gas, with traces $H_2O \approx 0\text{-}100$ ppm, and with a pressure of about 1.05 atm. The residence time, varying with reactor temperature as indicated (constant mass flow), applies to the isothermal part of the reactor (about 40 cm of the length).

is mainly through reaction $SO_3+H \rightleftharpoons SO_2+OH$ (4.3). The N_2O decomposed by reaction $N_2O(+M) \rightleftharpoons N_2+O(+M)$. This result confirmed that N_2O acting as an O source in the system. Even though the investigation presented in paper II suggests a high rate constant for reaction 4.2, experimental work with $SO_2/SO_3/N_2O$ system presented in paper III indicate that reaction 4.2 is slow and insignificant under conditions of interest in this study. However, it is important to notice that the $SO_2/SO_3/N_2O$ system investigated is very sensitive to traces of water, and there is uncertainty of the water content available in the system. Due to this uncertainty, the results of $SO_2/SO_3/N_2O$ system is not conclusive.
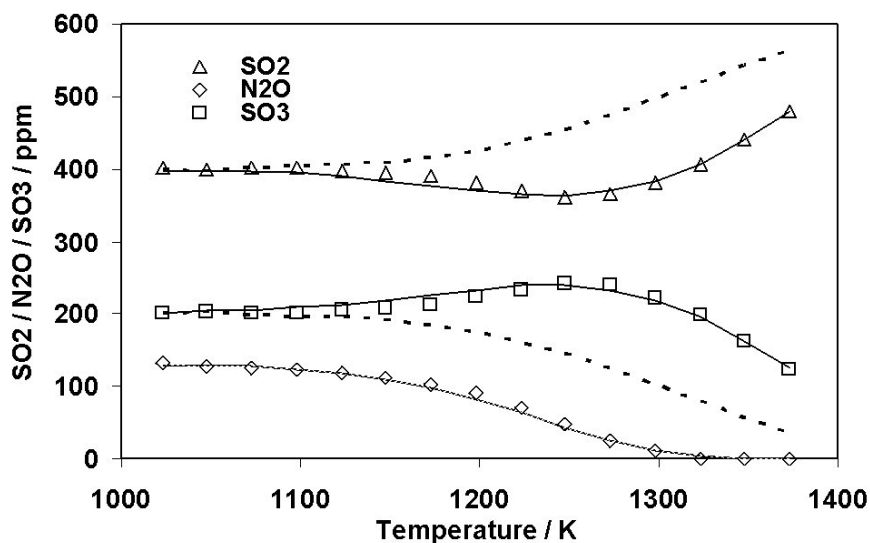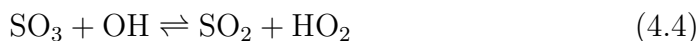
Figure 4.8: Comparison between experimental results from set 2 (symbols) and modeling predictions (lines) with a rate constant for reaction SO_3+O from paper II (dashed line) and Alzueta et al. [73] (solid line). Data set 2: $SO_3 = 201.2$ ppm, $SO_2 = 401$ ppm, $N_2O = 131$ ppm, $O_2 = 1.02$ %; residence time $1356.3/T[K]$. The experiments are carried out with N_2 as carrier gas, with traces of $H_2O \approx 5$-10 ppm, and with a pressure of about 1.05 atm.

4.4.3 Reactions of SO_3 with O/H Radical Pool

In order to further investigate the reactions important for SO_3/SO_2 ratio under combustion conditions, an ab initio study was conducted. The ab initio calculations were done by Paul Marshall using Gaussian 03 as presented in paper IV [100].

A number of reactions may conceivably affect the SO_3 concentration. Reactions of particular interest in this study are those of SO_3 with O, H and OH,

$$SO_3 + O \rightleftharpoons SO_2 + O_2 \tag{4.2}$$

$$SO_3 + H \rightleftharpoons SO_2 + OH \tag{4.3}$$

$$SO_3 + OH \rightleftharpoons SO_2 + HO_2 \tag{4.4}$$

In order to obtain a reliable estimate of reactions SO_3 with O/H radical pool in the temperature range of the present work, ab initio calculations were conducted. The results of ab initio calculations suggest a fast rate constant

for the reaction of SO_3 with H (reaction 4.3), but in contrary, the reactions of SO_3 with O (reaction 4.2) and OH (reaction 4.4) appear to be quite slow. The values of these rate constants are used to update the sulfur chemistry. The updated sulfur chemistry is evaluated using experimental data from literatures, as presented in detail in paper IV [100].

Several studies suggest a rate constant for reaction 4.2 that varies by several orders of magnitude [62, 73, 104–108]. Result from the present work for reaction 4.2 is not conclusive. On one hand, it supports a high value of the rate constant (paper II), while on another hand experimental work suggest that reaction 4.2 is quite slow (paper III).

The reaction $SO_3+H \rightleftharpoons SO_2+OH$ (4.3) is poorly characterized. Previous studies [63, 113] use an estimate value for a rate constant of this reaction.

The modeling results using the updated sulfur chemistry are compared to experimental data available in the literature as presented in detail in paper IV. Some of the comparison is described below.
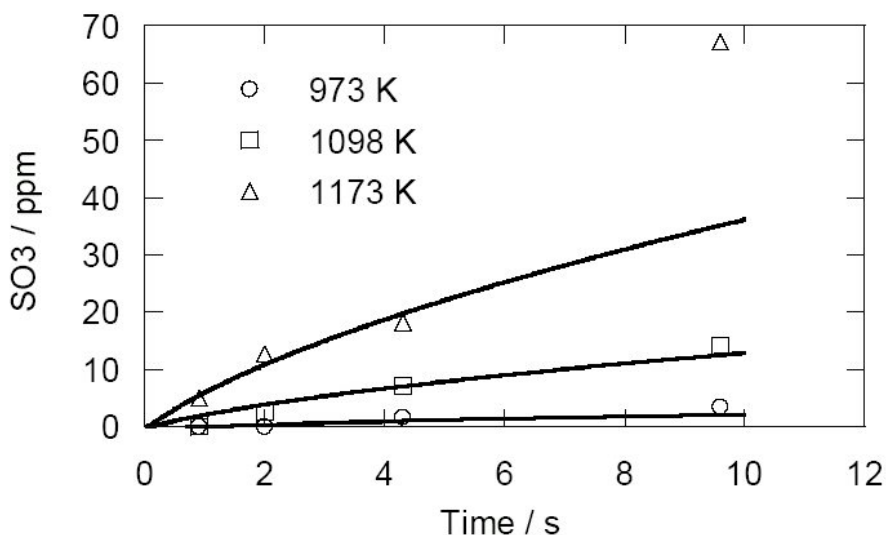

Figure 4.9: Comparison of experimental data [56] and modeling prediction for SO_3 formation in a quartz reactor at 973-1173 K. The inlet gases contained 8% H_2O, 0.14 % SO_2, and air to balance. Symbols denote experimental results, solid lines denote modeling prediction, as presented in paper IV [100].

Figure 4.9 compares modeling predictions with the flow reactor data of Flint and Lindsay [56]. Their experiments were conducted using an electrically heated quartz tube, 185 cm long and 1.6 cm internal diameter. Air containing 8% H_2O and 0.14% SO_2 was drawn at a controlled rate through the quartz tube. The temperature of the tube was maintained at selected

temperatures between 573 and 1173 K, and formation of SO_3 was detected only at 973 K and above. The residence time was varied by changing the gas flow rate. Except for a single data point, the modeling predictions are in good agreement with the flow reactor data.

Rate of production and sensitivity analysis indicate that the key reactions in SO_3 formation are

$$SO_2 + OH(+M) \rightleftharpoons HOSO_2(+M) \tag{4.5}$$

$$HOSO_2 + O_2 \rightleftharpoons SO_3 + HO_2 \tag{4.9}$$
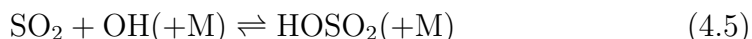
and to a less extent, reaction

$$SO_2 + HO_2 \rightleftharpoons SO_3 + OH \tag{4.4b}$$

and

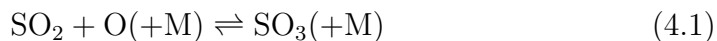$$SO_2 + OH \rightleftharpoons SO_3 + H \tag{4.3b}$$

It is noteworthy that modeling predictions with the high rate constant for the SO_3+O reaction (4.2) derived from flames [62, 104–108] lead to a significant overprediction of the SO_3 formation rate through the inverse step,

$$SO_2 + O_2 \rightleftharpoons SO_3 + O \tag{4.2b}$$

Radical formation from combustion has been shown to enhance the SO_2 oxidation rate significantly [12]. Glarborg et al. [63] studied SO_2 conversion during moist CO oxidation. The experiments were conducted using a quartz flow reactor (length 19 cm, inner diameter 0.45 cm), designed to approximate plug flow. The reactants CO, SO_2, O_2, and H_2O were heated separately and mixed in a cross flow at the reactor inlet. The product gas was quenched at the exit of the reactor with cooling air and dried prior to analysis. The experimental data are compared with modeling predictions as shown in figure 4.10. The agreement is within the experimental uncertainty. Compared to conditions in the absence of combustibles, the enhanced radical levels open up new pathways to formation and consumption of SO_3.

The dominating SO_3 formation reaction is now recombination of SO_2 with atomic O,

$$SO_2 + O(+M) \rightleftharpoons SO_3(+M) \tag{4.1}$$

while SO_3 decomposition proceeds mainly by the reactions

$$SO_3 + HO_2 \rightleftharpoons HOSO_2 + O_2 \tag{4.9b}$$

$$HOSO_2(+M) \rightleftharpoons SO_2 + OH(+M) \tag{4.5b}$$
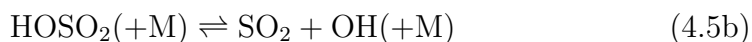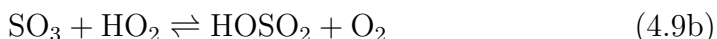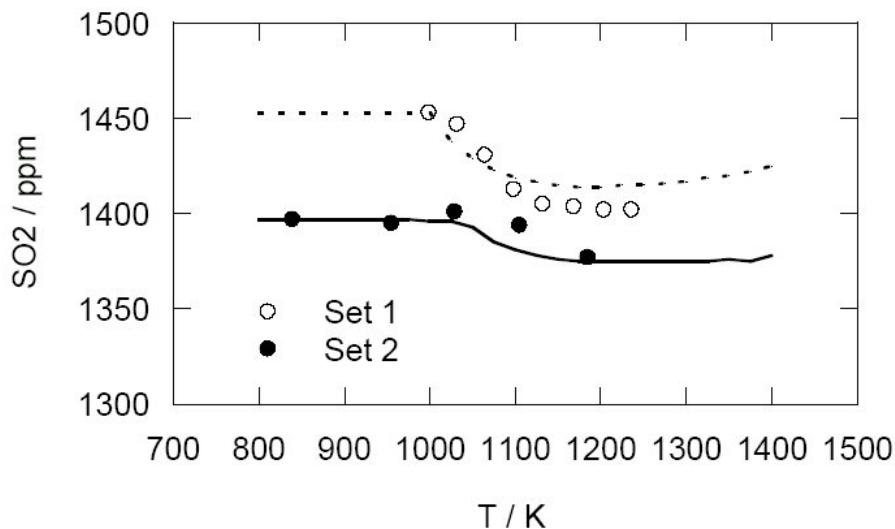
Figure 4.10: Comparison of experimental data [63] and modeling predictions for conversion of SO_2 as function of temperature during moist CO oxidation in a quartz flow reactor. Experimental data are shown as symbols, modeling predictions as lines. Data set 1: 448 ppm CO, 1453 ppm SO_2, 4.3 % O_2 and 1% H2O, residence time as a function of temperature 243[K]/T. Data set 2: 446 ppm CO, 1395 ppm SO_2, 4.1% O_2 and 8.7% H_2O, residence time as a function of temperature 244[K]/T. Symbols denote experimental results, lines denote modeling prediction [100].

$$SO_3 + H \rightleftharpoons SO_2 + OH \qquad (4.3)$$

While the revised rate constant for the SO_3+H reaction (4.3) has only a small impact compared to earlier modeling for the SO_2/SO_3 ratio in combustion, the updated value for reaction SO_3+O (4.2) has important implications. This reaction has been assumed to be an important consumption step for SO_3 in flames [62, 104, 106–108] and in flow reactor experiments [63, 73]. The present analysis indicates that reaction is too slow to be important in any of these systems. The observed SO_3 consumption must be attributed to other reactions, primarily SO_3+H (4.3). Also the reaction SO_3+OH (4.4) is generally too slow to be significant, but the reverse step between SO_2+HO_2 (4.4b) may contribute to SO_3 formation under conditions with low radical levels.

It appears that the work presented in paper II suggests a high rate constant for reaction 4.2. There is a significant O atom loss in the system, and it was partly attributed by reaction with SO_3, resulting a high rate constant for this reaction (SO_3 + O (4.2))in paper II. This interpretation is in conflict

with experimental results presented in paper III and the present ab initio value as presented in paper IV. The likely explanation is that there is loss of O on the reactor surface in the experimental results presented in paper II, but more work is required to confirm this.

4.5   Conclusions

Sulfur chemistry important for the SO_2/SO_3 ratio under combustion conditions has been updated. Modeling predictions with a revised reaction mechanism for SO_2/SO_3 chemistry are in good agreement with a range of experimental data from reactor experiments.

The calculations indicate that oxidation of SO_2 to SO_3 with and without presence of combustibles involve primarily recombination of SO_2 with O and OH radicals. The reaction SO_3+H may limit the SO_3 concentration, while SO_3 reactions with O or OH are unimportant for the SO_2/SO_3 ratio under most conditions of interest. In conclusion, the ratio of SO_2/SO_3 in the gas phase system is mainly determined by reactions $SO_2 +O/OH$, reactions involving intermediate $HOSO_2$, and reaction SO_3+H.

As presented in detail in papers II-IV, the work on sulfur chemistry has significantly improved our understanding of the mechanisms important for the SO_2/SO_3 ratio under combustion conditions. The modeling results using an updated chemistry give a good agreement when compared to experimental data for the SO_2/SO_3. Having the K/O/H/Cl and sulfur chemistry updated, the next step is to investigate their interactions important for sulfation process under combustion conditions as presented in the next chapter.

Chapter 5

Sulfate Aerosols Formation

5.1 Introduction

This chapter contains a study using K/O/H/Cl chemistry (from paper I), S chemistry (papers II-IV), and their interactions (K/O/H/Cl/S chemistry) to investigate the importance of homogeneous sulfation process prior to sulfate aerosol formation, as presented in detail in paper V. The K/O/H/Cl chemistry in general gives a good agreement when compared to the experimental data (paper I). The study of sulfur chemistry presented in paper IV (which is an update of work in papers II-III) suggests that modeling predictions with a revised reaction mechanism for SO_2/SO_3 chemistry are in good agreement with a range of experimental data from reactor experiments.

The objective of this study has been to investigate the active mechanism in the sulfate aerosols formation in biomass combustion. The experimental data using synthetic flue gas available in the studies from Iisa et al. [23] and Jensen et al. [17] are used to evaluate the model, taking into account the SO_2, O_2 inlet concentrations, residence time and temperature time history. In addition, data from a study by Jimenez and Ballester [114] on orujillo (a residue of the olive oil production process) combustion is also used to evaluate the model. The sulfate aerosol formation is modeled using different approaches:

- **Model A**

  - Detailed K/O/H/Cl chemistry from paper I.

  - Detailed S chemistry from paper IV.

  - Detailed K/O/H/Cl/S from Glarborg and Marshall [14].

- **Model B**

  – Detailed K/O/H/Cl chemistry from paper I.

  – Detailed S chemistry from paper IV.

  – Additional reaction involving KCl as a sink for the SO_3 formed to instantaneously generate sulfate aerosols (paper V).

- **Model C**

  – Detailed K/O/H/Cl chemistry from paper I.

  – Detailed S chemistry from paper IV.

  – Detailed K/O/H/Cl/S from Glarborg and Marshall [14] and additional chemistry from present work (paper V).

- **Model D**

  – Detailed K/O/H/Cl chemistry from paper I.

  – Detailed S chemistry from paper IV.

  – Detailed K/O/H/Cl/S from Glarborg and Marshall [14].

  – Clustering model for aerosol formation and catalytic reaction from present work (paper V).

The first model includes the previous work by Glarborg and Marshall with adjustments on the sulfur chemistry and K/O/H/Cl chemistry (model A). The second approach (model B) is where the SO_3 formation is assumed to be the rate limiting step in the sulfate formation, and all of the SO_3 formed is assumed to instantaneously generate K_2SO_4 aerosols when excess K is available in the system. The third model (model C) is an updated model of Glarborg and Marshall with some additional reactions in the K/O/H/Cl/S subset involving novel species $KHSO_3$ and KSO_4. The last modeling approach (model D), is where the surface (catalytic) reaction is added to the gas phase mechanism. This model consists of a mechanism suggested by Glarborg and Marshall with addition of clustering mechanism for sulfate aerosol formation. The formed aerosol will then catalyze the further sulfation process which leads to additional sulfate aerosols. The model predictions (A-C) are

compared to the experimental data from literature [17, 23, 114], while model D is used to only evaluate the experimental data of Jensen et al. [17].

The reactions that oxidize SO_2 into SO_3 are of special interest in this study since they are believed to be the rate limiting step in the K_2SO_4 formation prior to sulfate aerosols generation.

5.2   Detailed Kinetic Modeling

A gas phase model for interaction between sulfur, chlorine, and potassium earlier proposed by Glarborg and Marshall [14] is used as basis for the current modeling. The Senkin code [86] which runs in conjunction with Chemkin-II [87] was used in the modeling, assuming plug flow.

The reaction mechanism consists of subsets for O_2/H_2, chlorine chemistry, sulfur chemistry, potassium chemistry and the interaction between those species. The chlorine chemistry, involving reactions of HCl and Cl_2, is an update of the evaluation by Baulch et al. [70]. K/O/H/Cl chemistry is taken from previous work (paper I). As presented earlier, few of the rate constants in the K/O/H/Cl reaction subset have been determined experimentally. Therefore estimated values for the rate constants are assigned to most of the reactions. However from paper I, the modeling results give a good agreement when compared to experimental data. The sulfur subset was taken from recent work by the authors which include results from paper II-IV [98–100]. The sulfur subset includes reactions of SO_2 with O, OH, and HO_2 to form SO_3, reactions involving $HOSO_2$ intermediate and also reactions involving SO_3 and H, O, OH, HO_2, SO. All of the reactions mentioned may be important for the ratio of SO_2 to SO_3. The reactions that oxidize SO_2 into SO_3 is of special interest in this study since they are believed to be the rate limiting step in the K_2SO_4 formation prior to sulfate aerosols generation. The reactions involving K/O/H/Cl/S are listed in Table 5.1. Reactions 1-17 in the list are those from Glarborg and Marshall [14], while reactions 18-26 are part of the present work as presented in paper V.

Thermodynamic data used in the present study is taken from previous works [14, 109] and additional thermodynamic data for $KHSO_3$ and KSO_4 from the present work.

In model C, additional reactions are added to the K/O/H/Cl/S subset. The additional reactions involve the novel species $KHSO_3$ and KSO_4. The thermodynamic data of the additional species were calculated by Paul Marshall using Gaussian 03 [100]. Using the current thermodynamic properties, the exothermicity of the additional reactions can be estimated. The reactions are expected to be fast in the exothermic direction, and we assign some of

them a high rate constants of 1 x 10^{14} cm^3 mol^{-1} s^{-1}.

5.3 Results and Discussion

5.3.1 Model A

The updated detailed gas phase mechanism (model A) is used to simulate the conditions of experimental work from Iisa et al. [23], Jensen et al. [17] and Jimenez and Ballester [114]. The experiments from Iisa et al. were conducted at temperatures from 1173 to 1373 K in an entrained flow reactor. Solid KCl particles were introduced to the system together with a mixture of gases consisting of SO$_2$, O$_2$, H$_2$O, and N$_2$ to balance. The residence times of the gases in the reactor were in range from 0.3-1.5 s, after which a quenching system was applied to avoid further reaction. The comparison between the data from Iisa et al. [23] and predicted results are shown in figures 5.1-5.3. The modeling and validation were done following these two steps. First, the evaporation of solid potassium chloride was modeled as three-pseudo-first order reactions in series following Glarborg and Marshall [14]. The rate constants were fitted to match the experimental data by Iisa et al. [23].

The comparison between the degree of KCl vaporization and the predicted value as a function of residence times can be seen in figure 5.1. The comparison between observed degree of KCl sulfation in the entrained flow reactor as a function of the residence time at 1373 and 1173 K [23] and the predicted values from model A is shown in figure 5.2-5.3. The model under-predicts the sulfate formation for all sets by approximately factor two. The updated sulfur subset of the mechanism yields a lower oxidation rate for SO$_2$ and thereby a less satisfactory agreement with the sulfation data than the original scheme by Glarborg and Marshall [14].

Model A is then compared to the experimental data from Jensen et al. [17]. Jensen et al. conducted experiments in a laboratory tubular furnace reactor using synthetic flue gas contained a mixture of gaseous N$_2$, O$_2$, H$_2$O vapor, SO$_2$, and vapor KCl. Potassium chloride was added to the system by saturating the feed stream or part of it with salt vapors. The peak temperature is varied from 1043 to 1273 K (see figure 5, paper V). The experimental data, presented as the ratio S/(S+Cl) in the aerosols, are compared to predicted results in figure 5.4. The model strongly underpredicts the sulfur content in the aerosols. In contrast with the experimental findings, model A predicts the sulfation process to be insignificant under these experimental conditions.

Finally, model A is evaluated against experimental data from Jimenez and

70

Table 5.1: Rate coefficients for K/O/H/Cl/S chemistry, units are cm, mol, s, K.

| No	Reaction	A	n	E/R	Note
1.	K +SO$_2$(+M) $\rightleftharpoons$ KSO$_2$(+M)	3.7E14	0.00	0	[14]
	Low-pressure limit 5.2E23 -1.50 0				
2.	K +SO$_3$(+M) $\rightleftharpoons$ KSO$_3$(+M)	3.7E14	0.00	0	[14]
	Low-pressure limit 4.7E34 -4.90 0				
3.	K +SO$_3$ $\rightleftharpoons$ KO + SO$_2$	1.0E14	0.00	7840	[14]
4.	KO +SO$_2$(+M) $\rightleftharpoons$ KSO$_3$(+M)	3.7E14	0.00	0	[14]
	Low-pressure limit 5.2E23 -1.50 0				
5.	KOH +SO$_3$(+M) $\rightleftharpoons$ KHSO$_4$(+M)	1.0E14	0.00	0	[14]
	Low-pressure limit 2.6E42 -7.6 0				
6.	KSO$_2$ + O $\rightleftharpoons$ KO + SO$_2$	1.3E13	0.00	0	[14]
7.	KSO$_2$ + OH $\rightleftharpoons$ KOH +SO$_2$	2.0E13	0.00	0	[14]
8.	KSO$_2$ + KO$_2$ $\rightleftharpoons$ K$_2$SO$_4$	1.0E14	0.00	0	[14]
9.	KSO$_3$ + O $\rightleftharpoons$ KO + SO$_3$	1.3E13	0.00	0	[14]
10.	KSO$_3$ + OH $\rightleftharpoons$ KOH +SO$_3$	2.0E13	0.00	0	[14]
11.	KSO$_3$ + KO $\rightleftharpoons$ K$_2$SO$_4$	1.0E14	0.00	0	[14]
12.	KHSO$_4$ + KOH $\rightleftharpoons$ K$_2$SO$_4$ + H$_2$O	1.0E14	0.00	0	[14]
13.	KHSO$_4$ + KCl $\rightleftharpoons$ K$_2$SO$_4$ + HCl	1.0E14	0.00	0	[14]
14.	KCl+ SO$_3$(+M) $\rightleftharpoons$ KSO$_3$Cl(+M)	1.0E14	0.00	0	[14]
	Low-pressure limit 1.9E41 -7.80 0				
15.	KSO$_3$Cl +OH $\rightleftharpoons$ KHSO$_4$ + Cl	1.0E14	0.00	0	[14]
16.	KSO$_3$Cl +H$_2$O $\rightleftharpoons$ KHSO$_4$ + HCl	1.0E14	0.00	0	[14]
17.	KSO$_3$Cl +KOH $\rightleftharpoons$ K$_2$SO$_4$ + HCl	1.0E14	0.00	0	[14]
18.	KO$_2$+SO$_2$(+M) $\rightleftharpoons$ KSO$_4$(+M)	1.0E14	0.00	0	as KOH+SO$_3$
	Low pressure limit 2.6E42 -7.6 0				
19.	KSO$_2$+O$_2$(+M) $\rightleftharpoons$ KSO$_4$ (+M)	1.0E14	0.00	0	as KOH+SO$_3$
	Low pressure limit 2.6E42 -7.6 0				
20.	KO+SO$_3$(+M) $\rightleftharpoons$ KSO$_4$ (+M)	1.0E14	0.00	0	as KOH+SO$_3$
	Low pressure limit 2.6E42 -7.6 0				
21.	KHSO$_4$ +OH $\rightleftharpoons$ KSO$_4$+H$_2$O	1.0E14	0.00	0	
22.	KHSO$_3$+OH $\rightleftharpoons$ KSO$_3$ + H$_2$O	1.0E14	0.00	0	
23.	KHSO$_3$+OH $\rightleftharpoons$ KHSO$_4$ + H	1.0E14	0.00	0	
24.	KSO$_3$+O $\rightleftharpoons$ KSO$_4$	1.0E14	0.00	0	
25.	KSO$_4$+O$\rightleftharpoons$KSO$_3$+O$_2$	1.0E14	0.00	0	
26.	KOH+SO$_2$(+M)$\rightleftharpoons$KHSO$_3$(+M)	1.0E14	0.00	0	as KOH+SO$_3$
	Low pressure limit 2.6E42 -7.6 0				
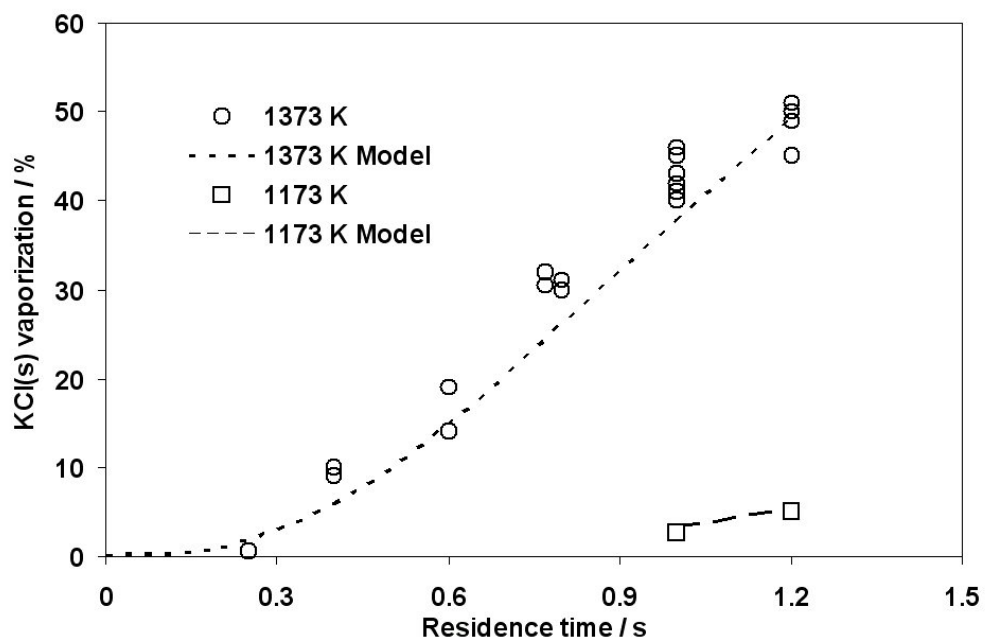
Figure 5.1: Vaporization of solid KCl as a function of residence time in an entrained flow reactor at 1173 and 1373K. Symbols denote experimental results [23], lines denote modeling result. KCl feed rate: 0,24 g/min
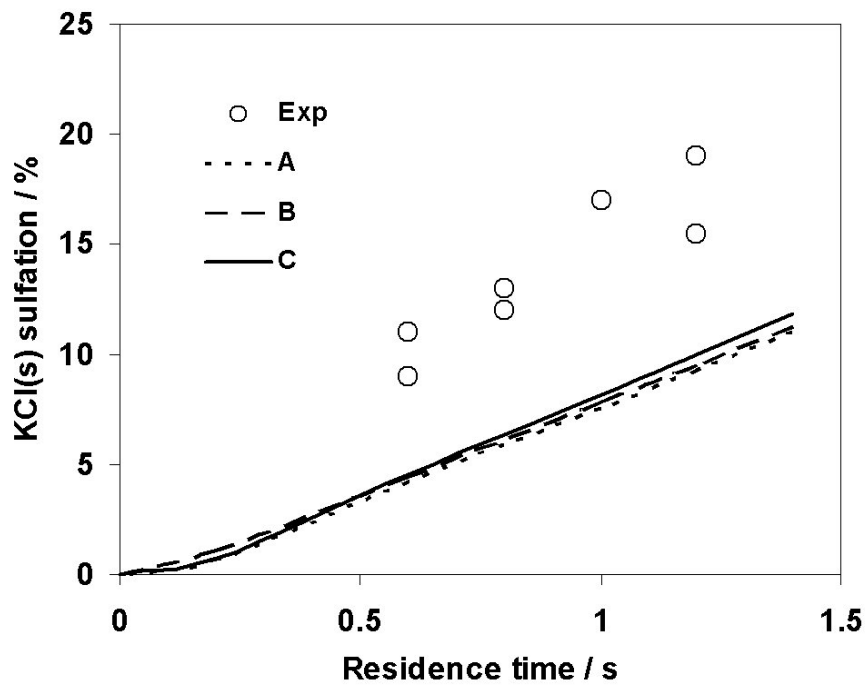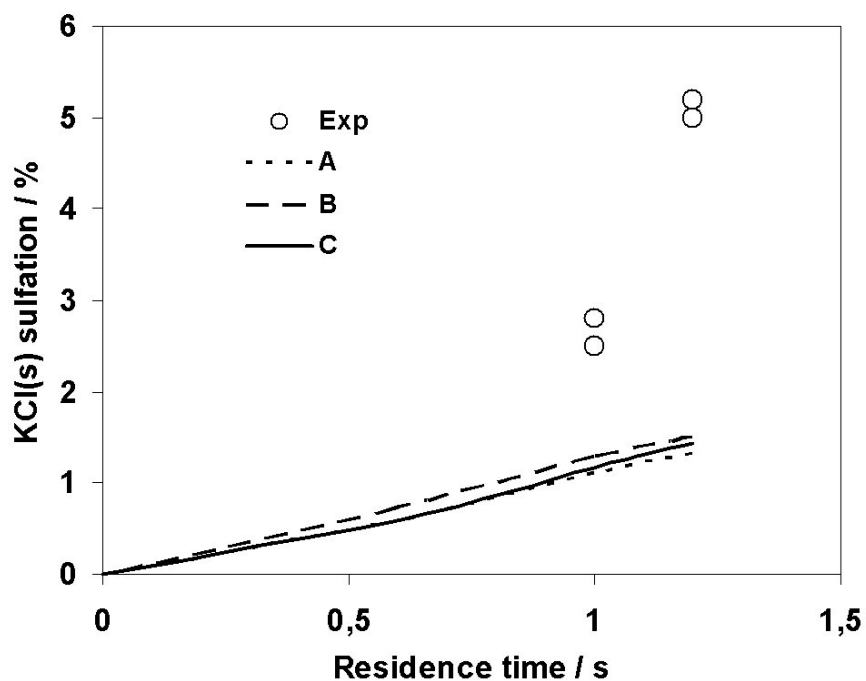
Figure 5.2: Fractional conversion of solid KCl to K_2SO_4 as a function of residence time in an entrained flow reactor at 1373 K. Symbols denote experimental results [23], lines denote modeling result (models A-C). Inlet feed contained 2 % SO_2, 5 % O_2, 10 % H_2O, N_2 to balanced and KCl feed rate : 0,24 g/min

.

Figure 5.3: Fractional conversion of solid KCl to K_2SO_4 as a function of residence time in an entrained flow reactor at 1173 K. Symbols denote experimental results [23], lines denote modeling result (models A-C). Inlet conditions contained 2 % SO_2, 5 % O_2, 10 % H_2O, N_2 to balanced and KCl feed rate : 0,24 g/min
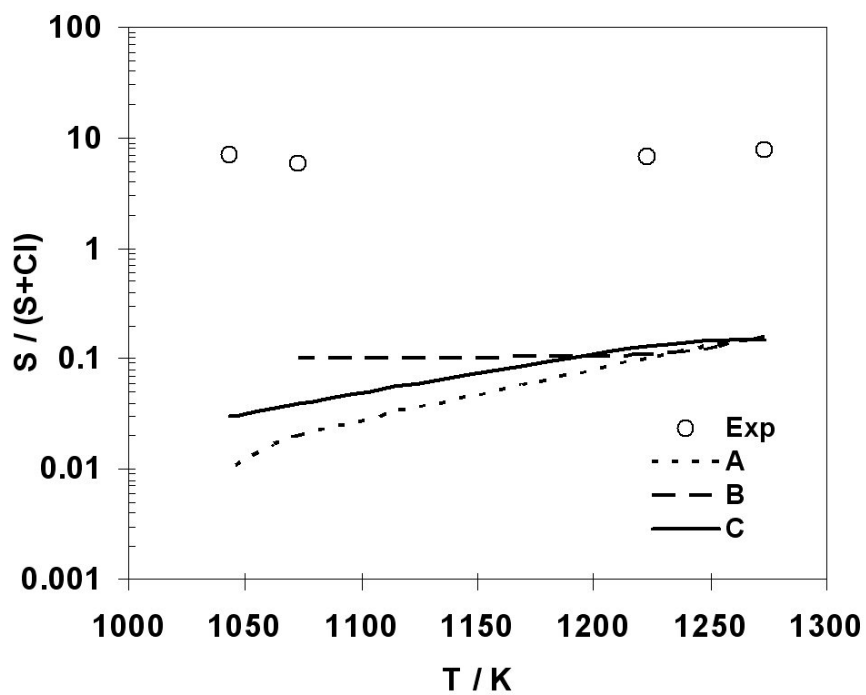
.

Figure 5.4: Comparison of the predicted results (from models A-C, lines) with the experimental data from Jensen et al. [17] (open symbols). Inlet conditions contained 200 ppm KCl, 200 ppm SO_2, 4 % O_2, 4 % H_2O, N_2 to balanced. The peak temperature is varied from 1043, 1073, 1223, or 1273 K, and residence time is around 3 s

.

Ballester [115]. These data were recently used by Jimenez and Balester [114] in modeling sulfate aerosols formation. The experiments were done using an entrained flow reactor [115]. The temperature profile measured along the cooling section for a reactor temperature of 1300 °C [115] is shown in paper V (figure 7). A comparison between the predictions of model A and the observed Cl/S ratio in the aerosols is presented in figure 5.5. Again, model A strongly underpredicts the sulfate formation, resulting in higher Cl/S values compared to the experimental data.
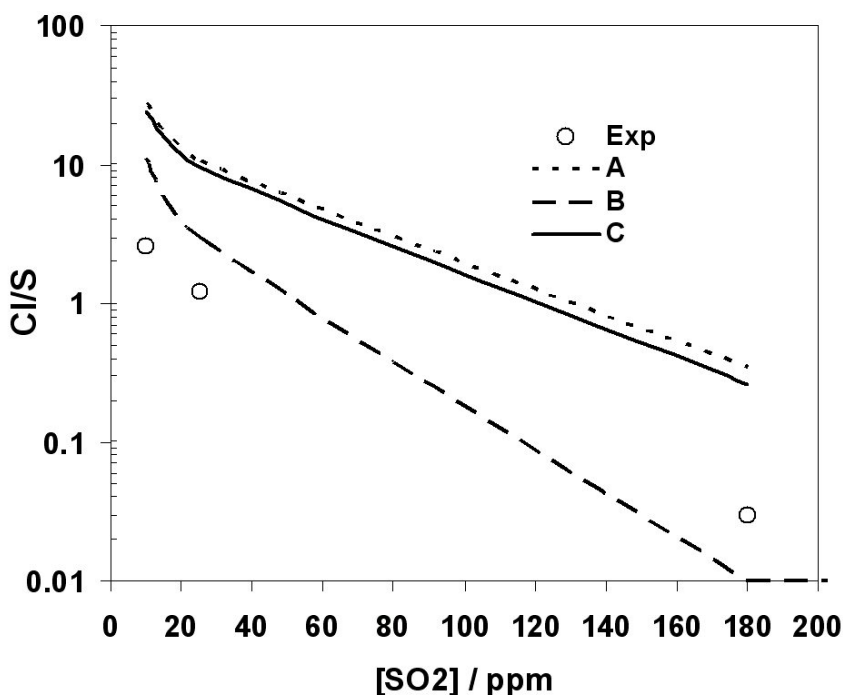

Figure 5.5: Comparison of the predicted results (from models A-C, lines) with the experimental data from Jimenez and Ballester [115] (open symbols). Inlet conditions contained 13 ppm KOH, 34 ppm HCl, 10/25/180 ppm SO_2, 5 % O_2, 20 % H_2O, 8 % CO_2 and N_2 to balanced, residence time is around 3 s

.

In general, the homogeneous gas phase model A underpredicts the degree of sulfation when compared to the experimental data. Previous work by Glarborg and Marshall [14] indicates that under the conditions investigated (Iisa et al. [23] at 1373 K), the degree of sulfation appears to be limited only

by the SO_2 oxidation rate. This has an implication that the sulfation rate would be expected to be independent of the alkali precursor (in this case KCl, KOH, or other).

5.3.2   Model B

The next modeling approach (model B) uses an assumption of SO_2 oxidation to SO_3 being the rate limiting step in the sulfation process prior to the aerosol formation. The SO_3 formed in the system will instantaneously form potassium sulfate and generate sulfate aerosols. The results of the model on the degree of sulfation is compared to the experimental data of Iisa et al. [23], Jensen et al. [17] and Jimenez and Ballester [114] as shown in figures 5.2-5.5. Model B underpredicts the degree of sulfation from experimental data under all of the conditions investigated. There is no significant difference between the results of model A and B when compared to the experimental data of Iisa et al. [23] and Jensen et al. [17]. However, for the conditions of Jimenez and Ballester (figure 5.5), model B predicts a degree of sulfation that is about an order of magnitude higher than model A, significantly improving the agreement with experiment. This difference is discussed further below.

The characteristic temperature profile used in the experiments by Jimenez and Ballester involved a higher peak temperature (1573 K) than the other experiments (1043-1373 K). At the higher temperature, the SO_3 formation rate is faster as a consequence of the higher O and OH radical concentrations. However, at the same time SO_3 is limited by the thermal equilibrium with SO_2. To convert a significant fraction of SO_2 to the higher oxidation state ($S^{IV} \rightarrow S^{VI}$), a fast, irreversible consumption of SO_3 to form K_2SO_4 is required. An immediate consumption of SO_3 (as in model B) shifts the reaction into producing more SO_3. In model A, even though the reaction between SO_3 and KOH/KCl occurs almost at collision frequency, the SO_3 consumption rate is limited due to the very low concentration of potassium (13 ppm KOH in the inlet). For this reason, SO_3 is only partly converted to K_2SO_4 and model A predicts a considerably lower degree of sulfation than model B.

According to the assumptions of models A and B, the homogeneous oxidation of SO_2 to SO_3 is a rate limiting step. However, both models underpredict the degree of sulfation observed experimentally.

The second modeling approach (model B) on formation of sulfate aerosols was based on the assumption that the SO_3 formation in the gas phase is the rate limiting step [10, 14, 17–19, 23] and that immediately after its formation, the SO_3 is consumed to form K_2SO_4. As shown above, the model consistently underpredicts the formation of sulfate aerosols under the conditions

of interest. The model B predictions suggest that the oxidation of SO_2 to SO_3 is low, below 1 % while in the experiments by Jensen et al. [17], the SO_2 conversion was quite high, around 5-16 %. The smallest discrepancy is found for the conditions of Iisa et al. [23], where the predicted SO_2 conversion of 0.4-2.8 % is compared to an observed value of 2-5 %.

It is important to point out that the sulfur subset in the present gas phase mechanism predicts well the homogeneous SO_2 oxidation over a wide range of conditions [100]. Therefore the difference between the experimental and modeling results cannot be explained in terms of uncertainties in this subset. Consequently, the discrepancy might be attributed to chemistry involving K-containing species or surface reactions.

The homogeneous oxidation of SO_2 by oxygen molecules at temperatures below 1173 K is very slow according to observations [11,56,57]. As presented in paper V (figure 9), a higher SO_2 consumption is found in the SO_2/O_2/alkali metal system [17, 23]. This suggests that the presence of alkali metals may promote oxidation of SO_2. In particular the experimental data of Jensen et al. [17] show very high conversion rates for SO_2.

It is clear that the oxidation of SO_2 in the sulfation experiments, in particular those of Jensen et al. [17], cannot be attributed solely to reactions in the gas-phase H/S/O system. The results suggest that either an unknown gas-phase mechanism or a catalytic reaction promotes formation of S^{VI} (SO_3 or sulfate). These possibilities are investigated further in the following.
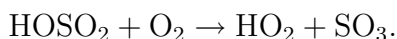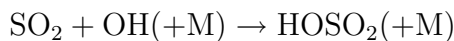
5.3.3 Model C

The third modeling approach (model C) takes into consideration that K-containing species may be involved actively in the SO_3 formation and sulfation process. A previous mechanism [14] contains a detailed reaction subset for K-containing species in the sulfation process. However, with the updated sulfur chemistry, the results of model A underpredicts the degree of sulfation when compared to the experimental data available in the literature [17, 23, 114]. In model C, the alkali subset of the detailed mechanism is supplemented with additional reactions of $KHSO_3$ and KSO_4, offering novel pathways to SO_3, as well as pathways to sulfation that do not involve SO_3 formation.

The comparison between the observed degree of KCl-sulfation in the entrained flow reactor as a function of the residence time, at 1373 and 1173 K [23], and the predicted value from model C, is also shown in figures 5.2-5.3. The results indicate that there is no significant difference in the modeling results for A and C when compared to the experimental data [17, 23, 114].
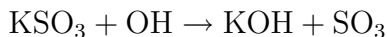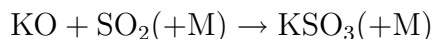
Sensitivity analysis and rate of production analysis for the conditions of

Iisa et al. [23], at 1373 K (figure 5.2), using model C, were conducted to investigate the reactions important for the homogeneous sulfate formation prior to aerosol formation. The previous model by Glarborg and Marshall supports the suggestion that the oxidation of SO_2 to SO_3 is the rate limiting step in the sulfation process. In the present study, the model C predictions suggest that while the oxidation of SO_2 to SO_3 has a significant role in the sulfation process, other steps involving reactions with K-containing species may also be active in the sulfation process.
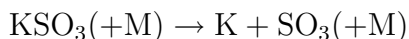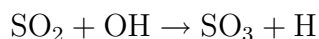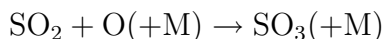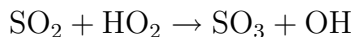
The pathways of SO_3 formation at 1373 K in the present study deviate somewhat from the suggestions by Glarborg and Marshall [14]. In their study, the SO_2 oxidation occurred mainly by OH addition to form $HOSO_2$ which then reacted with O_2 to form SO_3 and HO_2,

$$SO_2 + OH(+M) \rightarrow HOSO_2(+M)$$

$$HOSO_2 + O_2 \rightarrow HO_2 + SO_3.$$

According to the current mechanism, the oxidation of SO_2 to SO_3 may, in addition to this sequence, proceed through the reactions

$$KO + SO_2(+M) \rightarrow KSO_3(+M)$$

$$KSO_3 + OH \rightarrow KOH + SO_3$$

with smaller contributions from

$$SO_2 + HO_2 \rightarrow SO_3 + OH$$

$$SO_2 + O(+M) \rightarrow SO_3(+M)$$

$$SO_2 + OH \rightarrow SO_3 + H$$

$$KSO_3(+M) \rightarrow K + SO_3(+M)$$

The suggestion that KSO_3 may be a significant intermediate in SO_3 formation is novel compared to previous work.
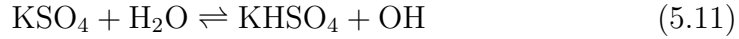
The pathway diagram for potassium transformations under the conditions of figure 5.2, with model C, is shown in figure 5.6. The main form of gaseous potassium under the present conditions is potassium chloride. In agreement with the previous studies [14, 85], KCl after vaporization is partly converted to KOH by reaction

$$KCl + H_2O \rightleftharpoons KOH + HCl \tag{5.9}$$

Part of the KCl is converted to KSO_3Cl following the reaction

$$KCl + SO_3(+M) \rightleftharpoons KSO_3Cl(+M) \tag{5.10}$$
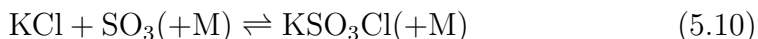
The KSO_3Cl reacts with H_2O in a mechanism similar to the previously suggested [14], and forms $KHSO_4$. This reaction contributes to more than 50 % of the $KHSO_4$ formed. The $KHSO_4$ is also formed through reaction

$$KSO_4 + H_2O \rightleftharpoons KHSO_4 + OH \qquad (5.11)$$

and additional contribution by reactions
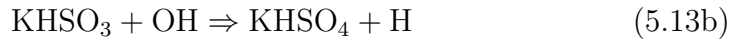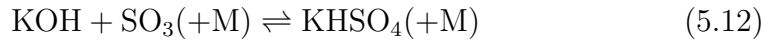
$$KOH + SO_3(+M) \rightleftharpoons KHSO_4(+M) \qquad (5.12)$$

$$KHSO_3 + OH \Rightarrow KHSO_4 + H \qquad (5.13b)$$

Similar to the suggestion by Glarborg and Marshall, potassium sulfate is formed by reaction

$$KHSO_4 + KCl \rightleftharpoons K_2SO_4 + HCl \qquad (5.14)$$
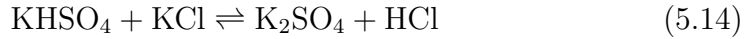
This reaction is the main consumption of $KHSO_4$ in the system and the only reaction that directly produces K_2SO_4.

According to the present model, the homogeneous gas phase sulfation may occur through sequences

$KCl \rightarrow KSO_3Cl \rightarrow KHSO_4 \rightarrow K_2SO_4$ (A) or

$KCl \rightarrow K \rightarrow KSO_2 \rightarrow KSO_4 \rightarrow KHSO_4 \rightarrow K_2SO4$ (B) or

$KCl \rightarrow KOH \rightarrow KSO_2 \rightarrow KSO_4 \rightarrow KHSO_4 \rightarrow K_2SO4$ (C) or

$KCl \rightarrow KOH \rightarrow KHSO_4 \rightarrow K_2SO_4$ (D) or

$KCl \rightarrow KOH \rightarrow KHSO_3 \rightarrow KHSO_4 \rightarrow K_2SO_4$ (E) or

$KCl \rightarrow KOH \rightarrow KO \rightarrow KSO_3 \rightarrow KSO_4 \rightarrow KHSO_4 \rightarrow K_2SO4$ (F).
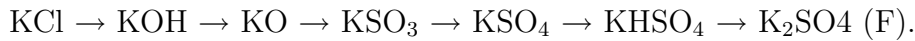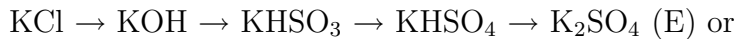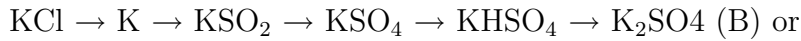
Six sequences having potentially significant roles in the sulfation mechanism. All of them should be taken into account in the gaseous sulfation process. From those six, the sequence (A) is found to be the most significant one followed by sequence (B), (C) and finally (D) and minor by (E) and (F). The pathways indicate that even alkali containing species such as KSO_2 and KSO_4 may contribute to the gaseous sulfation process.

The current model (model C) is also evaluated against experimental data from Iisa et al. [23] in terms of SO_2, O_2, and H_2O inlet variation at 1373 K. The predicted results using model C give similar trends to the previous study
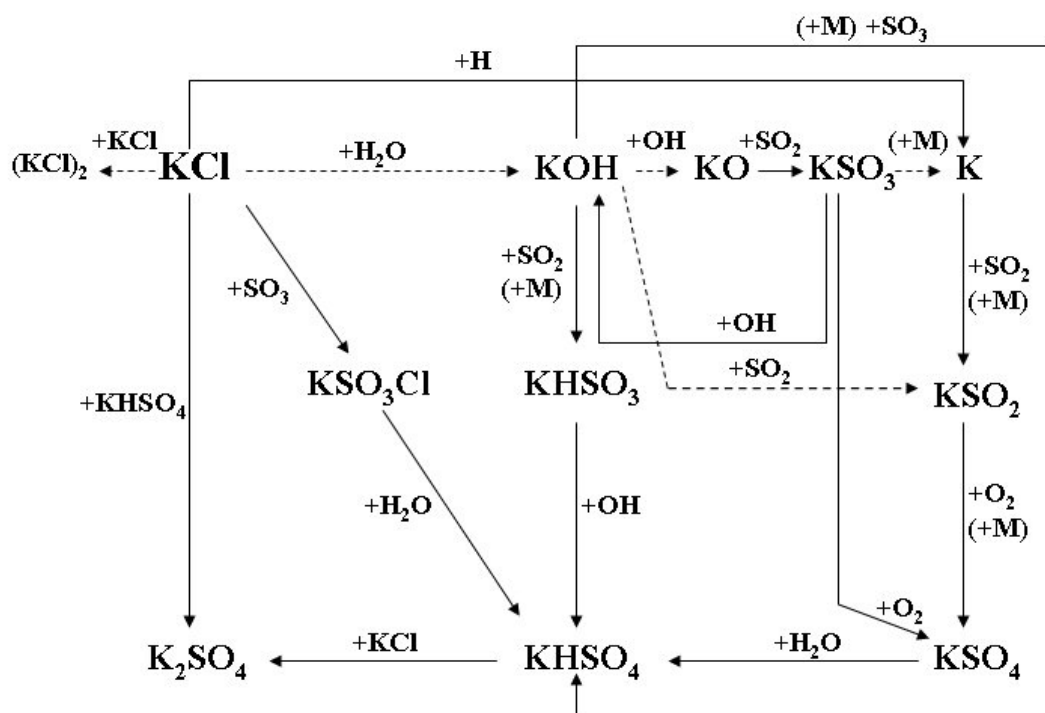
Figure 5.6: Pathway diagram for potassium transformations under the conditions of Iisa et al. [23] at 1373 K with model C.

by Glarborg and Marshall [14], except that the degree of sulfation from the model underpredicts the experimental data by around factor 2, as shown in figures 5.7-5.9. The present gaseous model (model C) suggests that apart from the SO_3-formation, the reactions of SO_2 and O_2 directly with some of the K-containing species may have a significant role in the gaseous sulfation process.
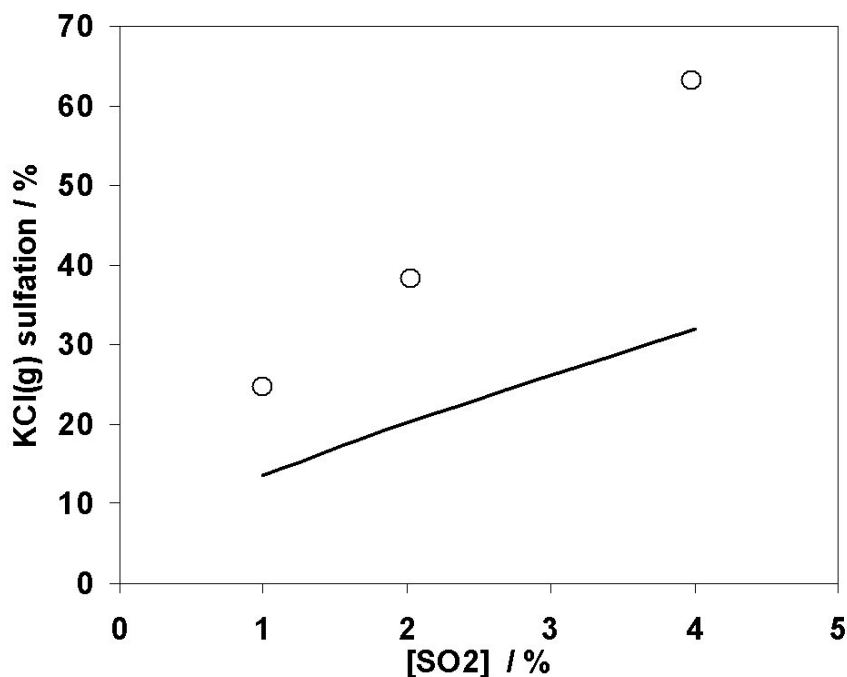

Figure 5.7: Fractional conversion of vaporized KCl to K_2SO_4 as a function of SO_2 concentration in an entrained flow reactor at 1373 K. Symbols denote experimental results [23], lines denote modeling result (model C). Inlet conditions contained 5 % O_2, 10 % H_2O, N_2 to balanced and KCl feed rate : 0,24 g/min

Comparison of predictions with model C to the experimental data by Jensen et al. [17] and Jimenez and Ballester [114] shows a significant underprediction of the sulfate aerosol formation (figures 5.4-5.5). As in figures 5.2 and 5.3, models A and C yields similar results, despite the changes in the potassium subset. The difference of about a factor of two between the observed and predicted sulfation rate for the conditions of Iisa et al. [23] may conceivably be attributed to uncertainties in the gas-phase K/O/H/Cl/S chemistry. However, for the conditions of Jensen et al. [17] and Jimenez

Figure 5.8: Fractional conversion of vaporized KCl to K_2SO_4 as a function of O_2 concentration in an entrained flow reactor at 1373 K. Symbols denote experimental results [23], lines denote modeling result (model C). Inlet conditions contained 2 % SO_2, 10 % H_2O, N_2 to balanced and KCl feed rate : 0,24 g/min
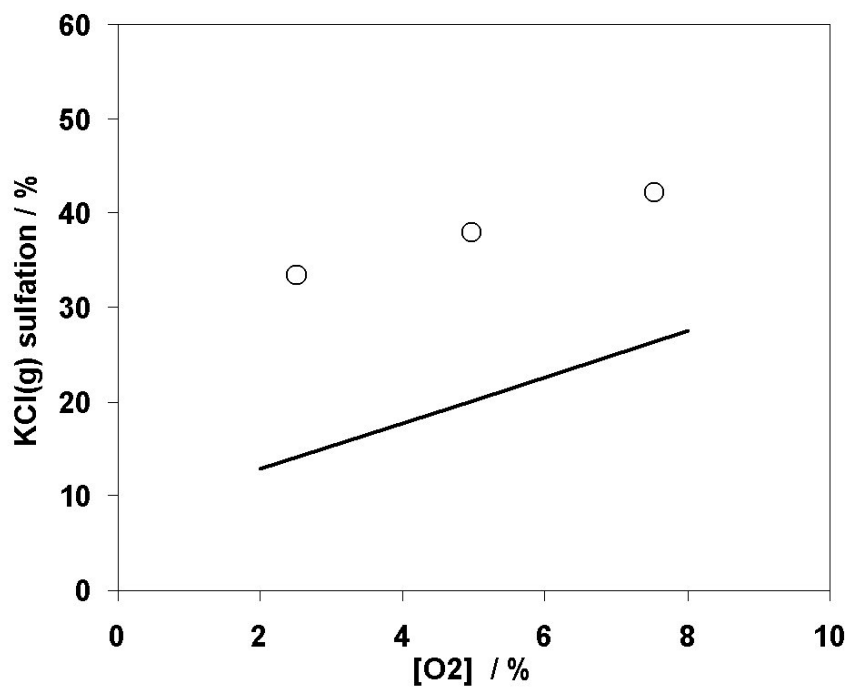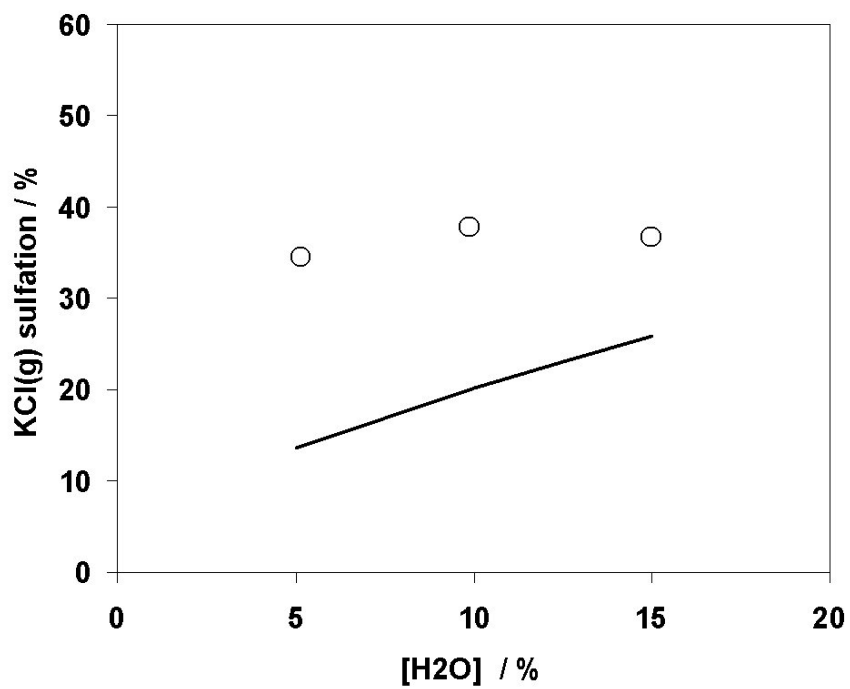
Figure 5.9: Fractional conversion of vaporized KCl to K_2SO_4 as a function of H_2O concentration in an entrained flow reactor at 1373 K. Symbols denote experimental results [23], lines denote modeling result (model C). Inlet conditions contained 2 % SO_2, 5 % O_2, N_2 to balanced and KCl feed rate : 0,24 g/min

and Ballester [114] the degree of sulfation from the experiments are significantly higher than the predicted values from the homogeneous models. In these cases, it seems that apart from the homogeneous mechanism involving K/O/H/Cl/S, some unknown mechanism for sulfate aerosol formation may be active. In order to investigate further the mechanisms which may be active in the system investigated [17], a discussion of the possible catalytic reactions in the system is presented. Independent of whether the sulfation process occurs mainly through a homogeneous or a heterogeneous mechanism, experimental evidence indicate that the availability of SO_3 in the system has a significant role. As discussed in the literature [29, 44, 48] the heterogeneous sulfation is promoted by the availability of SO_3 in the system. The sulfation of molten alkali chloride is suggested to be significantly faster compared to the solid alkali chloride sulfation [23]. At short residence times (a few seconds) as investigated in the present study, it is unlikely that a solid alkali chloride sulfation process is involved. Little is known about the sulfation of molten alkali chloride, but even in the presence of SO_3, it is a comparatively slow process [23]. Therefore in the present study, it seems that a homogeneous mechanism is active and the availability of SO_3 in the system has a significant role. The author's hypothesis is that the SO_3 formation rate is enhanced by catalytic reactions. This issue is discussed further below.

5.3.4   Model D

Field measurements [10, 116] of straw and other alkali containing biomass fuels usually show levels of sulfate similar to those observed by Jensen et al. [17] in the submicron aerosol particles formed by gas-to-particle conversion. Christensen et al. [10] concluded from analysis of data from combustion of several straw types that the observed level of sulfate formation is explained by a chemical equilibrium for the sulfation reaction being established in the gas phase at temperatures exceeding approximately 1073 K. The levels of sulfate formation in these studies are quite inconsistent with the much lower rate of gas phase sulfur dioxide oxidation computed by model A-C and support the suggestion that catalytic reactions may be involved in the sulfate aerosol formation.

A range of solids present in combustion systems has been shown to catalyze SO_2 oxidation. Fly ash has been shown in several studies to be an efficient catalyst. It has been observed that submicron-ash may catalyze the SO_2 oxidation to SO_3 in the convective passes of a coal-fired utility boiler, depending on the fuel, combustion conditions, and temperature profile in the convective section [58]. Both the iron oxide content [58, 59] and the calcium content [58] of the fly ash are important for the catalytic activity. A labo-

ratory study by Marier and Dibbs [59] showed that the degree of oxidation of SO_2 in the presence of fly ash was 10 - 30 %, increasing linearly with the iron oxide content of the ash, compared to a conversion below 1% in the absence of fly-ash. Graham and Sarofim [58] used submicrometer CaO to study the inorganic aerosols and their role in catalyzing sulfuric acid production in furnaces. The sulfation reaction of submicrometer CaO was reported to be fast. Also iron oxides on boiler walls and tube furnaces may be active as catalysts. A study on emissions of sulfur trioxide from coal-fired power plants [60] indicates that formation of SO_3 may be catalyzed by iron oxides at lower temperatures (427-593 °C) in the economizer region of the boiler. This formation depends on site-specific factors (e.g. cleanliness of the tube surfaces). An investigation on the SO_3 formation in a fluidized bed done by Dennis and Hayhurst [57] indicated that while homogeneous reactions results in a very minor conversion, heterogeneous catalytic reactions on the surface of the sand is active in the oxidation.

Under the experimental conditions of Jensen et al. [17] with the high reported sulfation levels, it is conceivable that the K_2SO_4-formation involves catalytic oxidation of SO_2 to SO_3. The available surfaces include the alumina reactor wall, a steel grid in the alkali feeder, alkali deposits in the feeding section, and alkali aerosols fed to the system or generated during reaction. Steel and to a lesser extent alumina have been shown to catalyze oxidation of SO_2 [117]. There are indications that also alkali metals may promote SO_2 oxidation. Experimental data by Zeuthen [118], obtained in the same set-up as that used by Jensen et al. [17], indicate that presence of K_2SO_4 nuclei promotes additional K_2SO_4 formation in the system. Experiments on sulfate aerosol formation with and without seed particles and with and without 50 ppm SO_2 (other inlet conditions are kept constant, 200 ppm KCl, 5 % H_2O and 5% O_2) show that while seed particles of K_2SO_4 will suppress nucleation of KCl it does not suppress nucleation of K_2SO_4, but the size of the particles is increased [118]. This can be explained by an increased formation of SO_3 on the surface of the particles prior to the K_2SO_4 nucleation. Henriksson and Warnqvist [47] proposed a mechanism for the heterogeneous reaction of solid NaCl by SO_2 in the absence of SO_3. According to their analysis, SO_2 and O_2 are adsorbed on the NaCl surface, and the adsorbed species react to form adsorbed SO_3 (SO_3(ads)). The SO_3(ads) reacts with adsorbed water and NaCl to form HCl and Na_2SO_4. The intermediates were proposed to be H_2SO_4(ads) and $NaHSO_4$(ads).

To assess whether surfaces in the inlet KCl feeding system may have acted as a catalyst for SO_3 formation, calculations using model C were conducted, assuming SO_2/SO_3 to be in equilibrium right after the feeder (around 990 K). The results are shown in Figure 5.10. The modeling predictions provide a

fairly close agreement with the experimental data of Jensen et al. According to the calculations, oxidation of SO_2 to SO_3 downstream of the feeder is negligible due to the low temperature. The SO_3 formed is largely converted to K_2SO_4, while $[SO_2]$ remains at the equilibrium value. These calculations also explain the lack of temperature dependence of the sulfation rate; the reactor peak temperature is downstream of the feeder where the catalyzed reaction takes place. From these calculations it is plausible that the solid surfaces in the KCl feeding system catalyze SO_2 oxidation, approaching an equilibrium concentration of SO_3 prior to the gas phase system where it reacts with other inlet gases to form K_2SO_4.

In the last modeling approach (model D), the possible scenario that K_2SO_4 aerosols, once formed, promote further SO_2 oxidation is investigated. Since the details of the catalytic mechanism is not known, a simplified approach will be taken, involving addition of a catalytic reaction to the homogeneous gas phase model A. The aerosol formation is modeled with a clustering approach, where a number of K_2SO_4 molecules will recombine to form a larger molecule. Eventually this molecule reaches a critical cluster number and precipitates to form a solid aerosol particle. The aerosol particle formed then acts as a catalyst for the further sulfation process by enhancing SO_3 formation in the system. The detailed modeling for the clustering phenomena is presented below.

Potassium sulfate nucleation can be modeled by a chemical clustering approach where gaseous potassium sulfate is allowed to cluster to form larger species by sequential polymerization steps. The value of the rate constant used in each step is assumed to be similar to that of the dimerization reaction NaCl+NaCl [14], which has been measured experimentally. Here, K_2SO_4 is treated as a monomer for the subsequent clustering process i.e.,

$$K_2SO_4 + K_2SO_4 \rightarrow (K_2SO_4)_2$$

$$(K_2SO_4)_2 + K_2SO_4 \rightarrow (K_2SO_4)_3$$

$$(K_2SO_4)_{n-1} + K_2SO_4 \rightarrow \text{Aerosol}$$

This sequence of irreversible reactions $(K_2SO_4)_{n-1} + K_2SO_4 \rightarrow (K_2SO_4)_n$ ($2 \leq n \leq 10$), with the nucleation taken to be completed for n = 10, can be used to assess the potential importance of homogeneous nucleation of K_2SO_4 from its gaseous form. The critical nucleus size of 10 potassium sulfate molecules is just a coarse estimation, the number can be in range of 1 to infinite, depending on the saturation ratio.

The rate of catalytic reaction by solid particles surfaces is estimated from gas kinetic theory following Gustavsson et al. [119]. The catalytic reaction
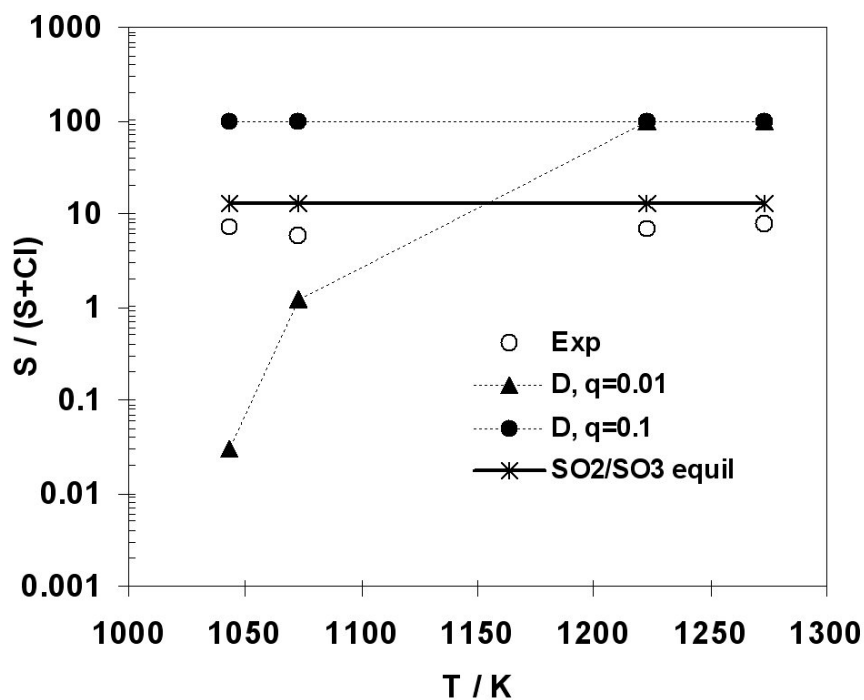
Figure 5.10: Comparison of model predictions (lines) with the experimental data from Jensen et al. [17] (open symbols), presented as $\frac{S}{(S+Cl)}$ in the aerosols. Results from predictions with model C, assuming that SO_2/SO_3 is in equilibrium at the inlet to the homogeneous gas phase system (after KCl feeding) are shown as a solid line. Results obtained with model D, using k_2 with collision efficiencies of 0.01 and 0.1, are shown as dotted lines. Inlet conditions contained 200 ppm KCl, 200 ppm SO_2, 4 % O_2, 4 % H_2O, N_2 to balanced. The peak temperature is varied from 1043, 1073, 1223, or 1273 K, and residence time is around 3 s.

is assumed as a pseudo second order reaction where the reaction rate (r_{SO_2}) = k[SO₂][Aerosol]= k_{cat}[SO₂]. Here k (cm³ mol⁻¹ s⁻¹) = k_{cat} (s⁻¹)/[aerosol]. And k_{cat} (s⁻¹) is the catalytic reaction of SO₂ by aerosol particles. The rate of collision between aerosol particles and SO₂ were calculated from the kinetic theory of gases. The aerosol particles are assumed to have zero velocity, since they are large compared with the gas phase species. The collision frequency, Z_{SO_2} (s⁻¹)= ν_{SO_2} n_p σ. The average velocity of SO₂ can be calculated as ν_{SO_2} (cm s⁻¹)=$\sqrt{3RT/M_{SO_2}}$, where n_p (cm⁻³) is the particle number density, and σ (cm²)= π r_p^2 is the collision cross section. The rate of catalytic SO₂ oxidation by aerosol particles then is k_{cat} (s⁻¹)= z_{SO_2} q_{SO_2}, where q_{SO_2} is the collision efficiency (the value is below or equal to 1). The particle number density (n_p) can be calculated from the aerosol concentration.

Particle agglomeration is not accounted for in this simplified model and two approaches have been adopted in the calculations. In the first approach (case 1) it is assumed that the agglomeration occurs immediately, resulting in a particle diameter similar to that reported by Jensen et al. [17], d_p=159 nm. This corresponds to a pseudo second-order rate constant of k_1= 2.4 · 10¹⁶ · T⁰·⁵ · q_{SO_2} (cm³ mol⁻¹ s⁻¹). In the second approach (case 2), no agglomeration is assumed, corresponding to d_p=1.36 nm (calculated from n=10, spherical particle) and k_2= 1.7 · 10¹² · T⁰·⁵ · q_{SO_2} (cm³ mol⁻¹ s⁻¹).

Model predictions for approach 2 are compared to the experimental data of Jensen et al. [17] in figure 5.10. Similar results are obtained for case 1. Collision efficiencies in the range 0.01 < q_{SO_2} < 0.1 cover the experimental data for most of the different peak temperatures (1043–1273 K). However, even with the assumed zero activation energy of the surface reaction, the predicted temperature dependence of the sulfation rate is considerable, in contrast to the experimental observations. For this reason, it appears unlikely that alkali sulfate aerosols strongly promote SO₂ oxidation in the investigated system.

The gas phase model consistently underpredicts the sulfate formation in the experiments of Iisa et al. [23], Jensen et al. [17], and Jimenez and Ballester [114]. The difference compared to the data of Iisa et al., about a factor of 2, may be caused by uncertainties in the gas phase mechanism. However, the underprediction of the sulfation rate observed by Jensen et al. and Jimenez and Ballester is an order of magnitude or higher. We attribute the higher observed sulfation rate mainly to presence of surfaces that may catalyze oxidation of SO₂. In the experiments of Jensen et al., reactor and deposit surfaces may be active, while for the conditions of Jimenez and Ballester the presence of fly ash may be of importance. However, the results of the present study are consistent with the previous finding that sulfate aerosol formation

occurs from homogeneous nucleation, following oxidation of SO_2 to SO_3 (or KSO_4). The sulfate aerosol formation is influenced by the SO_2, O_2, KCl inlet concentrations, residence time and temperature history. Apart from the SO_3 formation, other aspects such as reactions of SO_2 and O_2 with K-containing species or catalytic reaction by solid surfaces may be important limiting step in the sulfation process under present conditions investigated.

5.4 Conclusions

The K/O/H/Cl chemistry, sulfur chemistry, and their interaction (K/O/H/Cl/S chemistry) have been used to evaluate the degree of sulfation from available experimental data [17, 23, 114]. In general the modeling results underpredict the experimental data on the degree of sulfation and aerosol formation. Since the K/O/H/Cl and sulfur chemistry are quite valid, the underprediction may be attributed partly to the uncertainties in the K/O/H/Cl/S chemistry.

In this study, the sulfate aerosols formation was modeled using four different approaches (models A,B,C and D). The homogeneous gas phase models (A,B,C) in general underpredicts the experimental data on the degree of sulfation. The underprediction for the experimental data of Iisa et al. [23] by the model is around factor of 2. This may be attributed to the uncertainties in the gas phase K/O/H/Cl/S chemistry. However, the underprediction of the sulfation rate observed by Jensen et al. and Jimenez and Ballester is an order of magnitude or higher. The higher observed sulfation rate may be attributed mainly to the presence of surfaces that may catalyze oxidation of SO_2. In the experiments of Jensen et al., reactor and deposit surfaces may be active, while for the conditions of Jimenez and Ballester the presence of fly ash may be of importance. In general, the sulfate aerosols formation is influenced by the SO_2, O_2, KCl inlet concentrations, residence time and temperature history. Apart from the SO_3 formation, other aspects such as reactions of SO_2 and O_2 with K-containing species or solid surfaces may be important for the sulfation process under the conditions investigated in this study. Finally, experiments in a rigorously homogeneous system is needed to verify the proposed gas-phase sulfation mechanism and to gain more insight into the fundamental mechanisms controlling the sulfate aerosols formation which can be used for model improvement.

Chapter 6

General Conclusions

The objective of this project has been to improve the fundamental knowledge of the gas phase chemistry which is important for the gaseous emissions, aerosol or deposit formation during combustion of biomass and waste. The aim is to improve the available detailed chemical kinetic model for conversion of chlorine, sulfur and alkali-containing species and their interaction at high temperatures.

In the present work, the detailed kinetic model for gas phase sulfur, chlorine, alkali metal, and their interaction has been updated. The K/O/H/Cl chemistry, S chemistry, and their interaction can reasonably predict experimental data.

In general, understanding of the interaction between K-containing species and radical pool under combustion conditions has been improved. The available K/O/H/Cl chemistry has been updated by using both experimental work and detailed kinetic modeling. The experimental work was done by introducing gaseous KCl to CO oxidation system under reducing conditions. The experiments were performed using a laboratory flow reactor at atmospheric pressure and temperatures in the range of 773-1373 K, varying the CO inlet concentration and the KCl level. The addition of KCl results in a strong inhibition of the CO oxidation. The inhibition increases with the KCl level, but the effect levels off at high concentrations. The experimental data were interpreted in terms of a detailed chemical kinetic model and used to update the K/O/H/Cl chemistry. In general a satisfactory agreement between experimental data and kinetic modeling was achieved.

The oxidation of SO_2 to SO_3 under combustion conditions has been suggested to be the rate limiting step in the gaseous sulfation process prior to aerosol formation. While the overall mechanisms for SO_3 formation and destruction are fairly well known, kinetic modeling of the process still suffers from a lack of accurate kinetic data, and refinements are required in order to

establish a reliable mechanism. In this study, the sulfur chemistry important for the SO_2/SO_3 ratio under combustion conditions has been updated. In general the uncertainties of the important rate constants have been minimized. The mechanism of SO_3 formation and destruction has been better understood. Modeling predictions with a revised reaction mechanism for SO_2/SO_3 chemistry are in a good agreement with a range of experimental data from reactor experiments. The calculations indicate that oxidation of SO_2 to SO_3 with and without the presence of combustibles involve primarily recombination of SO_2 with O and OH radicals. Reaction SO_3+H may limit the SO_3 concentration, while reactions SO_3 with O or OH are unimportant for the SO_2/SO_3 ratio under most conditions of interest. The ratio of SO_2/SO_3 in the gas phase system is mainly determined by reactions SO_2 +O/OH, reactions involving intermediate $HOSO_2$, and reaction SO_3+H.

There has been a controversy regarding the fundamental mechanism of the sulfate aerosol formation. Alkali sulfate aerosol formation may either be initiated in the gas phase by homogeneous mechanism, or it may only involve a heterogeneous mechanism. In this PhD project, the updated K/O/H/Cl and S chemistry, also the interaction of those chemistry are used to investigate the importance of homogeneous gas phase sulfation process prior to aerosol formation. The results of the present study suggest that homogeneous gas phase sulfation may be active. However, heterogeneous mechanism involving catalytic oxidation of SO_2 by solid surfaces may also be active in the system investigated.

The homogeneous gas phase model for sulfation has been evaluated using experimental data available in the literature. The sulfate aerosols formation was modeled using four different approaches (models A,B,C and D). The homogeneous gas phase models (A,B,C) in general underpredicts the experimental data on the degree of sulfation. The underprediction for the experimental data of Iisa et al. [23] by the model is around factor of 2. This may be attributed to the uncertainties in the K/O/H/Cl/S chemistry. However, the underprediction of the sulfation rate observed by Jensen et al. and Jimenez and Ballester is an order of magnitude or higher. The higher observed sulfation rate may be attributed mainly to the presence of surfaces that may catalyze oxidation of SO_2. In the experiments of Jensen et al., reactor and deposit surfaces may be active, while for the conditions of Jimenez and Ballester the presence of fly ash may be of importance. In general, the sulfate aerosols formation is influenced by the SO_2, O_2, KCl inlet concentrations, residence time and temperature history. Apart from oxidation of SO_2 to SO_3, other aspects such as reactions of SO_2 and O_2 with K-containing species or solid surfaces may play an important role in the sulfation process under the conditions investigated in this study.

Chapter 7

Practical Applications and Future Work

In general, the results of chemistry in the present work can be implemented in reactor models and used to simulate the effect of fuel and process parameters on emissions and operation. The detailed kinetic model can be used to simulate gas phase potassium, chlorine, sulfur chemistry and their interaction under combustion conditions and cooling of the flue gas. The detailed kinetic modeling offers a tool to predict gas phase system of those species and their interaction of any interest.

The sulfur chemistry can be used to predict sulfur emission during coal or heavy fuel combustion under oxidizing conditions. The K/O/H/Cl/S chemistry can be used to predict the homogeneous sulfation process and aerosols formation during straw, wood or black liquor combustion (with additional Na subset), however some catalytic reactions may need to be taken into account. Apart from that, the model may also be used to simulate the reduction of NO/CO/S/Cl emissions by addition of K-containing additives. The mechanism of those pollution control processes may actually involve homogeneous gas phase reactions. Part of the model can also be used to investigate mechanism of K-containing additives involved in the reduction of carbon deposit during steam reforming.

With increasing the use of fuel blending (i.e. biomass and coal), the amounts of trace species of alkali metal, Cl, S can be varied, which may be an advantage of pollution control using the way pollutants interact. It seems that sulfur oxides, chlorine species, and alkali metals have the ability to either promote or inhibit reaction, depending on the reaction conditions.

For future work, more experimental study to investigate K/O/H/Cl chemistry in a broader range of operational conditions and alkali precursors is necessary in order to minimize the uncertainties in the mechanism and the

rate constants. Furthermore, more experimental work to investigate the sulfation process under combustion conditions and cooling of the flue gases are necessary in order to gain more insight into the fundamental mechanisms controlling the sulfate aerosol formation. In addition, experiments in a rigorously homogeneous system is called for to verify the proposed homogeneous sulfation mechanism.

Bibliography

[1] B. Sander. *Biomass Bioenergy*, 12:177–183, 1997.

[2] J.N. Knudsen, P.A. Jensen, W.G. Lin, F. Frandsen, and K. Dam-Johansen. *Energy Fuels*, 18:810–819, 2004.

[3] D.C. Dayton, R.J. French, and T.A. Milne. *Energy Fuels*, 9:855–865, 1995.

[4] D.C. Dayton, B.M. Jenkins, S.Q. Turn, R.R. Bakker, R.B. Williams, D. Belle-Oudry, and L.M. Hill. *Energy Fuels*, 13:860–870, 1999.

[5] P.A. Jensen, F.J. Frandsen, K. Dam-Johansen, and B. Sander. *Energy Fuels*, 14:1280–1285, 2000.

[6] J.N. Knudsen, P.A. Jensen, and K. Dam-Johansen. *Energy Fuels*, 18:1385–1399, 2004.

[7] D.C. Dayton and W.J. Frederick Jr. *Energy Fuels*, 10:284–292, 1996.

[8] J.N. Knudsen. *PhD Thesis, Technical University of Denmark*, ISBN 87-91435-11-0, 2004.

[9] S.C. van Lith, V.A. Ramirez, P.A. Jensen, F.J. Frandsen, and P. Glarborg. *Energy Fuels*, 20:964–978, 2006.

[10] K.A. Christensen, M. Stenholm, and H.Livbjerg. *J. Aerosol Sci.*, 294:421–444, 1998.

[11] C.F. Cullis and M.F.R. Mulcahy. *Combust. Flame*, 18:225–292, 1972.

[12] P. Glarborg. *Proc. Combust. Inst.*, 31:77–98, 2007.

[13] S.C. van Lith. *PhD Thesis, Technical University of Denmark*, ISBN 87-91435-29-3, 2005.

[14] P. Glarborg and P. Marshall. *Combust. Flame*, 141:22–39, 2005.

[15] H. Livbjerg. *International Seminar organised on behalf of International Energy Agency (IEA), Bioenergy Task 32 : Biomass Combustion and Cofiring*, 2001.

[16] J.T. Johannesen, K.A. Christensen, O. Simonsen, and H. Livbjerg. *Chem. Eng. Sci.*, 52:2541–2556, 1997.

[17] J.R. Jensen, L.B. Nielsen, C. Schultz-Møller, S.Wedel, and H.Livbjerg. *Aerosol Sci. Technol.*, 2000.

[18] K.A. Christensen and H.Livbjerg. *Aerosol Sci. Technol.*, 33:470–489, 2000.

[19] K.A. Christensen and H.Livbjerg. *Aerosol Sci. Technol.*, 25:185–199, 1996.

[20] F. Frandsen. *PhD Thesis, Technical University of Denmark*, ISBN 87-90142-03-9, 1995.

[21] H.P. Nielsen. *PhD Thesis, Technical University of Denmark*, ISBN 87-90142-47-0, 1998.

[22] P.A. Jensen, M. Stenholm, and P. Hald. *Energy Fuels*, 11:1048, 1997.

[23] K. Iisa, Y. Lu, and K. Salmenoja. *Energy Fuels*, 13:1184–1190, 1999.

[24] K. Salmenoja and K. Makela. *J. Inst. Energy*, 69:155, 1996.

[25] H.P. Michelsen, F. Frandsen, K. Dam-Johansen, and O.H. Larsen. *Fuel Proc. Tech.*, 54:95–108, 1998.

[26] S. Srinivasachar, J.J. Helble, D.O. Ham, and G. Domazetis. *Prog. Energy Combust. Sci.*, 16:303–309, 1990.

[27] C.A. Stearns, R.A. Miller, F.J. Kohl, and G.C. Fryburg. *J. Electrochem. Soc.*, 124:1145–1146, 1977.

[28] F.J. Kohl, G.J. Santoro, C.A. Stearns, and D.E. Rosner. *J. Electrochem. Soc.*, 126:1054–1061, 1979.

[29] W.L. Fielder, C.A. Stearns, and F.J. Kohl. *J. Electrochem. Soc.*, pages 2414–2417, 1984.

[30] M. Steinberg and K. Schofield. *Prog. Energy Combust. Sci.*, 16:311–317, 1990.

[31] M. Steinberg and K. Schofield. *Proc. Combust. Inst.*, 26:1835–1843, 1996.

[32] K. Schofield and M. Steinberg. *J. Chem. Phys.*, 96:715–726, 1992.

[33] R.A. Durie, J.W. Milne, and M.Y. Smith. *Combust. Flame*, 30:221–230, 1977.

[34] M.Steinberg and K. Schofield. *Combust. Flame*, 129:453–470, 2000.

[35] J.W. Hastie, E.R. Plante, and D.W. Bonnell. *ACS Symp. Ser.*, 179:543–600, 1982.

[36] P.J. Ficalora, O.M. Uy, D.W. Muenow, and J.L. Margrave. *J. Ceram. Soc.*, 51:574–577, 1968.

[37] I. Eliezer and R.A. Howald. *J. Chem. Phys.*, 65:3053–3062, 1976.

[38] D. Cubiciotti and F.J. Kenesha. *High. Temp. Sci.*, 4:32–40, 1972.

[39] R.E. Fryxell, C.A. Trythall, and R.J. Perkins. *Corrosion*, 29:423–428, 1973.

[40] J.C. Halle and K.H. Stern. *J. Phys. Chem.*, 84:1699–1704, 1980.

[41] K.H.Lau, R.D. Brittain, R.H. Lamoreaux, and D.L. Hildenbrand. *J. Electrochem. Soc.*, 132:3041–3048, 1985.

[42] V.Sricharoenchaikul, W.J. Frederick Jr., and T.M. Grace. *J. Pulp Paper Sci.*, 23:394–400, 1997.

[43] A.B.Anderson and N.C. Debnath. *J. Phys. Chem.*, 87:1938–1941, 1983.

[44] A.B.Anderson. *J. Am. Chem. Soc.*, 106:6262–6265, 1984.

[45] M. Steinberg and K. Schofield. *Combust. Flame*, 129:453–470, 2002.

[46] L.Boonsongsup, K. Iisa, and Jr. W.J. Frederick. *Ind. Eng. Chem. Res.*, 36:4212–4216, 1997.

[47] M. Henriksson and B. Warnqvist. *Ind.Eng.Chem.Process Des. Dev.*, 18:249–253, 1979.

[48] J.A.B. Satrio, S.B. Jagtap, and T.D. Wheelock. *Ind. Eng. Chem. Res.*, 41:3540–3547, 2002.

[49] S. Ozawa, K. Ito, and H. Matsuda. *Kagaku Kogaku Ronbushu*, 28:396–404, 2002.

[50] K. Schofield and M. Steinberg. *J. Phys. Chem.*, 96:715–726, 1992.

[51] J. Latva-Somppi, M. Moisio, E.L. Kauppinen, T. Valmari, P. Ahonen, and J. Keskinen. *J. Aerosol Sci.*, 29:461–480, 1998.

[52] A. Levy, E.L. Merryman, and W.T. Reid. *Environmental Sci. and Technol.*, 4:653–662, 1970.

[53] S.C. Hunter. *J. Eng. Power*, 104:44–51, 1982.

[54] A.B. Hedley. *J. Inst. Fuel*, 40:142, 1967.

[55] A. Dooley and G. Wittingham. *Trans. Faraday Soc.*, 42:354, 1946.

[56] D. Flint and A.W. Lindsay. *Fuel*, 30:288, 1952.

[57] J.S. Dennis and A.N. Hayhurst. *Combust. Flame*, 72:241–258, 1988.

[58] K.A. Graham and A.F. Sarofim. *J. Air Waste Manag. Ass.*, 48:106–112, 1998.

[59] P. Marier and H.P. Dibbs. *Thermochimica Acta*, 8:155–165, 1974.

[60] R.K. Srivastava, C.A. Miller, C. Erickson, and R. Jambhekar. *J. Air Waste Manag. Ass.*, 54(6):750–762, 2004.

[61] A.G. Gaydon. *Proc. Roy. Soc.*, 183A:111, 1944.

[62] C.P. Fenimore and G.W. Jones. *J. Phys. Chem*, 69:3593, 1965.

[63] P. Glarborg, D. Kubel, K. Dam Johansen, H. M. Chiang, and J.W. Bozzeli. *Int. J. Chem. Kinet.*, 28:773–790, 1996.

[64] J. Villadsen and H. Livbjerg. *Cat. Rev. Sci. Eng.*, 17(2):203–272, 1978.

[65] P. Glarborg, M.U. Alzueta, K. Kjaergaard, and K.Dam-Johansen. *Combust. Flame*, 132:629–638, 2003.

[66] J.A. Silver, A.C. Stanton, M.S. Zahniser, and C.E. Kolb. *J. Chem. Phys.*, 88:3123–3129, 1984.

[67] J.A. Silver and C.E. Kolb. *J. Phys. Chem.*, 90:3267–3269, 1986.

[68] J.M.C. Plane, B. Rajasekhar, and L. Bartolotti. *J. Chem. Phys.*, 91:6177–6186, 1989.

[69] M. Helmer and J.M.C. Plane. *J. Chem. Phys.*, 99:7696–7702, 1993.

[70] D.L. Baulch, J. Duxbury, S.J. Grant, and D.C. Montague. *J. Phys. Chem. Ref. Data Suppl.*, 10, 1981.

[71] O.I. Smith, S. Tseregounis, and S. N. Wang. *Ind. J. Inst. Energy*, 14:679, 1982.

[72] K.Chung, J.G. Calvert, and J.W. Bottenheim. *Int. J. Chem. Kinet.*, 7:161–182, 1975.

[73] M.U. Alzueta, R. Bilbao, and P. Glarborg. *Combust. Flame*, 127:2234, 2001.

[74] P. Dagaut, F. Lecomte, J. Mieritz, and P. Glarborg. *Int. J. Chem. Kinet.*, 35:564–575, 2003.

[75] A.Goumri, D. Laakso, J.D. Rocha, E. Francis, and P. Marshall. *J. Phys. Chem.*, 97:5295–5297, 1993.

[76] Y. Shi and P. Marshall. *J. Phys. Chem.*, 95:1654–1658, 1991.

[77] P.G. Ashmore. *Catalysis and Inhibition of Chemical Reactions*, Butterworths, London, 1963.

[78] The UCL Centre for Cosmic Chemistry and University College London Physics. http://www.chem.ucl.ac.uk/cosmicdust/er-lh.htm.

[79] A.J. Hynes, M. Steinberg, and K. Schofield. *J. Chem. Phys.*, 80:2585–2597, 1984.

[80] V.M. Zamansky, M.S. Sheldon, and P.M. Maly. *Proc. Combust. Inst.*, 27:3001–3008, 1998.

[81] V.M. Zamansky, P.M. Maly, L. Ho, V.V. Lissianski, D. Rusli, and W.C. Gardinger Jr. *Proc. Combust. Inst.*, 27:1443–1449, 1998.

[82] V.M. Zamansky, V.V. Lissianski, P.M. Maly, D. Rusli, and W.C. Gardinger Jr. *Combust. Flame*, 117:821–831, 1999.

[83] V.M. Zamansky, L. Ho, P.M. Maly, and W.R.Seeker. *Proc. Combust. Inst.*, 26:2075–2082, 1996.

[84] V.V. Lissianski, V.M. Zamansky, and P.M. Maly. *Combust. Flame*, 125:1118–1127, 2001.

[85] L. Hindiyarti, F. Frandsen, H. Livbjerg, and P. Glarborg. *Fuel*, 85:978–988, 2006.

[86] A.E.Lutz, R.J.Kee, and J.A. Miller. A Fortran Program for Predicting Homogeneous Gas Phase Chemical Kinetics with Sensitivity Analysis. Sandia National Laboratories, Report SAND87-8248, 1987.

[87] R.J.Kee, F. Rupley, and J.A. Miller. Chemkin II A Fortran Chemical Kinetics Package for the Analysis of Gas Phase Chemical Kinetics. Sandia National Laboratories, Report SAND89-8009, 1989.

[88] G. Klingenberg and J.M. Heimerl. *Prog. Astr. Aero.*, 139:241–260, 1992.

[89] P. Glarborg, D. Kubel, P.G. Kristensen, J. Hansen, and K. Dam-Johansen. *Combust. Sci. Technol.*, 110/111:461, 1995.

[90] C. Mueller, P. Kilpinen, and M. Hupa. *Combust. Flame*, 113:579–588, 1998.

[91] A.N. Baratov, L.P. Vogman, V.N. Kobzar, V.V. Azatyan, M.D. Museridze, Z.G. Dzotsenidze, D.I. Petviashvili, and M.A. Namoradze. *Combust. Explosions Shock Waves*, 12:61–64, 1976.

[92] M. Slack, J.W. Cox, A. Grillo, R. Ryan, and O. Smith. *Combust. Flame*, 77:311–320, 1989.

[93] D.E. Jensen, G.A. Jones, and A.C.H. Mace. *J. Chem. Soc. Faraday Trans I*, 75:2377–2385, 1979.

[94] D. Husain. *J. Chem. Soc. Faraday Trans. 2*, 85:85–130, 1989.

[95] D. Husain, J.M.C. Plane, and C.C.Xiang. *J. Chem. Soc. Faraday Trans. 2*, 80:1465, 1984.

[96] D. Husain, J.M.C. Plane, and C.C.Xiang. *J. Chem. Soc. Faraday Trans. 2*, 81:561, 1985.

[97] A.J. Hynes and M. Steinberg. *J. Chem. Phys*, 80:2585–2597, 1984.

[98] A. Yilmaz, L. Hindiyarti, A. Jensen, P. Glarborg, and P. Marshall. *J. Phys. Chem. A*, 110:6654–6659, 2006.

[99] L. Hindiyarti and P. Glarborg. *additional report*, 2006.

[100] L. Hindiyarti, P. Glarborg, and P. Marshall. *accepted to J. Phys. Chem. A*, 2007.

[101] M.A. Mueller, R.A. Yetter, and F.L. Dryer. *Int. J. Chem. Kin.*, 32:317–339, 2000.

[102] R. Atkinson and J.N. Pitts Jr. *Int. J. Chem. Kin.*, 10:1081–1090, 1978.

[103] D. Schwartz, R. Gadiou, J.F. Brilhac, G. Prado, and G. Martinez. *Ind. Eng. Chem. Res.*, 39:2183–2189., 2000.

[104] K. Schofield. *J. Phys. Chem. Ref. Data*, 2:25–84, 1973.

[105] N.A. Burdett, W.E. Langdon, and R.T. Squires. *J. Inst. Energy*, 57:373–376, 1984.

[106] E.L. Merryman and A. Levy. *Proc. Combust. Inst.*, 17:727–736, 1979.

[107] O.I. Smith, S. Tseregounis, and S.N. Wang. *Int. J. Chem. Kin.*, 14:679–697, 1982.

[108] O.I. Smith, S. Tseregounis, S.N. Wang, and C.K. Westbrook. *Combust. Sci. Technol.*, 30:241–271, 1983.

[109] C.L. Rasmussen, P. Glarborg, and P. Marshall. *Proc. Combust. Inst.*, 31:339–347, 2007.

[110] J. Naidoo, A. Goumri, and P. Marshall. *Proc. Combust. Inst.*, 30:1219–1225, 2005.

[111] P.G. Kristensen. *PhD Thesis, Department of Chemical Engineering, Technical University of Denmark*, ISBN 87-90142-18-7, 1997.

[112] D.C. Astholz, K. Glanzer, and J. Troe. *J. Chem. Phys.*, 70:2409–2413, 1979.

[113] M. Frenklach, J.H. Lee, J.N. White, and W.C. Gardinger JR. *Combust. Flame*, 41:1–16, 1981.

[114] S. Jimenez and J. Ballester. *Fuel*, 86:486–493, 2007.

[115] S. Jimenez and J. Ballester. *Combust. Flame*, 140:346–358, 2005.

[116] M. Joller, T. Brunner, and I. Obernberger. *Energy Fuels*, 19:311–323, 2005.

[117] T.L. Jørgensen, H. Livbjerg, and P. Glarborg. *submitted for publication*, 2007.

[118] J. Zeuthen. *PhD Thesis, Technical University of Denmark*, 2007.

[119] L. Gustavsson, P. Glarborg, and B. Leckner. *Combust. Flame*, 106:345–358, 1996.

Appendices

Paper I

Influence of Potassium Chloride on Moist CO Oxidation under Reducing
Conditions: Experimental and Kinetic Modeling Study.
(published in FUEL, 85, 978-988, 2006)

Paper II

Thermal Dissociation of SO_3 at 1100-1400 K.
(published in Journal of Physical Chemistry A, 110, 6654-6659, 2006)

Paper III

The Fate of SO_3/SO_2 in the System with N_2O Addition.
(additional report)

Paper IV

Reactions of SO_3 with O/H Radical Pool under Combustion Condition.
(accepted for publication in Journal of Physical Chemistry A, 2006)

Paper V

Mechanism of Alkali Sulfate Aerosols Formation during Biomass Combustion.
(accepted for publication in FUEL, 2007)

Paper I

Influence of potassium chloride on moist CO oxidation under reducing conditions: Experimental and kinetic modeling study

Lusi Hindiyarti, Flemming Frandsen, Hans Livbjerg, Peter Glarborg *

Department of Chemical Engineering, Technical University of Denmark, DK-2800 Lyngby, Denmark

Abstract

Experimental results on the influence of gas phase potassium on CO oxidation under reducing conditions have been obtained. The experiments were performed using a laboratory flow reactor at atmospheric pressure and temperatures in the range 773–1373 K, varying the CO inlet concentration and the KCl level. The addition of KCl results in a strong inhibition of the CO oxidation. The inhibition increases with the KCl level, but the effect levels off at high concentrations. The experimental data were interpreted in terms of a detailed chemical kinetic model. In general a satisfactory agreement between experimental data and kinetic modeling was achieved. Analysis of the modeling results indicates that the reaction $K + OH + M \rightleftharpoons KOH + M$ is rate controlling for the radical recombination. The experimental data support a high rate constant for this reaction, but an estimation of the value from the present work is difficult due to uncertainties in the potassium chemistry and in the experimental conditions. Experimental data in a wider range of conditions and alkali precursors are required for model improvement.
© 2005 Elsevier Ltd. All rights reserved.

Keywords: Alkali chemistry; Potassium; Radical recombination; Kinetics

1. Introduction

The concern of CO_2 emissions results in increasing use of biomass and its waste as fuels for energy and steam production. Biomass potentially used as fuel includes 1-year crops such as straw, which are known to have high a potassium and chlorine content in their structure. High concentrations of potassium and chlorine may increase fouling and corrosion problems in boilers, and potassium is also responsible for aerosol formation. Significant efforts in the past have focused on chlorine and sulfur chemistry, but the knowledge about alkali metal chemistry is still limited.

In high temperature flames, compounds containing halogen atoms are known to act as inhibitors (flame extinguishants) by catalyzing the recombination of H atoms and thus decreasing the radical pool [1]. Bulewicz and Janicka [2], found from experiments done in a laboratory-size fluidized bed combustor (FBC) that alkali metal halides affected the carbon monoxide level in the flue gases. The effect was similar if the halogen was introduced not as inorganic salt, but as volatile organic halide

(e.g. halon 1211, CF_2ClBr) or as a hydrogen halide. This indicated that the carbon monoxide level was controlled predominantly by gas phase interactions. It is known that CO is oxidized mainly by reacting with hydroxyl radical,

$$CO + OH \rightleftharpoons CO_2 + H$$
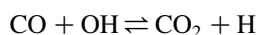
The inhibiting effect of the additives was explained in terms of a catalytic effect on free radical recombination, with the involvement of hydrogen halide molecules and free halogen atoms [3]. In the presence of free radical concentrations above equilibrium, the CO oxidation rate would decrease due to accelerated radical recombination.

Previous attempts to develop detailed reaction mechanisms for the potassium and sodium chemistry are limited. The first detailed mechanisms for alkali metal chemistry in flames were reported by Steinberg and co-workers [4–6]. They focused on alkali atom removal, catalyzed radical recombination, and sodium/sulfur interactions. Zamansky and co-workers [7–11] investigated sodium chemistry in relation to NO_x reduction in combustion and in reburning. In a recent kinetic study on gas phase potassium chemistry, Glarborg and Marshall [12] updated the thermochemistry and high-temperature gas-phase reaction mechanisms of sodium and potassium and proposed a mechanism for the gas phase formation of Na_2SO_4 and K_2SO_4.

Alkali-containing additives have been known for a long time as inhibitors on flame propagation [13]. Experiments have

---

* Corresponding author. Tel. +4525 2840; fax 4588 2258
E-mail address: pgl@kt.dtu.dk (P. Glarborg).

been reported from laminar premixed flames [4,14–23], laminar diffusion flames [24,25] and turbulent diffusion flames [26]. The inhibiting effect has been attributed mostly to gas phase radical removal reactions [14,24], but the mechanism is still in discussion. It is commonly believed that the most likely mechanism in fuel-rich flames is the sequence:

$$KOH + H \rightleftharpoons K + H_2O \tag{R15}$$

$$K + OH + M \rightleftharpoons KOH + M \tag{R2}$$

but other reactions have been proposed. The reaction numbers refer to the mechanism listed in Table 2.

Only a few flame studies have been sufficiently accurate to yield quantitative kinetic information. Jensen et al. [18] did flame-photometric measurements on the acceleration of H and OH radical recombination in flames by addition of potassium. Potassium was added in concentrations lower than 1000 ppm to fuel-rich, laminar, premixed, atmospheric-pressure H_2–O_2–N_2 flames. In the downstream region of these flames radical recombination occurs through the reactions:

$$H + H_2O \rightleftharpoons OH + H_2$$

$$H + H + M \rightleftharpoons H_2 + M$$

$$H + OH + M \rightleftharpoons H_2O + M$$
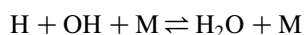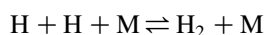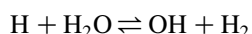
The observed acceleration of radical recombination in the presence of potassium was interpreted in terms of the gas phase reactions (R2) and (R15). Jensen et al. proposed that potassium-containing species other than K and KOH and flame species other than H, OH, H_2 and H_2O played no significant role in radical recombination in the flames. They based this on the assumption that such other species would have to undergo reactions with unreasonably high rate coefficients if these reactions were to compete with reactions (R2), (R15) and reactions involving the O/H radical pool. A similar mechanism was proposed for flames doped with sodium hydroxide [19].

The simple mechanism proposed by Jensen et al. has been questioned in later studies. Hynes et al. [4] found that the rate constant for $A + OH + M$ (A being Na or K) proposed by Jensen and coworkers [18,19] was too fast to be consistent with theory and proposed an additional reaction sequence involving an AO_2 adduct, for potassium:

$$K + O_2 + M \rightleftharpoons KO_2 + M \tag{R4}$$

$$KO_2 + H \rightleftharpoons KO + OH \tag{R18}$$

$$KO + H_2O \rightleftharpoons KOH + OH \tag{R13}$$

Slack et al. [22] measured hydroxyl radical decay rates in laminar atmospheric pressure CH_4–O_2–N_2–Ar flames. Their results were consistent with a five-reaction mechanism consisting of (R15, R2) + (R4, R18, R13) with a comparatively low value of the rate constant k_2, provided KO_2 has a sufficient thermal stability. However, the mechanism of (R15, R2) with

rate constants from Jensen et al. [18] also yielded a satisfactory agreement with their measurements.

The objective of the present work is to improve the understanding of potassium chemistry and its interactions with the radical pool in combustion by studying the effect of KCl on CO oxidation in a flow reactor under reducing conditions and 873–1373 K. The work involves both experiments and a kinetic modeling study. The moist CO oxidation system is well suited for studying additive interaction with the radical pool, since the reaction mechanism for CO is well established. A better understanding of the gas phase potassium chemistry may facilitate development of more efficient methods to minimize emission and operation problems in biomass or waste combustion systems.

2. Experimental

The experiments were done in an alumina tube reactor to simulate plug flow under well-controlled reaction conditions. The reactor design was similar to that used in previous experiments [27,28]. A schematic of the reactor can be seen in Fig. 1. The inner diameter of the main tube was 24 mm and it had a wall thickness of 3 mm. The length of the reactor and reaction zones was 750 and 300 mm, respectively. The alumina inner tube for KCl feeding was 12 mm in diameter and 150 mm in length, with a wall thickness of 2 mm.

The reactor inlet consisted of main and secondary inlet flows. Potassium was fed by saturating a nitrogen flow from the main inlet with potassium vapor in a packed bed of inert porous alumina pellets impregnated with potassium chloride. The packed bed of pellets was inserted in the inner tube close to the entrance section of the reactor. It was critical to maintain
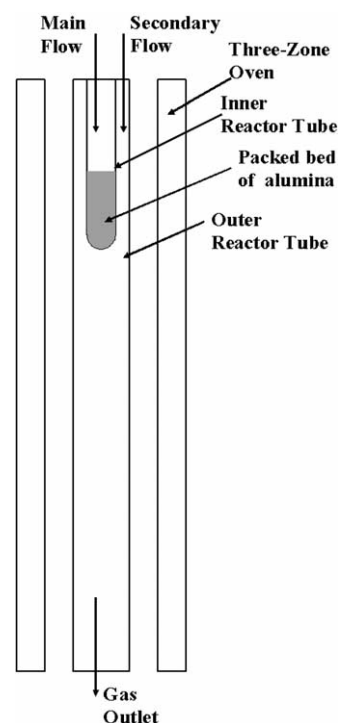

Fig. 1. A schematic of the reactor used in experiments.

a constant temperature in the potassium feeding section in order to get a certain amount of potassium vapor. In order to avoid contact with the KCl in the pellets, the reactive gas was fed to the secondary flow. The two inlet flows were merged at the end of the inner tube. A reactor set-up equipped with a three-heating-zone oven was used for the experiment. The separate heating zones were useful to maintain a constant temperature in the KCl feeding tube, and a certain setting temperature in the reaction zones.

The alumina pellets were prepared by heating them in an oven at a temperature of about 573 K for one day to remove the volatiles. Then the pellets were impregnated with a saturated KCl solution for about one day, and the slurry was filtered in order to separate the particles. The particles were gently flushed with water before being placed in an oven for 24 h at 473 K. The KCl solution was prepared by adding a sufficient amount of solid KCl in a beaker glass filled with distilled water, applying continuous agitation to the slurry until no more solid KCl dissolved in the water.

For the present investigation a total gas flow of about 1 NL/min was used. Feed gases contained CO, H_2O, and N_2. Two different CO inlet concentrations were used in the experiments and the amount of KCl vapor was varied by setting the flow to the alumina packed bed. The gas outlet was analyzed for CO and CO_2 after gas conditioning. The uncertainty in the CO and CO_2 gas analyzers used was around 4% of the measurement range. Pure CO oxidation experiments were done for reference.

The temperature profile along the reactor was measured by a K type thermocouple, which was displaced axially in small steps, allowing sufficient time for stabilization of the temperature between each reading.

To obtain a mass balance for potassium chloride, the amount of potassium condensed on the tube wall was measured. The alumina tube was withdrawn and flushed with distilled water. The wall condensate of potassium chloride was analyzed from the electrical conductivity of the flushed water.

3. Kinetic modeling

The Senkin code [29] which runs in conjunction with Chemkin-II [30] was used to model the flow reactor experiments, assuming plug flow. The reaction mechanism and thermodynamic properties used in this study were drawn

mainly from the work of Glarborg and Marshall [12]. Table 1 contains thermodynamic data for the key species, while rate coefficients for important reactions in the potassium subset are listed in Table 2.

The thermodynamic properties of alkali species from Glarborg and Marshall [12] were drawn from their own calculations, from data evaluations [31–33], and from recent high-level theoretical work [34–41]. Even though thermodynamic properties for alkali metals are surprisingly demanding to estimate theoretically [41], the theoretical work has narrowed the error margins for a number of the alkali oxide and hydroxide species significantly. In particular the bond energies of the alkali super oxides NaO_2 and KO_2 have been the subject of significant controversy in the past. Results from flame studies [6] and from observations of the equilibration of the $Na + O_2 + M = NaO_2 + M$ reaction [42,43] indicated a strong bond for NaO_2, of the order of 230–243 kJ/mol. However, these results appear to be in error, possibly due to underestimation of the NaO_2 consumption rates in the investigated systems [44]. The high value for the NaO_2 bond strength would make this species more stable than NaOH at intermediate temperatures, in conflict with experimental observations [45]. Theoretical studies [35,43,46,47] suggest a value of D_0 $(Na–O_2)$ of 151–159 kJ/mol, in reasonable agreement with estimates from mass spectrometric-effusion cell [48] and ionization potential experiments [49]. Glarborg and Marshall proposed a value of D_0 $(Na–O_2)$ of 151 kJ/mol [35,43], corresponding to $H_{f,298}$ $(NaO_2) = -46.0$ kJ/mol. Also the bond energy of KO_2 has been in question, but recent theoretical work favor values of 168–170 kJ/mol [39,47]. We adopt the recommendation of Glarborg and Marshall of D_0 $(K–O_2)$ of 169 kJ/mol, corresponding to $H_{f,298}$ $(KO_2) = -67.0$ kJ/mol. It is noteworthy that with the revised lower bond energies for KO_2 and NaO_2, these species are unlikely to play a major role for radical recombination in flames.

For NaOH and KOH the JANAF tables [31] report significant uncertainties in the heat of formation. Recent investigations for NaOH [32,37,41] are in fairly good agreement and have narrowed the error margin for this component. For KOH the uncertainty is larger. Based on an evaluation of available published data Gurvich et al. [33] proposed a heat of formation for KOH of -232 ± 3 kJ/mol, while Lee and Wright [40] estimate a value of -222 ± 4 kJ/mol from ab initio calculations. In the present work we have

Table 1
Thermodynamic properties for selected alkali species.

Species	$H_{f,298}$	S_{298}	$C_{p,300}$	$C_{p,400}$	$C_{p,500}$	$C_{p,600}$	$C_{p,800}$	$C_{p,1000}$	$C_{p,1500}$	Source
K	89.00	160.3	20.79	20.79	20.79	20.79	20.79	20.79	20.80	[31]
KH	123.1	198.0	31.11	32.70	34.00	35.05	36.39	37.14	38.23	[31]
KO	55.18	238.0	35.98	36.78	37.22	37.51	37.91	38.19	38.76	[31,38]
KOH	-222.0	238.3	49.24	51.18	52.18	52.81	53.76	54.71	57.02	[33,40]
(KOH)₂	-641.0	342.9	105.7	110.1	112.4	113.7	115.7	117.7	122.3	[33]
KO	-67.0	268.7	48.32	50.85	52.64	53.92	55.51	56.38	57.34	[39,47]
KCl	-214.7	239.1	36.51	37.06	37.36	37.57	37.85	38.06	38.50	[31]
(KCl)₂	-617.6	352.9	80.89	81.86	82.31	82.57	82.82	82.93	83.05	[31]

Units are kJ/mol ($H_{f,298}$) and J/mol-K (S_{298}, C_p).

Table 2
Rate coefficients for key reactions in the reaction mechanism

No	Reaction	A	N	E/R	Source
1.	$K+O+M \rightleftharpoons KO+M$	1.5×10^{21}	-1.50	0	Est[a], [62]
2.	$K+OH+M \rightleftharpoons KOH+M$	3.8×10^{19}	-0.65	0	See text
3.	$K+HO_2 \rightleftharpoons KOH+O$	1.0×10^{14}	0.0	0	Est[a]
4.	$K+O_2(+M) \rightleftharpoons KO_2(+M)$	1.2×10^{14}	0.00	0	Est[a], [63,64]
	Low pressure limit	5.4×10^{21}	-1.32	0	
5.	$K+H_2O_2 \rightleftharpoons KOH+OH$	2.5×10^{13}	0.00	0	Est[a], [65]
6.	$K+H_2O_2 \rightleftharpoons KO+H_2O$	1.6×10^{13}	0.00	0	Est[a], [65]
7.	$KO+H \rightleftharpoons K+OH$	2.0×10^{14}	0.00	0	Est[a]
8.	$KO+O \rightleftharpoons K+O_2$	2.2×10^{14}	0.00	0	Est[a], [57,67]
9.	$KO+OH \rightleftharpoons KOH+O$	2.0×10^{13}	0.00	0	Est[a]
10.	$KO+HO_2 \rightleftharpoons KOH+O_2$	5.0×10^{13}	0.00	0	Est[a]
11.	$KO+H_2 \rightleftharpoons KOH+H$	1.6×10^{13}	0.00	0	Est[a], [66]
12.	$KO+H_2 \rightleftharpoons K+H_2O$	3.1×10^{12}	0.00	0	Est[a], [66]
13.	$KO+H_2O \rightleftharpoons KOH+OH$	1.3×10^{14}	0.00	0	Est[a], [66]
14.	$KO+CO \rightleftharpoons K+CO_2$	1.0×10^{14}	0.00	0	Est[a], [67]
15.	$KOH+H \rightleftharpoons K+H_2O$	5.0×10^{13}	0.00	0	Est[b], [68]
16.	$KOH+KOH \rightleftharpoons K_2O_2H_2$	8.0×10^{13}	0.00	0	Est as NaCl+NaCl [69]
17.	$KO_2+H \rightleftharpoons K+HO_2$	2.0×10^{14}	0.00	0	Est[a]
18.	$KO_2+H \rightleftharpoons KO+OH$	5.0×10^{13}	0.00	0	Est[a]
19.	$KO_2+H \rightleftharpoons KOH+O$	1.0×10^{14}	0.00	0	Est[a]
20.	$KO_2+O \rightleftharpoons KO+O_2$	1.3×10^{13}	0.00	0	Est[a], [70]
21.	$KO_2+OH \rightleftharpoons OH+O_2$	2.0×10^{13}	0.00	0	Est[a]
22.	$KO_2+CO \rightleftharpoons KO+CO_2$	1.0×10^{14}	0.00	0	Est[a]
23.	$K+Cl+M \rightleftharpoons KCl+M$	1.8×10^{20}	-1.00	0	[71]
24.	$K+HCl \rightleftharpoons KCl+H$	9.1×10^{12}	0.00	594	[72]
	$K+HCl \rightleftharpoons KCl+H$	1.0×10^{14}	0.00	1830	[72]
25.	$K+Cl_2 \rightleftharpoons KCl+Cl$	4.4×10^{14}	0.00	0	Est[a], [73,74]
26.	$KO+HCl \rightleftharpoons KCl+OH$	1.7×10^{14}	0.00	0	Est[a], [65]
27.	$KOH+HCl \rightleftharpoons KCl+H_2O$	1.7×10^{14}	0.00	0	Est[a], [65]
28.	$KO_2+HCl \rightleftharpoons KCl+HO_2$	1.4×10^{14}	0.00	0	Est[a], [70]
29.	$KCl+KCl \rightleftharpoons K_2Cl_2$	8.0×10^{13}	0.00	0	Est[a], [69]
30.	$K+H+M \rightleftharpoons KH+M$	3.0×10^{17}	-1.00	0	[51] est
31.	$KH+H \rightleftharpoons K+H_2$	1.0×10^{14}	0.00	0	[51] est
32.	$KH+O \rightleftharpoons KO+H$	5.0×10^{13}	0.00	0	[51] est
33.	$KH+O \rightleftharpoons K+OH$	5.0×10^{13}	0.00	0	[51] est
34.	$KH+OH \rightleftharpoons K+H_2O$	1.0×10^{14}	0.00	0	[51] est
35.	$KH+OH \rightleftharpoons KOH+H$	1.0×10^{13}	0.00	0	[51] est
36.	$KH+O_2 \rightleftharpoons K+HO_2$	1.0×10^{14}	0.00	0	[51] est

Units are cm, mol, s, K.

[a] The rate constant is estimated from analogy with the corresponding sodium reaction [12].

[b] The rate constant is estimated from analogy with the corresponding lithium reaction [12].

adopted the value recommended by Lee and Wright of -222 kJ/mol. Further work on the thermodynamic properties of KOH is desirable.

The reaction mechanism consists of subsets for CO/H_2 oxidation, chlorine chemistry, and potassium chemistry. The chlorine chemistry, involving reactions of HCl and Cl_2, is an update of the evaluation by Baulch et al. [50]. Few of the rate constants in the K/H/O/CO reaction subset have been determined experimentally. Therefore estimated values for the rate constants are assigned to most of the reactions. While Glarborg and Marshall [12] focused on lean conditions, the present study involves strongly reducing conditions. For this reason we have included a reaction subset for KH (R30)–(R36), with rate constants as estimated by Klingenberg and Heimerl [51]. The most important reaction in the K/H/O/CO subset for the present investigation is the recombination of K with OH to form KOH (R2). The rate constant for this reaction is discussed further below.

Among the potassium/chlorine interactions, only one reaction has been determined experimentally, $K+HCl$ (R24). The other rate constants are estimated to be the same as the corresponding sodium reactions. Data on corresponding K and Na reactions show very similar rate constants [12]. The sodium and chlorine species interaction, primarily the reactions of Na, NaO, NaOH, and NaO_2 with HCl (or Cl_2 to form NaCl), is fairly well established, as all those reactions have been determined experimentally.

4. Results and discussion

Oxidation of CO by water vapor was studied in the range of temperature from 773 to 1373 K. Experiments were performed by increasing the temperature in steps of 25 K. The initial mole fractions of CO were around 1900–2150 ppm or 7800 ppm. The mole fraction of the oxidizing agent, H_2O, was kept constant as 0.052, with N_2 as balance gas. The KCl vapor

concentration was varied as 0, 157, 313, 470, or 626 ppm. Oxygen was present as an impurity due largely to diffusion through the teflon tubes in the feeding system; the concentration was estimated to be approximately 75 ppm. The isothermal zone residence times for the experiments were 0.95–1.70 s; it varied with temperature since the mass flow was held constant. Mass balance experiments performed at 1073 K showed a significant amount of KCl condensation in the reactor system (in the range of 40–80%), but we expect only a fraction of the KCl to deposit in the high temperature, isothermal part of the reactor.

5. CO oxidation without KCl present

The oxidation of carbon monoxide (CO) under very reducing conditions was studied as shown in Fig. 2, for a mixture of CO and H_2O with CO inlet concentrations around 1900 or 7800 ppm. The results from the experiments are shown as symbols, while solid lines denote modeling results. Comparing Fig. 2a and b, it can be seen that by increasing the inlet ratio between H_2O and CO, the oxidation of CO occurs at lower temperatures. The temperature for 50% conversion of CO, i.e. where CO and CO_2 reach the same value, is shifted from around 923 K (for the higher inlet ratio between H_2O and CO (a)) to around 1023 K (for the lower ratio (b)). This is caused by the reaction sequence $H_2O + H \rightleftharpoons OH + H_2$, $CO + OH \rightleftharpoons CO_2 + H$. The promoting effect of water vapor in larger amounts is opposite to what has been observed for CO oxidation under oxidizing condition; here an increase in the H_2O/CO inlet ratio will typically decelerate the CO oxidation [1,52].

From pathway analysis and sensitivity analysis the key reactions in the CO/H_2 subset under the present conditions were identified. The CO conversion is dominated by $CO + OH \rightleftharpoons CO_2 + H$, which is also the most sensitive reaction in the system. Since the OH radical is required for the reaction to occur, the availability of water will control the system. Most of the OH radicals are generated through the reaction $H_2O + H \rightleftharpoons OH + H_2$ and only a small amount is formed by the reaction $H_2O + O \rightleftharpoons OH + OH$.

In the interpretation of the flow reactor results, the potential impact of oxygen impurities and of reactions on the alumina reactor surface had to be taken into consideration. The presence of trace amounts of O_2 enhances the oxidation rate through $H + O_2 \rightleftharpoons O + OH$, and $O + H_2O \rightleftharpoons 2OH$. The amount of oxygen was estimated by kinetic modeling and assumed to be the same in all experiments.

Modeling predictions of the present experiments tend to overpredict the conversion of CO to CO_2. Since the rate constants for the key reactions in the system are well known, the difference between the experimental and modeling results cannot be explained in terms of uncertainties in the kinetic model. Consequently, the discrepancy was attributed to surface reactions. While data on moist CO oxidation have shown little indication of surface reactions on a quartz wall under lean to slightly reducing conditions [52–54], experiments on CO/H_2
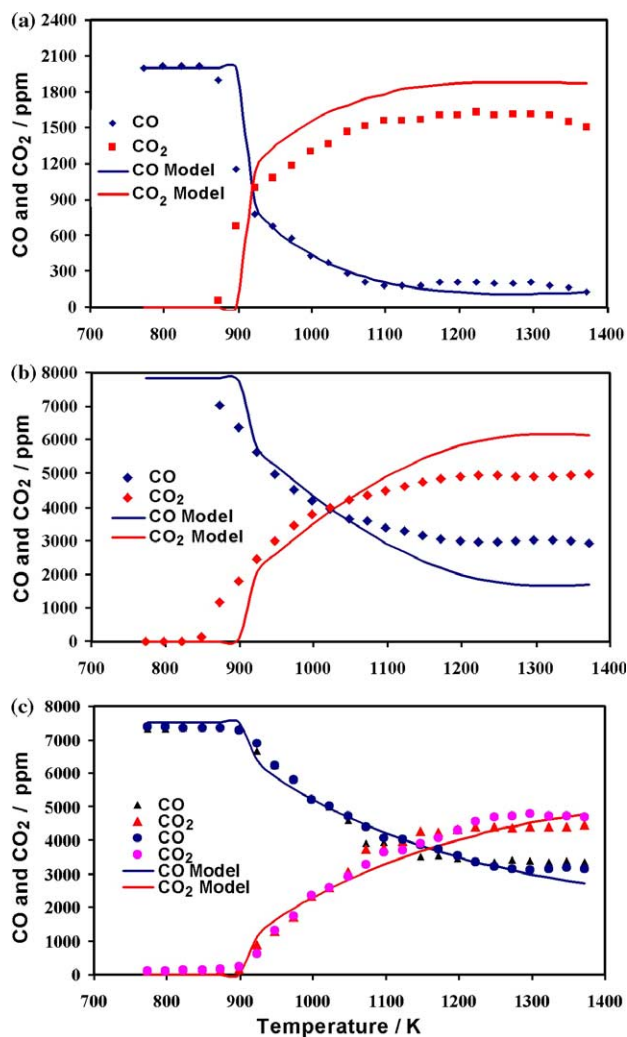

Fig. 2. The outlet mole fractions of CO and CO_2 in a CO oxidation experiment in a clean reactor for lower CO inlet concentration (a), for higher CO inlet concentration (b) and for higher CO inlet concentration with dirty reactor (c) without KCl addition in the gas phase. Inlet composition CO:1900 or 7800 ppm; H_2O: 0.052; N_2: balance gas and O_2 from kinetic modeling estimation (75 ppm), residence time: 0.95–1.70 s (1305/T[K]). The solid lines denote modeling results and the symbols are experimental results. Note that for the conditions of (2a) and (2b) the CO inlet concentration decreased slightly over the time of the experimental run.

oxidation under reducing conditions [55] indicate some radical recombination on the quartz reactor wall.

Following Dagaut et al. [55] the surface reaction was represented by a hydrogen atom loss at the reactor walls. As the O/H radical pool starts establishing, the presence of CO causes the production of hydrogen atoms through the reaction $CO + OH \rightleftharpoons CO_2 + H$. This reaction enhances the radical pool build-up. Hydrogen atom recombination kinetics at the surface was included by fitting a sticking probability to match the experimental results, assuming an activation energy of 9800 cal/mole as observed for quartz [55]. The resulting hydrogen loss rate constant for the (clean) alumina reactor, $k_{clean} = 5.0 \cdot \exp(-9800/RT)$ s^{-1}, was implemented in the mechanism and used in the plug-flow calculation. The results

of the model equipped with the hydrogen atom loss mechanism agree quite well with data for the clean reactor (Fig. 2a and b).

The presence of potassium chloride could be expected to alter the surface reactivity. Various potassium powders have been shown to enhance radical recombination on their surface [56]. Fig. 2(b) and (c) show results of CO oxidation experiments with the high CO inlet concentration in a clean and a dirty reactor, respectively. The dirty reactor has been exposed to KCl. The results show a significant inhibition of the CO oxidation in the dirty reactor, compared to the behavior in the clean reactor. In the clean reactor the initiation temperature is around 873 K; this value is shifted to 923 K in a dirty reactor. The temperature for 50% conversion of CO, i.e. where CO and CO_2 reach the same value, is shifted from around 1023 K (clean reactor) to around 1148 K (dirty reactor). These results suggest that the surface reactivity towards radicals has increased considerably due to the presence of potassium on the wall. Similar to the procedure used for the clean reactor, a hydrogen atom loss rate at the reactor wall was derived based on trial and error to achieve the closest agreement between modeling and experimental results. The resulting rate constant, $k_{dirty} = 2.8 \times 10^3 \exp(-9800/RT)$ s^{-1} for the dirty reactor is more than two orders of magnitude higher than the value for the clean reactor. We have assumed here for simplicity that the activation energy for the rate constant is similar to that of the clean surface. This revised mechanism subset for the dirty reactor is used in the subsequent modeling with KCl addition.

6. CO oxidation with KCl present

A number of experiments with KCl addition to the $CO/H_2O/N_2$ system were conducted, varying the CO and KCl inlet concentrations. The results are summarized in Figs. 3 and 4. The presence of KCl clearly has an inhibiting effect on the CO oxidation; as the inlet KCl level increases, the CO conversion into CO_2 decreases, resulting in a higher fraction of $CO/CO_{initial}$ (higher CO outlet). The inhibiting effect of KCl addition can be seen in the experimental data both with lower and higher CO inlet concentration. The addition of KCl in concentrations of 157, 313, 470, or 626 ppm to the CO oxidation system shifts the initiation temperature from around
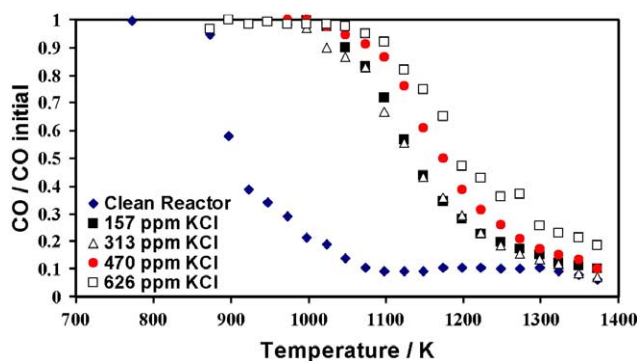
Fig. 3. The fractions of $CO/CO_{initial}$ from the reactor from a CO oxidation experiment with 0–626 ppm KCl addition, inlet composition CO: 2150 ppm; H_2O: 0.052; N_2: balance gas; and O_2 from kinetic modeling estimation (75 ppm).
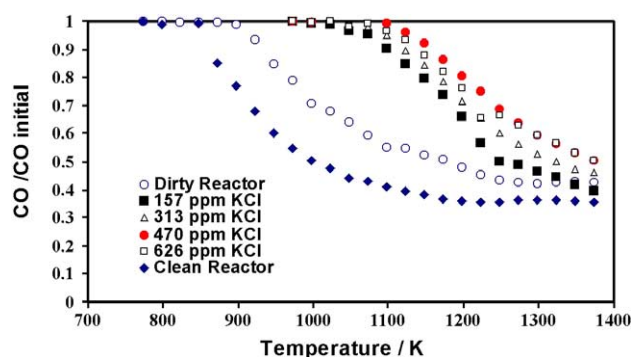
Fig. 4. The fractions of $CO/CO_{initial}$ from the reactor from CO oxidation experiment with 0–626 ppm KCl addition, inlet composition CO: 7800 ppm; H_2O: 0.052; N_2: balance gas; and O_2 from kinetic modeling estimation (75 ppm).

923 K for conditions without KCl addition to 1023 K for experiments with KCl present. The temperature for 50% conversion of CO is also shifted. Similar to what has been observed in flames [22] the effect of potassium is non-linear, with increasing seeding levels resulting only in minor additional inhibition of the oxidation.

To investigate the importance of surface deposits compared to gas phase potassium reactions additional experiments were conducted. Similar to the other experiments the inlet gases consisted of carbon monoxide, water vapor and nitrogen; the temperature was kept at 1073 K. The concentrations of CO and CO_2 from the gas outlet was measured continuosly during the course of the reaction. By passing a nitrogen flow through the packed alumina bed with KCl, KCl vapor was fed in a certain amount to the reaction zone. After around 2 h, when the outlet concentrations of CO and CO_2 had achieved steady state values, the nitrogen flow to the KCl feeding system was stopped, terminating the KCl vapor fed to the system. When the CO and CO_2 concentrations again achieved steady state, the nitrogen flow to the packed alumina bed with KCl was resumed.

The results from this experiment (Fig. 5) show that the CO and CO_2 concentrations depend strongly on the KCl feeding. Initially the potassium chloride causes a strong inhibition of CO oxidation. When the KCl feeding is terminated, the inhibition of the CO oxidation is reduced significantly, resulting in a lower CO outlet concentration. After an initial instant decrease, the CO concentration continues to decrease for 45–60 min, approaching the values typical of the dirty reactor experiments (Fig. 2c). The inhibition of CO oxidation may indicate that potassium is slowly released from the deposit on the surface to the gas phase. When the KCl feeding to the gas phase is resumed, the CO outlet concentration increases almost instantaneously to the initial level, followed by a slow further increase. The slow increase in CO at this point may be attributed to a slight increase in surface reactivity as the wall deposit builds up.

Overall the results confirm that the potassium deposited on the alumina reactor surface is chemically active and has some influence on the CO conversion in the reactor. However, the gas phase potassium chemistry dominates the CO oxidation
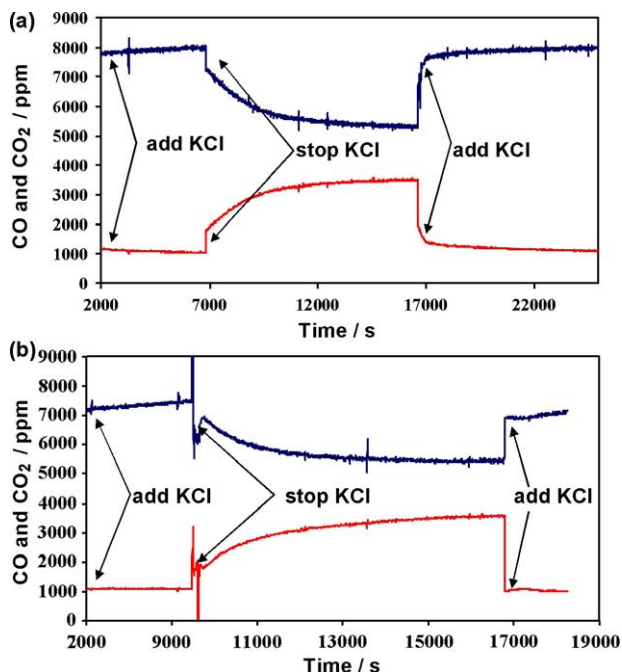
Fig. 5. The outlet mole fractions of CO and CO_2 in CO oxidation experiments with 157 (a) and 313 (b) ppm KCl addition, inlet composition CO: 7800 ppm; H_2O: 0.052; N_2: balance gas; and O_2 from kinetic modeling estimation (75 ppm). The KCl feeding was terminated after about 7000 s (upper) and 9500 s (lower), respectively, and resumed after nearly 17000 s.

rate and despite the surface reactions the experimental results are useful for characterizing the potassium/radical pool interaction.

Figs. 6 and 7 compare the experimental data with KCl feeding (Figs. 3 and 4) with kinetic modeling results. The modeling predictions agree well with the experimental data for the lower CO inlet concentration (Fig. 6), while the agreement for the data with higher CO inlet concentration is less satisfactory (Fig. 7). In general, for the higher CO inlet concentration the proposed kinetic scheme predicts a lower inhibition effect of the KCl addition compared to the experimental results.

Reaction-path analysis and sensitivity analysis were conducted to identify the key reactions under the present conditions. According to our kinetic model, the presence of KCl does not alter the key reactions for CO conversion. As discussed previously, CO oxidation mainly occurs by reaction with OH radicals, $CO + OH \rightleftharpoons CO_2 + H$. The hydroxyl radical is mostly formed by the reaction $H_2O + H \rightleftharpoons OH + H_2$, with a little amount generated through $H_2O + O \rightleftharpoons OH + OH$.

Fig. 8 is a pathway diagram for the potassium transformations at 1050 K with 313 ppm KCl addition for both high and low CO inlet concentration. The contribution of various elementary reactions in the production and destruction of a species is analyzed. The main form of gaseous potassium under the present conditions is potassium chloride, with small amounts of KOH and the K atom, their relative importance depending on the temperature and
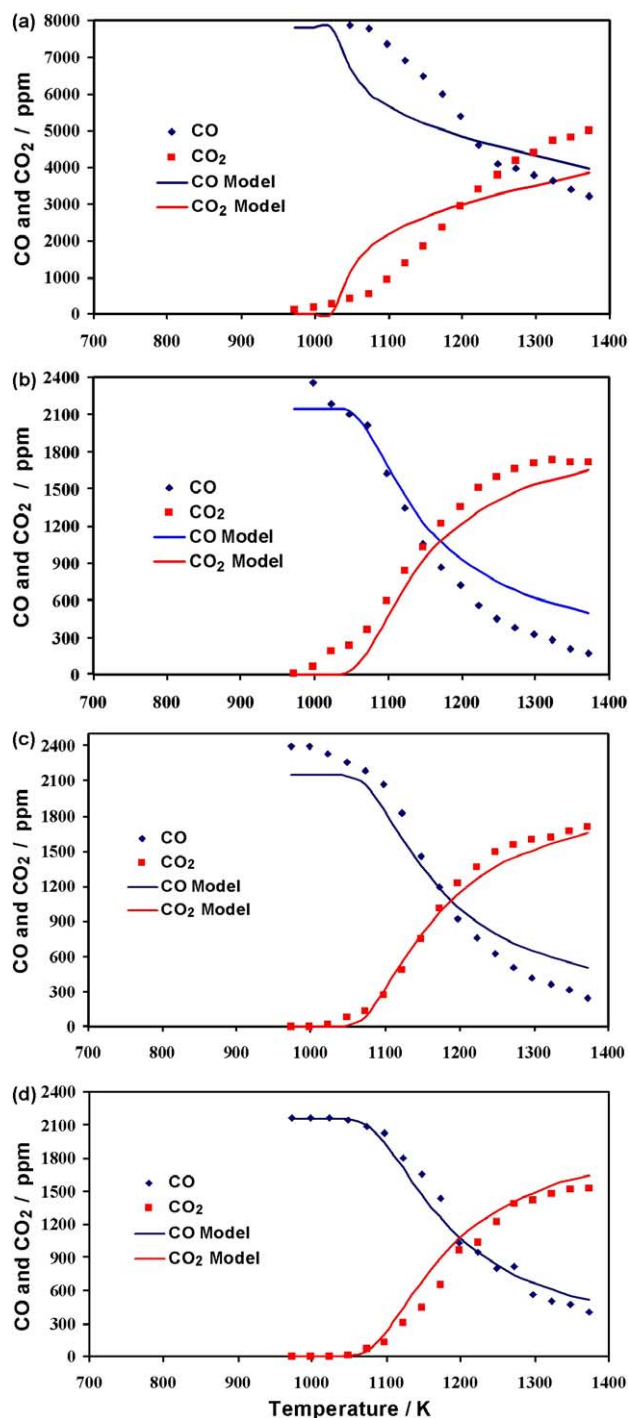
Fig. 6. The outlet molar fractions of CO and CO_2 in CO oxidation experiments with 157 (a), 313 (b), 470 (c), or 626 (d) ppm KCl addition respectively, inlet composition CO: 2150 ppm; H_2O: 0.052; N_2: balance gas; and O_2 from kinetic modeling estimation (75 ppm), residence time: 0.95–1.70 s (1305/T[K]). The solid lines denote modeling results and the symbols are experimental results.

residence time. Potassium hydride (KH) does not attain a significant concentration.

After vaporization, part of the KCl is converted to KOH by the reaction
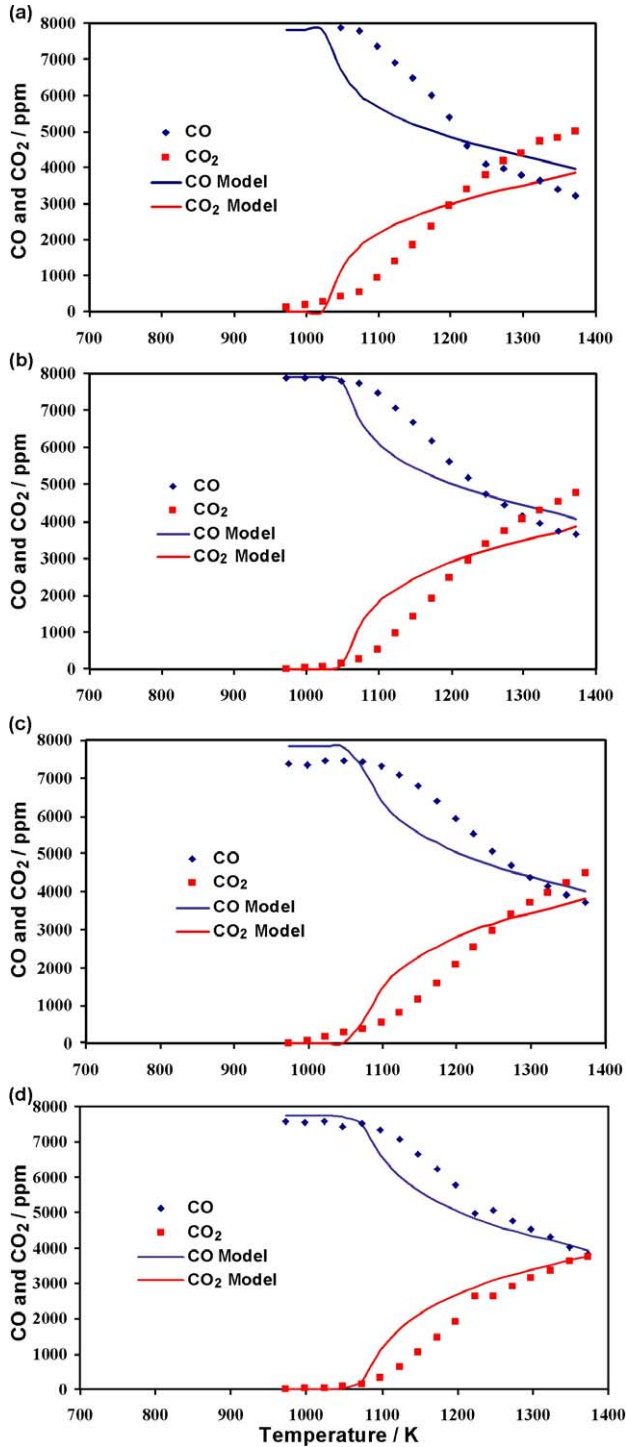
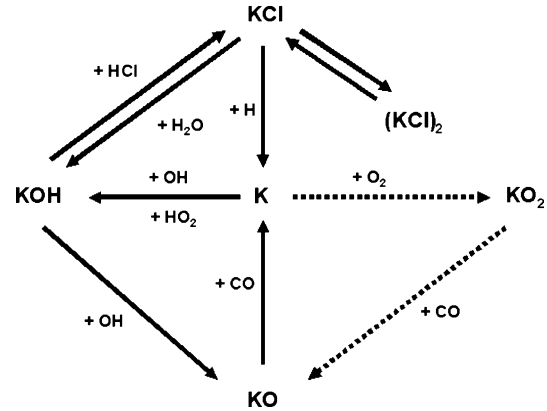$$KCl + H_2O \rightleftharpoons KOH + HCl \qquad (R27b)$$

Fig. 8. The pathway diagram for potassium transformation under the condition of temperature 1050 K with 313 ppm KCl addition for higher and lower CO inlet oncentration.

build up to a few ppm and then slowly decay. As the H atom concentration builds up, KCl is converted mainly to K atoms through reaction

$$KCl + H \rightleftharpoons K + HCl \qquad (R24b)$$

The K atom reacts through several reactions, mainly

$$K + HO_2 \rightleftharpoons KOH + O \qquad (R3)$$

$$K + OH + M \rightleftharpoons KOH + M \qquad (R2)$$

with minor contributions through reaction

$$K + O_2 + M \rightleftharpoons KO_2 + M \qquad (R4)$$

Potassium dioxide will form KO by reacting with CO through reaction below,

$$KO_2 + CO \rightleftharpoons KO + CO_2 \qquad (R22)$$

Potassium hydroxide will react further according to the reactions below,

$$KOH + HCl \rightleftharpoons KCl + H_2O \qquad (R27)$$

$$KOH + OH \rightleftharpoons KO + H_2O \qquad (R13b)$$

According to the model, KO reacts almost solely through reaction with CO,

$$KO + CO \rightleftharpoons K + CO_2 \qquad (R14)$$

During the course of reaction, potassium chloride remains the dominant form of potassium in the gas phase. Fig. 9 shows the predicted distribution of the minor potassium species as a function of temperature for conditions with a lower CO inlet concentration and 470 ppm KCl addition. At lower temperatures a major part of the KCl recombines to form the dimeric form of potassium chloride through the reaction $KCl + KCl \rightleftharpoons (KCl)_2$ (R29). As the temperature increases, KCl is thermodynamically favored compared to $(KCl)_2$ and the dimer becomes less important.

Apart from the KCl monomer and dimer, KOH is the most important potassium species over most of the temperature

Fig. 7. The outlet mole fractions of CO and CO_2 in CO oxidation experiments with 157 (a), 313 (b), 470 (c), or 626 (d) ppm KCl addition, respectively. Inlet composition CO: 7800 ppm; H_2O: 0.052; N_2: balance gas;and O_2 from kinetic modeling estimation (75 ppm), residence time: 0.95–1.70 s (1305/T[K]). The solid lines denote modeling results and the symbols are experimental results.

The b in (R27b) denotes a reverse reaction. In the early stage (within 0.5 ms) this reaction is the major consumption step for KCl, while at longer times (above 0.5 ms) it becomes a net producer of KCl. At 1050 K it reaches equilibrium very fast, in just about 1 ms. Potassium hydroxide is predicted to

Fig. 9. Concentration of $(KCl)_2$ (scaled by a factor of 1/10), K and KOH during the course of the gas phase reaction. Inlet composition: KCl: 470 ppm; CO: 2150 ppm; H_2O: 0.052; N_2: balance gas; and O_2 from kinetic modeling estimation (75 ppm), residence time: 0.95–1.70 s (1305/T[K]). The combined symbols and line denotes $(KCl)_2$, dashed line the KOH concentration and the solid line the K concentration.

range investigated. However, the K atom starts to build up above 1050 K and peaks at 1100 K, where it is present in higher concentrations than KOH. Above this temperature [K] decreases and at 1175 K it is again lower in concentration than KOH. Since key reactions, such as (R27), are close to equilibration, the relative importance of KOH and K will depend on the thermodynamic properties of the involved species, and particularly the heat of formation of KOH needs to be determined with higher accuracy. It should be noted that the trends from the simulations shown in Fig. 9 are different from what has been observed in flames [18] where most of the potassium is present as K but with a smaller, although significant, proportion present as KOH.

To identify the rate limiting steps in the inhibition of CO oxidation by KCl, an A-factor sensitivity analysis was performed. Fig. 10 shows the results of a first order sensitivity analysis of the predicted CO concentration with respect to the reaction rate constants for the conditions above. The analysis indicates that the oxidation rate is mainly sensitive to the reactions that generate or consume free radicals in the system. The oxidation rate is enhanced by reactions that increase the radical pools of OH and H such as $H_2O + H \rightleftharpoons OH + H_2$, $HO_2 + H_2O \rightleftharpoons H_2O_2 + OH$ and $H_2O + O \rightleftharpoons OH + OH$ and
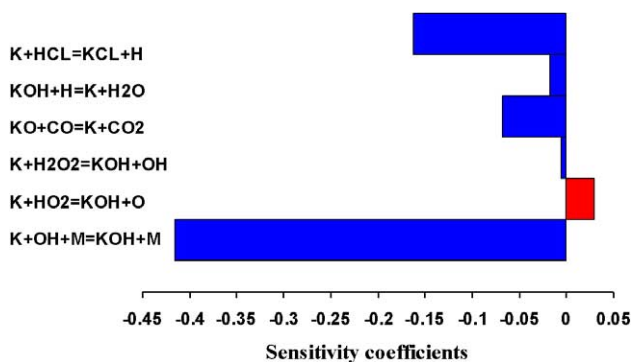
Fig. 10. A-factor sensitivity coefficients for key elementary reactions with respect to formation of CO_2 with conditions corresponding to the experiments in Fig. 9.

inhibited by chain terminating reactions mainly involving alkali species. The reactions $K + HCl \rightleftharpoons KCl + H$ (R24), $KOH + H \rightleftharpoons K + H_2O$ (R15), $KO + CO \rightleftharpoons K + CO_2$ (R14), $K + H_2O_2 \rightleftharpoons KOH + OH$ (R5), and $K + OH + M \rightleftharpoons KOH + M$ (R2) inhibit the CO oxidation, whereas the reaction $K + HO_2 \rightleftharpoons KOH + O$ (R3) enhances the CO oxidation. The analysis confirms that the inhibiting effect of potassium on the CO oxidation in the present work is caused by decreasing the availability of active radicals.

The sensitivity analysis indicates that the chain terminating reaction $K + OH + M \rightleftharpoons KOH + M$ (R2) is the rate limiting step of the potassium inhibition to the CO oxidation system. For this reason the value of rate constant for this reaction has a considerable impact on the model predictions. Glarborg and Marshall [12] adopted the rate constant proposed by Husain [57], $k_2 = 5.4 \times 10^{21} T^{-1.55}$ cm^6 mol^{-1} s^{-1}. Using this value, experimental results and modeling prediction agree qualitatively, but the inhibiting effect of KCl is underpredicted. The expression by Husain et al. was based on a direct measurement at 530 K (with He as bath gas) and an extrapolation to high temperatures by RRKM theory. In the present work, we have chosen a rate constant for (R2) of $k_2 = 3.8 \times 10^{19} T^{-0.65}$ cm^3 mol^{-1} s^{-1}. This value is in agreement with the measurement of Husain et al. at 530 K, assuming the collision efficiency of N_2 to be twice that of He, and with the high temperature data of Jensen et al. [18], obtained from analysis of $H_2/O_2/N_2$ flames doped with potassium.

Fig. 11 shows an Arrhenius plot for the $K + OH + M$ reaction (R2). The open symbols denote data from a direct measurement by Husain [58] and the indirect determination from the flame measurement by Jensen et al. [18]. The dashed line shows the theoretical values predicted by Husain et al. [59], while the solid line denotes the value recommended from the present work.

The chosen rate constant for (R2) results in a significantly improved agreement between modeling predictions and experimental results, compared to calculations with the lower rate constant proposed by Husain et al. [57]. However,
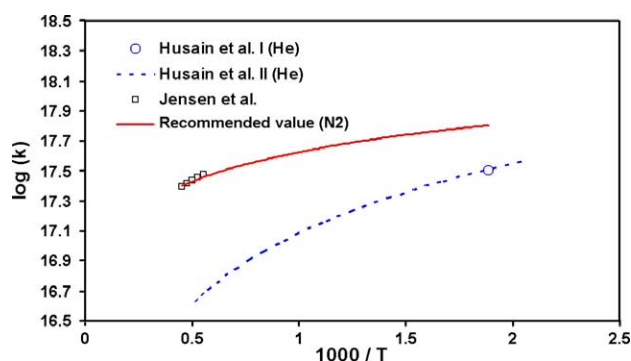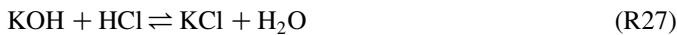

Fig. 11. Arrhenius plot for the $K + OH + M$ reaction. Units are Kelvin and cm^6 mol^{-2} s^{-1}. The open symbols denote data from a direct measurement by Husain et al. [58] and the indirect determination from the flame measurement by Jensen et al. [18]. The dashed line shows the theoretical values predicted by Husain et al. [59], while the solid line denotes the value recommended from the present work.

experimental uncertainties and uncertainties in the chemical kinetic model preclude a determination of k_2 from the present work. The experimental uncertainties include the amount of KCl fed to the gas phase, the oxygen concentration, and surface reactions at the reactor wall. The model uncertainties involve the heat of formation of KOH and the rate constants for potential key reactions, for instance the K+H+M reaction (R30) which could become an important chain terminating step if the rate constant was comparable to that of K+O+M (R1) and K+OH+M (R2).

The reaction-path analysis and sensitivity analysis indicate that there are several active mechanisms for catalyzed radical recombination by potassium. These include:

$$KCl + H \rightleftharpoons K + HCl \tag{R24b}$$

$$K + OH + M \rightleftharpoons KOH + M \tag{R2}$$

$$KOH + HCl \rightleftharpoons KCl + H_2O \tag{R27}$$

The net reaction is $H + OH \rightleftharpoons H_2O$.

$$KCl + H \rightleftharpoons K + HCl \tag{R24b}$$

$$K + HO_2 \rightleftharpoons KOH + O \tag{R3}$$

$$KOH + HCl \rightleftharpoons KCl + H_2O \tag{R27}$$

The net reaction is $H + HO_2 \rightleftharpoons H_2O + O$.

$$KOH + OH \rightleftharpoons KO + H_2O \tag{R13b}$$

$$KO + CO \rightleftharpoons K + CO_2 \tag{R14}$$

$$K + OH + M \rightleftharpoons KOH + M \tag{R2}$$

The net reaction is $CO + 2OH \rightleftharpoons CO_2 + H_2O$.

These mechanisms are different from those proposed based on flame studies. Jensen et al. [18] found the key reactions in fuel-rich flames to be,

$$KOH + H \rightleftharpoons K + H_2O \tag{R15}$$

$$K + OH + M \rightleftharpoons KOH + M \tag{R2}$$

Reaction (R2) is also important under our conditions, while (R15) is rapidly equilibrated and found not to be an important reaction in this work.

Research on sodium chemistry [8,60,61] indicate that the impact of alkali metals on oxidation is largely controlled by the reactions

$$A + OH + M \rightleftharpoons AOH + M \tag{R2'}$$

$$A + H_2O \rightleftharpoons AOH + H \tag{R15b'}$$

$$AOH + OH \rightleftharpoons AO + H_2O \tag{R13b'}$$

$$A + O_2 + M \rightleftharpoons AO_2 + M \tag{R4'}$$

$$AO_2 + H \rightleftharpoons AO + OH \tag{R18'}$$

The reactions numbers correspond to the similar steps in the potassium mechanism. The alkali superoxide AO_2 has also been suggested to be important in K-doped flames [22], but with the present thermochemistry it is doubtful that these compounds are sufficiently stable at high temperatures to play a role. In the present work at lower temperatures there is only trace amounts of oxygen present and KO_2 reactions are not significant.

It is interesting that alkali metals, similar to nitrogen oxides [52] and sulfur oxides [53], may act as sensitizers or inhibitors, depending on reaction conditions. All of these compounds have the ability to inhibit or catalyze some particular reactions depending on gas composition and reaction conditions. For example in the case of sulfur dioxide, it catalyzes CO oxidation under specific conditions even though it generally acts to inhibit fuel oxidation [53]. The idea that alkali metals can remove radicals if its concentration is sufficient is well documented in literature, e.g. [4–6], as well as in the present work. However, under other conditions addition of alkali metals may serve to promote reaction [7–11]. Zamansky and co-workers [7,11] propose that Na can add or remove radicals depending on factors such as concentrations of radicals, of other species, and temperature. They investigated the effect of sodium on the reburning process for NO_x reduction. It was found that Na atoms inhibited the combustion process by reducing H and OH if radical concentrations in the combustion system are high (main combustion zone and the initial part of the reburning zone where injection, mixing, and oxidation of the reburning fuel occurs). If radical concentrations were low (end of the reburning zone), Na atoms increased the concentrations of H and OH [11].

Promotion of reaction by alkali metals may occur through the reaction sequence

$$AOH + M \rightleftharpoons A + OH + M \tag{R2b'}$$

$$A + H_2O \rightleftharpoons AOH + H \tag{R15b'}$$

which corresponds to the net reaction $H_2O \rightleftharpoons H + OH$. More research in the interaction of the alkali species with the radical pool is desirable, as this chemistry may have important practical implications.

7. Conclusion

Experimental results on the influence of gas phase potassium on CO oxidation under reducing conditions have been obtained. The experiments were performed using a laboratory flow reactor at atmospheric pressure and temperatures in the range 773—1373 K, varying the CO inlet concentration and the KCl level. The addition of KCl results in a strong inhibition of the CO oxidation. The inhibition increases with the KCl concentration, but the effect levels off at high concentrations. The experimental data were interpreted in terms of a detailed chemical kinetic model. In general a satisfactory agreement between experimental data and kinetic modeling was achieved. Analysis of the modeling results

indicates that the reaction $K + OH + M \rightleftharpoons KOH + M$ is rate controlling for the radical recombination. The experimental data support a high rate constant for this reaction, but an estimation of the value from the present work is difficult due to uncertainties in the potassium chemistry and in the experimental conditions. Experimental data in a wider range of conditions and alkali precursors is required for model improvement.

Acknowledgements

References

[1] Mueller C, Kilpinen P, Hupa M. Combust Flame 1998;113:579–88.
[2] Bulewicz EM, Janicka EJ. Inst Energy Sept 1990;124.
[3] Anthony EJ, Bulewicz EM, Janicka EJ, Kandefer S. Fuel 1998;77(7): 713–28.
[4] Hynes AJ, Steinberg M, Schofield K. J Chem Phys 1984;80:2585–97.
[5] Steinberg M, Schofield K. Prog Energy Combust 1990;16:311–7.
[6] Schofield K, Steinberg M. J Chem Phys 1992;96:715–26.
[7] Zamansky VM, Sheldon MS, Maly PM. Proc Combust Inst 1998;27: 3001–8.
[8] Zamansky VM, Maly PM, Ho L, Lissianski VV, Rusli D, Gardinger Jr WC. Proc Combust Inst 1998;27:1443–9.
[9] Zamansky VM, Lissianski VV, Maly PM, Rusli D, Gardinger Jr WC. Combust Flame 1999;117:821–31.
[10] Zamansky VM, Ho L, Maly PM, Seeker WR. Proc Combust Inst 1996;26: 2075–82.
[11] Lissianski VV, Zamansky VM, Maly PM. Combust Flame 2001;125: 1118–27.
[12] Glarborg P, Marshall P. Combust Flame 2005;141:22–39.
[13] Dautriche CR. Seances Acad Sci 1908;146:535.
[14] Rosser WA, Inami SH, Wise H. Combust Flame 1963;7:107.
[15] van Tiggelen A, Dewitte M, Vrebosch J. Combust Flame 1964;8:257.
[16] Hoffmann W. Chem Ing Tech 1971;43:556–60.
[17] Iya K, Wollowitz S, Kaskan W. Proc Combust Inst 1975;15:329–36.
[18] Jensen DE, Jones GA, Mace ACH. J Chem Soc Faraday Trans I 1979;75: 2377–85.
[19] Jensen DE, Jones GA. J Chem Soc Faraday Trans I 1982;78:2843–50.
[20] Kim HT, Reuther JJ. Combust Flame 1984;57:313–7.
[21] Bulewicz EM, Kucnerowicz-Polak BJ. Combust Flame 1987;70:127–35.
[22] Slack M, Cox JW, Grillo A, Ryan R, Smith O. Combust Flame 1989;77: 311–20.
[23] Williams BA, Fleming JW. Proc Combust Inst 2002;29:345–51.
[24] Friedman R, Levy H. Combust Flame 1963;7:195.
[25] Dodding RA, Simmons RF, Stephens A. Combust Flame 1970;15:313–5.
[26] Birchall JD. Combust Flame 1970;14:85.
[27] Jensen JR, Nielsen LB, Schultz-Møller C, Wedel S, Livbjerg H. Aerosol Sci Technol 2000;33:490–509.
[28] Rasmussen CL, Master Thesis Report, CHEC Group, Department of Chemical Engineering, Technical University of Denmark,Lyngby; 2003.
[29] Lutz AE. Kee RJ, Miller JA. SENKW. A fortran program for predicting homogeneous gas phase chemical kinetics with sensitivity analysis. Sandia National Laboratories, Report SAND87-8248; 1987.
[30] Kee RJ, Rupley F, Miller JA. Chemkin II: a fortan chemical kinetics package for the analysis of gas phase chemical kinetics, Sandia National Laboratories, Report SAND89-8009; 1989.
[31] Chase Jr MW. NIST-JANAF Tables. J Phys Chem Ref Data Monogr 9 1998 [Am. Inst. Phys., Am. Chem. Soc., New York].
[32] Gurvich LV, Bergman GA, Gorokhov LN, Iorish VS, Leonidov VYa, Yungman VS. J Phys Chem Ref Data 1996;25:1211–76.
[33] Gurvich LV, Bergman GA, Gorokhov LN, Iorish VS, Leonidov VYa, Yungman VS. J Phys Chem Ref Data 1997;26:1031–110.
[34] Lee EPF, Soldan P, Wright TG. Chem Phys Lett 1998;295:354–8.
[35] Lee EPF, Soldan P, Wright TG. Chem Phys Lett 1999;301:317–24.
[36] Soldan P, Lee EPF, Wright TG. Phys Chem Chem Phys 1999;1:4947–54.
[37] Lee EPF, Wright TG. J Phys Chem 2002;106:8903–7.
[38] Lee EPF, Soldan P, Wright TG. J Phys Chem 2002;117:8241–7.
[39] Lee EPF, Wright TG. Chem Phys Lett 2002;363:139–43.
[40] Lee EPF, Wright TG. Mol Phys 2003;101:405–12.
[41] Sullivan MB, Iron MA, Redfern PC, Martin JML, Curtiss LA, Radom L. J Phys Chem A 2003;107:5617–30.
[42] Plane JMC, Rajasekhar B, Bartolotti L. J Phys Chem 1989;93:3141–5.
[43] Marshall P, Narayan AS, Fontijn A. J Phys Chem 1990;94:2998–3004.
[44] Schofield K. Int J Chem Kinet 1993;25:719–43.
[45] Perry RA, Miller JA. Int J Chem Kinet 1996;28:217–34.
[46] Horner DA, Allen WD, Csaszar AG, Schaefer III HF. Chem Phys Lett 1991;186:346–55.
[47] Partridge H, Bauschlischer Jr CW, Sodupe M, Langhoff SR. Chem Phys Lett 1992;195:200–6.
[48] Hildenbrand DL, Lau KH. J Chem Phys 1993;98:4076–81.
[49] Dyke JM, Shaw AM, Wright TG. In: Fontijn A, editor. Gas-phase metal reactions. Amsterdam: Elsevier; 1992. p. 467–91.
[50] Baulch DL, Duxbury J, Grant SJ, Montague DC. Evaluated kinetic data for high temperature reactions. Homogeneous gas phase reactions of halogen- and cyanide-containing species. J Phys Chem Ref Data Suppl 1981;4:10.
[51] Klingenberg G, Heimerl JM. Prog Astr Aero 1992;139:241–60.
[52] Glarborg P, Kubel D, Kristensen PG, Hansen J, Dam-Johansen K. Combust Sci Technol 1995;110/111:461.
[53] Alzueta MU, Bilbao R, Glarborg P. Combust Flame 2001;127:2234.
[54] Glarborg P, Kubel D, Dam-Johansen K, Chiang, HM, Bozzeli JW. Int J Chem Kinet 1996;28:773–90.
[55] Dagaut P, Lecomte F, Mieritz J, Glarborg P. Int J Chem Kinet 2003;35: 564–75.
[56] Baratov AN, Vogman LP, Kobzar VN, Azatyan VV, Museridze MD, Dzotsenidze ZG, et al. Combust Explosions Shock Waves 1976;12:61–4.
[57] Husain D. J Chem Soc Faraday Trans 1989;85:85–130.
[58] Husain D, Plane JMC, Xiang CC. J Chem Soc Faraday Trans 1984;80: 1465.
[59] Husain D, Plane JMC, Xiang CC. J Chem Soc Faraday Trans 1985;81: 561.
[60] Hynes AJ, Steinberg M. J Chem Phys 1984;80:2585–97.
[61] Schofield K, Steinberg M. J Phys Chem 1992;96:715–26.
[62] Griffin J, Worsnop DR, Brown RC, Kolb CE, Herchbach DR. J Phys Chem A 2001;92(105):1643–8.
[63] DeMore WB, Sander SP, Golden DM, Hampson RF, Kurylo MJ, Howard CJ, et al. Chemical kinetics and photochemical data for use in stratospheric modeling: evaluation number 12. JPL Publ 1997;97–4:115–65.
[64] Helmer M, Plane JMC. J Geophys Res 1993;98:207–22.
[65] Silver JA, Stanton AC, Zahniser MS, Kolb CE. J Phys Chem 1984;88: 3123–9.
[66] Ager III JW, Howard CJ. J Chem Phys 1987;87:921–5.
[67] Kolb CE, Worsnop DR, Zahniser MS, Robinson GN, Shi X, Herschbach DR. In: Fontijn A, editor. Gas phase metal reactions. Amsterdam: Elsevier; 1992. p. 15–27.
[68] Plane JMC, Rajasekhar B. J Chem Soc Faraday Trans 2 1988;84: 273–85.
[69] Alkemade U, Homann KH. Ber Bunsen Ges Phys Chem 1989;93: 434–9.
[70] Silver JA, Kolb CE. J Phys Chem 1986;90:3267–9.
[71] Jensen DE, Jones GA. Combust Flame 1978;32:1–34.
[72] Helmer M, Plane JMC. J Chem Phys 1993;99:7696–702.
[73] Silver JA. J Chem Phys 1986;84:4718–20.
[74] Talcott CL, Howard CJ, Ager III JW. J Chem Phys 1986;84:6161–9.

Paper II

Thermal Dissociation of SO$_3$ at 1000−1400 K[†]

Ayten Yilmaz, Lusi Hindiyarti, Anker D. Jensen, and Peter Glarborg*

Department of Chemical Engineering, Technical University of Denmark, DK-2800 Lyngby, Denmark

Paul Marshall

Department of Chemistry, University of North Texas, P.O. Box 305070, Denton, Texas 76203-5070

*Received: October 7, 2005; In Final Form: December 15, 2005*

The thermal dissociation of SO$_3$ has been studied for the first time in the 1000−1400 K range. The experiments were conducted in a laminar flow reactor at atmospheric pressure, with nitrogen as the bath gas. On the basis of the flow reactor data, a rate constant for SO$_3$ + N$_2$ → SO$_2$ + O + N$_2$ (R1b) of 5.7×10^{17} exp($-40000/T$) cm^3/(mol s) is derived for the temperature range 1273−1348 K. The estimated uncertainty is a factor of 2. The rate constant corresponds to a value of the reverse reaction of $k_1 \approx 1.8 \times 10^{15}$ cm^6 mol^{-2} s^{-1}. The reaction is in the falloff region under the investigated conditions. The temperature and pressure dependence of SO$_2$ + O (+N$_2$) was estimated from the extrapolation of low temperature results for the reaction, together with an estimated broadening parameter and the high-pressure limit determined recently by Naidoo, Goumri, and Marshall (*Proc. Combust. Inst.* **2005,** *30,* 1219−1225). The theoretical rate constant is in good agreement with the experimental results. The improved accuracy in k_1 allows a reassessment of the rate constant for SO$_3$ + O → SO$_2$ + O$_2$ (R2) based on the data of Smith, Tseregounis, and Wang (*Int. J. Chem. Kinet.* **1982,** *14,* 679−697), who conducted experiments on a low-pressure CO/O$_2$/Ar flame doped with SO$_2$. At the location in the flame where the net SO$_3$ formation rate is zero, $k_2 = k_1$[SO$_2$][M]/[SO$_3$]. A value of 6.9×10^{10} cm^3 mol^{-1} s^{-1} is obtained for k_2 at 1269 K with an uncertainty a factor of 3. A recommended rate constant $k_2 = 7.8 \times 10^{11}$ exp($-3065/T$) cm^3 mol^{-1} s^{-1} is consistent with other flame results as well as the present flow reactor data.

Introduction

Research in high-temperature sulfur chemistry has been motivated partly by the effect of sulfur species on flame characteristics and nitrogen chemistry and partly by the adverse effects of a high SO$_3$/SO$_2$ ratio in the flue gas. During the combustion of sulfur-containing fuels, most of the sulfur is converted to sulfur dioxide (SO$_2$) but a small fraction is oxidized further to form sulfur trioxide (SO$_3$). The presence of SO$_3$ enhances the corrosion potential of the flue gas,[1] and it has implications for the formation of aerosols in biomass-fired systems.[2−4]

The conversion of SO$_2$ to SO$_3$ is kinetically limited.[1] The reactions that may contribute to the formation of SO$_3$ involve the interaction of SO$_2$ with the radical pool.[5−7] In the presence of nitrogen oxides, there is a kinetic coupling of NO$_x$ and SO$_x$ chemistry via the radical pool.[5,7] While the overall mechanisms for SO$_3$ formation are fairly well-known, kinetic modeling of the process still suffers from a lack of accurate kinetic data and refinements are required in order to establish a reliable mechanism.[4,5]

Flow reactor studies of SO$_2$ oxidation under post-flame conditions[5,7] indicate fractional conversions of SO$_2$ to SO$_3$ of the order of a few percent. According to these studies, SO$_3$ formation occurs primarily through the reaction

$$\text{SO}_2 + \text{O (+M)} \rightarrow \text{SO}_3 \text{ (+M)} \qquad \text{(R1)}$$
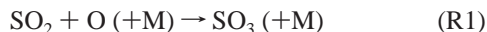
Direct measurements are available for this reaction in the 300−800 K range[8,9] and for the reverse reaction, thermal dissociation of SO$_3$, in the temperature range of 1700−2500 K.[10] Indirect determinations are available from flames[12−14] and shock tube experiments.[15] The rate constant increases with temperature at lower temperatures, peaks at around 750 K, and drops off as the temperature increases further.[9,10] The positive temperature dependence below 750 K arises from a barrier of about 16 kJ/mol to reaction,[9] while at higher temperatures the dominant effect becomes the limitations in collisional stabilization of the SO$_3^*$ intermediate, causing a decrease in the reaction rate. A Rice−Ramsperger−Kassel−Marcus (RRKM) extrapolation of the low-temperature measurements is in good agreement with data for both the forward and backward reaction over a temperature range of 220−2500 K for Ar as collision partner.[9] Even above 1000 K the reaction is in the falloff region at atmospheric pressure.[7,9]

Reaction 1 is important not only for the formation of SO$_3$ in combustion systems but also in some industrial processes. In the reverse direction

$$\text{SO}_3 \text{ (+M)} \rightarrow \text{SO}_2 + \text{O (+M)} \qquad \text{(R1b)}$$

it is believed to be a rate-limiting step in the conversion of spent sulfuric acid to SO$_2$.[11] Even though the rate constant for reaction R1 is probably known more accurately than most sulfur reactions, it is noteworthy that there are few measurements under the conditions of practical interest in combustion and industrial processes, that is, temperatures between 1000 and 1500 K. Recently, Hwang et al.[15] derived a rate constant for R1 in Ar

---

in the temperature range of 960−1150 K from modeling the effect of SO$_2$ addition on the OH concentration profile for H$_2$ oxidation in a shock tube. However, the only direct measurements of the rate constant using nitrogen as collision partner were obtained at room temperature.[8]

The objective of the present work is to derive a rate constant for the thermal dissociation of SO$_3$ in the 1000−1400 K range from flow reactor experiments with nitrogen as inert gas. A gas containing a mixture of SO$_2$ and O$_2$ in N$_2$ is led to a catalyst, where SO$_2$ is partly oxidized to SO$_3$ at 673 K. The resulting gas is then led to a flow reactor, where SO$_3$ is converted back to SO$_2$ by thermal dissociation. The fractional conversion of SO$_3$ in the homogeneous reactor provides a measure of the value of k_{1b}. The results are compared to the RRKM predictions for the SO$_2$ + O (+N$_2$) reaction. In addition, the more accurate value available for k_1 allows for a reassessment of the rate constant for the reaction SO$_3$ + O → SO$_2$ + O$_2$ (R2) obtained from flame measurements.[12−14]

Experimental Section

The source of SO$_3$ in the present study is oxidation of SO$_2$ over a KCl-doped V$_2$O$_5$−WO$_3$−TiO$_2$ catalyst. Oxidation of SO$_2$ to SO$_3$ is a concern in selective catalytic reduction (SCR), a common technology used for the removal of nitrogen oxides in flue gas by reaction with NH$_3$. Since the presence of SO$_3$ is detrimental to the ability of vanadium catalysts to remove NO,[16,17] oxidation of SO$_2$ over commercial catalysts has been the subject of recent research work. Zheng and Jensen[18] studied the kinetics of SO$_2$ oxidation over SCR catalysts provided by Haldor Topsøe A/S. They tested catalysts with different concentrations of the active component V$_2$O$_5$ (<10 wt %) and WO$_3$ (5−13 wt %). The catalysts were doped with KCl and K$_2$SO$_4$ at different levels by a wet impregnation method at room temperature at 0.8 bar absolute pressure followed by drying at 323 K for 15 h. Zheng and Jensen found that, at 673 K, the activity of the doped catalyst for SO$_2$ oxidation was more than an order of magnitude higher than that of a fresh catalyst and the SO$_2$ conversion efficiency was fairly constant over time. The catalyst used in this work is the KCl-doped 7.3 wt % V$_2$O$_5$−WO$_3$−TiO$_2$ catalyst from the work of Zheng and Jensen.[18]

The experimental setup consisted of two quartz reactors in series in separate ovens. In the first reactor, SO$_2$ was oxidized to SO$_3$ over the doped V$_2$O$_5$−WO$_3$−TiO$_2$ catalyst. The temperature along the catalytic reactor was set to 673 K. The product gas from the first reactor was fed into the second reactor through a heated line at 415 K in order to prevent condensation. The second reactor was homogeneous, operated at high temperatures (up to around 1400 K) to promote the conversion of SO$_3$ to SO$_2$.

A schematic of the experimental setup is presented in Figure 1. Sulfur dioxide, oxygen, and nitrogen were mixed in a cross-joint and directed either to bypass (the flow meter, G) or to the catalytic reactor (B). The bubble flow meter served to measure the flow of the input gases from the gas cylinders as a check for mass flow meters. The output of the catalytic reactor was directed either to the homogeneous reactor (C) or to the gas conditioning and analyzers (F). Bypass lines were available for both reactors so that input and output gases could be analyzed and the setup could be used in a flexible way. Prior to the analyzers, a condenser (D) and filters (E) were located to protect the analyzer from any aerosols and/or condensed liquids.

The catalytic reactor was a heterogeneous quartz reactor with a 2 cm inner diameter. The catalyst was cut into pieces (roughly 1.5 cm × 1.5 cm) and stacked upon a porous plate in the
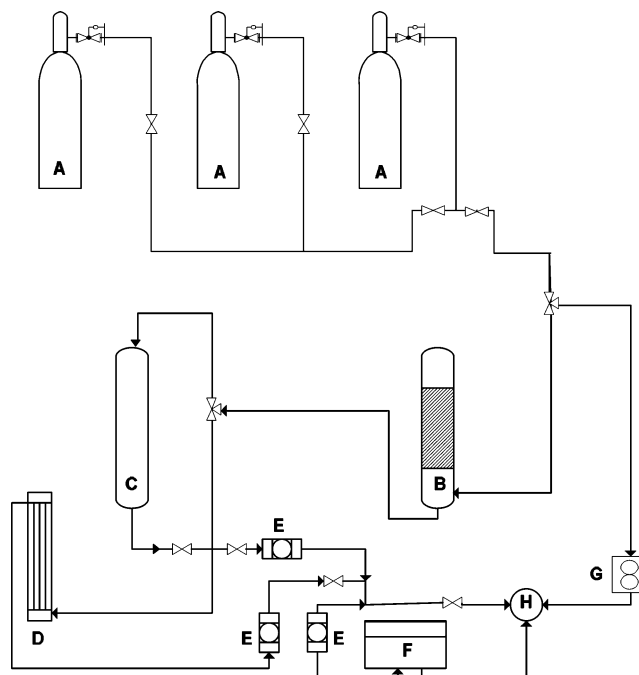
Figure 1. Schematic of the experimental setup: (A) gas cylinders (O$_2$, SO$_2$, N$_2$), (B) catalytic reactor, (C) homogeneous reactor, (D) condenser, (E) filter, (F) gas analyzers, (G) bubble flow meter, and (H) purging system.
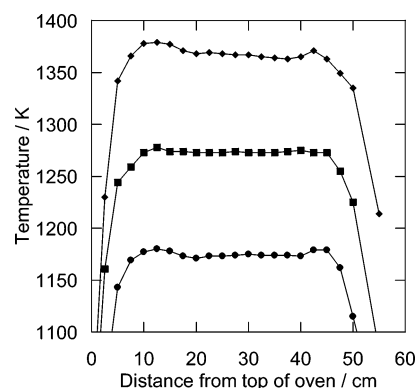

Figure 2. Characteristic temperature profile in the homogeneous reactor.

isothermal zone of the reactor. The total length of the reactor occupied by the catalyst material was 16 cm. This reactor was operated at 673 K, and the reactor residence time was about 3 s.

The homogeneous reactor consisted of a quartz tube located in a three-zone electrically heated oven. No gases were added to the mixture between the first and the second reactor and the reactants entered the homogeneous reactor premixed and were heated together. The tubes used for the second reactor were designed to approximate plug flow in the laminar flow regime.

The reactor temperatures were controlled with thermocouples with an accuracy of ±5 K. During experiments, the thermocouples were placed outside the reactor to avoid contact with the reacting gases but the temperature profiles were obtained from probing inside the reactor with an inert flow. Characteristic temperature profiles for the reactor are shown in Figure 2. In most of the temperature range investigated, a flat temperature profile was obtained in the isothermal region of the reactor, but at the highest temperatures, variations within ±15 K were observed.The concentration of SO$_2$ was measured continuously by a UV analyzer with an accuracy of ±3%.

TABLE 1: Selected Reactions from the H/S/O Subset[a]

	A	β	E_a/R	ref
1. $SO_2 + O (+N_2) \rightleftharpoons SO_3 (+N_2)$	3.7×10^{11}	0.00	850	9, pw
low-pressure limit	2.9×10^{27}	-3.58	2620	
Troe parameters: 0.43, 371, 7442				
$SO_2 + O (+Ar) \rightleftharpoons SO_3 (+Ar)$	3.7×10^{11}	0.00	850	9
low-pressure limit	2.4×10^{27}	-3.60	2610	
Troe parameters: 0.442, 316, 7442				
2. $SO_3 + O \rightleftharpoons SO_2 + O_2$	7.8×10^{11}	0.00	3070	12, pw
3. $SO_2 + OH \rightleftharpoons SO_3 + H$	4.9×10^{2}	2.69	12000	5
4. $SO_2 + OH (+M) \rightleftharpoons HOSO_2 (+M)$	5.7×10^{12}	-0.27	0	21
low-pressure limit	1.7×10^{27}	-4.09	0	
Troe parameters: 0.10, 1×10^{-30}, 1×10^{30}				
5. $HOSO_2 + O_2 \rightleftharpoons SO_3 + HO_2$	7.8×10^{11}	0.00	330	22

[a] Units are in mol, cm, s, and K.

Numerical Procedure and Reaction Mechanism

The experimental results were interpreted in terms of a detailed reaction mechanism. Since the homogeneous reactor was designed to approximate plug flow, the reactor results were modeled with SENKIN,[19] which is part of the CHEMKIN library.[20] SENKIN performs an integration in time. The results of the SENKIN calculations were compared to experimental data using the nominal residence time in the isothermal part of the reactor.

The reaction mechanism consisted of a H_2/O_2 subset and a full description of the H/S/O reaction system. The H_2/O_2 subset was included in the model to account for effects of water vapor. Presence of water vapor, even in small concentrations, may conceivably lead to an O/H radical pool, initiated by the reaction

$$O + H_2O \rightleftharpoons OH + OH$$

The SO_2/SO_3 subset of the mechanism is listed in Table 1. With a few exceptions, the H/S/O subset and the corresponding thermochemistry were adopted from previous work by the authors.[4,6] The rate coefficients for $SO_2 + O (+N_2) = SO_3$ $(+N_2)$ (R1b) were estimated from RRKM calculations as part of this study (described below) and used in the modeling. In addition to thermal dissociation of SO_3 (R1b), reactions that consume SO_3 include $SO_3 + O$ (R2), $SO_3 + H$ (R3b), and $SO_3 + HO_2$ (R4b). Also, the oxidation of SO_2 to SO_3 must be taken into consideration; this may occur through the reaction of SO_2 with O (R1) or with OH, either directly (R3) or through $HOSO_2$ (R4, R5).

The reaction $SO_3 + O = SO_2 + O_2$ (R2), an important consumption step for SO_3 under the present conditions, has not been measured directly, and the rate constant is associated with a considerable uncertainty.[5,6] To obtain a reliable estimate of R2 in the temperature range of the present work, we reinterpreted the flame data of Smith et al.[12] They conducted experiments on a low-pressure $CO/O_2/Ar$ flame doped with SO_2. On the basis of measured profiles of SO_2, SO_3, O_2, and O, Smith et al. were able to derive rate constants for reactions R1$_{Ar}$ and R2 in the temperature range of 1435−1850 K. We take a different approach and look at the lower temperature part of the flame closer to the burner surface. In this part, $[SO_3]$ builds up and peaks at a location corresponding to a temperature of 1269 K. At this point in the flame, the net SO_3 formation rate $\dot{R}_{SO_3} = 0$. A reaction analysis shows that SO_3 is formed by reaction R1$_{Ar}$ and consumed almost solely by reaction R2; the temperature is too low for reaction R2b to contribute significantly to the decomposition of SO_3. At this location
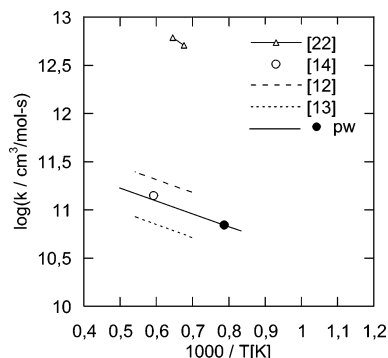
$$\dot{R}_{SO_3} = k_{1,Ar}[SO_2][O][M] - k_2[SO_3][O] = 0 \quad (1)$$

Figure 3. Arrhenius plot for the reaction $SO_3 + O \rightarrow SO_2 + O_2$ (R2). The data shown are obtained in the present work (pw) and from flame measurements: Schofield,[23] Merriman and Levy,[14] and Smith et al.[12,13]

The value of k_2 is then easily derived

$$k_2 = \frac{k_{1,Ar}[SO_2][O][M]}{[SO_3][O]} = \frac{k_{1,Ar}[SO_2][M]}{[SO_3]} \quad (2)$$

Since the concentration of the O atom drops out of the equation, the uncertainty in the value of k_2 is associated with uncertainties in $k_{1,Ar}$ (adopted from Naidoo et al.[9]) and the measurements of $[SO_2]$, $[SO_3]$, and flame temperature. We obtain a value of k_2 (1269 K) = 6.9×10^{10} cm^3 mol^{-1} s^{-1} with an estimated uncertainty of less than a factor 3. The rate coefficient for R2 is then estimated by adopting the activation energy of 25.5 kJ/mol for the reaction determined by Smith et al.[12] (see Table 1), yielding a rate constant of $k_2 = 7.8 \times 10^{11} \exp(-3065/T)$ cm^3 mol^{-1} s^{-1}. This expression is in excellent agreement with the results of Merryman and Levy[14] who obtained a value of $k_2 = 1.5 \times 10^{11}$ cm^3 mol^{-1} s^{-1} at 1685 K in an atmospheric-pressure flame. A reevaluation of their data with a revised value of $k_{1,Ar}$[9] yields only a small correction in this value (k_2 (1685 K) = 1.4×10^{11} cm^3 mol^{-1} s^{-1}).

Our preferred rate constant for R2 is compared with values reported from flame studies in Figure 3. Apart from the high value recommended by Schofield[23] from a review of early flame measurements, the data are in good agreement. Data from reactor studies of the reaction in the same temperature range (not shown) span more than 5 orders of magnitude and are clearly outside the uncertainty limits of the present recommendation. The flow reactor work of Burdett et al.[24] on the reverse reaction $SO_2 + O_2 = SO_3 + O$ (R2b) in the 900−1350 K range must be in error, since their derived value of k_{2b} corresponds to $k_2 \approx 10^{17}$ cm^3 mol^{-1} s^{-1} at 1000 K, that is, much larger than collision frequency. On the other hand, the value proposed by Alzueta et al.[6] from the analysis of batch reactor data[25] at 1173−1323 K is 2 orders of magnitude lower than the rate constants derived from flames. Such a low value is incompatible with the flame results as well as with the present experimental results; this is discussed further below. Our current thinking is that the batch reactor data may have been influenced by surface loss of SO_3.

Results and Discussion

The experiments were performed at atmospheric pressure with temperatures in the homogeneous reactor in the range 973−1423 K. Typical conditions involved SO_3 and SO_2 concentrations into the homogeneous reactor of about 500 ppm, with around 5% O_2 in N_2. Also, trace amounts of water vapor were present, estimated to be in the range of 30−150 ppm.[26] A typical experimental run is shown in Figure 4. At $t = 0$, only the nitrogen and oxygen valves were turned on and the two reactors
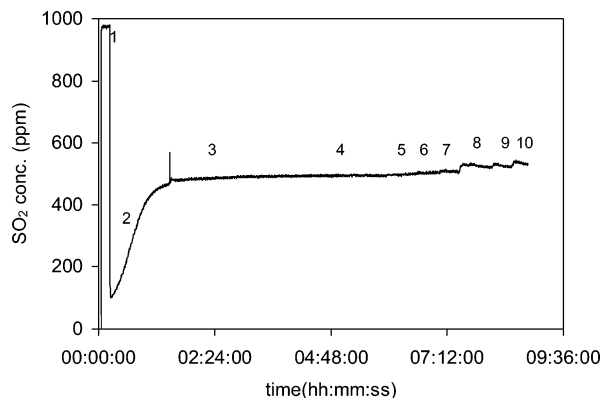
Figure 4. Characteristic SO$_2$ profile as a function of time in an experiment. The inlet gas contains 975 ppm SO$_2$ and 4.7 O$_2$, with trace amounts of water vapor and N$_2$ as the carrier gas: (1) The input concentration of SO$_2$ is analyzed. (2) The gas is fed to the catalytic reactor, bypassing the homogeneous reactor. The products from the catalytic reactor are analyzed. (3) After the catalytic reactor has achieved steady-state operation, the product gas from this reactor is fed into the homogeneous reactor (operated at 923 K). The product gas from the homogeneous reactor is analyzed. (4–10) Step 3 is repeated for temperatures of 948, 973, 998, 1023, 1048, 1073, and 1176 K.

were bypassed. Then, SO$_2$ was supplied to the system, and the inlet SO$_2$ concentration was measured. The reactant gas mixture was then fed into the catalytic reactor, resulting in a rapid oxidation of SO$_2$. The initial conversion was more than 80%, but over time the conversion efficiency decreased, and in about 45 min, the SO$_2$ concentration stabilized at about 500 ppm. The conversion efficiency of the catalytic reactor depended on the SO$_2$/O$_2$ ratio; a 35–60% conversion of SO$_2$ to SO$_3$ was observed for SO$_2$/O$_2$ ratios between 0.01 and 0.1. Once the SO$_2$ concentration out of the catalytic reactor was stabilized, the product gas was fed into the homogeneous reactor. The temperature in the homogeneous reactor was increased in steps of 25 K above the chosen starting temperature, securing steady-state conditions between each temperature increment. As indicated by the results of Figure 4, thermal dissociation of SO$_3$ was very slow below 1100 K and subsequent experiments emphasized temperatures above this value.

Experimental results for the decomposition of SO$_3$ in the temperature range of 1050–1425 K are shown in Figure 5. The five experimental runs cover sulfur oxide levels in the range of 580–1050 ppm and oxygen concentrations of 2.6–5.0%. Over this temperature range, the SO$_3$ conversion increased from being negligible to being almost complete. The oxygen level affects the oxidation of SO$_2$ to SO$_3$ in the catalytic reactor but has little effect on the SO$_3$ decomposition in the homogeneous reactor.

Figure 6 compares selected experimental data (sets 1 and 4) to modeling predictions with the detailed reaction mechanism (solid lines). Without any adjustments, the kinetic model is seen to describe the experimental results quite well. For all sets, the kinetic model is in agreement with the experimental data within experimental uncertainty.

Sensitivity analysis of the calculations with the detailed chemical kinetic model shows that the SO$_3$ decomposition rate is only sensitive to two reactions

$$SO_3 \, (+M) \rightleftharpoons SO_2 + O \, (+M) \qquad (R1b)$$

$$SO_3 + O \rightleftharpoons SO_2 + O_2 \qquad (R2)$$
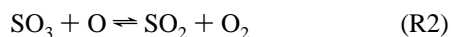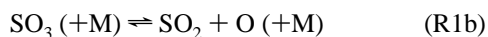
The chemistry is not affected by the trace impurities of water vapor present.
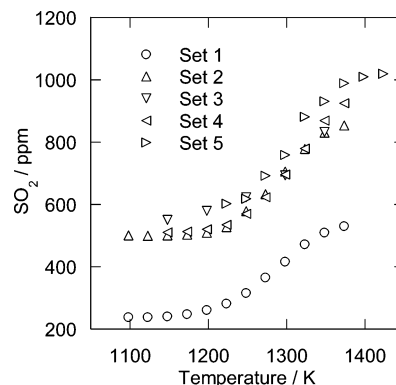
Figure 5. Experimental results for thermal decomposition of SO$_3$. Set 1: SO$_3$ = 342 ppm, SO$_2$ = 238 ppm, O$_2$ = 4.7%; residence time 2320/T(K). Set 2: SO$_3$ = 420 ppm, SO$_2$ = 500 ppm, O$_2$ = 2.6%; residence time 2550/T(K). Set 3: SO$_3$ = 406 ppm, SO$_2$ = 540 ppm, O$_2$ = 4.7%; residence time 2901/T(K). Set 4: SO$_3$ = 487 ppm, SO$_2$ = 510 ppm, O$_2$ = 4.7%; residence time 2164/T(K). Set 5: SO$_3$ = 467 ppm, SO$_2$ = 578 ppm, O$_2$ = 5.0%; residence time 1873/T(K). All experiments are carried out with N$_2$ as the carrier gas, with H$_2$O $\approx$ 100 ppm, and with a pressure of about 1.05 atm. The residence time (s), varying with reactor temperature as indicated (constant mass flow), applies to the isothermal part of the reactor (about 40 cm of the length).
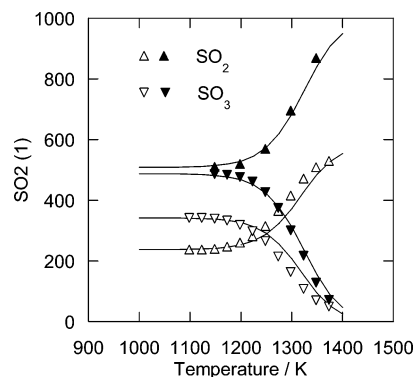

Figure 6. Comparison between experimental results (symbols) and modeling predictions (solid lines) for thermal decomposition of SO$_3$. Set 1 (open symbols): SO$_3$ = 342 ppm, SO$_2$ = 238 ppm, O$_2$ = 4.7%; residence time 2320/T(K). Set 4 (closed symbols): SO$_3$ = 487 ppm, SO$_2$ = 510 ppm, O$_2$ = 4.7%; residence time 2164/T(K). The outlet SO$_3$ concentration is calculated as the difference between the inlet and outlet SO$_2$. The experiments are carried out with N$_2$ as the carrier gas, with H$_2$O $\approx$ 100 ppm, and with a pressure of about 1.05 atm.

The rate constant of reaction R1b was determined from optimization of the value of k_{1b} at selected experimental conditions using the detailed chemical kinetic model. Figure 7 summarizes the values of k_{1b} obtained from the experimental runs. We have disregarded data obtained at low (<20%) or high (>80%) conversions of SO$_3$. There is some scatter in the data, but within the uncertainty, values appear to be independent of the SO$_x$ inlet level and the O$_2$ concentration, as would be expected. The flow reactor data are consistent with a rate constant for SO$_3$ + N$_2$ $\rightleftharpoons$ SO$_2$ + O + N$_2$ of 5.7 × 10^{17} exp-(−40000/T) cm^3/(mol s) in the temperature range of 1273–1348 K.

Similar, but slightly lower, values of k_{1b} could be obtained from a simple analysis of the R1b–R2 reaction sequence, assuming the oxygen atom is in the steady state. Reaction R2 can be assumed to be irreversible, since the reverse step, SO$_2$ + O$_2$, is endothermic by about 150 kJ/mol. The decomposition rate for SO$_3$ can be written as

$$\dot{R}_{SO_3} = -k_{1b}[SO_3][M] - k_2[SO_3][O] + k_1[SO_2][M] \quad (3)$$

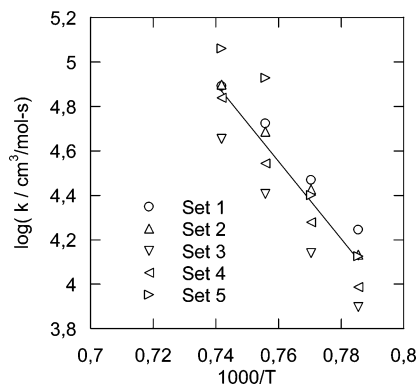**Figure 7.** Values of the rate constant for $SO_3 + N_2$ (R1b) determined from the results of the flow reactor experiments. The solid line is a best-fit line to the data, corresponding to $k_{1b} = 5.7 \times 10^{17} \exp(-40000/T)$ cm^3/(mol s). The values were obtained from data at fractional conversions of SO_3 between 20 and 80%.

The steady-state concentration of O is then

$$[O]_{ss} = \frac{k_{1b}[SO_3][M]}{k_1[SO_2][M] + k_2[SO_3]} \qquad (4)$$

Inserting the expression for $[O]_{ss}$, we get after some manipulation

$$\dot{R}_{SO_3} = k_{1b}[SO_3][M]\left[\frac{k_1[SO_2][M] - k_2[SO_3]}{k_1[SO_2][M] + k_2[SO_3]} - 1\right] \quad (5)$$

An assumption that $k_2[SO_3] \gg k_1[SO_2][M]$ leads to a simple expression for the SO_3 consumption rate, $-\dot{R}_{SO_3} = 2k_{1b}[SO_3]$-[M], from which k_{1b} can easily be obtained. Since R2 is comparatively fast according to the flame measurements, the inequality is almost fulfilled and the error in the values in k_{1b} from the simple analysis, compared to the detailed analysis, is only of the order of 30%. It is noteworthy that a very low value for k_2, such as that proposed by Alzueta et al.,[6] leads to k_1-$[SO_2][M] \gg k_2[SO_3]$ and thereby $\dot{R}_{SO_3} = 0$. This is in conflict with the experimental observations; the present flow reactor data support the comparatively high value for k_2 derived from flames.

The error analysis conducted includes an experimental uncertainty and a modeling uncertainty. The experimental uncertainty involves uncertainty in inlet concentrations, outlet concentrations, reactor residence time in the isothermal zone, reactor temperature, and the potential loss of SO_3 or O atoms on the reactor surface; the modeling uncertainty involves uncertainty in the value of k_2. Of special concern, is the potential impact of reactions on the surface of the quartz reactor. Sulfur trioxide is known to absorb on glass surfaces where it may act to promote the recombination of atomic oxygen.[27,28] However, an experiment conducted in a flow reactor with half the diameter (i.e., twice the surface-to-volume ratio) of the standard reactor yielded a value of k_{1b}, which within the scatter was in agreement with the data from the larger reactor. From an assessment of each contribution, we estimate the overall uncertainty in k_{1b} to be a factor of 2.

Figure 8 compares the data for the thermal dissociation rate of SO_3 with the only other measurements of this reaction, the shock tube study of Astholz et al.[10] While the present study involved nitrogen as collision partner, Astholz et al. conducted their experiments in argon. The two sets of data appear to be consistent, but a direct comparison is difficult due to the differences in the temperature regime and bath gas.
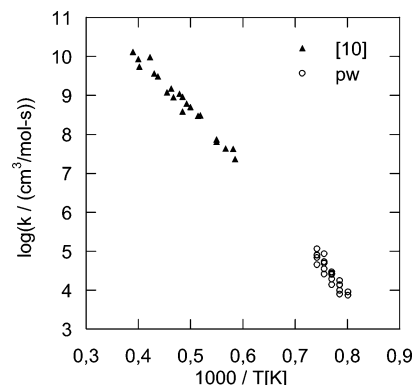
Figure 8. Arrhenius plot for the reaction $SO_3 + M \rightarrow SO_2 + O + M$ (R1b). The open symbols denote values obtained in the present work (pw), while the closed symbols represent the measurements of Astholz et al.[10] with Ar as the third body.
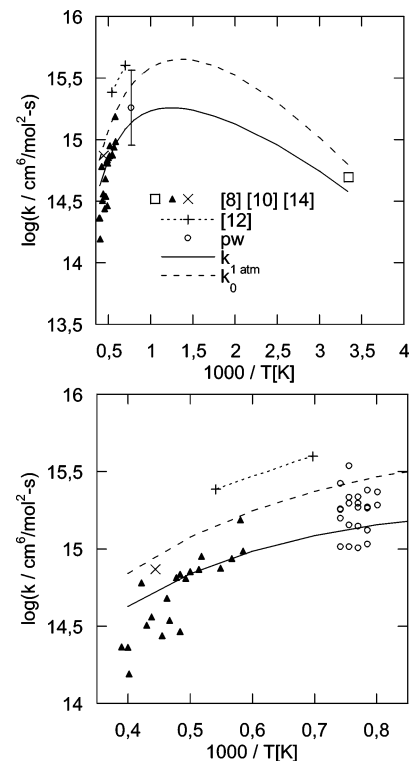
Figure 9. Arrhenius plot for the reaction $SO_2 + O + M \rightarrow SO_3 + M$ (R1). The upper part shows results for the 300−2500 K temperature range, while the lower part emphasizes the high-temperature results. The lines represent RRKM calculations originally adjusted to fit measurements for M = Ar but rescaled for N_2. The solid lines are the rate constant at 1 atm, while the dashed lines represent the low-pressure limit. The data shown are from the present work (pw) and from the literature: Atkinson and Pitts, Jr.,[8] Merriman and Levy,[14] Astholz et al.,[10] and Smith et al.[12] All data refer to the $SO_2 + O + N_2$ reaction, except the measurements of Astholz et al.[10] and Smith et al.,[12] which were performed with Ar as the third body.

In Figure 9, the results are compared with the theoretical rate constant for the reverse reaction, $SO_2 + O + N_2 \rightarrow SO_3 + N_2$ (R1), as well as selected literature results. The latter include the room-temperature result of Atkinson and Pitts, Jr.[8] and indirect measurements by Merryman and Levy from flames.[14] The results from the flow reactor study of Mueller et al.[7] and the shock tube study of Hwang et al.[15] on the reaction are not included, since they were obtained at higher pressures. The high-temperature data of Astholz et al.[10] and Smith et al.[12] are shown, even though they relate to argon as a bath gas. The values of k_1

from the present work and from Astholz et al. were derived from k_{1b} through the equilibrium constant for the reaction.

The upper part of Figure 9 shows results over a broad range of temperature, while the lower part emphasizes the high-temperature results. The solid and dashed lines in Figure 9 denote the theoretical rate constant for SO$_2$ + O (+N$_2$) at 1 atm and at the low-pressure limit, respectively. The high-pressure limit was taken from Naidoo et al.[9] Troe's unimolecular formalism has previously been applied to R1 with M = Ar, to obtain the broadening parameter F_c and, by fitting to measurements over 290−840 K, the average energy transfer per collision $-\langle \Delta E \rangle = 3000 \, J(T/298)^{-0.42}$.[9] That representation of the falloff curves was reevaluated in this study for M = N$_2$. Collision rates with the bath gas were calculated in the same way as outlined earlier[9] based on $\sigma = 3.62$ and $\epsilon/k = 97.5$ K for N$_2$. To match the ratio $k_{1,0}(N_2)/k_{1,0}(Ar) = 1.3$ determined by Atkinson and Pitts at room temperature,[8] we chose $-\langle \Delta E \rangle = 5740$ J for N$_2$ collisions and assumed the same temperature dependence as for Ar. The new broadening parameter is given in Table 1, along with the $k_{1,0}$ expression for M = N$_2$. This expression fits the Troe formulation to within about 15%. Comparison with the expression for M = Ar[9] indicates similar rate constants at the low-pressure limit, with $k_{1,0}(N_2)/k_{1,0}(Ar) \approx 1.2$ and little temperature dependence of this ratio.

The results in Figure 9 confirm that the recombination of sulfur dioxide with oxygen atoms has a positive activation energy at low temperatures, while at high temperatures the reaction rate decreases with temperature. The reaction appears to be in the falloff region at atmospheric pressure over a wide range of temperature, including the conditions of the present work. The value of k_1 derived from the flow reactor data is seen to be in good agreement with the theoretical rate coefficients. According to the present study, the rate constant using N$_2$ as collision partner does not deviate much from that using Ar. It is worthwhile to compare the present results with those of Mueller et al.,[7] who studied the high-pressure falloff behavior of the reaction. Under the conditions of the present work (1000−1400 K, atmospheric pressure), their proposed rate constant for SO$_2$ + O (+N$_2$) is in very good agreement with the present work, being within 25% of our theoretical value. Within the uncertainty, the present results are also in agreement with the shock tube results of Hwang et al.;[15] they derived a value of k_1 of $(3.9 \pm 2.0) \times 10^{15}$ cm^6 mol^{-2} s^{-1} at 960−1150 K and pressures of 1.3−2.7 atm.

Concluding Remarks

On the basis of experiments conducted in a laminar flow reactor, a rate constant for SO$_3$ + N$_2$ → SO$_2$ + O + N$_2$ (R1b) of $5.7(^{+5.7}_{-2.9}) \times 10^{17}$ exp($-40000/T$) cm^3/(mol s) was derived for the temperature range of 1273−1348 K and atmospheric pressure. The temperature and pressure dependence of the reverse reaction, SO$_2$ + O (+N$_2$), were estimated based on RRKM calculations for SO$_2$ + O (+Ar),[9] rescaling for N$_2$. The theoretical rate coefficients agree with the experimental value within the uncertainty. On the basis of the flame measurements of Smith et al.[12] and the present value of $k_{1,Ar}$, the rate constant for SO$_3$ + O → SO$_2$ + O$_2$ (R2) was estimated to be 6.9×10^{10} cm^3 mol^{-1} s^{-1} at 1269 K, with an uncertainty factor of 3. The

recommended rate constant $k_2 = 7.8 \times 10^{11}$ exp($-3065/T$) cm^3 mol^{-1} s^{-1} is consistent with other flame results as well as the present flow reactor data.

References and Notes

(1) Johnsson, J. E.; Glarborg, P. Sulfur Chemistry in Combustion I - Sulfur in Fuels and Combustion Chemistry. *Pollutants from Combustion. Formation Mechanisms and Impact on Atmospheric Chemistry*; Vovelle, C., Ed.; Kluwer Academic Publisher: Boston, MA, 2000; pp 283−301.

(2) Christensen, K. A.; Livbjerg, H. *Aerosol Sci. Technol.* **1996**, *25*, 185−199.

(3) Jensen, J. R.; Nielsen, L. B.; Schultz-Møller, C.; Wedel, S.; Livbjerg, H.; *Aerosol Sci. Technol.* **2000**, *33*, 490−509.

(4) Glarborg, P.; Marshall, P. *Combust. Flame* **2005**, *141*, 22−38.

(5) Glarborg, P.; Kubel, D.; Dam-Johansen, K.; Chiang, H. M.; Bozzelli, J. W. *Int. J. Chem. Kinet.* **1996**, *28*, 773−790.

(6) Alzueta, M. U.; Bilbao, R.; Glarborg, P. *Combust. Flame* **2001**, *127*, 2234−2251.

(7) Mueller, M. A.; Yetter, R. A.; Dryer, F. L. *Int. J. Chem. Kinet.* **2000**, *32*, 317−339.

(8) Atkinson, R.; Pitts, J. N., Jr. *Int. J. Chem. Kinet.* **1978**, *10*, 1081−1090.

(9) Naidoo, J.; Goumri, A.; Marshall, P. *Proc. Combust. Inst.* **2005**, *30*, 1219−1225.

(10) Astholz, D. C.; Glänzer, K.; Troe, J. *J. Chem. Phys.* **1979**, *70*, 2409−2413.

(11) Schwartz, D.; Gadiou, R.; Brilhac, J. F.; Prado, G.; Martinez, G. *Ind. Eng. Chem. Res.* 2000, 39, 2183-2189.

(12) Smith, O. I. Tseregounis, S.; Wang, S.-N. *Int. J. Chem. Kinet.* **1982**, *14*, 679−697.

(13) Smith, O. I. Tseregounis, S.; Wang, S.-N.; Westbrook, C. K. *Combust. Sci. Technol.* **1983**, *30*, 241−271.

(14) Merryman, E. L.; Levy, A. *Proc. Combust. Inst.* **1979**, *17*, 727−736.

(15) Hwang, S. M.; Cooke, J. A.; DeWitt, K. J.; Rabinowitz, M. J. Determination of Rate Coefficients of SO$_2$ + O + M → SO$_3$ + M Reaction. 30th International Symposium on Combustion, Work-In−Progress poster, Chicago, IL, July 25−30, 2004.

(16) Dunna, J. P.; Stenger, H. G., Jr.; Wachs, I. E. *Catal. Today* **1999**, *51*, 301−318.

(17) Giakoumelou, I. Parvulescu, V.; Boghosian, S. *J. Catal.* **2004**, *225*, 337−349.

(18) Zheng, J.; Jensen, A. D. Unpublished results.

(19) Lutz, A.; Kee, R. J.; Miller, J. A. *SENKIN: A Fortran Program for Predicting Homogeneous Gas-Phase Chemical Kinetics with Sensitivity Analysis*; Sandia Report SAND87-8248; Sandia National Laboratories: Livermore, CA, 1987.

(20) Kee, R. J.; Rupley, F. M.; Miller, J. A. *CHEMKIN-II: A Fortran Chemical Kinetics Package for the Analysis of Gas-Phase Chemical Kinetics*; Sandia Report SAND89-8009; Sandia National Laboratories: Livermore, CA, 1989.

(21) Blitz, M. A.; Hughes, K. J.; Pilling, M. J. *J. Phys. Chem. A* **2003**, *107*, 1971−1978.

(22) Atkinson, R.; Baulch, D. L.; Cox, R. A.; Hampson, R. F.; Kerr, J. A.; Troe, J. *J. Phys. Chem. Ref. Data* **1992**, *21*, 1125−1568.

(23) Schofield, K. *J. Phys. Chem. Ref. Data* **1973**, *2*, 25−84.

(24) Burdett, N. A.; Langdon, W. E.; Squires, R. T. *J. Inst. Energy* **1984**, 373.

(25) Cullis, C. F.; Henson, R. M.; Trimm, D. L. *Proc. R. Soc. London, Ser. A* **1966**, *295*, 72−83.

(26) Kristensen, P. G. Nitrogen Burnout Chemistry. Ph.D. Thesis, Department of Chemical Engineering, Technical University of Denmark, Lyngby, Denmark, 1997.

(27) Kaufman, F. *Proc. R. Soc. London, Ser. A* **1958**, *247*, 123−139.

(28) Cullis, C. F.; Mulcahy, M. F. R. *Combust. Flame* **1972**, *18*, 225−292.

Paper III

The Fate of SO_3/SO_2 in the System with N_2O Addition

Lusi Hindiyarti and Peter Glarborg
Department of Chemical Engineering, Technical University of Denmark,
DK–2800 Lyngby, Denmark

Abstract

The fate of SO_3/SO_2 in a system with N_2O addition were investigated. Experiments using flow reactors in range temperature of 1073 to 1373 K were conducted to investigate the importance of reaction $SO_3+O \rightleftharpoons SO_2+O_2$ for the ratio of SO_3/SO_2. Experimental results agree favorably when compared to the predicted results from a detailed kinetic modeling. The experimental data supports a low rate constant for reaction $SO_3+O \rightleftharpoons SO_2+O_2$. This reaction plays insignificant role for the SO_3/SO_2 ratio under most conditions of interest in this study. The mechanism of SO_3 decomposition only involves reaction of SO_3 with H.

Keywords: fate, SO_3/SO_2, mechanism, N_2O

Introduction

The combustion of fuel containing sulfur results in oxides sulfur formation mainly SO_2 and SO_3. The presence of SO_3 enhances the corrosion potential of the flue gas [1] and it has implications for formation of aerosols in biomass-fired systems [2, 3, 4].

Oxidation of SO_2 to SO_3 is kinetically limited [1]. The reactions that may contribute to the formation of SO_3 involve interaction of SO_2 with the radical pool [5, 6, 7]. In the presence of nitrogen oxides there is a kinetic coupling of NO_x and SO_x chemistry via the radical pool [5, 7]. While the overall mechanisms for SO_3 formation are fairly well known, kinetic modeling of the process still suffers from a lack of accurate kinetic data, and refinements are required in order to establish a reliable mechanism [4, 5].

It is generally believed that reaction $SO_3 + O \rightleftharpoons SO_2 + O_2$ is important for the ratio of SO_2/SO_3 in the system under combustion condition or industrial processes [8, 9, 10]. Despite the importance of this reaction, there is a significant uncertainty in its rate constant. A recent study by authors [10] indicates a fairly high rate constant for this reaction. Other data from literature study suggest a rate constant which vary by several orders of magnitude [6, 11, 12, 13, 14, 15, 16]. While most of the data support a high rate constant for this reaction; only the investigation by Alzueta et al. [6] suggest a low rate constant.

The objective of the present work is to study the rate of reaction $SO_3 + O \rightleftharpoons SO_2 + O_2$ in the range of temperature from 1073 to 1373 K using experimental work. The experimental results are compared to a detailed kinetic modeling for the fate of SO_3/SO_2 using an updated sulfur mechanism from a recent work [17]. The N_2O gas is used during the experiments in this study as an O source. Fate of SO_3/SO_2 in the system with N_2O addition under those conditions is discussed. A gas containing a mixture of SO_2 and O_2 in N_2 is led to a catalyst, where SO_2 is partly oxidized to SO_3 at 673 K. The resulting gas is then led to a flow reactor, where N_2O is introduced to the mixture gases. The SO_3 in the homogeneous reactor may be converted back to SO_2 by reaction with O, H, HO_2, OH and by thermal dissociation.

Experimental

The experimental setup is described in more detail elsewhere [10] consists of two quartz reactors in series in separate ovens. In the first reactor, SO_2 was oxidized to SO_3 over a doped V_2O_5-WO_3-TiO_2 catalyst. The temperature along the catalytic reactor was set to 673 K. The product gas from the first reactor was fed into the second reactor through a heated line at 415 K in order to prevent condensation. N_2O was introduced to the gases prior to entering the homogeneous reactor as a source of O. The second reactor was homogeneous, operated at high temperatures (up to 1373 K) and the availability of O in the system was expected to promote conversion of SO_3 to SO_2.
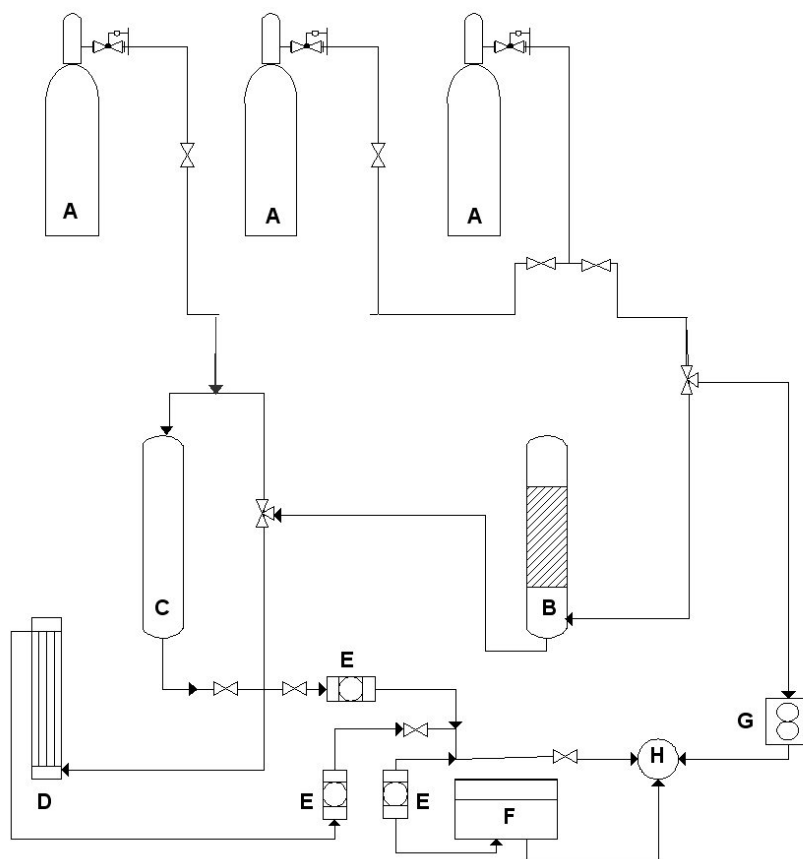
Figure 1: Schematic of the experimental setup. A. Gas cylinders (O_2, SO_2, N_2O). B. Catalytic reactor. C. Homogeneous reactor. D. Condenser. E. Filter. F. Gas analyzers. G. Bubble flow meter. H. Purging system.

A schematic of the experimental setup is presented in figure 1. Sulfur dioxide, oxygen and nitrogen were mixed and directed either to bypass (the flow meter -
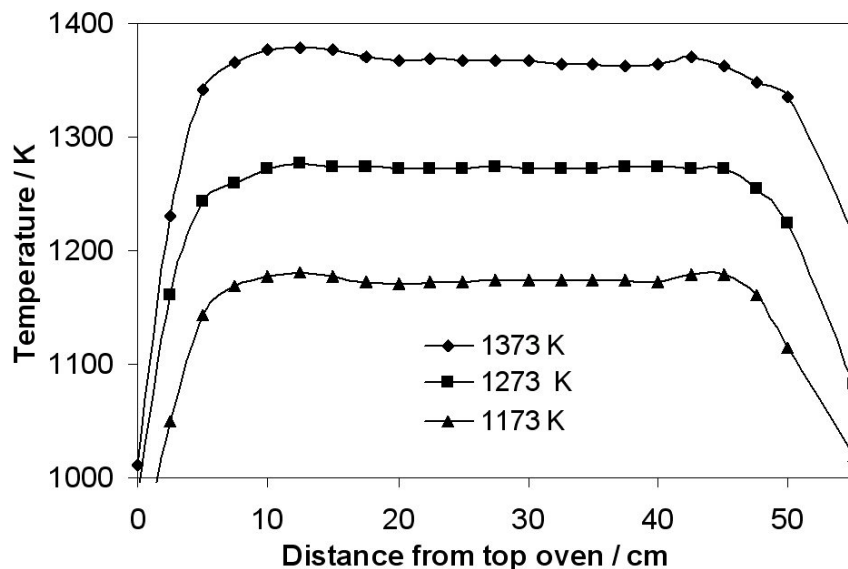
Figure 2: Characteristic temperature profile in the homogeneous reactor.

G) or to the catalytic reactor (B). The bubble flow meter served to measure the flow of the input gases from the gas cylinders as a check for mass flow meters. The output of the catalytic reactor was directed either to the homogeneous reactor (C) or to the gas conditioning and analyzers (F). By-pass lines were available for both reactors so that input and output gases could be analyzed and the setup could be used in a flexible way. Prior to the analyzers, a condenser (D), two filters (E) and a condense alarm were located to protect the analyzer from any aerosols and/or condensed liquids.

The catalytic reactor was a heterogeneous quartz reactor with a 2 cm inner diameter. The catalyst was cut into pieces and stacked upon a porous plate in the isothermal zone of the reactor. The total length of the reactor occupied by the catalyst material was 16 cm. This reactor was operated at 673 K and the reactor residence time was about 3 s.

The homogeneous reactor consisted of a quartz tube located in a three-zone electrically heated oven. N_2O gas was added to the mixture between the first and the second reactor. The reactants entered the homogeneous reactor premixed and were heated together. The tubes used for the second reactor were designed to approximate plug flow in the laminar flow regime. Characteristic temperature profiles for the reactor are shown in figure 2. In most of the temperature range investigated, a flat temperature profile was obtained in the isothermal region

4

of the reactor, but at the highest temperatures variations within ±15 K were observed.

The reactor temperatures were controlled with thermocouples with an accuracy of ±5K. During experiments the thermocouples were placed outside the reactor to avoid contact with the reacting gases, but the temperature profiles were obtained from probing inside the reactor with an inert flow. The concentration of SO_2 was measured continuously by a UV analyzer with an accuracy of ±3%.

Detailed Kinetic Model

The experimental results were interpreted in terms of a detailed reaction mechanism. Since the homogeneous reactor was designed to approximate plug flow, the reactor results were modeled with SENKIN [18], which is part of the CHEMKIN library [19]. SENKIN performs integration in time. The results of the SENKIN calculations were compared to experimental data using the nominal residence time in the isothermal part of the reactor.

The reaction mechanism consisted of a H_2/O_2 subset and a full description of the H/S/O subset. The H_2/O_2 subset was included in the model to account for effects of water vapor. Presence of water vapor, even in small concentrations, may conceivably lead to an O/H radical pool, initiated by the reaction

$$O + H_2O \rightleftharpoons OH + OH$$
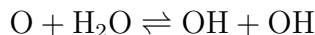
The H/S/O subset and the corresponding thermochemistry were adopted from previous work [4, 6, 10, 17].

Results and Discussion

The experiments were performed at atmospheric pressure with temperatures in the homogeneous reactor in the range 1073 to 1373 K. Typical conditions involved SO_3 and SO_2 concentrations into the homogeneous reactor of about 150-400 ppm, with around 1-4% O_2 in N_2. Also trace amounts of water vapor were present. It is previously estimated to be in the range 30-150 ppm [20], but in the present study a significantly lower amount of water traces is proposed. The conversion efficiency of the catalytic reactor depended on the SO_2/O_2 ratio; 35% to 60% conversion of SO_2 to SO_3 was observed for $SO_2:O_2$

ratios between 0.01 and 0.1. Once the SO_2 concentration out of the catalytic reactor was stabilized, the product gas was fed into the homogeneous reactor. The N_2O was added to the gases prior entering the homogeneous reactor. The temperature in the homogeneous reactor was increased in steps of 25 K above the chosen starting temperature, securing steady-state conditions between each temperature increment.
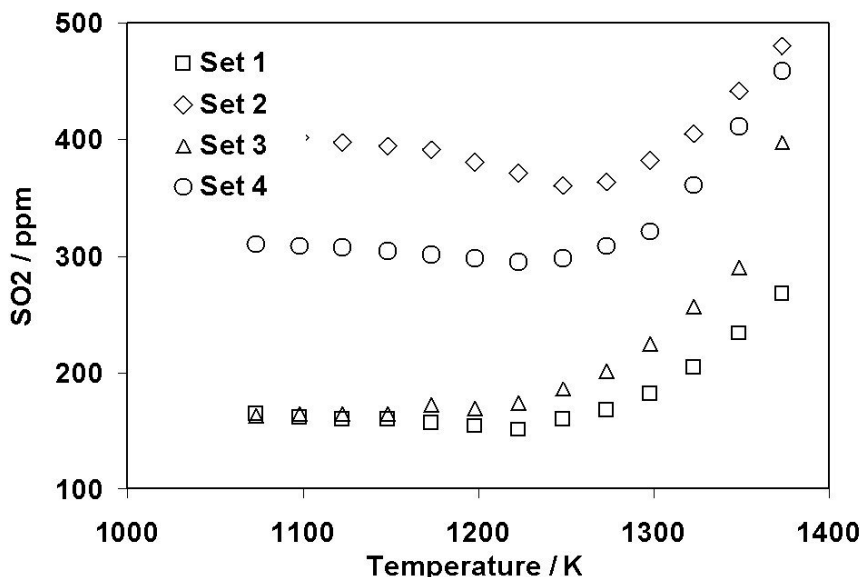
Figure 3: Experimental results for the decomposition of SO_3 in $SO_3/SO_2/N_2O$ system. Set 1: SO_3 = 214.7 ppm, SO_2 = 156 ppm, N_2O = 164 ppm, O_2 = 4.07 %; residence time 1441.28/T[K]. Set 2: SO_3 = 201.2 ppm, SO_2 = 401 ppm, N_2O = 131 ppm, O_2 = 1.02 %; residence time 1356.3/T[K]. Set 3: SO_3 = 387.4 ppm, SO_2 = 156 ppm, N_2O = 176 ppm, O_2 = 4.27%; residence time 1519.65/T[K]. Set 4: SO_3 = 310.8 ppm, SO_2 = 300.4 ppm, N_2O = 143 ppm, O_2 = 1.02%; residence time 1377.45/T[K]. All experiments are carried out with N_2 as carrier gas, with traces $H_2O \approx$ 0-100 ppm, and with a pressure of about 1.05 atm. The residence time, varying with reactor temperature as indicated (constant mass flow), applies to the isothermal part of the reactor (about 40 cm of the length).

Experimental results for SO_3 decomposition in the temperature range 1073 to 1373 K are shown in Figure 3. Over this temperature range the SO_3 decompositon increased from being negligible to being significant. The oxygen level affects the oxidation of SO_2 to SO_3 in the catalytic reactor, but has little effect on the SO_3 decomposition in the homogeneous reactor.

In the present study, SO_3 is expected to decompose through reaction involving
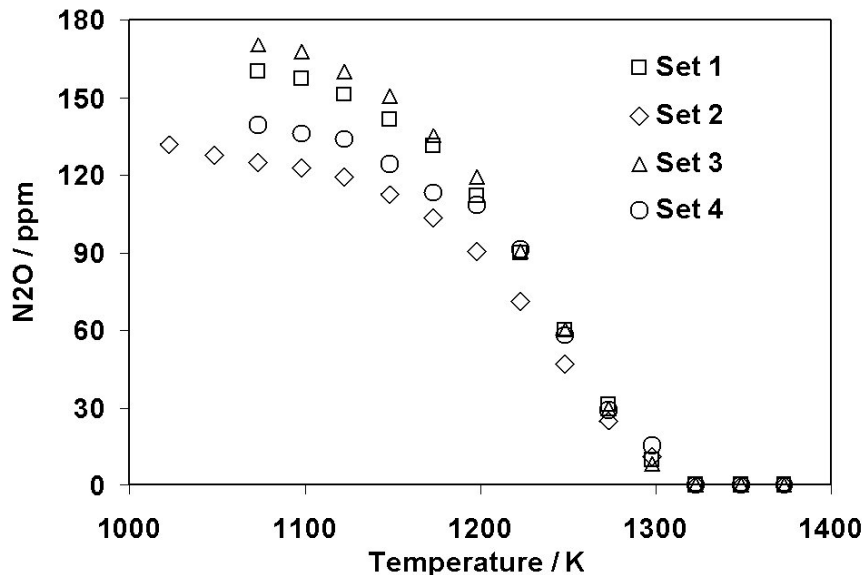
Figure 4: Experimental results for the decomposition of N_2O in $SO_3/SO_2/N_2O$ system. Set 1: SO_3 = 214.7 ppm, SO_2 = 156 ppm, N_2O = 164 ppm, O_2 = 4.07 %; residence time 1441.28/T[K]. Set 2: SO_3 = 201.2 ppm, SO_2 = 401 ppm, N_2O = 131 ppm, O_2 = 1.02 %; residence time 1356.3/T[K]. Set 3: SO_3 = 387.4 ppm, SO_2 = 156 ppm, N_2O = 176 ppm, O_2 = 4.27%; residence time 1519.65/T[K]. Set 4: SO_3 = 310.8 ppm, SO_2 = 300.4 ppm, N_2O = 143 ppm, O_2 = 1.02%; residence time 1377.45/T[K]. All experiments are carried out with N_2 as carrier gas, with traces $H_2O \approx$ 0-100 ppm, and with a pressure of about 1.05 atm. The residence time, varying with reactor temperature as indicated (constant mass flow), applies to the isothermal part of the reactor (about 40 cm of the length).

O, since a recent work [10] suggest a fairly high rate constant for reaction $SO_3+O \rightleftharpoons SO_2+O_2$, which means that this reaction would participate in the SO_3 decomposition when there is enough available O in the system.

Figure 4 shows the decomposition of N_2O from the experimental data. The four experimental data cover N_2O levels in the range 125-176 ppm. Over this temperature range the N_2O decomposition increased from being negligible to being almost complete.

In order to investigate the mechanism active for SO_3 decomposition, and to study the importance of reaction $SO_3+O \rightleftharpoons SO_2+O_2$ in the system investigated, the experimental data were introduced to a detailed kinetic model from a recent work [17] without any adjustment in the sulfur chemistry. The results signif-

icantly overpredict the SO_3 decomposition into SO_2. The sensitivity analysis suggests that rate constant for reaction $SO_3+O \rightleftharpoons SO_2+O_2$ is the most sensitive in the system investigated.

A significantly lower rate constant for reaction $SO_3+O \rightleftharpoons SO_2+O_2$ from Alzueta et al. [6] is then used in the detailed kinetic modeling. The results of modeling are compared to the experimental data on the concentration of SO_2, SO_3, and N_2O.

The results are shown in figure 5. By applying this detailed kinetic model, and traces of water (4-11 ppm), the predicted results is seen to describe the experimental data both for SO_2, SO_3 and N_2O quite well. For all sets the kinetic model is in good agreement with the experimental data within the experimental uncertainty. The decomposition of SO_3 starts to speed up at around 1273 K. In this study, the experimental data appears to support the suggestion of a low rate constant for reaction $SO_3+O \rightleftharpoons SO_2+O_2$, contrary to a suggestion from a recent work [10].

If a higher rate constant for reaction $SO_3+O \rightleftharpoons SO_2+O_2$ previously suggested [10] is applied, the agreement between experimental data and the predicted results is not achieved. While applying a low rate constant from Alzueta et al. [6], a good agreement is achieved. The results are shown in figure 6. These results support the suggestion of reaction $SO_3+O \rightleftharpoons SO_2+O_2$ being very slow. In this study, this reaction is found to be slow and insignificant under most condition investigated. However, a determination of a rate constant from this study is difficult due to the uncertainty of water traces available in the system.

It is noteworthy that a very limited trace amount of water was introduced in the detailed kinetic modeling. The present system investigated is very sensitive to the availability of water in the system. The water available in the system is assumed to be originated from water content in the air which diffused to the system through teflon lines during experiments. The result of detailed kinetic modeling, where the water concentration introduced to the model is varied, compared to the experimental data from set 2 is shown in figure 7. It is clear that the water concentration has a significant influence on the results of the model predictions. From the simulation, around 4-11 ppm water concentration appears to be the favored concentration for the model to achieve a good agreement with the experimental data.

Sensitivity analysis from the model shows that the SO_3 decomposition is only sensitive to the reaction,

$$SO_2 + O(+M) \rightleftharpoons SO_3(+M)$$

8
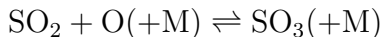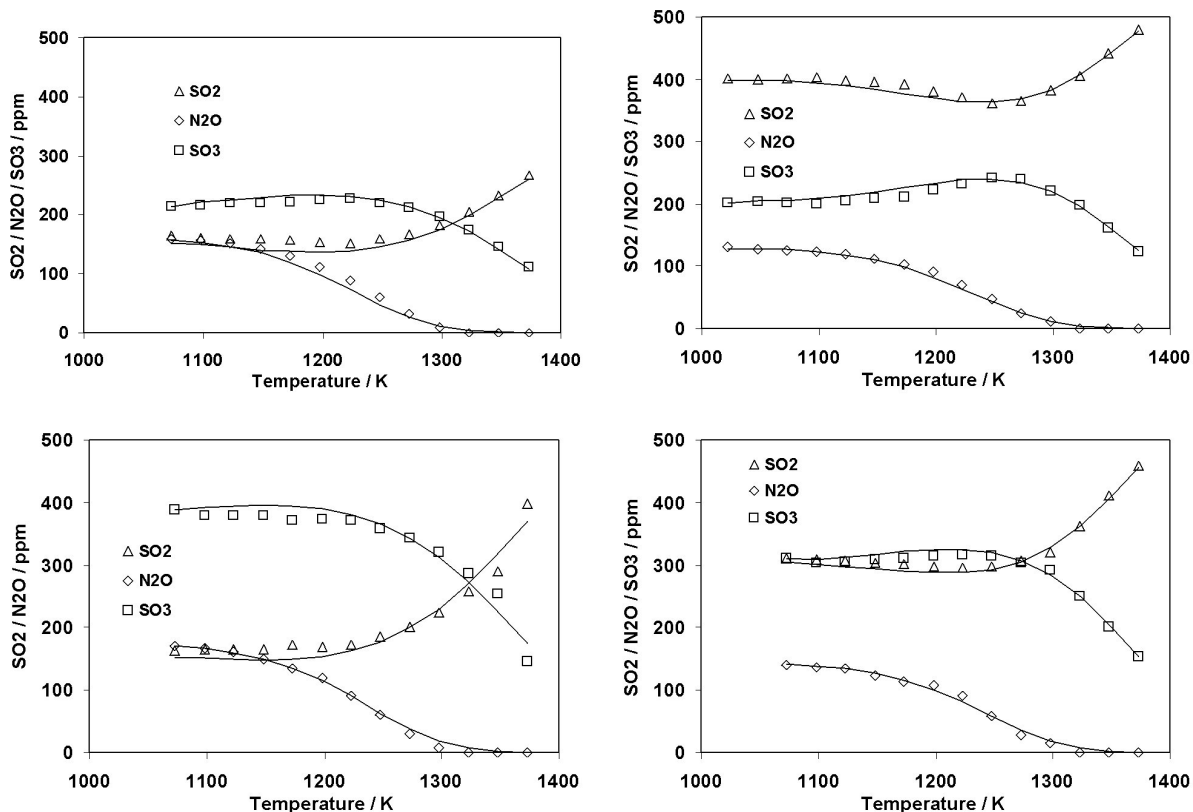
Figure 5: Comparison of the experimental data (symbols) to the predicted results (lines). Clockwise (from top left) Set 1: $SO_3 = 214.7$ ppm, $SO_2 = 156$ ppm, $N_2O = 164$ ppm, $O_2 = 3.07$ %; residence time $1441.28/T[K]$. Set 2: $SO_3 = 201.2$ ppm, $SO_2 = 401$ ppm, $N_2O = 131$ ppm, $O_2 = 1.02$ %; residence time $1356.3/T[K]$. Set 3: $SO_3 = 387.4$ ppm, $SO_2 = 156$ ppm, $N_2O = 176$ ppm, $O_2 = 4.27$%; residence time $1519.65/T[K]$. Set 4: $SO_3 = 310.8$ ppm, $SO_2 = 300.4$ ppm, $N_2O = 143$ ppm, $O_2 = 1.02$%; residence time $1377.45/T[K]$. All experiments are carried out with N_2 as carrier gas, with traces $H_2O \approx 0\text{-}100$ ppm, and with a pressure of about 1.05 atm. The residence time, varying with reactor temperature as indicated (constant mass flow), applies to the isothermal part of the reactor (about 40 cm of the length).

The results can be seen in figure 8 for both 4 ppm and 100 traces water introduced to the model.

The reaction $SO_3+O \rightleftharpoons SO_2+O_2$, which is previously suggested to be an important consumption step for SO_3 decomposition, is found to be slow and plays insignificant role under most condition of interest in this study. By applying
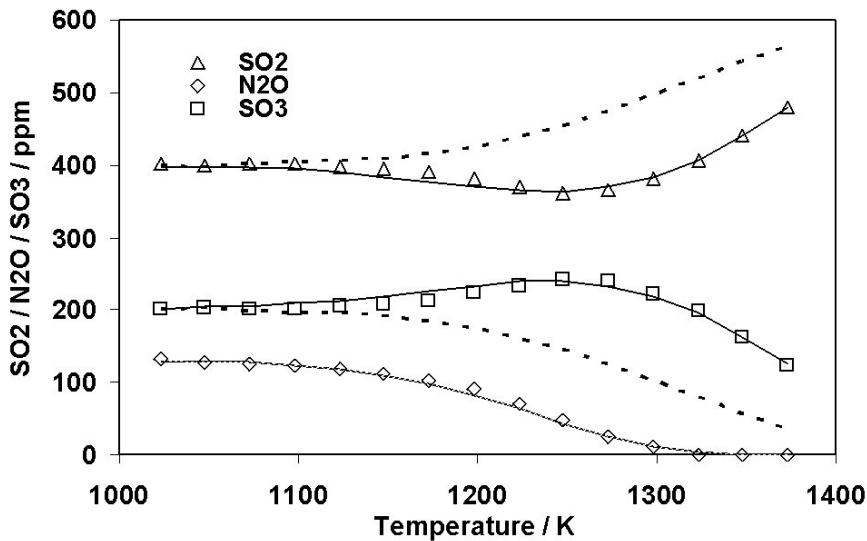
9

Figure 6: Comparison between experimental results from set 2 (symbols) and modeling predictions (lines) with a rate constant for reaction SO_3+O from Yilmaz et al. [10](dashed line) and Alzueta et al. [6] (solid line). Data set 2: SO_3 = 201.2 ppm, SO_2 = 401 ppm, N_2O = 131 ppm, O_2 = 1.02 %; residence time 1356.3/T[K]. The experiments are carried out with N_2 as carrier gas, with traces of $H_2O \approx$ 5-10 ppm, and with a pressure of about 1.05 atm.

both 4 or 100 ppm H_2O concentration in the model, rate production analysis suggest that the consumption of SO_3 is mainly through reaction SO_3+H $\rightleftharpoons SO_2$+OH. The N_2O decomposed through reaction N_2O(+M) $\rightleftharpoons N_2$+O(+M) and provide O.

In the present study, the experimental data supports a low rate constant for reaction SO_3+O$\rightleftharpoons SO_2$+O_2 as proposed by Alzueta et al.[6]. The agreement between predicted results and experimental data is good when a very low water concentration is introduced in the model prediction. However, the result of $SO_2/SO_3/N_2O$ system is not conclusive, since the system investigated is very sensitive to traces of water, and there is uncertainty of the water content available in the system.
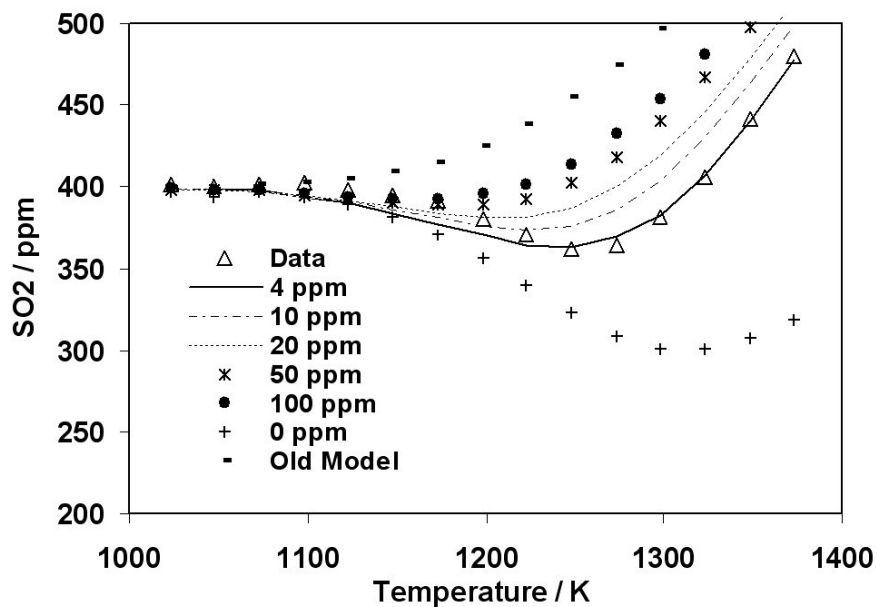
Figure 7: Comparison between experimental results from set 2 (open triangle symbols) and modeling predictions by varying the H_2O inlet to the model (solid, dashed lines and other symbols, old model (model with a high rate for SO_3+O) for SO_2 outlet concentration. Set 2: $SO_3 = 201.2$ ppm, $SO_2 = 401$ ppm, $N_2O = 131$ ppm, $O_2 = 1.02$ %; residence time 1356.3/T[K]. The experiments are carried out with N_2 as carrier gas, with $H_2O \approx 0\text{-}100$ ppm, and with a pressure of about 1.05 atm.
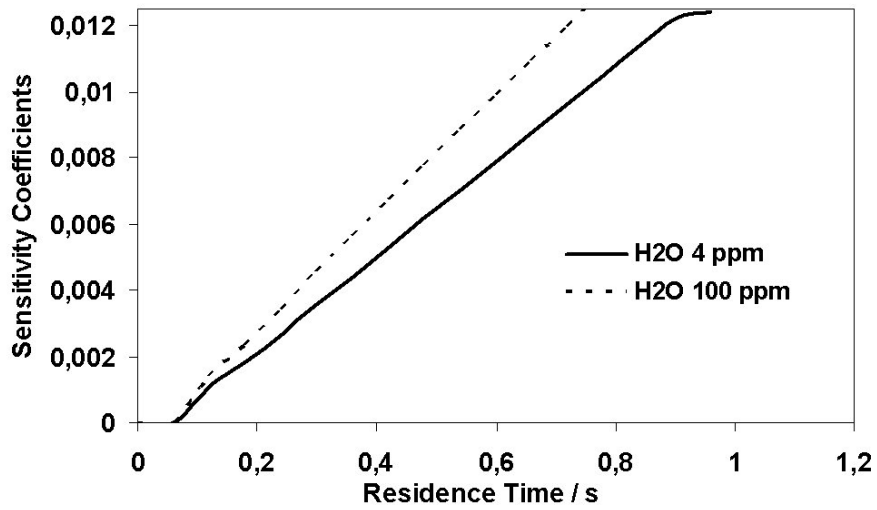
Figure 8: Sensitivity coefficients of reaction $SO_2+O(+M)=SO_3(+M)$ toward SO_3 decomposition at 1350 K for the system presented in figure 7.

Conclusions

In the present study, experiments to investigate the fate of SO_3/SO_2 in the system with N_2O addition under combustion condition has been conducted. The experimental data supports a low rate constant for reaction $SO_3+O \rightleftharpoons SO_2+O_2$. This reaction plays insignificant role for the SO_3/SO_2 ratio under most conditions of interest. The SO_3 decomposition mainly involves reaction of SO_3 with H. However, it is important to point out that the $SO_2/SO_3/N_2O$ system investigated in this study is very sensitive to traces of water, and there is uncertainty of the water content available in the system. Due to this uncertainty, the results of $SO_2/SO_3/N_2O$ system is not conclusive.

Acknowledgments

References

[1] Johnsson, J.E. and Glarborg, P.; "Sulfur Chemistry in Combustion I – Sulfur in Fuels and Combustion Chemistry.", Pollutants from Combustion. Formation Mechanisms and Impact on Atmospheric Chemistry, C. Vovelle (ed.), Kluwer Academic Publisher, pp. 283–301 (2000).

[2] Christensen, K.A. and Livbjerg, H.; Aerosol Sci. Technol. 1996, 25, 185-199.

[3] Jensen, J.R., Nielsen, L.B., Schultz-Møller, C., Wedel, S., and Livbjerg, H.; Aerosol Sci. Technol. 2000, 33, 490-509.

[4] Glarborg, P. and Marshall, P.; Combust. Flame 2005, 141, 22-38.

[5] Glarborg, P., Kubel, D., Dam–Johansen, K., Chiang, H.M., and Bozzelli, J.W.; Int. J. Chem. Kinet. 1996, 28, 773-790.

[6] Alzueta, M.U., Bilbao, R., and Glarborg, P.; Combust. Flame 2001, 127, 2234-2251.

[7] Mueller, M.A., Yetter, R.A., and Dryer, F.L.; Int. J. Chem. Kin. 2000, 32, 317-339.

[8] Cullis, C.F., and Mulcahy, M.F.R.; Combust. Flame 1972, 18, 225-292.

[9] Levy, A., Merryman, E.L., and Reid, W.T.; Environmental Sci. and Technol. 1970, 4, 653-662.

[10] Yilmaz, A., Hindiyarti, L., Jensen A.D., Glarborg P., J. Phys. Chem A. 2006,110, 6654-6659.

[11] Schofield,K.; J. Phys. Chem. Ref. Data 1973, 2, 25-84.

[12] Burdett, N.A., Langdon, W.E., and Squires, R.T.; J. Inst. Energy, 57, 373-376, 1984.

[13] Smith, O.I. Tseregounis, S., and Wang, S.-N.; Int. J. Chem. Kin. 1982, 14, 679-697.

[14] Smith, O.I. Tseregounis, S., Wang, S.-N., and Westbrook, C.K.; Combust. Sci. Technol. 1983, 30, 241-271.

[15] Merryman, E.L. and Levy, A.; Proc. Combust. Inst. 1979, 17, 727-736.

[16] Fenimore, C.P., and Jones, G.W.; J. Phys. Chem. 1965, 69, 3593.

[17] Rasmussen, C.L., Glarborg P., Marshall P., Proc. Combust. Inst. 2007, 31, 339-347.

[18] Lutz, A., Kee, R.J., and Miller, J.A., "SENKIN: A Fortran Program for Predicting Homogenous Gas Phase Chemical Kinetics with Sensitivity Analysis", Sandia Report SAND87–8248, Sandia National Laboratories, Livermore, CA (1987).

[19] Kee, R.J., Rupley, F.M., and Miller, J.A., "CHEMKIN–II: A Fortran Chemical Kinetics Package for the Analysis of Gas-Phase Chemical Kinetics", Sandia Report SAND89-8009, Sandia National Laboratories, Livermore, CA (1989).

[20] Kristensen, P.G., "Nitrogen Burnout Chemistry", PhD Thesis, Department of Chemical Engineering, Technical University of Denmark (1997).

Paper IV

Reactions of SO_3 with the O/H radical pool under combustion conditions

Lusi Hindiyarti and Peter Glarborg

Department of Chemical Engineering, Technical University of Denmark,
DK–2800 Lyngby, Denmark

Paul Marshall

Center for Advanced Scientific Computation and Modeling
Department of Chemistry, University of North Texas, P.O. Box 305070,
Denton, Texas 76203-5070

The reactions of SO_3 with H, O, and OH radicals have been investigated by ab initio calculations. For the SO_3+H reaction (1), the lowest energy pathway involves initial formation of HSO_3 and rearrangement to $HOSO_2$, followed by dissociation to OH + SO_2. The reaction is fast, with $k_1 = 8.4 \cdot 10^9$ $T^{1.22}$ exp(-13.9 kJ mol^{-1}/RT) cm^3 mol^{-1} s^{-1} (700-2000 K). The SO_3+O $\rightarrow$ SO_2+O_2 reaction (2) may proceed both on the triplet and singlet surface, but due to a high barrier the reaction is predicted to be slow. The rate constant can be described as $k_2 = 2.8 \cdot 10^4$ $T^{2.57}$ exp(-122.3 kJ mol^{-1}/RT) cm^3 mol^{-1} s^{-1} for T > 1000 K. The SO_3+OH reaction to form SO_2+HO_2 (3) proceeds by direct abstraction, but is comparatively slow, with $k_3 = 4.8 \cdot 10^4$ $T^{2.46}$ exp(-114.1 kJ mol^{-1}/RT) cm^3 mol^{-1} s^{-1} (800-2000 K). The revised rate constants and detailed reaction mechanism are consistent with experimental data from batch reactors, flow reactors, and laminar flames on oxidation of SO_2 to SO_3. The SO_3+O reaction is found to be insignificant during most conditions of interest; even in lean flames, SO_3+H is the major consumption reaction for SO_3.

1

Introduction

High temperature sulfur reactions continue to be of both theoretical and practical interest [1]. The combustion of fuel-bound sulfur results in formation of oxides of sulfur, mainly SO_2 and SO_3. Sulfur trioxide in combustion systems causes formation of sulfuric acid, which will condense and corrode metal surfaces at temperatures below the dew point [2, 3]. In addition it may contribute to aerosols and particulate emissions [4, 5, 6]. A better understanding of the mechanisms for SO_3 formation and destruction is a necessary step in the effort to minimize these problems. A number of reactions may conceivably affect the SO_3 concentration. Reactions of particular interest are those of SO_3 with H, O, and OH,

$$SO_3 + H \rightleftharpoons SO_2 + OH \tag{1}$$

$$SO_3 + O \rightleftharpoons SO_2 + O_2 \tag{2}$$

$$SO_3 + OH \rightleftharpoons SO_2 + HO_2. \tag{3}$$
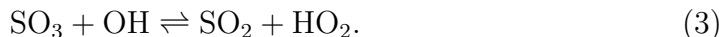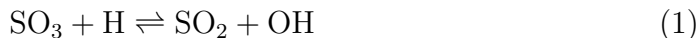
Depending on the reaction conditions, these steps may serve to either consume SO_3 (forward direction) or form SO_3 (reverse direction). Another important reaction for the SO_3/SO_2 ratio is the pressure-dependent step,

$$SO_2 + O(+M) \rightleftharpoons SO_3(+M) \tag{4}$$
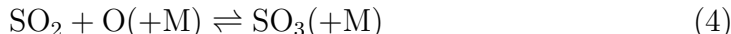
Under the excess oxygen conditions typical of the post-flame region in a combustion system it is believed that the SO_3/SO_2 ratio is mainly controlled by the sequence (4), (2) [2, 7, 8, 9, 10], while reactions (1) and (3) presumably are less important. While the SO_3 formation step (4) is characterized over a wide temperature and pressure range [11, 12], there is a significant uncertainty in the rate constants for the consumption reactions (1-3). There are no reported measurements for the SO_3+H reaction; kinetic models for sulfur chemistry rely on estimated values for k_1 [13, 14, 15] or adopt a QRRK estimate [7] for the reverse reaction SO_2+OH [10, 16, 17]. The rate constant for the reaction between SO_3 and O (2) has not been measured directly and reported data vary by several orders of magnitude. Indirect determinations have been reported based on results from laminar premixed flames [18, 19, 20, 21, 22] and, for the reverse step, from reactor experiments [10, 23]. A recent re-interpretation of selected flame results [12], based on a more accurate value of k_4, indicates a fairly high rate constant for reaction $SO_3+O \rightleftharpoons SO_2+O_2$, in agreement with earlier evaluations [20, 21, 22], and a fast reaction is also supported by other experiments [18, 19, 23]. In conflict with these results, Alzueta et al. [10] recommend a very low rate constant, which indicates that the reaction is insignificant under most conditions of interest. In the absence of measurements, the SO_3+OH reaction

(3) has been omitted from most previous modeling studies of sulfur chemistry [7, 10, 14, 15, 16], but it is potentially an important step.

The objective of the present work is to use ab initio calculations to obtain reliable estimates for the reactions of SO_3 with H, O, and OH. A recent reaction mechanism for sulfur chemistry [17] is updated with the new values for k_1, k_2, and k_3, and predictions with the revised model are compared to a range of experimental results from literature on the oxidation of SO_2 to SO_3. Finally, the implications for modeling the SO_3/SO_2 ratio in practical combustion systems are outlined.

Ab initio calculations

Computational methodology

The geometries of reactants, bound minima, products and connecting transition states (TSs) were derived with the B3LYP level of density functional theory combined with the 6-311G(2d,d,p) basis set [24]. These results are shown in Fig. 1. Vibrational frequencies at the same level of theory were scaled by a standard factor of 0.99 [24] and are listed in Table 1. For thermochemistry calculations all internal motions were treated as harmonic oscillators, with the usual assumption of separability of rotations and vibrations. Improved single-point energies were obtained with the CBS-QB3 composite approach of Petersson and coworkers, which approximates CCSD(T) calculations extrapolated to the infinite basis set limit and has been shown to give atomization energies with mean absolute deviation of 2.4 kJ mol^{-1} [24]. Simple transition state theory (TST) was applied to obtain rate constants k, in the form

$$k = \frac{k_B T}{h} \frac{Q_{TS}}{Q_{reactants}} \exp(-E_0/RT)$$

where the partition functions Q and the 0 K energy barriers E_0 were derived from the CBS-QB3 data.

The SO_3+O reaction

The potential energy diagram is shown in Fig. 2. Several states of SO_4 have been investigated in the past [25, 26], which arise from symmetry breaking in

tetrahedral SO_4. Here we focus on the lowest energy singlet and triplet states. Direct abstraction to form $^3O_2 + SO_2$ via TS2 is found to have a high barrier of 139 kJ mol^{-1}. The computed $\Delta_r H_0$ is -155.5 kJ mol^{-1}, which compares well with the JANAF evaluation of -151.1±0.7 kJ mol^{-1} [27]. TST yields a rate constant of $4.1 \cdot 10^7$ T$^{1.71}$ exp(-138.1 kJ mol^{-1}/RT) cm^3 mol^{-1} s^{-1} for T > 1000 K. By contrast, spin-allowed addition via TS1 to form triplet SO_4 is predicted to occur with a small barrier of only 2 kJ mol^{-1}. This low barrier may be consistent with the experiments over 300-500 K of Westenberg and de Haas [28], who argued in favor of pressure-dependent adduct formation (they did not observe SO_4 by mass spectrometry. Possibly the adduct decomposed before or during ionization). The computed bond dissociation enthalpy at 0 K, D_0(O-SO_3) = 85.8 kJ mol^{-1}, implies $\Delta_f H_0(^3SO_4)$ = -229.0 kJ mol^{-1}, with an uncertainty of around 5 kJ mol^{-1}. However, at combustion temperatures this triplet adduct will not be thermodynamically stable. We have not been able to find a reaction path for the spin-allowed dissociation of $^3SO_4$ to $^3O_2 + SO_2$, but intersystem crossing to the somewhat more stable singlet SO_4 (predicted $\Delta_f H_0(^1SO_4)$ = -256.8 kJ mol^{-1}) may be possible, especially if collisionally assisted. Spin-allowed dissociation of this singlet adduct to $^1O_2 + SO_2$ via TS3 has a computed barrier of 123 kJ mol^{-1}. Treatment of this step as the bottleneck with the assumption that $^1SO_4$ is in rapid equilibrium with the reactants via TST leads to a rate constant of $1.1 \cdot 10^7$ T$^{1.55}$ exp(-120.5 kJ mol^{-1}/RT) cm^3 mol^{-1} s^{-1} for T > 1000 K. The single-reference CBS-QB3 energy for $^1O_2 + SO_2$ is poorly defined because singlet oxygen is a multireference species. The experimental 0 K enthalpies of SO_2 with O_2 in the a $^1\Delta_g$, b $^1\Delta_g^+$ and c $^1\Sigma_u$ states, relative to the reactants, are -56.8, -5.8 and 239.6 kJ mol^{-1} [27]. As expected, these values bracket the computed $\Delta_r H_0$ of -36 kJ mol^{-1}, which presumably corresponds to some combination of the singlet states of O_2. Multireference studies of this pathway may be needed.

An alternative approach is based on density functional theory (DFT). For comparison we reoptimized the O+SO_3 stationary points at the B3LYP/aug-cc-pV(T+d)Z level of theory, where the basis set includes tight d functions on sulfur [29]. The energies, including unscaled zero point vibrational energies, are summarized in Table 2. For singlet oxygen the spin-restricted wavefunction is unstable with respect to becoming spin-unrestricted, with an expectation value for the spin operator, $<S^2>$, equal to 1.005. An improved estimate of the $^1O_2$ energy which corrects for spin contamination is obtained via the procedure of Yamaguchi et al. [30], and the result is shown in Table 2. The derived $^3\Sigma - ^1\Delta$ gap for O_2 is 84 kJ mol^{-1}, in good accord with the experimental value of 95 kJ mol^{-1} [27]. For the other singlet species the spin-restricted DFT results were stable with respect to relaxation of spin constraints, although this does not rule

out some multireference character in the wavefunctions. As may be seen from the relative enthalpies shown in Table 2, the DFT results underestimate ΔH_0 for O-atom abstraction from SO_3 by about 30 kJ mol^{-1}. DFT yields lowered reaction barriers, by 8 to 36 kJ mol^{-1}. DFT also reverses the order of singlet and triplet states for SO_4 by comparison with CBS-QB3 theory. A singlet ground state was obtained by McKee [25] and, until multireference calculations are available, we prefer CBS-QB3 data for the transition state theory analysis.

The singlet and triplet paths have similar rate constants above 1000 K, as may be seen in Fig. 3. The current recommendation for k_2 is the sum of both channels, $k_2 = 2.8 \cdot 10^4 \; T^{2.57} \exp(\text{-}122.3 \text{ kJ mol}^{-1}/RT) \text{ cm}^3 \text{ mol}^{-1} \text{ s}^{-1}$. It is several orders of magnitude lower than values derived from flames [12, 20, 21, 22], but a low value is in agreement with the recommendation of Alzueta et al. [10] based on batch reactor data [31]. The flame and batch reactor results are discussed further below.

The SO_3+H reaction

Two bound minima, corresponding to formation of an S-H or an O-H bond by H-atom addition, were characterized and are shown in Fig. 4. TSs were found for both addition processes and, like in the analogous H + SO_2 system [32], formation of the less strongly bound HSO_3 species is more kinetically favorable than formation of the more thermodynamically stable $HOSO_2$ molecule. Isomerization between these addition products is also possible, and is important because the lowest energy pathway on Fig. 4 involves initial formation of HSO_3 followed by rearrangement to $HOSO_2$, followed by dissociation to OH + SO_2. As a check on the accuracy of the CBS-QB3 energies we compute $\Delta_r H_0$ for the overall reaction to be -84.5 kJ mol^{-1}, which compares well with the experimental value of -83.2 kJ mol^{-1}, which is based on JANAF data [27] except for OH [33].

The predicted binding enthalpies of the adducts at 0 K are D_0(H-SO_3) = 79.1 kJ mol^{-1} and D_0(H-OSO_2) = 197.2 kJ mol^{-1}, respectively. The corresponding $\Delta_f H_0$ are -253.1 and -371.2 kJ mol^{-1}, respectively, and the computed $\Delta_f H_{298}$($HOSO_2$) = -379.2 kJ mol^{-1} agrees with -373$\pm$6 kJ mol^{-1} measured by Pilling and co-workers based on the OH + SO_2 equilibrium [34]. At low temperatures HSO_3 could be a sink for H atoms, but this molecule is not stable at high temperatures. We found no barrier for the initial addition H + $SO_3 \rightarrow$ HSO_3 and the bottleneck in the overall reaction will be at TS5. This controls isomerization to $HOSO_2$ which, being created with an internal energy well in

excess of the threshold for OH + SO$_2$ production (see Fig. 4), is expected to dissociate immediately. TS5 was analyzed via TST for the temperatures of interest, 700-2000 K, and the results may be summarized as k = 8.4 $\cdot$ 10^9 T$^{1.22}$ exp(-13.9 kJ mol^{-1}/RT) cm^3 mol^{-1} s^{-1}. Because the reaction is fast, k $\approx$ 10^{13} cm^3 mol^{-1} s^{-1}, tunneling contributions can be neglected. In Fig. 5 the present value of k$_1$ is compared with the only other literature determination, the QRRK estimate for the reverse reaction by Bozzelli and coworkers [7]. The two rate constants are seen to be in agreement within a factor of two in the investigated temperature range.

The SO$_3$+OH reaction

Computational results for an adduct formed between OH and SO$_3$ were reported by Wang et al. [26] and Wang and Hou [35]. Our similar computed structure is shown in Fig. 1. We derive a binding enthalpy D$_0$(HO-SO$_3$) = 120.1 kJ mol^{-1}. This implies Δ_fH$_0$(HO-SO$_3$) = -473.0 kJ mol^{-1}. Under atmospheric conditions this addition path could be a loss process for SO$_3$. However, in flames the adduct is insufficiently stable to be a sink for SO$_3$. For example, at 800 K the calculated equilibrium constant for OH + SO$_3$ $\rightleftharpoons$ HSO$_4$ is K$_c$ = 1.5 $\cdot$ 10^6 cm^3 mol^{-1}. With a conservative upper limit for [OH] of 10^{-8} mol cm^{-3}, then on the assumption that [SO$_3$] < [OH], the equilibrium fraction of SO$_3$ bound as adduct is less than 2%. At higher temperatures and/or lower [OH], an even smaller fraction of the SO$_3$ will be bound at equilibrium.

A small concentration of HOSO$_3$ could be significant if it rapidly reacts to new products before decomposing thermally back to OH + SO$_3$. By contrast to the analogous OH + SO$_2$ adduct, which reacts readily with O$_2$, the thermochemistry for O$_2$ + HOSO$_3$ $\rightarrow$ HO$_2$ + SO$_4$ is unfavorable. The latest Δ_fH$_0$(HO$_2$) = 15.2$\pm$0.3 kJ mol^{-1} [36] implies Δ_rH$_0$ = 231 kJ mol^{-1} for HO$_2$ formation. O atom elimination from HOSO$_3$ is predicted to be endothermic by 349 kJ mol^{-1} and can therefore be ignored. We have not found a reaction path for elimination of O$_2$. Wang and Hou [35] assigned a transition state for elimination of HO$_2$ from HOSO$_3$ but our own investigations, including following the intrinsic reaction coordinate, suggest instead this TS (labeled TS6 in Fig. 1) corresponds to direct abstraction by OH from SO$_3$. TS6 for direct abstraction lies 120.0 kJ mol^{-1} above OH + SO$_3$ and the corresponding rate constant for HO$_2$ + SO$_2$ formation is summarized over 800-2000 K as 4.8 $\cdot$ 10^4 T$^{2.46}$ exp(-114.1 kJ mol^{-1}/RT) cm^3 mol^{-1} s^{-1}.
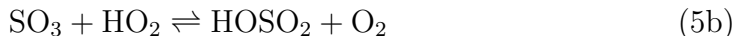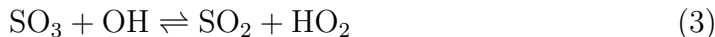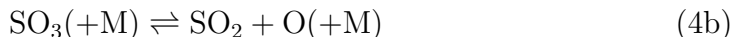
6

Detailed kinetic model

The revised rate constants for the SO_3+H (1), SO_3+O (2), and SO_3+OH (3) reactions were implemented in a detailed chemical kinetic model for high temperature sulfur chemistry, drawn largely from recent work by the authors [12, 17]. The reaction mechanism consists of a H_2/O_2 subset and a full description of the H/S/O reaction system. The mechanism contains the elementary steps that could conceivably influence the SO_2/SO_3 ratio at high temperatures. The sulfur oxides subset of the mechanism is listed in Table 3. The formation of SO_3 may proceed by a direct oxidation of SO_2,

$$SO_2 + O(+M) \rightleftharpoons SO_3(+M) \tag{4}$$

$$SO_2 + OH \rightleftharpoons SO_3 + H \tag{1b}$$

$$SO_2 + O_2 \rightleftharpoons SO_3 + O \tag{2b}$$

$$SO_2 + HO_2 \rightleftharpoons SO_3 + OH, \tag{3b}$$

or it may involve $HOSO_2$ as an intermediate,

$$SO_2 + OH(+M) \rightleftharpoons HOSO_2(+M) \tag{5}$$

$$HOSO_2(+M) \rightleftharpoons SO_3 + H(+M) \tag{7}$$

$$HOSO_2 + O \rightleftharpoons SO_3 + OH \tag{9}$$

$$HOSO_2 + OH \rightleftharpoons SO_3 + H_2O \tag{10}$$

$$HOSO_2 + O_2 \rightleftharpoons SO_3 + HO_2 \tag{11}$$
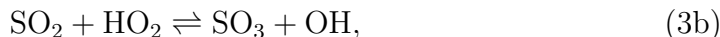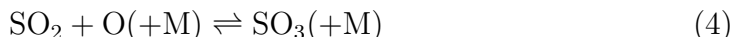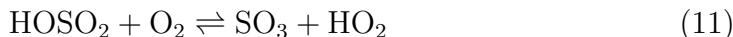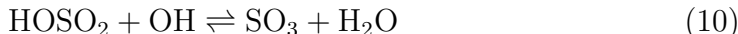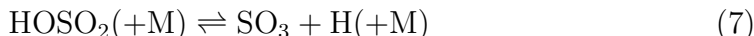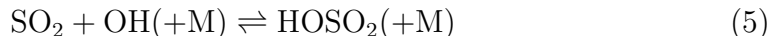
The destruction of SO_3 may occur by,

$$SO_3(+M) \rightleftharpoons SO_2 + O(+M) \tag{4b}$$

$$SO_3 + H \rightleftharpoons SO_2 + OH \tag{1}$$

$$SO_3 + O \rightleftharpoons SO_2 + O_2 \tag{2}$$

$$SO_3 + OH \rightleftharpoons SO_2 + HO_2 \tag{3}$$

$$SO_3 + HO_2 \rightleftharpoons HOSO_2 + O_2 \tag{5b}$$

$$SO_3 + SO \rightleftharpoons SO_2 + SO_2. \tag{6b}$$

Most of the reactions and rate constants have been discussed in some detail in previous work [7, 10, 11, 12, 16, 17]. In addition to k_1, k_2, and k_3, only one rate constant has been modified in the present work. For the SO_2+SO_2 reaction (6) we use an estimate, based on batch reactor results on $SO_2 + O_2$ [31], discussed below, and shock tube results on SO_2 decomposition [37]. Both studies indicate a reaction with a high activation energy, in the range 275–315 kJ/mol.

Modeling results and discussion

Predictions with the detailed chemical kinetic mechanism were compared with experimental results from the literature on oxidation of SO_2 to SO_3. The purpose of the modeling part has been to evaluate whether the novel values of k_1, k_2 and k_3 are consistent with the available experimental results and to discuss the implications. Results from batch reactors and flow reactors (assuming plug flow) were modeled with SENKIN [39], which is part of the CHEMKIN library [40]. SENKIN performs an integration in time. The results of the SENKIN calculations were compared to flow reactor data using the nominal residence time in the isothermal part of the reactor.

The experimental data on SO_3 formation from SO_2 include results from premixed flames [18, 19, 20, 21, 22], batch reactors [31], and flow reactors [7, 23, 43]. The flame results have consistently been interpreted in terms of a fast rate constant for the SO_3+O reaction (2). Based on a more accurate value of k_4, the authors [12] recently re-analyzed the results of Smith and coworkers [21, 22] and Merryman and Levy [20] to obtain a value of $k_2' = 7.8 \cdot 10^{11} \exp(-3065/T)$ $cm^3/(mole\ s)$, in support of the earlier estimates. The flame interpretations [12, 20, 21, 22] were all based on the assumption that the SO_3 level resulted from a balance between formation by SO_2+O(+M) (4) and consumption by SO_3+O (2), i.e. that the SO_3+H and SO_3+OH reactions could be disregarded due to a high O/H ratio in these flames. The present work indicates that the SO_3+O reaction is too slow to be an important consumption step for SO_3, even at the high temperatures in flames.

For the flames of Smith and coworkers [21, 22], which contained only trace amounts of water vapor as a hydrogen source, as well as for the flame of Merryman and Levy [20], we estimate from kinetic modeling an O/H ratio ≈ 100 at the location where $d[SO_3]/dt = 0$ (at 1269 K [12, 21, 22] and 1685 K [20], respectively). According to the results of the present study $k_1/k_2 \approx 10^5$, indicating that the SO_3+H reaction (1), not SO_3+O (2), is the controlling SO_3 consumption reaction in these lean flames. This is supported by the fact that the ratio k_1/k_2' is about the same order of magnitude, ≈ 100, as the estimated O/H ratio in these flames. This means that there is no conflict between the present estimate for k_2 and the flame results, even though the flame data have been used to support a much higher value for k_2 previously.

Support for a high value of k_2 came recently from work by the authors on thermal dissociation of SO_3 in a quartz flow reactor [12]. In this work, a sink for atomic oxygen was required to explain the experimental results, and the

8

loss of O was attributed partly to reaction with SO_3 (2). This interpretation is in conflict with the present value of k_2. The most likely explanation is loss of O on the reactor surface, but more work is required to confirm this. Sulfur trioxide is known to absorb strongly on glass surfaces where it acts to promote recombination of atomic oxygen [2, 41, 42].

There are only few results reported in literature on the oxidation of SO_2 by O_2 in the absence of combustibles. Cullis *et al.* [31] studied gaseous oxidation of SO_2 by O_2 in a silica batch reactor in the temperature range 1173–1323 K (the upper limit dictated by the position of equilibrium between SO_2 and SO_3). The conversion of reactants was detected by measuring the pressure change in the vessel. It was confirmed by changes in the surface to volume ratio that the reaction observed was essentially homogeneous. Cullis et al. did not use the data to derive rate coefficients, partly because of considerable scatter and partly because the mechanism of SO_3 formation was uncertain. Due to the fairly small conversion of SO_2 under the reaction conditions, rate measurements were difficult and not readily reproducible; however, the data obtained were average results of a large number of experiments.

Figures 6 and 7 compare the experimental results of Cullis et al. [31] to modeling predictions with the detailed mechanism. The data indicate that the reaction increases roughly linearly with the concentration of sulfur dioxide, but only slightly with the concentration of oxygen (Fig. 6), and that it has a high activation energy, about 315 kcal/mol (Fig. 7). Assuming the presence of trace amounts of water vapor (50 ppm), calculations indicate that SO_3 is formed mainly by the sequence,

$$SO_2 + OH(+M) \rightarrow HOSO_2(+M) \tag{4}$$

$$HOSO_2 + O_2 \rightarrow SO_3 + HO_2 \tag{11}$$

$$SO_2 + HO_2 \rightarrow SO_3 + OH. \tag{5}$$
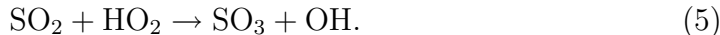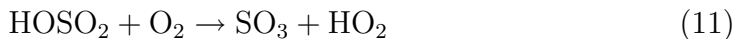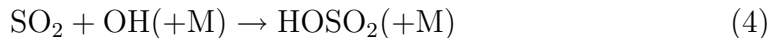
As the temperature increases, the sequence $SO_2 + SO_2 \rightarrow SO_3 + SO$ (6), $SO + O_2 \rightarrow SO_2 + O$, $SO_2 + O + M \rightarrow SO_3 + M$ (4), becomes more important. The modeling predictions are probably in agreement with the batch reactor results within the experimental uncertainty (Figs. 6 and 7), but the mechanism of SO_3 formation under these conditions is still in question.

According to our modeling, the reaction sequence, $SO_2 + O_2 \rightarrow SO_3 + O$ (2b), $SO_2 + O(+M) \rightarrow SO_3(+M)$ (4), is not important for the SO_3 formation. However, the batch reactor data can be used to obtain an upper limit for k_2. Assuming that O is in steady–state, we obtain $d[SO_3]/dt = 2k_{2b}[SO_2][O_2]$. From

this equation, an upper limit of 14 cm^3 mol^{-1} s^{-1} can be derived for k_{2b} at 1223 K, corresponding to k_2(1223 K) $\leq 1.6 \cdot 10^9$ cm^3/(mole s) (Fig. 3).

Experiments on oxidation of SO_2 to SO_3 by O_2 under flow reactor conditions have been reported by Flint and Lindsay [43], Burdett et al. [23] and Jørgensen [44]. These studies were all conducted at atmospheric pressure in electrically heated laminar flow reactors made of quartz or silica. In the present work the data from Flint and Lindsay and from Jørgensen are selected for model validation; the results from Burdett et al. suffer from uncertainty in the reactor temperature profile.

Figure 8 compares modeling predictions with the data of Flint and Lindsay [43]. Their experiments were conducted with 1400 ppm SO_2 and 8% H_2O in air at temperatures between 573 and 1173 K. Formation of SO_3 was detected only at 973 K and above. Except for a single data point, the modeling predictions are in good agreement with the flow reactor data. Flint and Lindsay attributed the SO_3 formation to the influence of catalysis by silica, but the present work indicates that it is largely a homogeneous reaction.

Figure 9 compares modeling predictions with the data of Jørgensen [44]. These experiments were conducted about 480 ppm SO_2, 60% O_2, water vapor (trace amounts or 1%) in N_2 at temperatures between 1023 and 1323 K. Again the modeling predictions are in good agreement with the experimental results, both under semi-dry and moist conditions. At the highest temperatures in the moist set, the SO_3 concentration becomes limited by thermal equilibrium and the predicted SO_2 level decreases.

Rate of production and sensitivity analysis indicate that the key reactions in SO_3 formation are $SO_2 + OH(+M) \rightarrow HOSO_2(+M)$ (5), $HOSO_2 + O_2 \rightarrow HO_2 + SO_3$ (11), and to a less extent $SO_2 + HO_2 \rightarrow SO_3 + OH$ (3b) and $SO_2 + OH \rightleftharpoons SO_3 + H$ (1b). Modeling predictions with the high rate constant for the $SO_3 + O$ reaction (2) derived from flames [12, 20, 21, 22] lead to a significant overprediction of the SO_3 formation rate through the inverse step, $SO_2 + O_2 \rightarrow SO_3 + O$ (2b) under the conditions of Figs. 8 and 9. This is in support of the low value of k_2 estimated in the present work.

The experiments discussed above [23, 31, 43, 44] were all conducted in the absence of combustibles. Radical formation from combustion has been shown to enhance the SO_2 oxidation rate significantly [45]. Glarborg et al. [7] studied SO_2 conversion during moist CO oxidation. The experiments were conducted using a quartz flow reactor, designed to approximate plug flow. It was placed in a three zone electrically heated oven, allowing a uniform temperature profile

with an uncertainty of ± 10 K over the reactor length. The reactants CO, SO_2, O_2, and H_2O were heated separately and mixed in a cross flow at the reactor inlet. The product gas was quenched at the exit of the reactor with cooling air and dried prior to analysis.

The experimental data are compared with modeling predictions in Fig. 10. The agreement is within the experimental uncertainty. Compared to conditions in the absence of combustibles, the enhanced radical levels open up new pathways to formation and consumption of SO_3. The dominating SO_3 formation reaction is now recombination of SO_2 with atomic O,

$$SO_2 + O(+M) \rightarrow SO_3(+M), \tag{4}$$

while SO_3 decomposition proceeds mainly by the reactions

$$SO_3 + HO_2 \rightarrow HOSO_2 + O_2 \tag{11b}$$

$$HOSO_2(+M) \rightarrow SO_2 + OH(+M), \tag{5b}$$

$$SO_3 + H \rightarrow SO_2 + OH \tag{1}$$
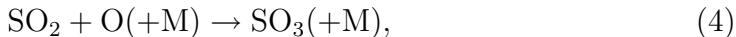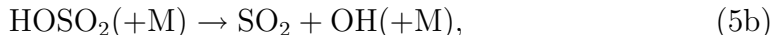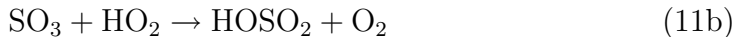
It is noteworthy that while the reactions (5, 11) are important for SO_3 formation in moist SO_2/O_2 systems, they proceed in the reverse direction (11b, 5b) at higher radical levels and serve to consume SO_3.

While the revised rate constant for the SO_3+H reaction (1) has only a small impact compared to earlier modeling for the SO_2/SO_3 ratio in combustion, the updated value for the SO_3+O reaction (2) has important implications. This reaction has been assumed to be an important consumption step for SO_3 in flames [18, 19, 20, 21, 22] and in flow reactor experiments [7, 10], while the reverse step between SO_2 and O_2 (2b) has been believed to contribute to SO_3 formation in SO_2/O_2 systems [6, 23]. The present analysis indicate that reaction (2) is too slow to be important in any of these systems and that the observed SO_3 consumption must be attributed to other reactions, primarily SO_3+H (1). Also the SO_3+OH reaction (3) is generally too slow to be significant, but the reverse step between SO_2 and HO_2 (3b) may contribute to SO_3 formation under conditions with low radical levels.

Conclusions

In the present study, ab initio calculations were carried out to estimate rate constants for the reactions of SO_3 with H, O and OH at high temperatures.

The $SO_3+H \rightarrow SO_2+OH$ reaction (1) is fast, with $k_1 = 8.4 \cdot 10^9$ T$^{1.22}$ exp(-13.9 kJ mol^{-1}/RT) cm^3 mol^{-1} s^{-1}. Contrary to reaction (1), the reactions of SO_3 with O (2) and OH (3) appear to be quite slow due to high barriers to reaction, $k_2 = 2.8 \cdot 10^4$ T$^{2.57}$ exp(-122.3 kJ mol^{-1}/RT) and $k_3 = 4.8 \cdot 10^4$ T$^{2.46}$ exp(-114.1 kJ mol^{-1}/RT) cm^3 mol^{-1} s^{-1}. Modeling predictions with a revised reaction mechanism for SO_2/SO_3 chemistry are in good agreement with a range of experimental data from reactor experiments. The calculations indicate that oxidation of SO_2 to SO_3 with and without presence of combustibles involve primarily recombination of SO_2 with O and OH radicals. Reaction (1) may limit the SO_3 concentration, while reactions (2) and (3) are unimportant for the SO_2/SO_3 ratio under most conditions of interest.

Acknowledgments

References

[1] Miller, J.A. and Klippenstein, S.J. *J. Phys. Chem. A* **2006**, *110*, 10528-10544

[2] Cullis, C.F. and Mulcahy, M.F.R. ; *Combust. Flame* **1972**, *18*, 225-292

[3] Srivastava, R.K., Miller, C.A., Erickson, C., and Jambhekar, R. *J. Air Waste Manage. Assoc.* **2004**, *54*, 750-762

[4] Christensen, K.A. and Livbjerg, H. *Aerosol Sci. Technol.* **1996**, *25*, 185-199.

[5] Jensen, J.R., Nielsen, L.B., Schultz-Møller, C., Wedel, S., and Livbjerg, H. *Aerosol Sci. Technol.* **2000**, *33*, 490-509.

[6] Glarborg, P. and Marshall, P. *Combust. Flame* **2005**, *141*, 22-38.

[7] Glarborg, P., Kubel, D., Dam–Johansen, K., Chiang, H.M., and Bozzelli, J.W.; *Int. J. Chem. Kinet.* **1996**, *28*, 773-790.

[8] Johnsson, J.E. and Glarborg, P.; "Sulfur Chemistry in Combustion I – Sulfur in Fuels and Combustion Chemistry.", Pollutants from Combustion. Formation Mechanisms and Impact on Atmospheric Chemistry, C. Vovelle (ed.), Kluwer Academic Publisher, pp. 283–301 (2000).

[9] Mueller, M.A., Yetter, R.A., and Dryer, F.L. *Int. J. Chem. Kin.* **2000**, *32*, 317-339.

[10] Alzueta, M.U., Bilbao, R., and Glarborg, P. *Combust. Flame* **2001**, *127*, 2234-2251.

[11] Naidoo, J., Goumri, A., and Marshall, P.; *Proc. Combust. Inst.* **2005**, *30*, 1219-1225.

[12] Yilmaz, A., Hindiyarti, L., Jensen A.D., Glarborg P., and Marshall, P. *J. Phys. Chem. A* **2006**, *110*, 6654-6659

[13] Frenklach, M., Lee, J.H., White, J.N. and Gardiner Jr., W.C. *Combust. Flame* **1981**, *41*, 1-16.

[14] Cerru, F.G., Kronenburg, A., and Lindstedt, R.P. *Proc. Combust. Inst.* **2005**, *30*, 1227-1235

[15] Cerru, F.G., Kronenburg, A., and Lindstedt, R.P. *Combust. Flame* **2006**, *146*, 437-455

[16] Dagaut, P., Lecomte, F., Mieritz, J., and Glarborg, P. *Int. J. Chem. Kin.* **2003**, 35, 564-575.

[17] Rasmussen, C.L., Glarborg P., Marshall P. *Proc. Combust. Inst.* **2007**, *31*, 339-347.

[18] Fenimore, C.P., and Jones, G.W. *J. Phys. Chem.* **1965**, *69*, 3593.

[19] Schofield, K. *J. Phys. Chem. Ref. Data* **1973**, *2*, 25-84.

[20] Merryman, E.L. and Levy, A. *Proc. Combust. Inst.* **1979**, *17*, 727-736.

[21] Smith, O.I. Tseregounis, S., and Wang, S.-N. *Int. J. Chem. Kin.* **1982**, *14*, 679-697.

[22] Smith, O.I. Tseregounis, S., Wang, S.-N., and Westbrook, C.K. *Combust. Sci. Technol.* **1983**, *30*, 241-271.

[23] Burdett, N.A., Langdon, W.E., and Squires, R.T. *J. Inst. Energy* **1984** September, 373.

[24] Montgomery Jr., J.A., Frisch, M.J., Ochterski, J.W., and Petersson, G.A. *J. Chem. Phys.* **1999**, *110*, 2822.

[25] McKee, M.L. *J. Am. Chem. Soc.* **1993**, *115*, 9136.

[26] Wang, X-B., Nicholas, J.B., and Wang, L-S. *J. Phys. Chem. A* **2000**, *104*, 504.

[27] NIST-JANAF Thermochemical Tables; 4th ed.; Chase, M. W., Jr., Ed.; American Chemical Society and the American Institute of Physics: Woodbury, N.Y., 1998.

[28] Westenberg, A.A. and deHaas, N.J. *J. Chem. Phys.* **1975**, *62*, 725.

[29] Dunning, T.H.,Jr.; Peterson, K.A.; Wilson, A.K. *J. Chem. Phys.* **2001**, *114*, 9244.

[30] Yamaguchi, K.; Jensen, F.; Dorigo, A.; Houk, K.N. *Chem. Phys. Lett.* **1988**, *149*, 537.

[31] Cullis, C.F.,Henson, R.M., and Trimm, D.L. *Proc. Roy. Soc. A* **1966**, *295*, 72-83.

[32] Goumri, A., Roucha, J.D-R. Laakso, D., Smith, C.E., and Marshall, P. *J. Phys. Chem. A* **1999**, *103*, 11328.

[33] Joens, J.A. *J. Phys. Chem. A* **2001**, *105*, 11041.

[34] Blitz, M.A., Hughes, K.J., and Pilling, M.J. *J. Phys. Chem. A* **2003**, *107*, 1971-1978.

[35] Wang, B. and Hou, H. *Chem. Phys. Lett.* **2005**, *410*, 235-241.

[36] Ruscic, B., Pinzon, R.E., Morton, M.L., Srinivasan, N.K., Su, M-C., Sutherland, J.W., and Michael, J.V. *J. Phys. Chem. A* **2006**, *110*, 6592-6601.

[37] Raju, M.T., Babu, S.V., and Rao, V.S. *Chem. Phys.* **1980**, *48*, 411-416.

[38] Atkinson, R., Baulch, D.L., Cox, R.A., Hampson, R.F., Kerr, J.A., and Troe, J.; J. Phys. Chem. Ref. Data **1992**, *21*, 1125-1568.

[39] Lutz, A., Kee, R.J., and Miller, J.A., "SENKIN: A Fortran Program for Predicting Homogenous Gas Phase Chemical Kinetics with Sensitivity Analysis", Sandia Report SAND87–8248, Sandia National Laboratories, Livermore, CA (1987).

[40] Kee, R.J., Rupley, F.M., and Miller, J.A., "CHEMKIN–II: A Fortran Chemical Kinetics Package for the Analysis of Gas-Phase Chemical Kinetics", Sandia Report SAND89-8009, Sandia National Laboratories, Livermore, CA (1989).

[41] Kaufman, F. *Proc. Royal Soc. London A* **1958**, *247*, 123.

[42] Mulcahy, M.F.R., Stevens, J.R., Ward, J.C., and Williams, D.J. *Proc. Combust. Inst.* **1969**,*12*, 323.

[43] Flint, D. and Lindsay, A.W. *Fuel* **1952**, *30*, 288.

[44] Jørgensen, T.L. B.Sc. thesis, Department of Chemical Engineering, Technical University of Denmark, 2007 (in Danish)

[45] Glarborg, P. *Proc. Combust. Inst.* **2007**,*31*, 77-98.

Table 1: CBS-QB3 energies (0 K, in au. 1 au = 2625.5 kJ mol^{-1}) and B3LYP/6-311G(2d,d,p) vibrational frequencies (cm^{-1}, scaled by 0.99) computed for the reactants, intermediates, products and transition states in the H, O, and OH reactions with SO$_3$ shown in Fig. 1.

Molecule	Energy, au	Frequencies, cm^{-1}
O ^{3}P	-74.98763	–
SO$_3$ ^{1}A$'_1$	-623.15539	488, 508, 508, 1034, 1350, 1350
SO$_4$ ^{1}A$_1$	-698.18631	299, 464, 465, 480, 635, 654, 895, 1224, 1403
SO$_4$ ^{3}A$''$	-698.17571	299, 350, 384, 384, 438, 779, 780, 941, 1159
TS1 ^{3}A$''$	-698.14226	214i, 125, 130, 469, 494, 499, 1022, 1267, 1346
TS2 ^{3}A$''$	-698.09006	897i, 96, 167, 436, 461, 511, 748, 1114, 1303
TS3 ^{1}A	-698.09604	530i, 142, 286, 412, 468, 654, 841, 1177, 1376
O$_2$ $^3\sum$	-150.16462	1625
^{1}O$_2$	-150.11901	1611
SO$_2$ ^{1}A$_1$	-548.03762	508, 1141, 1335
HSO$_3$ ^{2}A$_2$	-623.68528	178, 178, 567, 944, 944, 1039, 1104, 1104, 2580
HOSO$_2$ ^{2}A	-623.73026	262, 399, 405, 507, 679, 1059, 1105, 1265, 3715
TS4 ^{2}A$'$	-623.63844	975i, 178, 297, 490, 498, 550, 977, 1255, 1334
TS5 ^{2}A$'$	-623.64774	1486i, 406, 463, 525, 643, 775, 1139, 1334, 1887
OH $^2\prod$	-75.64969	3668
H ^{2}S	-0.49982	–
HOSO$_3$ ^{2}A$''$	-698.85077	214, 266, 361, 408, 429, 522, 791, 840, 1022, 1150, 1240, 3724
TS6 ^{2}A	-698.75939	745i, 87, 175, 243, 444, 469, 515, 743, 1082, 1102, 1281, 3711

Table 2: B3LYP/aug-cc-pV(T+d)Z energies (including zero point energies) for stationary points on the O+SO$_3$ potential energy surface, and enthalpies at 0 K relative to reactants.

Species	B3LYP energy (au)	B3LYP enthalpy (kJ/mol)	CBS-QB3 enthalpy (kJ/mol)
^{3}O	-75.09418	0	0
SO$_3$	-623.93744		
O$_2$	-150.38092	-180	-155, -151[a]
SO$_2$	-548.71939		
^{3}SO$_4$	-699.07583	-116	-86
^{1}SO$_4$	-699.06654	-92	-114
TS1	-699.03623	-12	2
TS2	-698.99222	103	139
TS3	-698.98777	115	123
^{1}O$_2$	-150.34887[b]	-87[c]	-36[c], -57[a,c]

a: Experiment [27].
b: Corrected spin-unrestricted result (see text).
c: Includes SO$_2$.

Table 3: Rate coefficients for key reactions in the reaction mechanism. Units are cm, mol, s, K.

No	Reaction	A	n	E/R	Source
1.	$SO_3+H \rightleftharpoons SO_2+OH$	8.4E09	1.22	1670	pw
2.	$SO_3+O \rightleftharpoons SO_2+O_2$	2.8E04	2.57	14700	pw
3.	$SO_3+OH \rightleftharpoons SO_2+HO_2$	4.8E04	2.46	13700	pw
4.	$SO_2+O(+M) \rightleftharpoons SO_3(+M)^a$	3.7E11	0.00	850	[11]
	Low pressure limit	2.4E27	-3.60	2610	
	Troe parameters 0.442 316 7442				
	Low pressure limit (N_2)	2.9E27	-3.58	2620	[12]
	Troe parameters (N_2) 0.43 371 7442				
5.	$SO_2+OH(+M) \rightleftharpoons HOSO_2(+M)^b$	5.7E12	-0.27	0	[34]
	Low pressure limit	1.7E27	-4.09	0	
	Troe parameters 0.10 1E-30 1E30				
6.	$SO_2+SO_2 \rightleftharpoons SO_3+SO$	5.0E07	2.00	37750	[37], est
7.	$HOSO_2 \rightleftharpoons SO_3+H$	1.4E18	-2.91	27630	[7], 1 atm
8.	$HOSO_2+H \rightleftharpoons SO_2+H_2O$	1.0E12	0.00	0	[7]
9.	$HOSO_2+O \rightleftharpoons SO_3+OH$	5.0E12	0.00	0	[7]
10.	$HOSO_2+OH \rightleftharpoons SO_3+H_2O$	1.0E12	0.00	0	[7]
11.	$HOSO_2+O_2 \rightleftharpoons HO_2+SO_3$	7.8E11	0.00	330	[38]

a: Enhanced third body coefficients: N_2=0, SO_2=10, H_2O=10
b: Enhanced third body coefficients: N_2=1, SO_2=5, H_2O=5
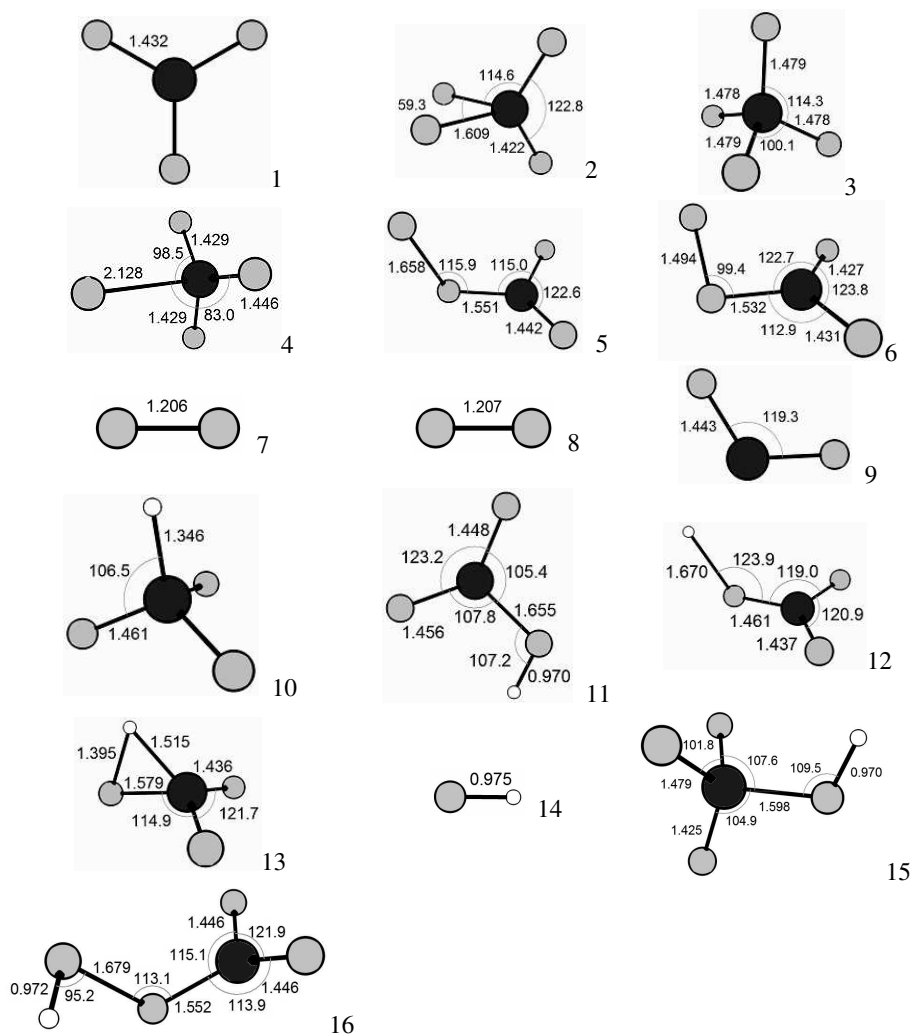
Figure 1: Computed B3LYP/6-311G(2d,d,p) geometries (distances in 10^{-10} m and angles in degrees): 1 D_{3h} SO_3 $^1A'_1$, 2 C_{2v} SO_4 $^1A_1$, 3 C_{2v} SO_4 $^3A_2$, 4 C_s TS1 $^3A''$, 5 C_{2v} TS2 $^3A''$, 6 C_1 TS3 ^1A, 7 O_2 $^3\sum$, 8 $^1O_2$, 9 C_{2v} SO_2 $^1A_1$, 10 C_{3v} HSO_3 $^2A_2$, 11 C_1 $HOSO_2$ ^2A, 12 C_s TS4 $^2A'$, 13 C_s TS5 $^2A'$, 14 OH $^2\prod$, 15 $HOSO_3$ $^2A''$, 16 C_1 TS6 ^2A.

19
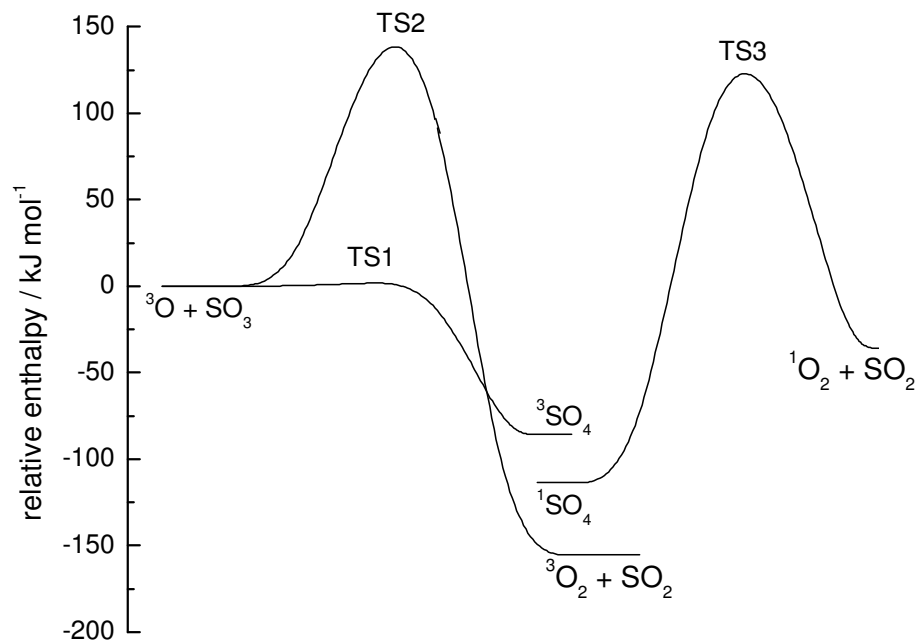
Figure 2: Potential energy diagram for O + SO$_3$ based on CBS-QB3 calculations, showing relative enthalpies at 0 K.
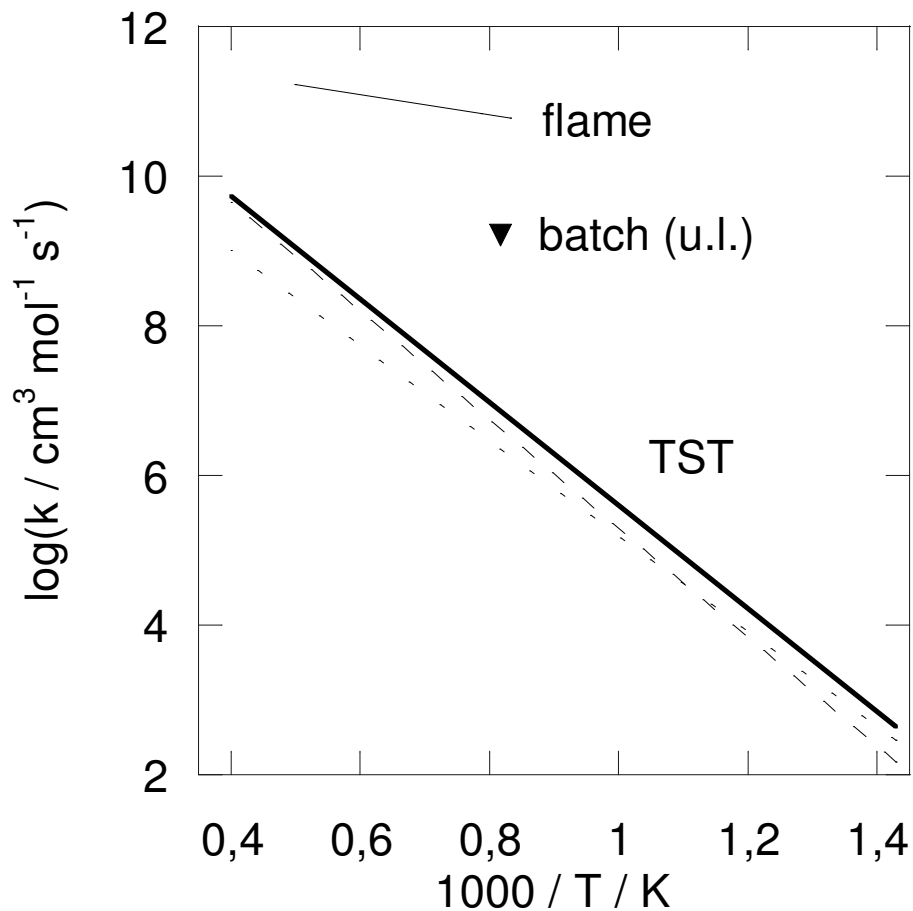
Figure 3: Arrhenius plot for the SO_3+O reaction. Thin solid line: the rate constant derived by Yilmaz et al. [12] based on flame measurements [20, 21, 22]. Solid triangle: upper limit ([10], present work) based on batch reactor data [31]. Long-dashed line: TST for $O + SO_3$ triplet abstraction; short-dashed line: TST for $O + SO_3$ singlet addition/elimination. Thick solid line: TST total rate constant.
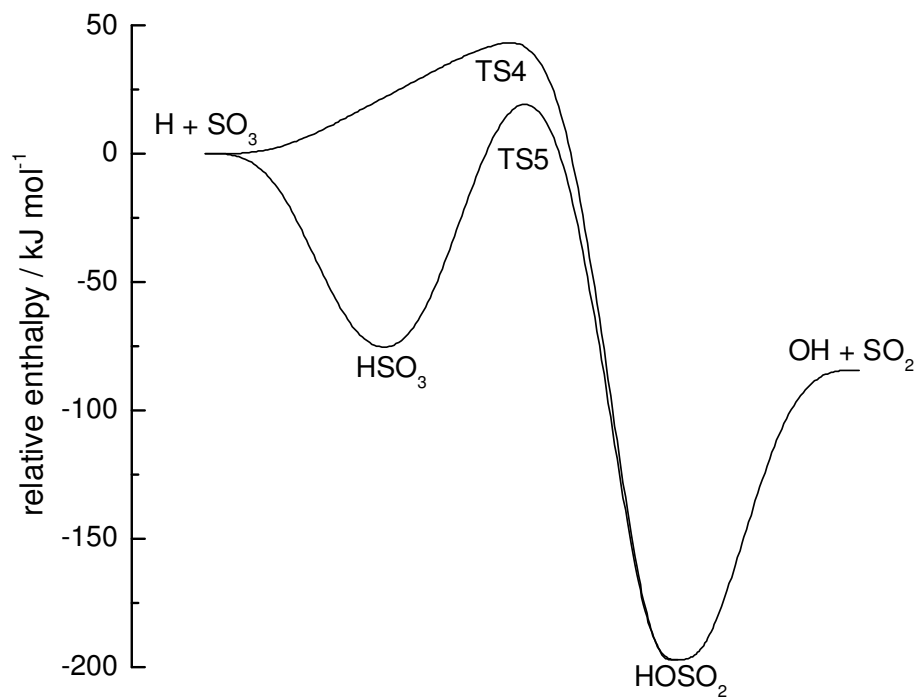
Figure 4: Potential energy diagram for H + SO$_3$ based on CBS-QB3 calculations, showing relative enthalpies at 0 K.
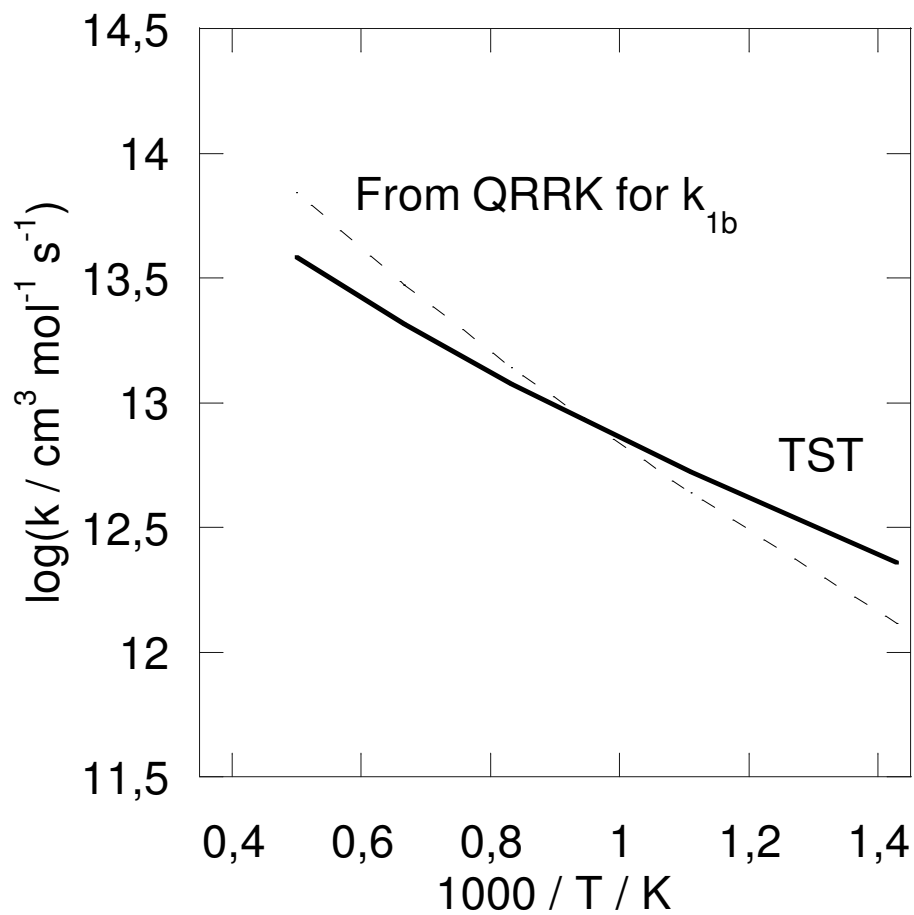
Figure 5: Arrhenius plot for the SO_3+H reaction. Dashed line: the rate constant derived from the QRRK estimate for the reverse reaction by Glarborg et al. [7]. Solid line: TST rate constant from the present work.
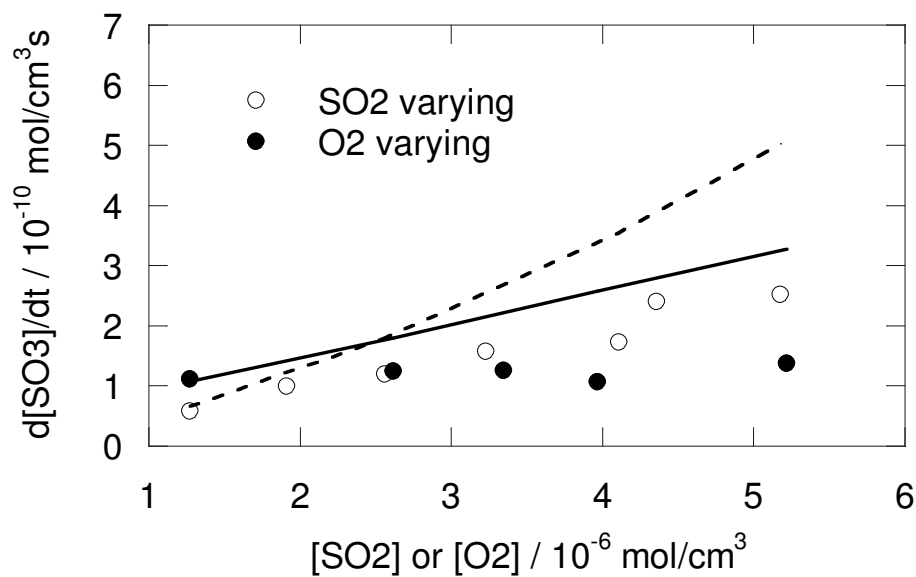
Figure 6: Comparison of experimental data [31] and modeling predictions for the SO_3 formation rate in a quartz batch reactor at a temperature of 1223 K and varying concentrations of SO_2 and O_2. In the modeling trace amounts of water vapor (50 ppm) have been assumed to be present. Experimental data are shown as symbols, modeling predictions as solid (O_2 varying) or dashed (SO_2 varying) lines.
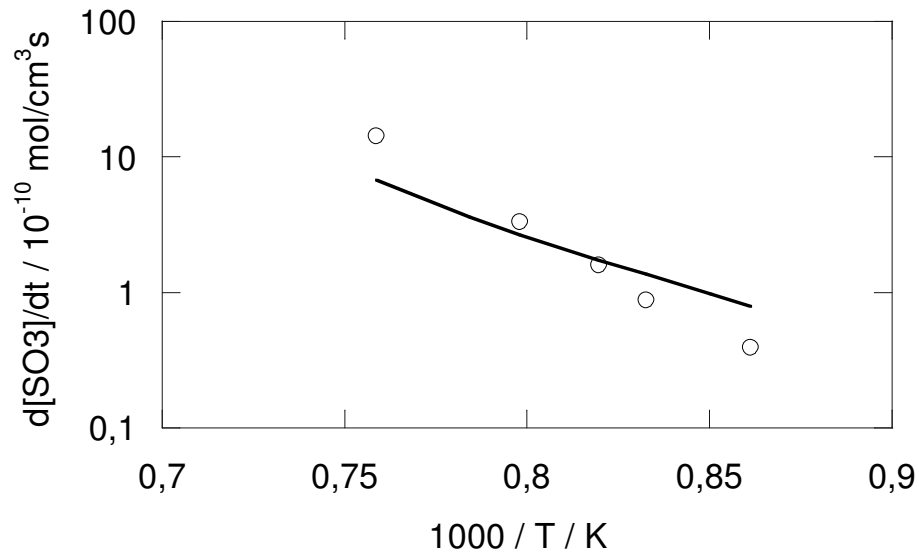
Figure 7: Comparison of experimental data [31] and modeling predictions for the SO_3 formation rate in a quartz batch reactor for $[SO_2] = [O_2] = 2.6 \cdot 10^{-6}$ mol cm^{-3} and varying temperature. In the modeling trace amounts of water vapor (50 ppm) have been assumed to be present. Experimental data are shown as symbols, modeling predictions as lines.
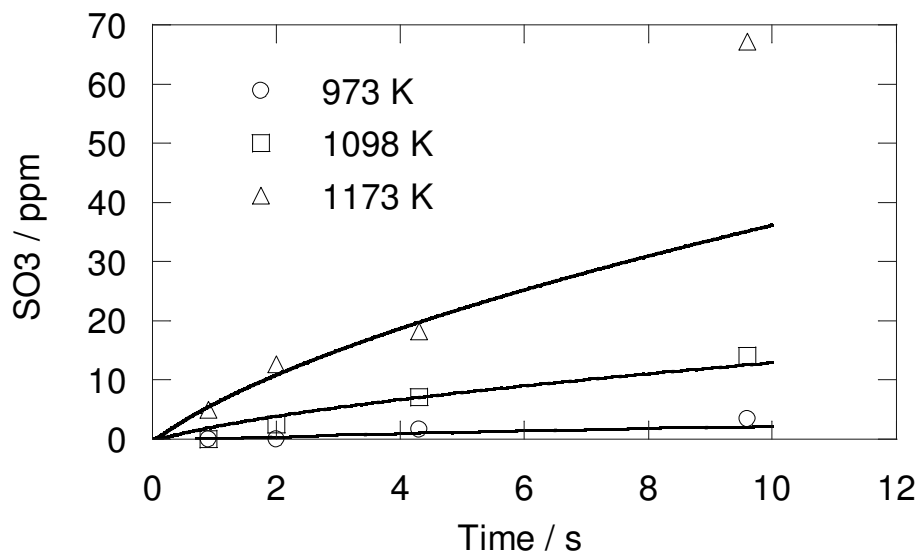
Figure 8: Comparison of experimental data [43] and modeling predictions for SO_3 formation in a quartz reactor at temperatures of 973–1173 K and atmospheric pressure. The quartz tube was 185 cm long and 1.6 cm internal diameter (S/V = 1.3 cm^{-1}). The inlet gases contained 0.14 % SO_2, 8% H_2O, and air to balance. Symbols denote experimental results, solid lines denote modeling predictions.
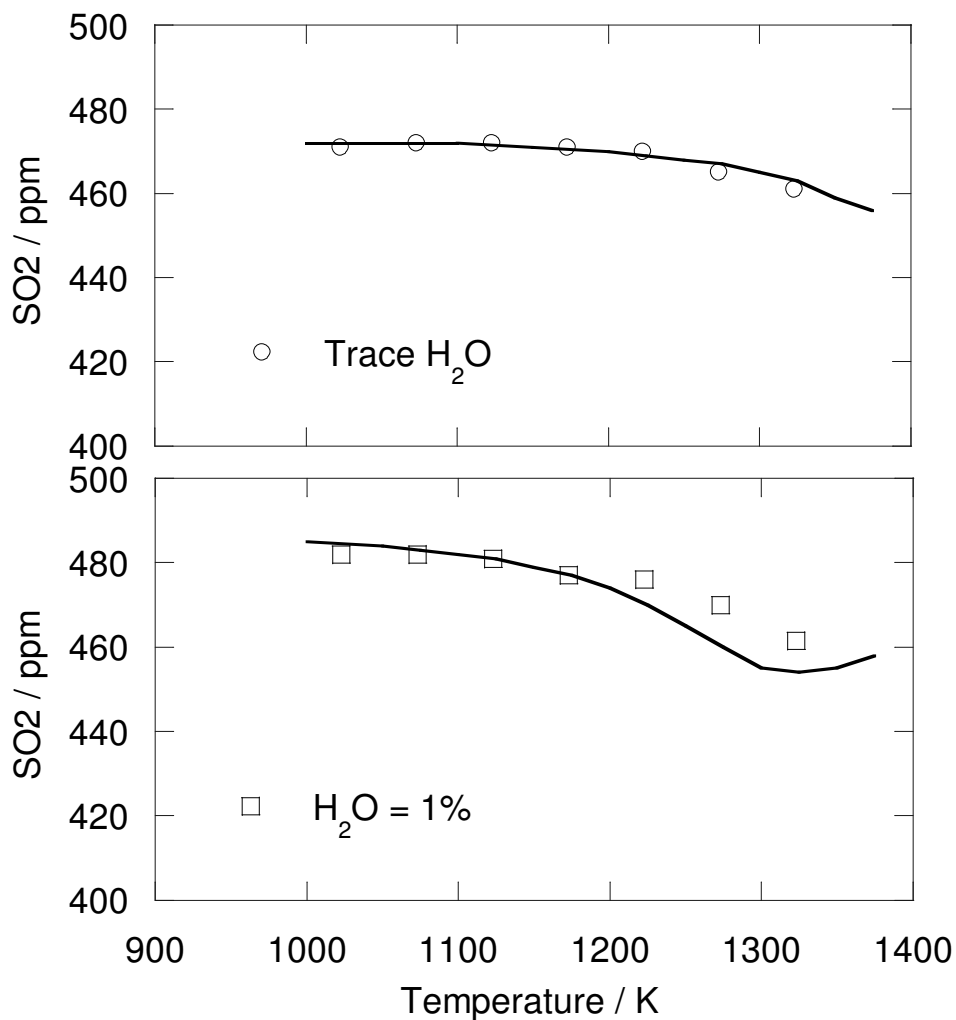
Figure 9: Comparison of experimental data [44] and modeling predictions for SO_2 oxidation in a quartz reactor at temperatures of 1023–1323 K and atmospheric pressure. The isothermal zone was 40 cm long and the reactor had a 3.15 cm internal diameter ($S/V = 0.6$ cm^{-1}). The inlet gas compositions were: 472 ppm SO_2, 60% O_2, trace H_2O (assumed 200 ppm), and N_2 to balance (upper figure); 485 ppm SO_2, 60% O_2, 1% H_2O, and N_2 to balance (lower figure). The residence time as a function of temperature is 5380[K]/T. Symbols denote experimental results, solid lines denote modeling predictions.

27
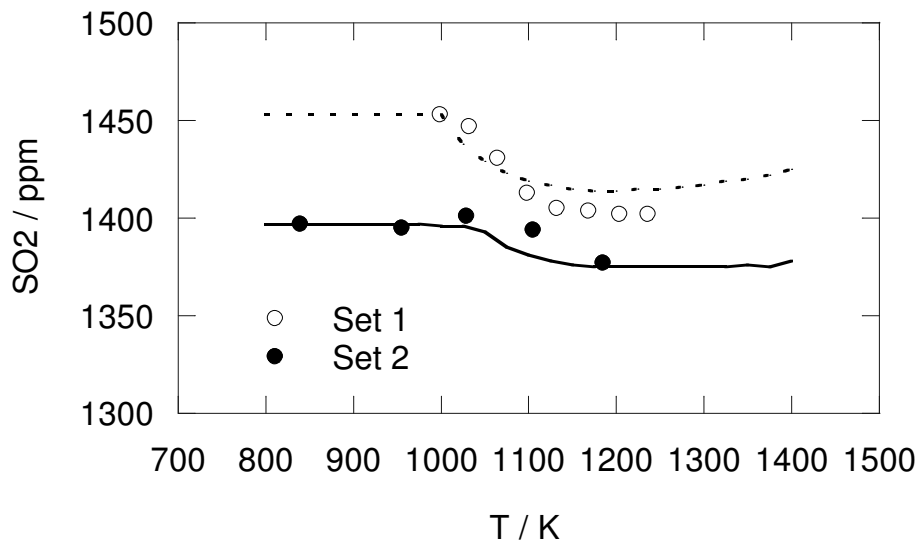
Figure 10: Comparison of experimental data [7] and modeling predictions for conversion of SO_2 as function of temperature during moist CO oxidation in a quartz flow reactor. Experimental data are shown as symbols, modeling predictions as lines. Data set 1: 448 ppm CO, 1453 ppm SO_2, 4.3% O_2 and 1% H_2O, residence time as a function of temperature 243[K]/T. Data set 2: 446 ppm CO, 1395 ppm SO_2, 4.1% O_2 and 8.7% H_2O, residence time as a function of temperature 244[K]/T.

Paper V

Mechanism of Alkali Sulfate Aerosol Formation during Biomass Combustion

Lusi Hindiyarti, Flemming Frandsen, Hans Livbjerg, and Peter Glarborg
Department of Chemical Engineering
Technical University of Denmark
DK-2800 Lyngby, Denmark

Paul Marshall
Department of Chemistry and Center for Advanced Scientific Computing
and Modeling, University of North Texas, P.O. Box 305070, Denton, Texas
76203-5070

Abstract

It is still an open question whether alkali sulfate aerosols in biomass combustion are formed in the gas phase by a homogeneous mechanism or involve heterogeneous contact between a solid or condensed alkali salt and gas phase S-containing species. This study investigates sulfate aerosol formation using gas phase modeling validated with data from laboratory experiments available in the literature. The sulfate aerosol formation was simulated using the following modeling approaches: 1) a simplified scheme with oxidation of SO_2 to SO_3 as the rate limiting step, 2) a full, updated gas-phase K/S/Cl reaction mechanism, and 3) a full gas-phase mechanism together with a simplified description of catalyzed formation of SO_3. It has been suggested that the rate limiting step in the gas phase sulfate aerosol formation is the oxidation of SO_2 to SO_3. This study suggests that apart from the homogeneous oxidation of SO_2 to SO_3, there may be other limiting steps which include reactions of SO_2 and O_2 with K-containing species. The results suggest that the SO_2 oxidation rate may be enhanced by catalytic reactions on particle or reactor surfaces. In general, the sulfate aerosol formation is influenced by the concentrations of SO_2, O_2, and KCl, as well as residence time and temperature history.

Keywords: sulfate aerosols, gas phase, modeling, sulfur oxide, catalytic

Introduction

In Denmark there is a significant amount of straw available as byproducts from farming. Previous experience with combustion of some biomass fuels, including straw, has revealed serious problems with the formation of sub-micron aerosol particles, deposits, corrosion, and emissions. These problems are closely linked to the chemical composition of the biomass. The content of inorganics in annual biomass fuels is about 5-10% of the total mass, and in straw the alkali content, especially potassium, is very high [1].

The formation of aerosols is not favorable for the environment or for human health, since they affect the health of living creatures. The sub-micron particles are formed by condensation of volatilized material, mainly alkali salts. Their main constituents are the chlorides and sulfates of the alkali metals. Their formation also has negative effects on the boiler operation because they penetrate particle filters more easily than larger combustion particles, and they are usually accompanied by corrosive deposits on boiler surfaces [2].

The characteristics of aerosols formed in the combustion of different biomass fuels, in a wide range of boiler scales from domestic heat producers to a large electricity generation plants, have been reported [3,4]. The relevance of alkali and chlorine in the deposit formation and boiler corrosion was pointed out in several studies [5–8]. Alkali metals may combine with aluminosilicates, causing lower melting temperatures of boiler deposits. Without the presence of the alkali, the boiler deposits do not melt at typical biomass combustion temperatures. Therefore the presence of alkali will increase the fouling tendency in biomass-fired power plants compared to coal-fired boilers [5,6,9].

Alkali sulfates play an important role in the formation of submicron particle formation [2, 3, 10, 11]. Alkali sulfate aerosols have been detected in biomass combustion [2, 3, 11] and in experiments using a laboratory flow reactor [12, 13]. It is still in discussion to what extent alkali sulfate aerosol formation is initiated in the gas phase by a homogeneous mechanism or involves a heterogeneous mechanism. Only a small fraction of the equilibrium value for gas phase alkali sulfate is expected to form according to early gas phase kinetic considerations [14]. The work by Steinberg and Schofield [14–16] on homogeneous interactions of sodium and sulfur in the burned gas of flames implied that kinetic limitations ruled out homogeneous Na_2SO_4 formation mechanisms in flames. Instead, the formation was reported to be a surface phenomenon, occuring at a rate that was directly proportional to the total sodium content of the flame [14]. In this case the

alkali metal (sodium/potassium) was expected to condense as chlorides. The condensed chloride would react with available S-containing gas species to form sulfates in the condensed (solid) phase. More recent studies suggest that sulfate aerosols may be formed in the gas phase by recondensation of alkali, volatilized in the combustion zone [2, 3, 11, 13, 17]. According to these studies, the particles are formed from alkali sulfate vapors by homogeneous nucleation of salt seeds, which grow by condensation and coagulation. The process is controlled by chemical reactions in the gas between, e.g. alkali, chlorine, and sulfur species [2]. An investigation on sulfation under combustion conditions by Iisa et al. [13] indicates that the sulfation rate is slow in the condensed phase, while the sulfation in the gas phase is quite fast. The sulfation of solid and molten alkali chloride by SO_2, H_2O, and O_2, is assumed to be too slow to be involved in the aerosol formation. The formation of aerosol particles by homogeneous nucleation from supersaturated vapors is practically immediate, once a certain treshold of supersaturation is exceeded.

In biomass combustion, the particles are believed to be formed by nucleation/condensation of volatilized mineral matter, in a mechanism similar to that described for coal combustion [2]. A model of particle formation during cooling of a flue gas from the combustion of fuels rich in volatile alkali species was developed by Christensen et al. [2, 3, 11, 18]. They suggest that sulfate seeds are formed by homogeneous nucleation of K_2SO_4 vapors at approximately 800 °C. When the flue gas cools down, KCl condenses on these nuclei at lower temperatures. Experiments in a flow reactor [12] support this suggestion. Further experimental support for this suggestion was found by Jimenez and Ballester [19] in laboratory experiments of orujillo (a residue of the olive oil production process) combustion.

The objective of this study is to investigate the active mechanism in the sulfate aerosol formation in biomass combustion. Recent advances in our understanding of the SO_2 oxidation chemistry [20–22] and K/Cl/S interactions [17, 23] are supplemented with an investigation of plausible novel pathways for gas-phase K_2SO_4 formation, based on ab initio methods, to yield an updated detailed reaction mechanism for sulfate formation. Modeling predictions are compared to experimental data on aerosol formation from Iisa et al. [13], Jensen et al. [12], and Jimenez and Ballester [24]. These data cover a range of experimental techniques, as well as variations in SO_2 and O_2 inlet concentration, residence time, and temperature time history.

In addition to calculations with the full mechanism, modeling predictions

3

were conducted with a simplified scheme considering only oxidation of SO_2 to SO_3. Several reports suggest that the rate limiting step in the formation of gas phase sulfate aerosol in biomass combustion is the oxidation of SO_2 to SO_3 [2,3,11,13,17]. Also the possibility of heterogeneously catalyzed SO_2 oxidation is discussed.
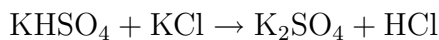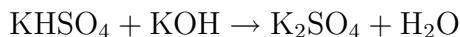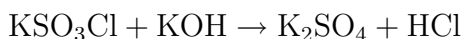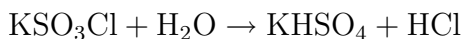
Mechanisms of Alkali Sulfate Formation

The available literature on alkali sulfate formation has been summarized in a previous work [17]. It was pointed out that there is still an open discussion regarding the relative importance of homogeneous and heterogeneous mechanisms of alkali sulfate formation prior to aerosol generation during biomass combustion. Recent work [17, 24] suggests that a homogeneous gas-phase mechanism is active and that SO_3-formation is the rate limiting step. However, the results are not conclusive. In this work, a broader range of data available in the literature is used to investigate further the sulfation phenomena.

Modeling predictions [17], supported by experimental observations [11, 13], indicate that the oxidation of SO_2 to SO_3 is the first and perhaps rate-limiting step in the gaseous alkali sulfate formation. The subsequent step according to Glarborg and Marshall [17] is most likely an association reaction involving KOH or KCl with SO_3:

$$KOH + SO_3(+M) \rightarrow KHSO_4(+M)$$

$$KCl + SO_3(+M) \rightarrow KSO_3Cl(+M)$$
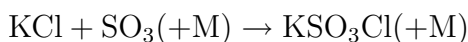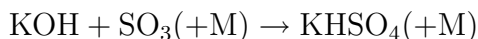
If the potassium hydrogen sulfate and potassium oxysulfur chloride (the complexes formed in these reactions) are sufficiently stable at high temperatures, they may participate in a series of shuffle reactions leading to alkali sulfate formation by the following reactions :

$$KSO_3Cl + H_2O \rightarrow KHSO_4 + HCl$$

$$KSO_3Cl + KOH \rightarrow K_2SO_4 + HCl$$

$$KHSO_4 + KOH \rightarrow K_2SO_4 + H_2O$$

$$KHSO_4 + KCl \rightarrow K_2SO_4 + HCl$$

4

This proposed mechanism indicates a fast and efficient gas phase sulfation process, with oxidation of SO_2 being the rate limiting step rather than alkali transformations. The plausibility of the mechanism depends on the thermal stability of the alkaline hydrogen sulfates and the alkaline oxysulfur chlorides in the gas phase [17].

In the present study, the sulfate aerosol formation is modelled using various approaches. All of these approaches, models A–D, take into account the updated sulfur chemistry from recent work [20–22], but describe the alkali chemistry differently. In model A, the alkali subset from Glarborg and Marshall [17] is adopted without any adjustments. In model B the SO_3 formation is assumed to be the rate limiting step in the sulfate formation, and all of the SO_3 formed is assumed to instantaneously generate aerosols K_2SO_4 when excess K is available in the system. In model C the importance of homogeneous sulfation pathways not involving SO_3 formation is investigated. Specifically, the K/S/O/H subset of Glarborg and Marshall (model A) is updated with additional reactions involving $KHSO_3$ and KSO_4. Finally, the last modeling approach (called model D) adds a surface-catalyzed oxidation of SO_2 to SO_3 to the gas phase mechanism. Model D consists of model A with addition of a clustering mechanism for sulfate aerosol formation. The aerosol formed may then catalyze SO_2 oxidation. The model predictions are compared to selected experimental data from literatures; model A-C to the full set [12, 13, 24], while model D is compared only to the experimental data of Jensen et al. [12].

Since the plausibility of the proposed novel gaseous reactions involving $KHSO_3$ and KSO_4 (model C) depends on their thermal stability, in the present work we estimate the thermodynamic properties of $KHSO_3$ and KSO_4 as described in the following section. These species have not been detected in the gas phase, and no data are available on their thermochemistry.

Thermodynamic Properties of Additional Potential Alkali Sulfate Precursors

A detailed explanation of the ab initio calculation method used in this study can be found elsewhere [17]. The A here represents alkali metal species either as potassium (K) or sodium (Na). The neutral alkali species ASO_4 and $AHSO_3$ (see Fig. 1) are unknown experimentally, so their properties are predicted via ab initio methods. Details of the approach have been given

previously [17]. Briefly, the Gaussian-3 methodology [25], as modified for alkali metals [26], was employed to derive the 0 K molecular energies listed in Table 1. Computations were carried out with the Gaussian 03 program suite [27]. These energies were used to compute the 0 K enthalpy changes for the isodesmic processes.

$$OH + AHSO_4 \rightarrow H_2O + ASO_4$$

$$OH + AHSO_3 \rightarrow H_2O + ASO_3$$
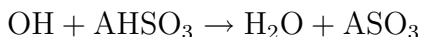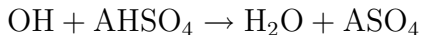
Next, moments of inertia and vibrational frequencies scaled by 0.99, computed at the B3LYP/6-311G(d,p) level of theory and given in Table 1, were used to calculate the temperature-dependent heat capacities and other thermodynamic properties (see Table 2), and thus to correct the reaction enthalpies to 298 K. We then used our earlier thermochemistry for $AHSO_4$ and ASO_3 [17], together with values for OH [28] and H_2O [29] to find $\Delta_f H_{298}$ for the unknown species. The C_{2V} structure for ASO_4 shows the binding to a pair of S-O bonds highlighted previously [17] in several other alkali-sulfur species, and is in accord with the calculations of Wang et al. [30]. The $AHSO_3$ molecules exhibit an unusual structure suggestive of binding not only to the two S-O groups but also to the hydroxyl group (see Fig. 1).

Detailed Chemical Kinetic Model

A gas phase model for interactions between sulfur, chlorine, and potassium earlier proposed by Glarborg and Marshall [17] is used as basis for the current modeling. The Senkin code [31] which runs in conjunction with Chemkin-II [32] was used in the modeling, assuming plug flow.

The reaction mechanism consists of subsets for H_2/O_2, chlorine chemistry, sulfur chemistry, potassium chemistry and the interactions between those species. The thermodynamic data used in the present study are taken from previous work [17, 21], except for $KHSO_3$ and KSO_4 (see Table 1).

The chlorine chemistry, involving reactions of HCl and Cl_2, is an update of the evaluation by Baulch et al. [33]. The sulfur subset was taken from recent work by the authors [20–22]. The reactions that oxidize SO_2 to SO_3 are of special interest in this study since they are believed to be the rate limiting steps in the K_2SO_4 formation prior to sulfate aerosol formation. Previously, the SO_2 and SO_3 concentrations in the gas phase were believed

to be determined by the reactions $SO_2+O(+M) \rightleftharpoons SO_3(+M)$ and $SO_3+O \rightleftharpoons SO_2+O_2$ [34]. However, in a recent study [22] the reaction $SO_3+O \rightleftharpoons SO_2+O_2$ was found to be insignificant. The sulfur subset includes reactions of SO_2 with O, OH, and HO_2 to form SO_3, reactions involving the $HOSO_2$-intermediate and also reactions involving SO_3 and H, O, OH, HO_2 radicals. All of these reactions may be important for the ratio of SO_2 to SO_3.

Few of the rate constants in the K/Cl/S/H/O reaction subset have been determined experimentally. Therefore estimated values for the rate constants are assigned to most of the reactions [17, 23]. In model C, some additional reactions are added to the K/H/S/O subset. These reactions, which are listed in Table 3, involve the novel species $KHSO_3$ and KSO_4. Using the current thermodynamic properties, the exothermicity of the reactions can be estimated. The reactions are expected to be fast in the exothermic direction, and following previous work [17] we assign a high rate constant of 10^{14} cm^3 mol^{-1} s^{-1} to these steps.

Results and Discussion

Model A

The updated detailed gas phase mechanism (called model A) is used to simulate the experimental data from Iisa et al. [13], Jensen et al. [12] and Jimenez and Balester [24]. The experiments from Iisa et al. were conducted at temperatures 1173, 1273, and 1373 K in an entrained flow reactor. Solid KCl particles were introduced to the system together with a mixture of gases consisting of SO_2, O_2, and H_2O, with N_2 to balance. The residence time of the gases in the reactor was in the range 0.3-1.5 s, after which a quenching system was applied to avoid further reaction. The comparison between the data from Iisa et al. [13] and the predicted results are shown in Figs. 2-4. The modeling and validation were done following these two steps. First, the evaporation of solid potassium chloride was modeled as three-pseudo-first order reactions in series following Glarborg and Marshall [17]. The rate constants were fitted to match the experimental data by Iisa et al. [13]. A comparison between the degree of KCl vaporization and the predicted value as a function of residence times can be seen in Fig. 2. A comparison between the observed degree of KCl sulfation in the entrained flow reactor as a function of the residence time at 1373 and 1173 K [13] and the predicted values from model

7

A is shown in Figs. 3-4. The model underpredicts the sulfate formation for all sets by approximately factor two. The updated sulfur subset of the mechanism yields a lower oxidation rate for SO_2 and thereby a less satisfactory agreement with the sulfation data than the original scheme by Glarborg and Marshall [17].

Model A is then compared to the experimental data from Jensen et al. [12]. Jensen et al. conducted experiments in a laboratory tubular furnace reactor using a synthetic flue gas containing a mixture of gaseous KCl, SO_2, H_2O, O_2, and N_2. Potassium chloride was added to the system by saturating the feed stream or part of it with salt vapors. The peak temperature was varied between 1043 and 1273 K. A characteristic temperature profile is shown in Fig. 5. The experimental data, presented as the ratio S/(S+Cl) in the aerosols, are compared to predicted results in Fig. 6. The model strongly underpredicts the sulfur content in the aerosols. In contrast with the experimental findings, model A predicts the sulfation process to be insignificant under these experimental conditions.

Finally, model A is evaluated against experimental data from Jimenez and Ballester [19]. These data were recently used by Jimenez and Balester [24] in modeling sulfate aerosols formation. The experiments were done using an entrained flow reactor [19]. Figure 7 shows the temperature profile measured along the cooling section for a reactor temperature of 1300 °C [19]. A comparison between the predictions of model A and the observed Cl/S ratio in the aerosols is presented in Fig. 8. Again, model A strongly underpredicts the sulfate formation, resulting in higher Cl/S values compared to the experimental data.
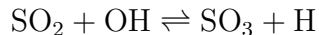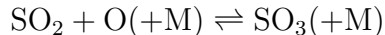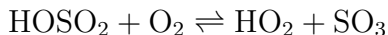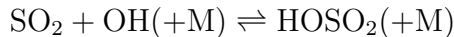
In general, the homogeneous gas phase model A underpredicts the degree of sulfation when compared to the experimental data. Previous work by Glarborg and Marshall [17] indicates that under the conditions investigated (Iisa et al. [13] at 1373 K), the degree of sulfation appears to be limited only by the SO_2 oxidation rate. This has an implication that the sulfation rate would be expected to be independent of the alkali precursor (in this case KCl, KOH, or other).
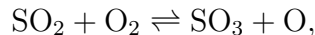
Model B

The next modeling approach (model B) uses an assumption of SO_2 oxidation to SO_3 being the rate limiting step in the sulfation process prior to the

aerosol formation. This modeling approach was used earlier by Jimenez and Ballester [24]. In this approach, the SO_3 formed in the system will instantaneously form potassium sulfate and subsequently generate sulfate aerosols irreversibly. Again, modeling predictions are compared to the experimental data of Iisa et al. [13], Jensen et al. [12] and Jimenez and Ballester [24] as shown in Figs. 3-4, 6 and 8. Similar to model A, model B underpredicts the degree of sulfation under all of the conditions investigated. There is no significant difference between the results of models A and B under the conditions of Iisa et al. (Figs. 3-4) and Jensen et al. (Fig. 6). However, for the conditions of Jimenez and Ballester (Fig. 8), model B predicts a degree of sulfation that is about an order of magnitude higher than model A, significantly improving the agreement with experiment. This difference is discussed further below.

In order to analyze which reactions govern the oxidation rate, sensitivity analysis and rate of production analysis for SO_3 formation were performed for the reaction conditions at 1373 K from Iisa et al. [13]. The calculations suggest that the important reactions involved in the formation of SO_3 are

$$SO_2 + OH(+M) \rightleftharpoons HOSO_2(+M)$$

$$HOSO_2 + O_2 \rightleftharpoons HO_2 + SO_3$$

$$SO_2 + O(+M) \rightleftharpoons SO_3(+M)$$

$$SO_2 + OH \rightleftharpoons SO_3 + H$$

$$SO_2 + HO_2 \rightleftharpoons SO_3 + OH.$$

The reaction

$$SO_2 + O_2 \rightleftharpoons SO_3 + O,$$
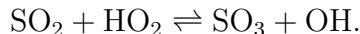
proposed earlier [17] to contribute to SO_3 formation, is now known to be too slow to be significant [22].

The characteristic temperature profile used in the experiments by Jimenez and Ballester involved a higher peak temperature (1573 K) than the other experiments (1043-1373 K). At the higher temperature, the SO_3 formation rate is faster as a consequence of the higher O and OH radical concentrations. However, at the same time SO_3 is limited by the thermal equilibrium with SO_2. To convert a significant fraction of SO_2 to the higher oxidation state ($S^{IV} \rightarrow S^{VI}$), a fast, irreversible consumption of SO_3 to form K_2SO_4 is required. An immediate consumption of SO_3 (as in model B) shifts the

reaction into producing more SO_3. In model A, even though the reaction between SO_3 and KOH/KCl occurs almost at collision frequency, the SO_3 consumption rate is limited due to the very low concentration of potassium (13 ppm KOH in the inlet). For this reason, SO_3 is only partly converted to K_2SO_4 and model A predicts a considerably lower degree of sulfation than model B.

According to the assumptions of models A and B, the homogeneous oxidation of SO_2 to SO_3 is a rate limiting step. However, both models underpredict the degree of sulfation observed experimentally.

The second modeling approach (model B) on formation of sulfate aerosols was based on the assumption that the SO_3 formation in the gas phase is the rate limiting step [2,3,11–13,17,35] and that immediately after its formation, the SO_3 is consumed to form K_2SO_4. As shown above, the model consistently underpredicts the formation of sulfate aerosols under the conditions of interest. The model B predictions suggest that the oxidation of SO_2 to SO_3 is low, below 1 % while in the experiments by Jensen et al. [12], the SO_2 conversion was quite high, around 5-16 %. The smallest discrepancy is found for the conditions of Iisa et al. [13], where the predicted SO_2 conversion of 0.4-2.8 % is compared to an observed value of 2-5 %.

It is important to point out that the sulfur subset in the present gas phase mechanism predicts well the homogeneous SO_2 oxidation over a wide range of conditions [22]. Therefore the difference between the experimental and modeling results cannot be explained in terms of uncertainties in this subset. Consequently, the discrepancy might be attributed to chemistry involving K-containing species or surface reactions.

There are several reported studies on SO_3 formation, both homogeneously [36–38] and heterogeneously/catalyzed [35, 39, 40]. The homogeneous oxidation of SO_2 by oxygen molecules at temperatures below 1173 K is very slow according to observations [34, 37, 39]. Figure 9 compares the SO_2 conversion in different experiments [12, 13, 37, 38]. As discussed above, the SO_2 consumption is quite low in the SO_2/O_2 system [37]. A study of SO_2 oxidation during moist CO oxidation [38] shows a higher conversion of SO_2 due to the generation of radicals. Despite the absence of combustibles, an even higher SO_2 consumption is found in the SO_2/O_2/alkali metal system [12,13]. This suggests that the presence of alkali metals may promote oxidation of SO_2. In particular the experimental data of Jensen et al. [12] show very high conversion rates for SO_2.

It is clear that the oxidation of SO_2 in the sulfation experiments, in particular those of Jensen et al. [12], cannot be attributed solely to reactions in the gas-phase H/S/O system. The results suggest that either an unknown gas-phase mechanism or a catalytic reaction promotes formation of S^{VI} (SO_3 or sulfate). These possibilities are investigated further in the following.
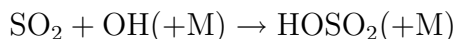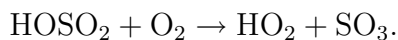
Model C

The third modeling approach (model C) takes into consideration that K-containing species may be involved actively in the SO_3 formation and sulfation process. A previous mechanism [17] contains a detailed reaction subset for K-containing species in the sulfation process. However, with the updated sulfur chemistry, the results of model A underpredicts the degree of sulfation when compared to the experimental data available in the literature [12,13,24]. In model C, the alkali subset of the detailed mechanism is supplemented with additional reactions of $KHSO_3$ and KSO_4, offering novel pathways to SO_3, as well as pathways to sulfation that do not involve SO_3 formation (Table 3).

The comparison between the observed degree of KCl-sulfation in the entrained flow reactor as a function of the residence time, at 1373 and 1173 K [13], and the predicted values from model C, is also shown in Figs. 3-4. The results indicate that there is no significant difference in the modeling results for A and C when compared to the experimental data; the model still underpredicts the degree of sulfation by around a factor of 2.
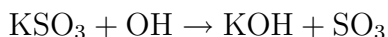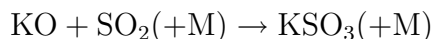
Sensitivity analysis and rate of production analysis for the conditions of Iisa et al. [13], at 1373 K (Fig. 3), using model C, were conducted to investigate the reactions important for the homogeneous sulfate formation prior to aerosol formation. The previous model by Glarborg and Marshall supports the suggestion that the oxidation of SO_2 to SO_3 is the rate limiting step in the sulfation process. In the present study, the model C predictions suggest that while the oxidation of SO_2 to SO_3 has a significant role in the sulfation process, other steps involving reactions with K-containing species may also be active in the sulfation process.

The pathways of SO_3 formation at 1373 K in the present study deviate somewhat from the suggestions by Glarborg and Marshall [17]. In their study, the SO_2 oxidation occurred mainly by OH addition to form $HOSO_2$ which then reacted with O_2 to form SO_3 and HO_2,

$$SO_2 + OH(+M) \rightarrow HOSO_2(+M)$$
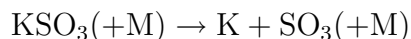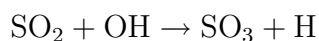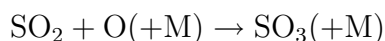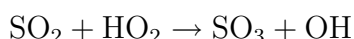
$$HOSO_2 + O_2 \rightarrow HO_2 + SO_3.$$

According to the current mechanism, the oxidation of SO_2 to SO_3 may, in addition to this sequence, proceed through the reactions

$$KO + SO_2(+M) \rightarrow KSO_3(+M)$$

$$KSO_3 + OH \rightarrow KOH + SO_3$$

with smaller contributions from

$$SO_2 + HO_2 \rightarrow SO_3 + OH$$

$$SO_2 + O(+M) \rightarrow SO_3(+M)$$

$$SO_2 + OH \rightarrow SO_3 + H$$

$$KSO_3(+M) \rightarrow K + SO_3(+M)$$

The suggestion that KSO_3 may be a significant intermediate in SO_3 formation is novel compared to previous work.

A pathway diagram for potassium transformations according to model C under the conditions of Fig. 3 is shown in Fig. 10. The main form of gaseous potassium under the present conditions is potassium chloride. In agreement with the previous studies [17, 23], KCl is after vaporization partly converted to KOH by reaction
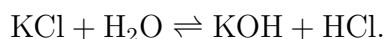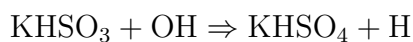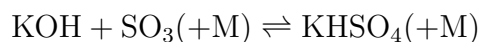
$$KCl + H_2O \rightleftharpoons KOH + HCl.$$

Part of the KCl is converted to KSO_3Cl following the reaction

$$KCl + SO_3(+M) \rightleftharpoons KSO_3Cl(+M)$$
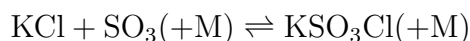
The KSO_3Cl reacts with H_2O in a mechanism similar to the previously suggested [17], and forms $KHSO_4$. This reaction contributes to more than 50 % of the $KHSO_4$ formed. The $KHSO_4$ is also formed through the reaction

$$KSO_4 + H_2O \rightleftharpoons KHSO_4 + OH$$
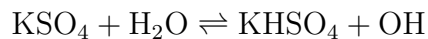
with an additional contribution by reactions

$$KOH + SO_3(+M) \rightleftharpoons KHSO_4(+M)$$

$$KHSO_3 + OH \Rightarrow KHSO_4 + H$$

12

Similar to the suggestion by Glarborg and Marshall, potassium sulfate is formed by reaction

$$KHSO_4 + KCl \rightleftharpoons K_2SO_4 + HCl$$
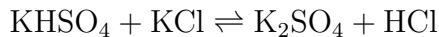
This reaction is the main consumption of $KHSO_4$ in the system and the only reaction that directly produces K_2SO_4.

The results of the sensitivity analysis of the predicted K_2SO_4 with respect to the reaction rate constants for the conditions of Fig. 3 is shown in Fig. 11. The analysis indicates that the sulfation rate is not only sensitive to the reactions that generate or consume free radicals in the system. According to the present model, the homogeneous gas phase sulfation may occur through the sequences

$KCl \rightarrow KSO_3Cl \rightarrow KHSO_4 \rightarrow K_2SO_4$ (a)

$KCl \rightarrow K \rightarrow KSO_2 \rightarrow KSO_4 \rightarrow KHSO_4 \rightarrow K_2SO_4$ (b)

$KCl \rightarrow KOH \rightarrow KSO_2 \rightarrow KSO_4 \rightarrow KHSO_4 \rightarrow K_2SO_4$ (c)

$KCl \rightarrow KOH \rightarrow KHSO_4 \rightarrow K_2SO_4$ (d)

$KCl \rightarrow KOH \rightarrow KHSO_3 \rightarrow KHSO_4 \rightarrow K_2SO_4$ (e)

$KCl \rightarrow KOH \rightarrow KO \rightarrow KSO_3 \rightarrow KSO_4 \rightarrow KHSO_4 \rightarrow K_2SO_4$ (f).
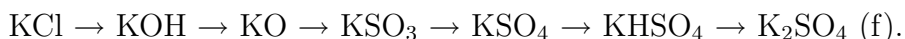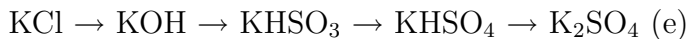
These six sequences have potentially significant roles in the sulfation mechanism. All of them should be taken into account in the gaseous sulfation process. From those six, sequence (a) is found to be the most significant one followed by sequence (b), (c) and (d), with minor contributions from (e) and (f). The pathways indicate that even alkali containing species such as KSO_2 and KSO_4 may contribute to the gaseous sulfation process.

The current model (model C) is also evaluated against experimental data from Iisa et al. [13] in terms of SO_2, O_2, and H_2O inlet variation at 1373 K. The predicted results using model C are similar to those of the previous study by Glarborg and Marshall [17], except that the current model underpredicts the degree of sulfation by around a factor of 2. According to model C, direct reactions of SO_2 and O_2 with some of the K-containing species may have a significant role in the gaseous sulfation process.

Comparison of predictions with model C to the experimental data by Jensen et al. [12] and Jimenez and Ballester [24] shows a significant underprediction of the sulfate aerosol formation (Figs. 6 and 8). As in Figs. 3 and 4, models A

and C yields similar results, despite the changes in the potassium subset. The difference of about a factor of two between the observed and predicted sulfation rate for the conditions of Iisa et al. [13] may conceivably be attributed to uncertainties in the gas-phase K/O/H/Cl/S chemistry. However, for the conditions of Jensen et al. [12] and Jimenez and Ballester [24] the degree of sulfation from the experiments are significantly higher than the predicted values from the homogeneous models. In these cases, it seems that apart from the homogeneous mechanism involving K/O/H/Cl/S, some unknown mechanism for sulfate aerosol formation is active. In order to investigate further the mechanisms which may be active in the system investigated [12], a discussion of the possible catalytic reactions in the system is presented. Independent of whether the sulfation process occurs mainly through a homogeneous or a heterogeneous mechanism, experimental evidence indicate that the availability of SO_3 in the system has a significant role. As discussed in the literature [41–43] the heterogeneous sulfation is promoted by the availability of SO_3 in the system. The sulfation of molten alkali chloride is suggested to be significantly faster compared to the solid alkali chloride sulfation [13]. At short residence times (a few seconds) as investigated in the present study, it is unlikely that a solid alkali chloride sulfation process is involved. Little is known about the sulfation of molten alkali chloride, but even in the presence of SO_3, it is a comparatively slow process [13]. Therefore in the present study, it seems that a homogeneous mechanism is active and the availability of SO_3 in the system has a significant role. The author's hypothesis is that the SO_3 formation rate is enhanced by catalytic reactions. This issue is discussed further below.

Model D

Field measurements [11, 44] of straw and other alkali containing biomass fuels usually show levels of sulfate similar to those observed by Jensen et al. [12] in the submicron aerosol particles formed by gas-to-particle conversion. Christensen et al. [11] concluded from analysis of data from combustion of several straw types that the observed level of sulfate formation is explained by a chemical equilibrium for the sulfation reaction being established in the gas phase at temperatures exceeding approximately 1073 K. The levels of sulfate formation in these studies are quite inconsistent with the much lower rate of gas phase sulfur dioxide oxidation computed by model A-C and support the suggestion that catalytic reactions may be involved in the sulfate aerosol formation.

14

A range of solids present in combustion systems has been shown to catalyze SO_2 oxidation. Fly ash has been shown in several studies to be an efficient catalyst. It has been observed that submicron-ash may catalyze the SO_2 oxidation to SO_3 in the convective passes of a coal-fired utility boiler, depending on the fuel, combustion conditions, and temperature profile in the convective section [40]. Both the iron oxide content [35, 40] and the calcium content [40] of the fly ash are important for the catalytic activity. A laboratory study by Marier and Dibbs [35] showed that the degree of oxidation of SO_2 in the presence of fly ash was 10 - 30 %, increasing linearly with the iron oxide content of the ash, compared to a conversion below 1% in the absence of fly-ash. Graham and Sarofim [40] used submicrometer CaO to study the inorganic aerosols and their role in catalyzing sulfuric acid production in furnaces. The sulfation reaction of submicrometer CaO was reported to be fast. Also iron oxides on boiler walls and tube furnaces may be active as catalysts. A study on emissions of sulfur trioxide from coal-fired power plants [45] indicates that formation of SO_3 may be catalyzed by iron oxides at lower temperatures (427-593 °C) in the economizer region of the boiler. This formation depends on site-specific factors (e.g. cleanliness of the tube surfaces). An investigation on the SO_3 formation in a fluidized bed done by Dennis and Hayhurst [39] indicated that while homogeneous reactions results in a very minor conversion, heterogeneous catalytic reactions on the surface of the sand is active in the oxidation.

Under the experimental conditions of Jensen et al. [12] with the high reported sulfation levels, it is conceivable that the K_2SO_4-formation involves catalytic oxidation of SO_2 to SO_3. The available surfaces include the alumina reactor wall, a steel grid in the alkali feeder, alkali deposits in the feeding section, and alkali aerosols fed to the system or generated during reaction. Steel and to a lesser extent alumina have been shown to catalyze oxidation of SO_2 [46]. There are indications that also alkali metals may promote SO_2 oxidation. Experimental data by Zeuthen [47], obtained in the same set-up as that used by Jensen et al. [12], indicate that presence of K_2SO_4 nuclei promotes additional K_2SO_4 formation in the system. Experiments on sulfate aerosol formation with and without seed particles and with and without 50 ppm SO_2 (other inlet conditions are kept constant, 200 ppm KCl, 5 % H_2O and 5% O_2) show that while seed particles of K_2SO_4 will suppress nucleation of KCl it does not suppress nucleation of K_2SO_4, but the size of the particles is increased [47]. This can be explained by an increased formation of SO_3 on the surface of the particles prior to the K_2SO_4 nucleation. Henriksson and Warnqvist [48] proposed a mechanism for the heterogeneous reaction of solid NaCl by SO_2 in the absence of SO_3. According to their analysis, SO_2
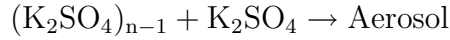
and O_2 are adsorbed on the NaCl surface, and the adsorbed species react to form adsorbed SO_3 (SO_3(ads)). The SO_3(ads) reacts with adsorbed water and NaCl to form HCl and Na_2SO_4. The intermediates were proposed to be H_2SO_4(ads) and $NaHSO_4$(ads).

To assess whether surfaces in the inlet KCl feeding system may have acted as a catalyst for SO_3 formation, calculations using model C were conducted, assuming SO_2/SO_3 to be in equilibrium right after the feeder (around 990 K). The results are shown in Fig. 12. The modeling predictions provide a fairly close agreement with the experimental data of Jensen et al. According to the calculations, oxidation of SO_2 to SO_3 downstream of the feeder is negligible due to the low temperature. The SO_3 formed is largely converted to K_2SO_4, while [SO_2] remains at the equilibrium value. These calculations also explain the lack of temperature dependence of the sulfation rate; the reactor peak temperature is downstream of the feeder where the catalyzed reaction takes place. From these calculations it is plausible that the solid surfaces in the KCl feeding system catalyze SO_2 oxidation, approaching an equilibrium concentration of SO_3 prior to the gas phase system where it reacts with other inlet gases to form K_2SO_4.

In the last modeling approach (model D), the possible scenario that K_2SO_4 aerosols, once formed, promote further SO_2 oxidation is investigated. Since the details of the catalytic mechanism is not known, a simplified approach will be taken, involving addition of a catalytic reaction to the homogeneous gas phase model A. The aerosol formation is modeled with a clustering approach, where a number of K_2SO_4 molecules will recombine to form a larger molecule. Eventually this molecule reaches a critical cluster number and precipitates to form a solid aerosol particle. The aerosol particle formed then acts as a catalyst for the further sulfation process by enhancing SO_3 formation in the system. The detailed modeling for the clustering phenomena is presented below.

Potassium sulfate nucleation can be modeled by a chemical clustering approach where gaseous potassium sulfate is allowed to cluster to form larger species by sequential polymerization steps. The value of the rate constant used in each step is assumed to be similar to that of the dimerization reaction NaCl+NaCl [17], which has been measured experimentally. Here, K_2SO_4 is treated as a monomer for the subsequent clustering process i.e.,

$$K_2SO_4 + K_2SO_4 \rightarrow (K_2SO_4)_2$$

$$(K_2SO_4)_2 + K_2SO_4 \rightarrow (K_2SO_4)_3$$

16

$$(K_2SO_4)_{n-1} + K_2SO_4 \rightarrow \text{Aerosol}$$

This sequence of irreversible reactions $(K_2SO_4)_{n-1} + K_2SO_4 \rightarrow (K_2SO_4)_n$ ($2 \leq n \leq 10$), with the nucleation taken to be completed for n = 10, can be used to assess the potential importance of homogeneous nucleation of K_2SO_4 from its gaseous form. The critical nucleus size of 10 potassium sulfate molecules is just a coarse estimation, the number can be in range of 1 to infinite, depending on the saturation ratio.

The rate of catalytic reaction by solid particles surfaces is estimated from gas kinetic theory following Gustavsson et al. [49]. The catalytic reaction is assumed as a pseudo second order reaction where the reaction rate (r_{SO_2}) = k[SO$_2$][Aerosol]= k_{cat}[SO$_2$]. Here k (cm^3 mol^{-1} s^{-1}) = k_{cat} (s^{-1})/[aerosol]. And k_{cat} (s^{-1}) is the catalytic reaction of SO$_2$ by aerosol particles. The rate of collision between aerosol particles and SO$_2$ were calculated from the kinetic theory of gases. The aerosol particles are assumed to have zero velocity, since they are large compared with the gas phase species. The collision frequency, Z_{SO_2} (s^{-1})= ν_{SO_2} n_p σ. The average velocity of SO$_2$ can be calculated as ν_{SO_2} (cm s^{-1})=$\sqrt{3RT/M_{SO_2}}$, where n_p (cm^{-3}) is the particle number density, and σ (cm^2)= π r_p^2 is the collision cross section. The rate of catalytic SO$_2$ oxidation by aerosol particles then is k_{cat} (s^{-1})= z_{SO_2} q_{SO_2}, where q_{SO_2} is the collision efficiency (the value is below or equal to 1). The particle number density (n_p) can be calculated from the aerosol concentration.

Particle agglomeration is not accounted for in this simplified model and two approaches have been adopted in the calculations. In the first approach (case 1) it is assumed that the agglomeration occurs immediately, resulting in a particle diameter similar to that reported by Jensen et al. [12], d_p=159 nm. This corresponds to a pseudo second-order rate constant of k_1= 2.4 $\cdot$ 10^{16} $\cdot$ T$^{0.5}$ $\cdot$ q_{SO_2} (cm^3 mol^{-1} s^{-1}). In the second approach (case 2), no agglomeration is assumed, corresponding to d_p=1.36 nm (calculated from n=10, spherical particle) and k_2= 1.7 $\cdot$ 10^{12} $\cdot$ T$^{0.5}$ $\cdot$ q_{SO_2} (cm^{3}mol^{-1} s^{-1}).

Model predictions for approach 2 are compared to the experimental data of Jensen et al. [12] in Fig. 12. Similar results are obtained for case 1. Collision efficiencies in the range $0.01 < q_{SO_2} < 0.1$ bracket the experimental data for most of the different peak temperatures (1043–1273 K). However, even with the assumed zero activation energy of the surface reaction, the predicted temperature dependence of the sulfation rate is considerable, in contrast to the experimental observations. For this reason, it appears unlikely that alkali sulfate aerosols strongly promote SO$_2$ oxidation in the investigated system, but more work is required to confirm this.

The gas phase model consistently underpredicts the sulfate formation in the experiments of Iisa et al. [13], Jensen et al. [12], and Jimenez and Ballester [24]. The difference compared to the data of Iisa et al., about a factor of 2, may be caused by uncertainties in the gas phase mechanism. However, the underprediction of the sulfation rate observed by Jensen et al. and Jimenez and Ballester is an order of magnitude or higher. We attribute the higher observed sulfation rate mainly to presence of surfaces that may catalyze oxidation of SO_2. In the experiments of Jensen et al., reactor and deposit surfaces may be active, while for the conditions of Jimenez and Ballester the presence of fly ash may be of importance. To what extent sulfate aerosols, once formed, may catalyze further SO_2 oxidation is not yet resolved. However, the results of the present study are consistent with the previous finding that sulfate aerosol formation occurs from homogeneous nucleation, following oxidation of SO_2 to SO_3 (or KSO_4). The sulfate aerosol formation is influenced by the SO_2, O_2, KCl inlet concentrations, residence time and temperature history. Apart from the SO_3 formation, other aspects such as reactions of SO_2 and O_2 with K-containing species or catalytic reaction by sulfate aerosols particles may be important limiting step in the sulfation process under present conditions investigated.

Discussion

Sulfation of alkali metals is known to proceed readily (but slow) in condensed and solid phase. However, it is unlikely that sulfates, once formed, are released from a surface to the gas-phase as aerosols. We believe that alkali sulfate aerosols are formed from homogeneous nucleation following a series of steps including oxidation of SO_2 (S^{IV}) to a higher oxidation state (S^{VI} – mainly SO_3) and subsequent sulfation. Such a mechanism is consistent with experimental observations [12,13,24] as well as with ab initio calculations on the thermal stability of the proposed complex intermediates ([17], present work) and the observation that molecule–molecule reactions involving alkali species are very fast, proceeding close to collision frequency [17]. The proposed mechanism currently cannot be proven, since reported experimental results are all obtained in systems where surfaces are present, i.e. reactor walls, deposits, and alkali and/or flyash particles. There are indications that some or all of these surfaces may catalyze oxidation of SO_2 to SO_3, but their role in alkali sulfate aerosol formation is still in discussion. Experiments in a rigorously homogeneous system is called for to verify the proposed gas-phase sulfation mechanism.

Conclusions

In this study, the sulfate aerosol formation was simulated using the following modeling approaches: 1) a simplified scheme with oxidation of SO_2 to SO_3 as the rate limiting step, 2) a full, updated gas-phase K/S/Cl reaction mechanism, and 3) a full gas-phase mechanism together with a simplified description of catalyzed formation of SO_3. The K/S/Cl mechanism was extended with reactions involving $KHSO_3$ and KSO_4 (thermodynamic properties from ab initio calculations) to investigate alkali interactions with the SO_2/SO_3 ratio and possible novel pathways to formation of K_2SO_4. Modeling predictions were compared with selected experimental data from the literature. The rate of gas phase sulfur dioxide oxidation computed by the homogeneous gas-phase models is much lower than the observed levels of sulfate formation in laboratory and field studies. This inconsistency supports the suggestion that catalytic reactions may be involved in the sulfate aerosol formation. The oxidation of SO_2 to SO_3, which we believe is a rate-limiting step in the sulfation process, proceeds readily on the surface of fly-ash particles present in solid fuel combustion. Additional experimental work is needed in order to gain more insight into the fundamental mechanisms controlling the sulfate aerosol formation.

Acknowledgments

References

[1] B. Sander. *Biomass Bioenergy*, 12:177–183, 1997.

[2] K.A. Christensen and H.Livbjerg. *Aerosol Sci. Technol.*, 33:470–489, 2000.

[3] K.A. Christensen and H.Livbjerg. *Aerosol Sci. Technol.*, 25:185–199, 1996.

[4] L.S. Johansson, C. Tullin, B. Leckner, and P. Sjövall. *Biomass Bioenergy*, 25(4):435–446, 2003.

[5] H.P. Michelsen, F. Frandsen, K. Dam-Johansen, and O.H. Larsen. *Fuel Proc. Tech.*, 54:95–108, 1998.

[6] T. Heinzel, V. Siegle, H. Spliethoff, and K.R.G. Hein. *Fuel Proc. Tech.*, 54:109–125, 1998.

[7] L.A.Hansen, H.P. Nielsen, F.J. Frandsen, K. Dam-Johansen, S. Hørlyck, and A. Karlsson. *Fuel Proc. Tech.*, 64:189–209, 2000.

[8] H.P. Nielsen, F.J. Frandsen, K. Dam-Johansen, and L.L. Baxter. *Prog. Energy Combust. Sci.*, 26:283–298, 2000.

[9] J. Boow. *Fuel*, 51:170–173, 1972.

[10] J. Latva-Somppi, M. Moisio, E.L. Kauppinen, T. Valmari, P. Ahonen, and J. Keskinen. *J. Aerosol Sci.*, 29:461–480, 1998.

[11] K.A. Christensen, M. Stenholm, and H.Livbjerg. *J. Aerosol Sci.*, 294:421–444, 1998.

[12] J.R. Jensen, L.B. Nielsen, C. Schultz-Møller, S.Wedel, and H.Livbjerg. *Aerosol Sci. Technol.*, 33:490–509, 2000.

[13] K. Iisa, Y. Lu, and K. Salmenoja. *Energy Fuels*, 13:1184–1190, 1999.

[14] M. Steinberg and K. Schofield. *Prog. Energy Combust. Sci*, 16:311–317, 1990.

[15] K. Schofield and M. Steinberg. *J. Phys. Chem.*, 96:715–726, 1992.

[16] M. Steinberg and K. Schofield. *Combust. Flame*, 129:453–470, 2002.

[17] P. Glarborg and P. Marshall. *Combust. Flame*, 141:22–39, 2005.

[18] K.A. Christensen. *PhD Thesis, Department of Chemical Engineering, Technical University of Denmark*, ISBN 87-90142-04-7, 1995.

[19] S. Jimenez and J. Ballester. *Combust. Flame*, 140:346–358, 2005.

[20] A. Yilmaz, L. Hindiyarti, A. Jensen, P. Glarborg, and P. Marshall. *J. Phys. Chem. A*, 110:6654–6659, 2006.

[21] C.L. Rasmussen, P. Glarborg, and P. Marshall. *Proc. Combust. Inst.*, 31:339–347, 2007.

[22] L. Hindiyarti, P. Glarborg, and P. Marshall. Reactions of SO_3 with the O/H radical pool under combustion conditions. *J. Phys. Chem. A*, 2007, in press.

[23] L. Hindiyarti, F. Frandsen, H. Livbjerg, and P. Glarborg. *Fuel*, 85:978–988, 2006.

[24] S. Jimenez and J. Ballester. *Fuel*, 86:486–493, 2007.

[25] L. A. Curtiss, K. Raghavachari, P. C. Redfern, V. Rassolov, and J. A. Pople. *J. Phys. Chem.*, 109:7764, 1998.

[26] L. A. Curtiss, P. C. Redfern, V. Rassolov, G. Kedziora, and J. A. Pople. *J. Chem. Phys.*, 114:9287, 2001.

[27] M. J. Frisch, G. W. Trucks, H. B. Schlegel, G. E. Scuseria, M. A. Robb, J. R. Cheeseman, J.A. Montgomery Jr., T. Vreven, K.N. Kudin, J.C. Burant, J.M. Millam, S.S. Iyengar, J. Tomasi, V. Barone, B. Mennucci, M. Cossi, G. Scalmani, N. Rega, G.A. Petersson, H. Nakatsuji, M. Hada, M. Ehara, K. Toyota, R. Fukuda, J. Hasegawa, M. Ishida, T. Nakajima, Y. Honda, O. Kitao, H. Nakai, M. Klene, X. Li, J.E. Knox, H. P. Hratchian, J.B. Cross, V. Bakken, C. Adamo, J. Jaramillo, R. Gomperts, R.E. Stratmann, O. Yazyev, A.J. Austin, R. Cammi, C. Pomelli, J.W. Ochterski, P.Y. Ayala, K. Morokuma, G.A. Voth, P. Salvador, J.J. Dannenberg, V.G. Zakrzewski, S. Dapprich, A.D. Daniels, M.C. Strain, O. Farkas, D.K. Malick, A.D. Rabuck, K. Raghavachari, J.B. Foresman, J.V. Ortiz, Q. Cui, A.G. Baboul, S. Clifford, J. Cioslowski, B.B. Stefanov, G. Liu, A. Liashenko, P. Piskorz, I. Komaromi, R.L. Martin, D.J. Fox, T. Keith, M.A. Al-Laham, C.Y. Peng, A. Nanayakkara, M. Challacombe, P.M.W. Gill, B. Johnson, W. Chen, M.W. Wong, C. Gonzalez, and J.A. Pople. *Gaussian 03, Revision D.02, Gaussian, Inc., Wallingford CT*, 2004.

[28] B. Ruscic, A.F. Wagner, L.B. Lawrence, L.B. Harding, L. R. Asher, D. Feller, D.A. Dixon, K.A. Peterson, Y. Song, X. Qian, C. Yiu Ng, J. Liu, W. Chen, and D.W. Schwenke. *J. Phys. Chem. A*, 106:2727, 2002.

[29] L.V. Gurvich, G.A. Bergman, L.N. Gorokhov, V.S. Iorish, V.Ya. Leonidov, and V.S. Yungman. *J. Phys. Chem. Ref. Data*, 26:1031–1110, 1997.

[30] X-B. Wang, C-F. Ding, J.B. Nicholas, D.A.Dixon, and L-S. Wang. *J. Phys. Chem. A.*, 103:3423, 1999.

[31] A.E. Lutz, R.J. Kee, and J.A. Miller. A Fortran Program for Predicting Homogeneous Gas Phase Chemical Kinetics with Sensitivity Analysis. Sandia National Laboratories, Report SAND87-8248, 1987.

[32] R.J. Kee, F. Rupley, and J.A.Miller. Chemkin II- A Fortran Chemical Kinetics Package for the Analysis of Gas Phase Chemical Kinetics. Sandia National Laboratories, Report SAND89-8009, 1989.

[33] D.L. Baulch, J. Duxbury, S.J. Grant, and D.C. Montague. Evaluated kinetic data for high temperature reactions. Vol.4 : Homogeneous gas phase reactions of halogen- and cyanide-containing species. *J. Phys. Chem. Ref. Data Suppl.*, 10, 1981.

[34] C.F. Cullis and M.F.R. Mulcahy. *Combust. Flame*, 18:225–292, 1972.

[35] P. Marier and H.P. Dibbs. *Thermochimica Acta*, 8:155–165, 1974.

[36] N.A. Burdett, W.E. Langdon, and R.T. Squires. *J. Inst. Energy*, 57:373–376, 1984.

[37] D. Flint and A.W. Lindsay. *Fuel*, 30:288, 1952.

[38] P. Glarborg, D. Kubel, K. Dam Johansen, H. M. Chiang, and J.W. Bozzeli. *Int. J. Chem. Kinet.*, 28:773–790, 1996.

[39] J.S. Dennis and A.N. Hayhurst. *Combust. Flame*, 72:241–258, 1988.

[40] K.A. Graham and A.F. Sarofim. *J. Air Waste Manag. Ass.*, 48:106–112, 1998.

[41] W.L. Fielder, C.A. Stearns, and F.J. Kohl. *J. Electrochem. Soc.: Solid-State Science and Technology*, 131:2414–2417, 1984.

[42] J.A.B. Satrio, S.B. Jagtap, and T.D. Wheelock. *Ind. Eng. Chem. Res.*, 41:3540–3547, 2002.

[43] A.B. Anderson. *J. Am. Chem. Soc.*, 106:6262–6265, 1984.

[44] M. Jöller, T. Brunner, and I. Obernberger. *Energy Fuels*, 19:311–323, 2005.

[45] R.K. Srivastava, C.A. Miller, C. Erickson, and R. Jambhekar. *J. Air Waste Manag. Ass.*, 54(6):750–762, 2004.

[46] T.L. Jørgensen, H. Livbjerg, and P. Glarborg. Homogeneous and heterogenously catalyzed oxidation of SO_2. 2007, submitted for publication.

[47] J. Zeuthen. *PhD Thesis, Department of Chemical Engineering, Technical University of Denmark*, 2007.

[48] M. Henriksson and B. Warnqvist. *Ind.Eng.Chem.Process Des. Dev.*, 18:249–253, 1979.

[49] L. Gustavsson, P. Glarborg, and B. Leckner. *Combust. Flame*, 106:345–358, 1996.

Tables

Table 1: Ab initio results for alkali metal species.

Molecule	G_3 energy (au)[a]	ΔH_{f298} (kJ mol 1)	Symmetry	Inertia product (GHz3)[b]	Vibrational frequencies (cm-1)b
NaHSO$_3$	-786.44191	-668.3	C$_1$	58.22	129, 166, 306, 322, 417, 454, 498, 579, 990, 1025, 1094, 3750
NaSO$_4$	-860.97449	-655.8	C$_{2v}$(2B1)	24.34	84, 219, 282, 327, 384, 427, 515, 580, 765, 915, 1090, 1117
KHSO$_3$	-1224.04538	-690.7	C$_1$	23.19	117, 149, 235, 304, 396, 427, 494, 572, 990, 1028, 3752
KSO$_4$	-1298.58048	-698.1	C$_{2v}$(2B1)	10.36	58, 173, 215, 333, 370, 430, 513, 564, 762, 918, 1108, 1117

[a] 1 au ≈ 2625.5 kJ mol-1.

[b] B3LYP/6-311G(d,p)result. Frequencies scaled by 0.99.

Table 2: Thermodynamic properties for selected alkali species. Units are kcal/mol (H$_{f,298}$) and cal/mol-K (S$_{298}$, C$_p$).

Species	H$_{f,298}$	S$_{298}$	C$_{p,300}$	C$_{p,400}$	C$_{p,500}$	C$_{p,600}$	C$_{p,800}$	C$_{p,1000}$	C$_{p,1500}$
NaHSO$_3$	-153.27	78.26	20.47	23.04	24.92	26.26	27.83	28.57	29.87
NaSO$_4$	-152.47	81.02	21.21	24.10	26.15	27.60	29.25	29.96	30.93
KHSO$_3$	-165.07	79.63	21.44	23.78	25.46	26.64	27.99	28.66	29.95
KSO$_4$	-166.84	82.19	22.18	24.86	26.78	28.10	29.56	30.18	31.10

Table 3: Rate coefficients for additional reactions, units are cm, mol, s, K.

No	Reaction	A	n	E	Note
1.	$KO_2+SO_2(+M) \rightleftharpoons KSO_4(+M)$	1.0E14	0.0	0.0	as $KOH+SO_3$ [17]
	Low pressure limit/2.6E42 -7.6 0/				
2.	$KSO_2+O_2(+M) \rightleftharpoons KSO_4 (+M)$	1.0E14	0.0	0.0	as $KOH+SO_3$ [17]
	Low pressure limit /2.6E42 -7.6 0/				
3.	$KO+SO_3(+M) \rightleftharpoons KSO_4 (+M)$	1.0E14	0.0	0.0	as $KOH+SO_3$ [17]
	Low pressure limit /2.6E42 -7.6 0/				
4.	$KHSO_4 +OH \rightleftharpoons KSO_4+H_2O$	1.0E14	0.0	0.0	
5.	$KHSO_3+OH \rightleftharpoons KSO_3 + H_2O$	1.0E14	0.0	0.0	
6.	$KHSO_3+OH \rightleftharpoons KHSO_4 + H$	1.0E14	0.0	0.0	
7.	$KSO_3+O \rightleftharpoons KSO_4$	1.0E14	0.0	0.0	
8.	$KSO_4+O \rightleftharpoons KSO_3+O_2$	1.0E14	0.0	0.0	
9.	$KOH+SO_2(+M) \rightleftharpoons KHSO_3(+M)$	1.0E14	0.0	0.0	as $KOH+SO_3$ [17]
	Low pressure limit/2.6E42 -7.6 0/				
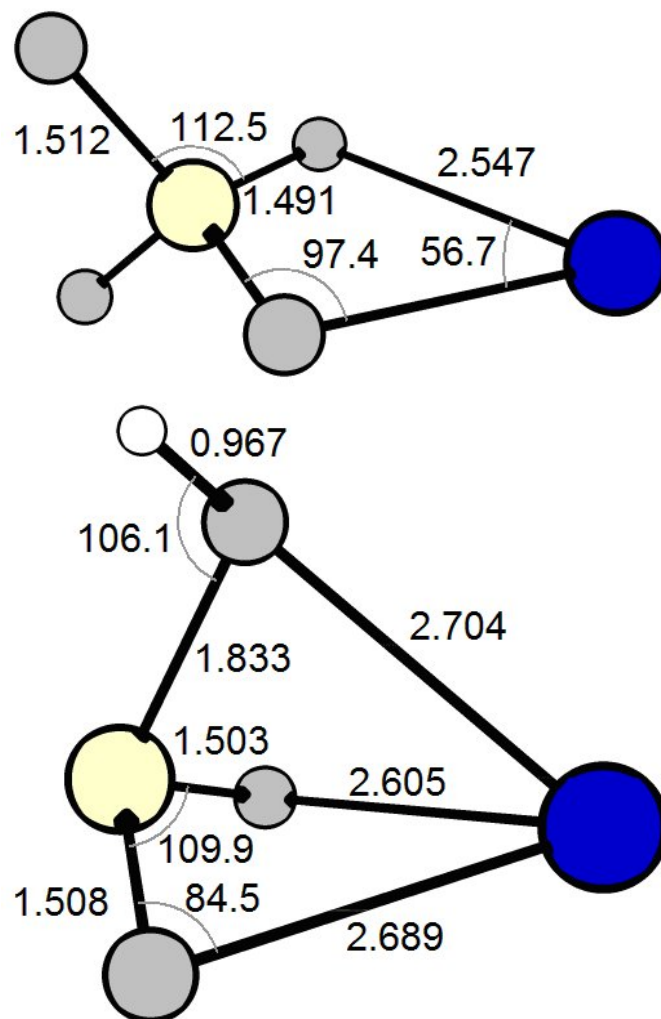
Figures

Figure 1: B3LYP/6-311G(d,p) geometries computed for KSO_4 and $KHSO_3$. Distances in 10^{-10} m and angles in degrees
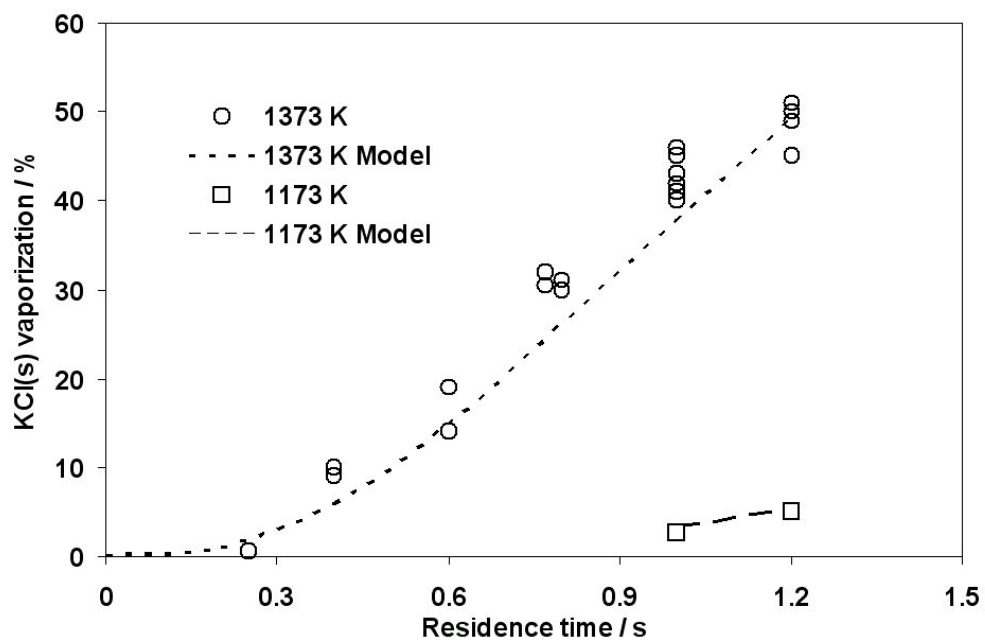
Figure 2: Vaporization of solid KCl as a function of residence time in an entrained flow reactor at 1173 and 1373K. Symbols denote experimental results [13], lines denote modeling result. KCl feed rate : 0,24 g/min
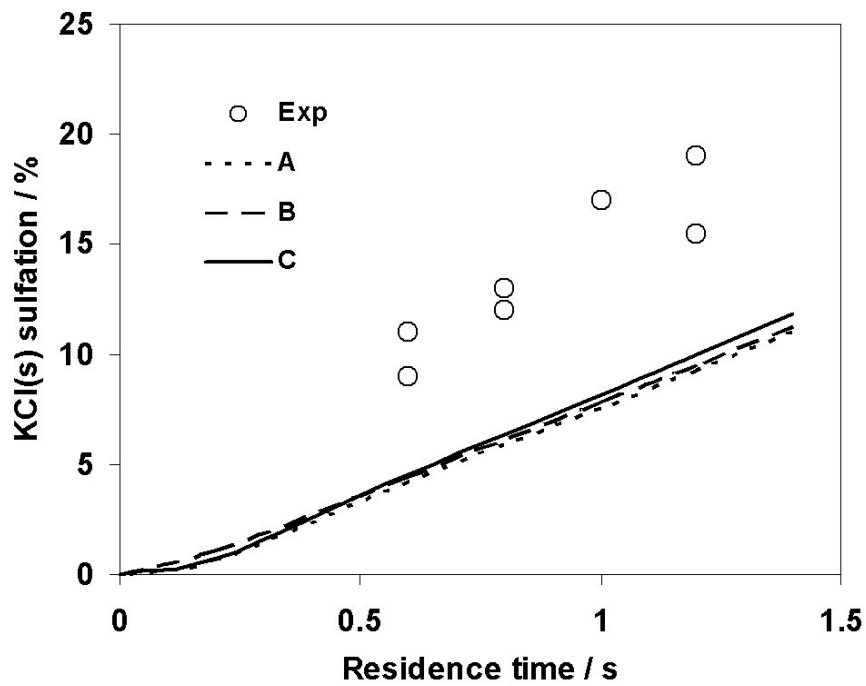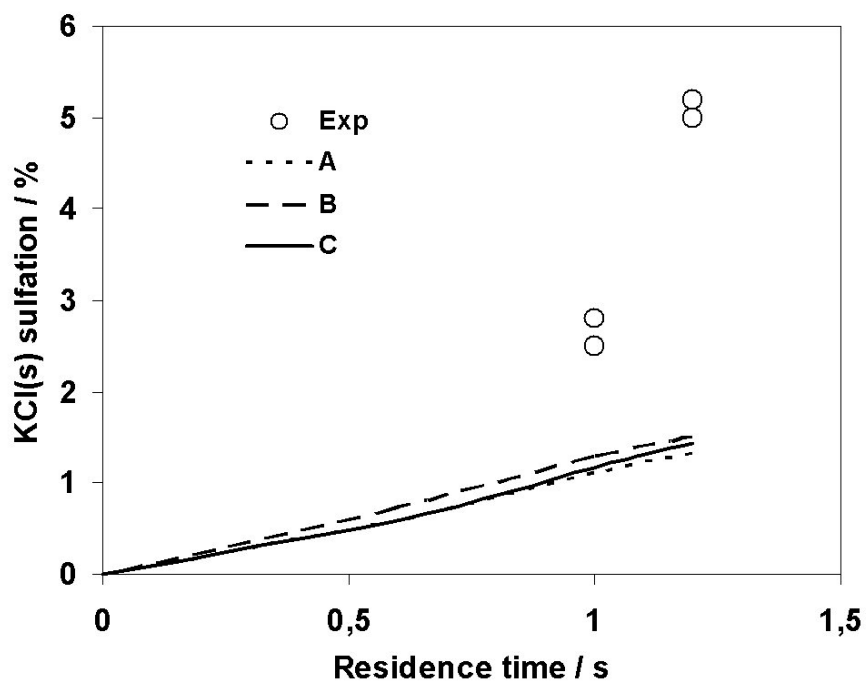
Figure 3: Fractional conversion of solid KCl to K_2SO_4 as a function of residence time in an entrained flow reactor at 1373 K. Symbols denote experimental results [13], lines denote modeling result (Models A-C). Inlet feed contained 2 % SO_2, 5 % O_2, 10 % H_2O, N_2 to balanced and KCl feed rate : 0,24 g/min

.

Figure 4: Fractional conversion of solid KCl to K_2SO_4 as a function of residence time in an entrained flow reactor at 1173 K. Symbols denote experimental results [13], lines denote modeling result (Models A-C). Inlet conditions contained 2 % SO_2, 5 % O_2, 10 % H_2O, N_2 to balanced and KCl feed rate : 0,24 g/min

.
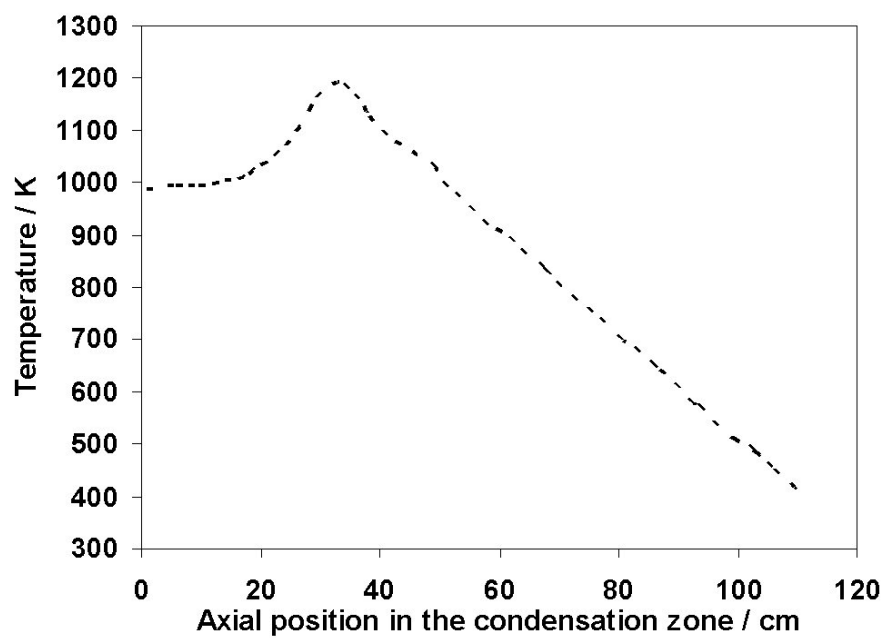
Figure 5: Measured temperature profile of the reactor wall, the peak temperature is varied from 1043-1273 K. [12]
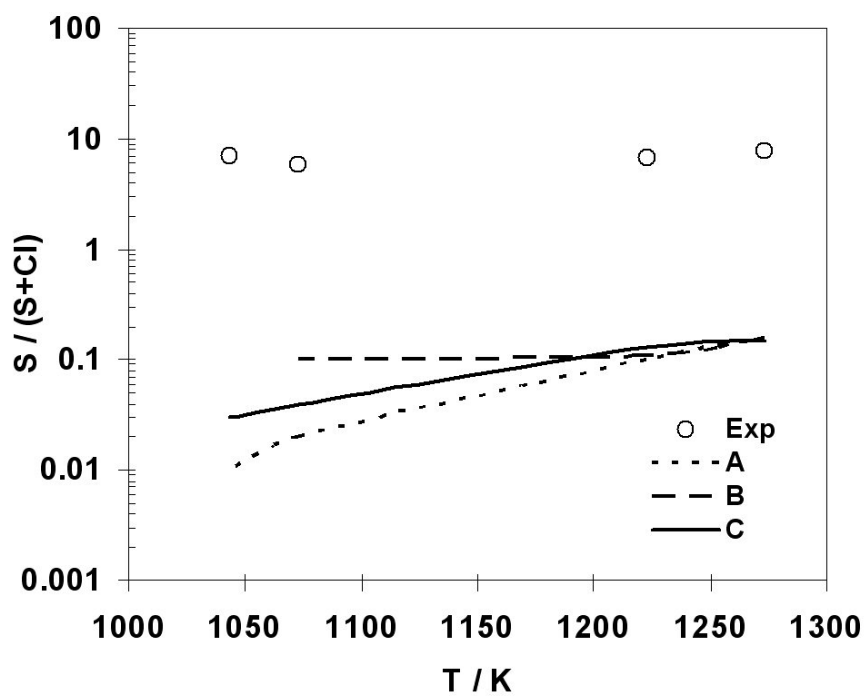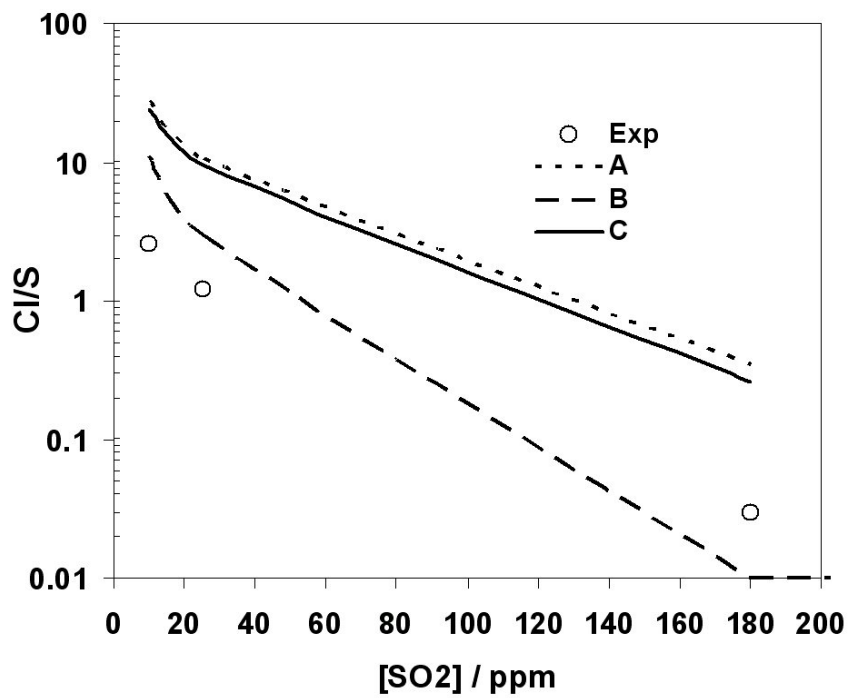
Figure 6: Comparison of the predicted model (A,B, and C, lines) with the experimental data from Jensen et al. [12] (open symbols), presented as $\frac{S}{(S+Cl)}$ in the aerosols. Inlet conditions contained 200 ppm KCl, 200 ppm SO_2, 4 % O_2, 4 % H_2O, N_2 to balanced. The peak temperature is varied from 1043, 1073, 1223, or 1273 K, and residence time is around 3 s.
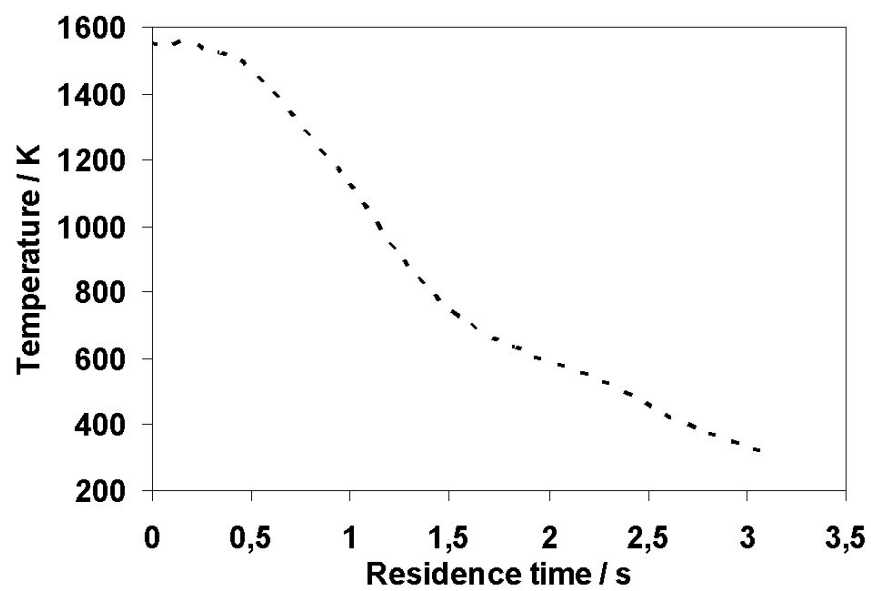
Figure 7: Measured temperature profile along the cooling section of the reactor from Jimenez and Ballester [24]

Figure 8: Comparison of the predicted model (A,B, and C, lines) with the experimental data from Jimenez and Ballester [19] (open symbols). Inlet conditions contained 13 ppm KOH, 34 ppm HCl, 10/ 25/180 ppm SO_2, 5 % O_2, 2 0 % H_2O, 8 % CO_2 and N_2 to balanced, residence time is around 3 s
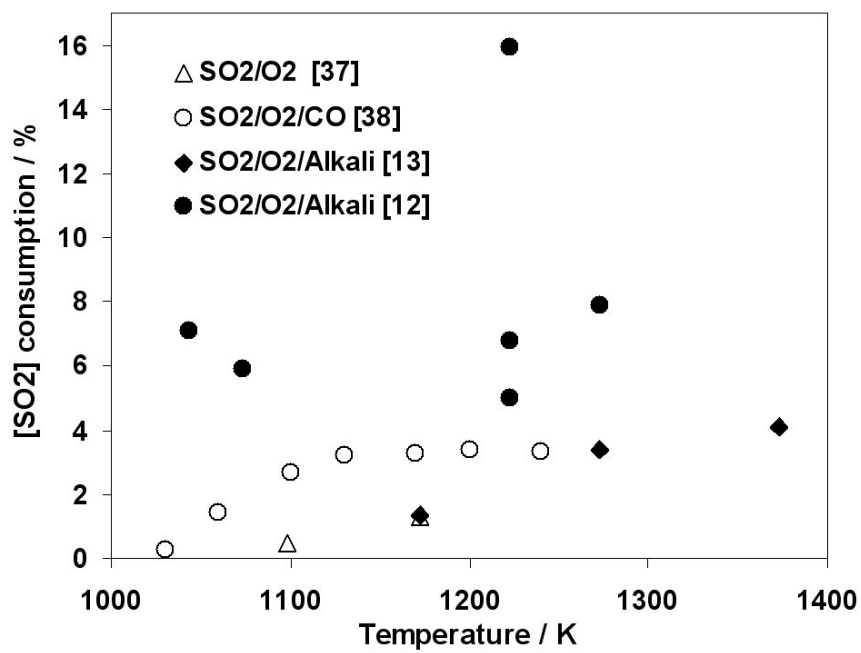
.

Figure 9: The SO$_2$ consumption (%) from different experiments [12,13,37,38] as a function of temperature/peak temperature.
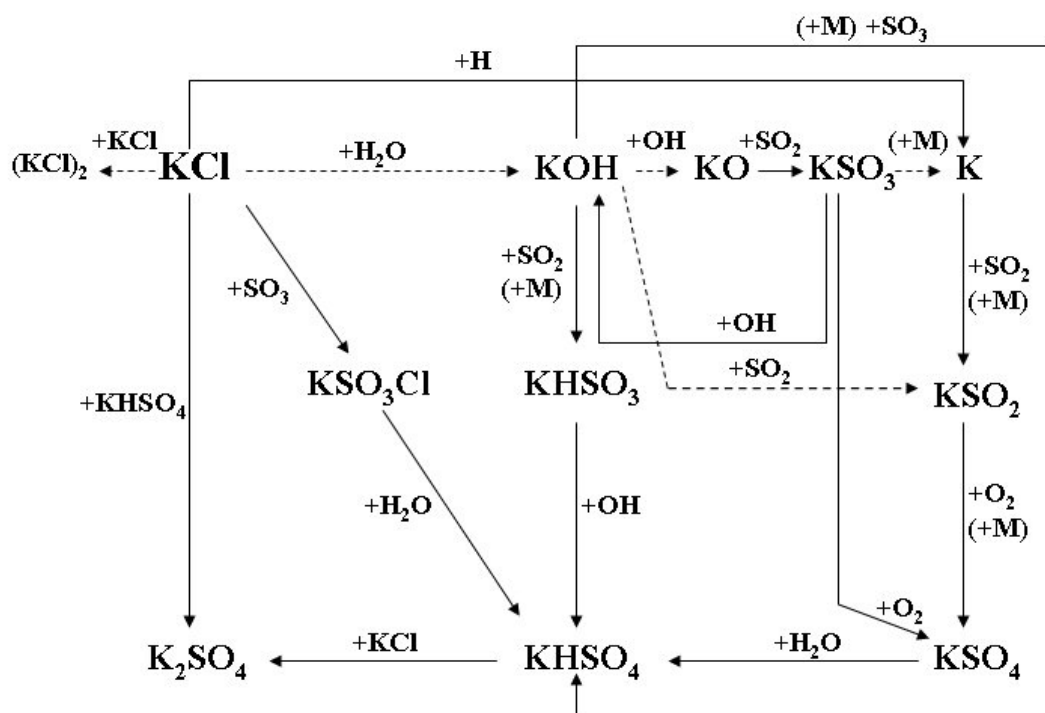
Figure 10: Pathway diagram for potassium transformations under the conditions of Iisa et al. [13] at 1373 K with model C.
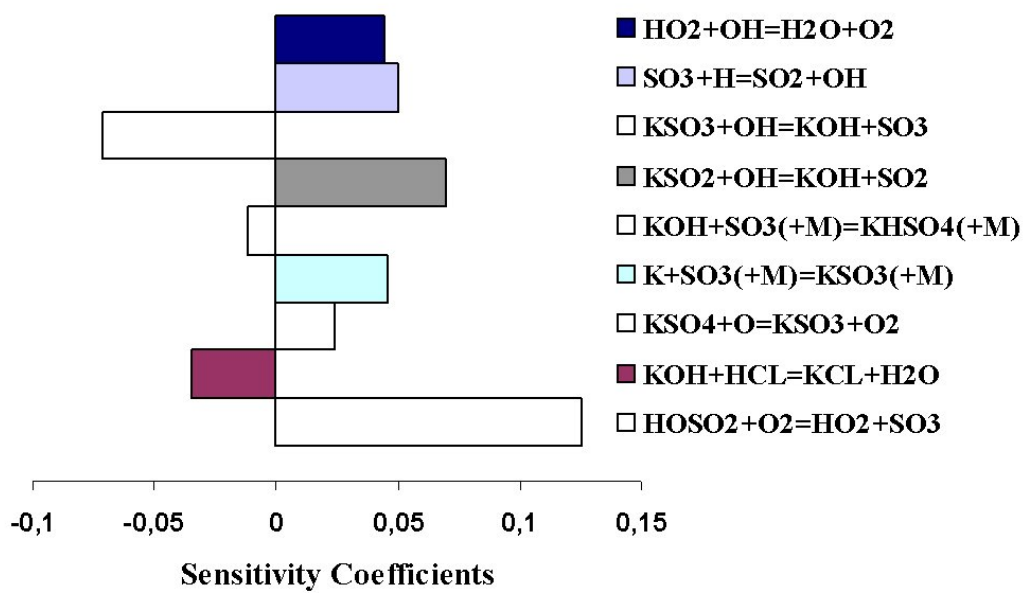
Figure 11: Sensitivity coefficients for the elementary reactions towards the K_2SO_4 formation for conditions corresponding to Iisa et al. [13] at 1373 K and with a residence time of 1.2 s with model C.
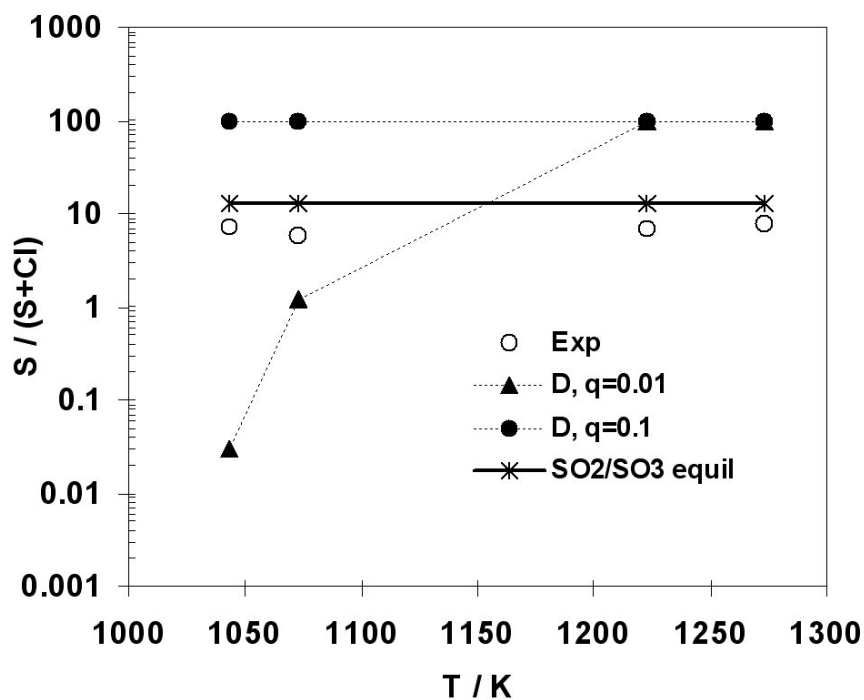
Figure 12: Comparison of model predictions (lines) with the experimental data from Jensen et al. [12] (open symbols), presented as $\frac{S}{(S+Cl)}$ in the aerosols. Results from predictions with model C, assuming that SO_2/SO_3 is in equilibrium at the inlet to the homogeneous gas phase system (after KCl feeding) are shown as a solid line. Results obtained with model D, using k_2 with collision efficiencies of 0.01 and 0.1, are shown as dotted lines. Inlet conditions contained 200 ppm KCl, 200 ppm SO_2, 4 % O_2, 4 % H_2O, N_2 to balanced. The peak temperature is varied from 1043, 1073, 1223, or 1273 K, and residence time is around 3 s.